TEMPLATING NANOSTRUCTURES IN EPOXY RESIN USING STYRENIC BLOCK COPOLYMERS

A THESIS SUBMITTED TO THE

CENTRAL DEPARTMENT OF CHEMISTRY
INSTITUTE OF SCIENCE AND TECHNOLOGY
TRIBHUVAN UNIVERSITY, KIRTIPUR
KATHMANDU, NEPAL

FOR THE AWARD OF THE DEGREE OF
DOCTOR OF PHILOSOPHY
IN CHEMISTRY

BY

RAJESH PANDIT

JUNE 2015 (JESTHA 2072)

TEMPLATING NANOSTRUCTURES IN EPOXY RESIN USING STYRENIC BLOCK COPOLYMERS

A THESIS SUBMITTED TO THE

CENTRAL DEPARTMENT OF CHEMISTRY
INSTITUTE OF SCIENCE AND TECHNOLOGY
TRIBHUVAN UNIVERSITY, KIRTIPUR
KATHMANDU, NEPAL

FOR THE AWARD OF THE DEGREE OF
DOCTOR OF PHILOSOPHY
IN CHEMISTRY

BY

RAJESH PANDIT

JUNE 2015 (JESTHA 2072)

DECLARATION

The thesis entitled **“Templating Nanostructures in Epoxy Resin Using Styrenic Block Copolymers”** which is being submitted to the Institute of Science and Technology (IOST), Central Department of Chemistry, Tribhuvan University, Nepal for the award of the degree of Doctor of Philosophy (Ph. D.), is a research work carried out by me under the supervision and guidance of Assoc. Prof. Dr. Rameshwar Adhikari, Central Department of Chemistry, Tribhuvan University, Nepal.

This research work is original and has not been submitted earlier in part or full in this or any other form to any university or institute, here or elsewhere, for the award of any degree.

…………………..

Rajesh Pandit

RECOMMENDATION

This is to recommend that **Mr. Rajesh Pandit** has carried out research entitled ***"*Templating Nanostructures in Epoxy Resin Using Styrenic Block Copolymers*"*** for the award of Doctor of Philosophy (Ph. D.) in **Chemistry** under my supervision. To my knowledge, this work has not been submitted for any other degree.

He has fulfilled all the requirements laid down by the Institute of Science and Technology (IOST), Tribhuvan University, Kirtipur for the submission of the thesis for the award of Ph. D. degree.

Dr. Rameshwar Adhikari
Supervisor
(Associate Professor)
Central Department of Chemistry
Tribhuvan University
Kirtipur, Kathmandu, Nepal

June 2015

CERTIFICATE OF APPROVAL

Date: 11/06/2015

On the recommendation of Associate Prof. Dr. Rameshwar Adhikari, this Ph. D. thesis work submitted by Mr. Rajesh Pandit**,** entitled **“Templating Nanostructures in Epoxy Resin Using Styrenic Block Copolymers”** is forwarded by Central Department of Research Committee (CDRC) to the Dean, Institute of Science and Technnology (IOST), Tribhuvan University, Kirtipur, Kathmandu.

…………………………………………
Dr. Megh Raj Pokharel
Professor,
Head,
Central Department of Chemistry
Tribhuvan University
Kirtipur, Kathmandu**,** Nepal

ACKNOWLEDGEMENTS

I would like to express my sincere gratitude to my supervisor Associate Prof. Dr. Rameshwar Adhikari for the continuous support of my Ph. D. research, for his motivation, enthusiasm, and immense knowledge. His guidance favoured me in all the time of research and writing of this thesis.

I am thankful to Prof. Dr. Megh Raj Pokharel, Head of the Department and Prof. Dr. Kedar Nath Ghimire, former Head of Department, Central Department of Chemistry, Tribhuvan University, Kathmandu for their cooperation to carry out the research.

I am extremely grateful to Prof. Dr. Albrecht Berkessel, University of Cologne, Germany for providing scholarship, laboratory facilities and research stay in Germany. I am indeed grateful to Prof. Dr. Georg H. Michler and his research group for microscopic investigations of my sample at Institute of Physics, Martin Luther University Halle-Wittenberg, Halle, Germany. I am grateful to Prof Dr. Wolfgang Grellemen and Dr. Ralf Lach, for helping me for the microhardness indentation test at Centre for Engineering Sciences, Martin Luther University, Halle, Germany.

I would like to extend my gratitude to Prof. Dr. Jean Marc Saiter and his group for providing laboratory facility to perform thermal characterization of samples and scientific stay at University of Rouen, Rouen, France.

I would like to thank Dr. Netra Lal Bhandari, Mrs. Sharmila Pradhan, Mrs. Jyoti Giri, Mr. Santosh Khanal, Mr. Bhushan Shakya, and Mrs. Shanta Pokhrel for making fruitful discussion during the weekly presentation in the department. I would like to extend my thanks to Mr. Santosh Thapa, Mr. Shankar Khatiwada and Mr. Sushant Ghimire for their help. Likewise, I would like to acknowledge Mr. Ashok Koirala and Mr. Mahesh Ojha for their inspiration and support.

I am truly indebted to my brothers Mr. Ram Chandra Pandit, Mr. Mani Raj Pandit, my wife Mrs. Sabina Pandit, my kids Shrijesh Pandit, Sambridhi Pandit and all other my family members for their care, support and encouragement from the very beginning of my study. Finally, I wish to thank all the persons who directly or indirectly helped me to complete this work.

Rajesh Pandit
June, 2015

ABSTRACT

Styrenic block copolymers based on polystyrene (PS) and poplybutadiene (PB) having various molecular architectures were subjected to epoxidation reaction to different degrees by various methods using *m*-chloroperoxy benzoic acid (MCPBA), performic acid (PFA), peracetic acid (PAA), and hexafluoro isopropanol (HFIP). The epoxidized copolymers were blended with diglycidyl ether of bisphenol-A (DGEBA) based epoxy resin, an amorphous material. Further, the nanocomposites with boehmite and layered silicate nanofiller were prepared.

The materials were characterized by different techniques such as fourier transform infrared (FTIR) spectroscopy, scanning electron microscopy (SEM) and transmission electron microscopy (TEM), thermogravimetric analysis (TGA), differential scanning calorimetry (DSC), and depth sensing microhardness measurements. The chemical modification of the block copolymers was confirmed by FTIR spectroscopy.

All the methods used for the epoxidation of block copolymers were found to be feasible. However, the MCPBA method was found to be practical and most selective one in terms of time, cost and ease of controlling reaction conditions. The FTIR peak intensity at 966 cm^{-1} corresponding to the *cis* conformation of C=C double bond decreased with increase of degree of epoxidation implying that the epoxidation reaction favoured at *cis* - position of the double bonds.

Highly cross-linked network was formed between the epoxy rings and amino groups in blend. The macrophase-separated spherical domains of epoxy resin were formed at lower epoxidation degree the block copolymer in epoxy resin blend. Highly ordered nanostructures were induced by the epoxidized block copolymers in the epoxy resin at higher degree of epoxidation.

The ordered structures thus formed in epoxy resin blends had periodicity of 50 nm, the dimension well below the wavelength of visible light indicating that the nanostructures were templated by the block copolymer. Hence, the dispersion of nanofiller was homogeneous in composites and most of the composites were transparent to visible light.

The addition of epoxidized copolymer offered the possibility to increase, besides imparting an enhanced toughness, the thermostability of the materials but lowering the flame retardancy. In contrast to highly brittle behaviour of the neat epoxy resin, the micro- and nanostructured blends exhibited highly ductile behaviour. The blending of the epoxy resin with 30 wt.-% of epoxidized block copolymer caused a decrease in hardness by more than 50% while the addition of 3 wt.-% of nano-boehmite significantly compensated the loss in the hardness. The epoxy resin blends as well as their nanocomposites revealed intense plastic deformation as demonstrated by fine fibrillar structures leading simultaneously to enhanced toughness and stiffness of the materials. The observed phenomena may open up the opportunity of synthesizing transparent nanostructured epoxy resins with tailored stiffness-toughness ratio over a wide range.

Keywords: epoxy resin, block copolymer, nanostructures, FTIR spectroscopy, electron microscopy, epoxidation, microhardness, deformation behavior

LIST OF ACRONYMS/ABBREVIATIONS

AFM	Atomic Force Microscopy
BCC	Body Centered Cubic
BCPs	Block Copolymers
DDM	Diamino Diphenylmethane
DGEBA	Diglycidyl Ether of Bisphenol-A
DTG	Derivative Thermogravimetry
DSC	Differential Scanning Calorimetry
e(SB)x	Epoxidized Poly(Styrene-Butadiene) Star Block Copolymer
EP	Epoxy Resin
FTIR	Fourier Transform Infrared Spectroscopy
g	Gram
G	Gyroid
h_{max}	Maximun Indentation Depth
HM	Martens Hardness
HFIP	Hexafluoro Isopropanol
HMTA	Hexamethylene Tetramine
LS	Layered Silicate
LOI	Limiting Oxygen Index
MCPBA	Meta-Chloroperoxy Benzoic Acid
MDA	Methylene Dianiline
MDP	Microhardness Dissipation Parameter
µm	Micrometer
mg	Milligram
mL	Milliliter
mm	Millimeter
mN	Milli Newton
MPa	Mega Pascal
M_W	Molecular Weight
nJ	Nano Joule
nm	Nano Meter

ODT	Order-Disorder Transition
OOT	Order-Order Transitions
PAA	Peracetic Acid
PFA	Performic Acid
PB	Polybutadiene
PCL	Poly(ε-Caprolactone)
PE	Polyethylene
PS	Polystyrene
SB	Polystyrene-*block*-polybutadiene
SBS	Polystyrene-*block*-polybutadiene-*block*-polystyrene
SE	Secondary Electron
SEM	Scanning Electron Microscopy
SEBS	Poly(Styrene-*block*-(Ethylene/Butadiene)-*block*- Styrene)
SIS	Poly(Styrene-*block*-Isoprene-*block*-Styrene)
TEM	Transmission Electron Microscopy
TETA	Triethylene Tetramine
TGA	Thermogravimetric Analysis
TM	Tapping Mode
TPE	Thermoplastic Elastomers
Wt	Weight
UV	Ultra Violet

LIST OF SYMBOLS

^{o} C	Degrees Celsius
ΔC_p	Specific Heat Capacity
E	Elastic Modulus (Young’s Modulus)
E_{IT}	Indentation Modulus
f_A	Volume Fraction
χ	Flory-Huggin Interaction Parameter
h	Indentation Depth
L	Lamellae Phase
N	Total Degree of Polymerization
P	Load
OS	Boehmite
T_c	Curing Temperature
T_g	Glass Transition Temperature
T_i	Initial Degradation Temperature
T_1	First Degradation Temperature
T_2	Second Degradation Temperature
T_3	Third Degradation Temperature
T_f	Final Degradation Temperature
U_{pl}	Plastic Deformation Energy
U_{el}	Elastic Deformation Energy

LIST OF TABLES

Page No.

Table 2.1: A summary of epoxy resin/block copolymer blend systems investigated in the literatures…………………………………….. 48

Table 2.2: A summary of morphology of epoxy resin/block copolymer blend systems investigated in the literature …………………………….. 55

Table 3.1: Characteristics of block copolymers sample code, architecture, butadiene content in wt.-% and molar mass (g/mol) …………….. 58

Table 3.2: List of epoxidized copolymers prepared by different methods 62

Table 3.3: Determination of epoxy value by titration method ……………… 63

Table 3.4: List of epoxy resin blends and nanocomposites; all cured at 80 ^{o}C and 140 ^{o}C for 12 hr and 24 hr respectively 66

Table 4.1: The average diameter of PS cylinders and thickness of epoxy phase in blend of EP/e(SB)$_X$-25, EP/e(SB)$_X$-50 and EP/e(SB)$_X$-100 84

Table 4.2: The average size of PS cylinders and thickness of epoxy phase in different architecture of copolymer epoxy blends of EP/e(SB)$_X$-100, EP/eSBS-100 and EP/eSB-100 87

Table 4.3: Mean thickness of epoxy phase in composition variations blends EP/e(SB)$_X$-50 (85/15), EP/e(SB)$_X$-50 (55/45) and EP/e(SB)$_X$-50 (40/60) 89

Table 4.4: The average size of dispersion of nanofillers in epoxy resin and blend composites of EP/OS, EP/LS, EP/e(SB)$_X$-50/OS, EP/e(SB)$_X$-100/OS 91

Table 4.5: Characteristics data extracted from the TGA curves of epoxidation degree variations... 94

Table 4.6: The data obtained from the TGA curves of various architectures of copolymers.. 97

Table 4.7: Characteristics data received from the TGA curves of method variations.. 99

Table 4.8: Characteristics data extracted from the TGA curves of composition variations.. 101

Table 4.9: Activation energy values for the thermal decomposition of epoxy resin, $(SB)_X$ and their blends.. 103

Table 4.10: The characteristics T_g and ΔC_p data obtained from the DSC thermograms of EP and EP/e$(SB)_X$ blends of epoxidation degree variation.. 107

Table 4.11: Characteristics T_g and ΔC_p data obtained from the DSC thermograms of epoxy resin and epoxy resin/block copolymer blends……………………………………………………………….. 110

Table 4.12: Characteristics T_g and ΔC_p data obtained from the DSC thermograms of epoxy resin and EP/e$(SB)_X$ blends prepared by different method ……………………………………………….. 112

Table 4.13: The characteristics of T_g and ΔC_p value extracted from the DSC thermograms of epoxy resin and EP/e$(SB)_X$ blends with composition variation 113

Table 4.14: The characteristics data of HM and E_{IT} of $(SB)_X$, epoxy resin (EP) and their epoxy resin/e$(SB)_X$ blends ……………………... 117

Table 4.15: The characteristics data of HM and E_{IT} of epoxy/architecture of copolymer blends 119

Table 4.16: The characteristics data of HM, E_{IT} , W_t and h_{max} of epoxy resin (EP), epoxy resin/e$(SB)_X$-25 blends and thier nanocomposites 122

Table 4.17: Characteristic plastic (U_{pl}) and elastic (U_{el}) energies data obtained from the microhardness measurements of the epoxy resin (EP) and EP/e$(SB)_X$ blend with epoxidation degree variation 123

Table 4.18: The characteristic microhardness dissipation parameter (MDP) data of specimens ………………………………………………… 125

LIST OF FIGURES

Page No.

Figure 1.1: Theoretical phase diagram of diblock copolymer morphology showing close packed sphere (CPS), body centred cube (BCC), hexagonal cylinder (H), gyroid (G) and lamellar (L) structure………………………………..................................... 2

Figure 1.2: Scanning electron micrographs of fracture surfaces of epoxy/ DETDA/ CTPEHA systems cured at; a) 140 °C and b) 180 °C, the amount of CTPEHA was 10 phr……………………………... 4

Figure 1.3: Transmission electron micrographs of DGEBA/Pip/PPO stained with RuO_4 shows; a) the presence of small 2 μm PPO particles; b) the large PPO particles contain epoxy inclusions……………... 4

Figure 2.1: Phase diagram for a polymer blend showing an upper critical solution temperature, UCST (apex of lower curve), and a lower critical solution temperature, LCST (apex of upper curve)……… 8

Figure 2.2: TEM images of phase morphology of a) graft copolymers and IPNs of SBR rubber and polystyrene b) polystyrene–*block*–polybutadiene–*block*–polystyrene (40% butadiene), illustrating the existence of the cylindrical structures ……………………….. 9

Figure 2.3: a) Illustration of high impact polystyrene (HIPS) morphology showing a phase-within-a-phase-within-a-phase organization, with polystyrene being the continuous phase, b) TEM image of phase morphology of HIPS…………... 10

Figure 2.4: a) Phase diagram of epoxy resin/PEO–PEP diblock without hardener, a implication of what the complete diagram may look like as given in the inset (L = lamellar, G = gyroid, C = hexagonally packed cylinders, S = spheres). b) Variation of principal (d)-spacing in the 52 wt% diblock system with increasing epoxy molecular weight (open circles) and with cure (filled squares)………………………………………………… 11

Figure 2.5: Transmission electron micrographs of: a) $(PI)_2PS$ and b) $(PI)_3PS$

miktoarm polymers with approximately 50 volume % PS............ 13
Figure 2.6: Schematic representations of; a) disorder state, b) vesicle, and c) micelles for the amphiphilic diblock copolymer nanocomposite. The red lines = hydrophobic blocks, blue lines = hydrophilic blocks, and circles filled with green color = nanoparticles……..... 15
Figure 2.7: a) Tapering mode-AFM image intercalated SBS/CLO-BDHA nanocomposite for 2 phr content and b) Height-magnifications TEM image of showing intercalation of OMMT in SBS lamella... 16
Figure 2.8: Stress–strain (σ/ε) curve of different types of polymeric materials 19
Figure 2.9: TEM images of; a) fibrillar structures spanning the craze in polystyrene, b) shear bands structures of section of polystyrene deformed at 60°C, observed between crossed polarizers………… 20
Figure 2.10: Reaction scheme for the synthesis of DGEBA-type epoxy resin... 21
Figure 2.11: Reaction scheme for the synthesis of novolac phenolic resin......... 22
Figure 2.12: Reaction mechanisms for the formation of resole phenolic resin... 23
Figure 2.13: Reaction steps for synthesis of urea-formaldehyde resin.............. 23
Figure 2.14: Reaction step for the synthesis of furan resin................................ 23
Figure 2.15: Reaction for the synthesis of unsaturated polyester resin.............. 24
Figure 2.16: Molecular structures of commonly used amine curing agents........ 24
Figure 2.17: Reaction scheme of the epoxy-terminated poly (aryl ether sulphone)s…………………………………………………... 25
Figure 2.18: Reaction scheme of the formation of siliconized epoxy hydroxyl-terminated polydimethylsiloxane structure................................... 26
Figure 2.19: A proposed reaction scheme for epoxy resin with NBR................ 26
Figure 2.20: Reaction steps involved in the preparation of polybutadiene-epoxy resin block copolymer from isocyanate-terminated polybutadiene (NCOTPB)……………………………………….. 27
Figure 2.21: Reaction schemes involved in the preparation of polybutadiene-epoxy resin block copolymer from carboxyl-terminated polybutadiene (CTPB)…………………………………………… 27
Figure 2.22: Reaction steps for glycidyl ester of styrene-itaconic acid based copolymer (SIAGE).. 28
Figure 2.23: TEM images of cured epoxy novolac (DER383/PN) containing

5% by weight of a) PBO–PEO-2 vesicles, b) PBO–PEO-4 wormlike micelles, and c) PBO–PEO-6 spherical micelles..................... 30

Figure 2.24: SEM images of prepared samples a) epoxy and b) CTBN modified epoxy.. 31

Figure 2.25: a) TGA of neat epoxy and 31 wt.% PCL4000 containing epoxy in air with 10 K/min heating rate and b) DSC thermograms of EP/PFR composites containing i) 0, ii) 5, iii) 10, and iv) 15 wt% PFR contents... 32

Figure 2.26: a) Tensile strength and b) impact strength of epoxy resin, epoxy/NR blend, and epoxy/ENR blends.................................... 34

Figure 2.27: Dynamic mechanical spectrum of 88/12 DDM cured epoxy resin/PEK-C blends……………………………………………. 35

Figure 2.28: Schematic diagram of toughening mechanisms proposed for thermoplastic-modified epoxies: 1) crack pinning, 2) particle bridging, 3) crack path deflection, 4) particle yielding, 5) particle-yielding induced shear banding, and 6) microcracking…. 37

Figure 2.29: Scanning electron micrographs of the fracture surfaces of; a) 20 phr CTBN-modified epoxy resin. b) 15 phr DGEBA/PEEKMOH blends... 39

Figure 2.30: a) TEM images of the crack tip DN-4PB specimen of BCP-toughened epoxy; wormlike structure cavitation or fragmentation after severe stretching, and b) Representative engineering stress-strain curves of CET600, CET600/sphere, and CET600/worm..... 41

Figure 2.31: a) SEM image of fracture surfaces of epoxy/10 wt.% poly(ether ester) blend containing 80 wt % soft-segment content (SSC), b) Comparison plots of tensile modulus and fracture toughness of epoxy resins/10 wt % poly(ether ester) (PEE) as functions of modifier composition.. 43

Figure 2.32: Different magnifications of scanning electron micrographs of fracture surfaces of epoxy blends with 10 wt % SSEBS-c-PCL containing 2.4 wt % PCL.. 44

Figure 2.33: Fracture toughness against nanoparticles volume content plots for EP/Al_2O_3 and EP/TiO_2 nanocomposites and the fracture

toughness increase with increasing diameter to distance ratio ($2r_0/2c$) curves of the fillers.. 46

Figure 2.34: TEM image and SAXS pattern for cured 20 wt- % MG-I/epoxy blends.. 49

Figure 2.35: Higher magnification transmission electron micrographs for DGEBA/MCDEA blends containing 30 wt % of; a) 40 mol.-% SepB and b) 61 mol.-% SepB modified systems........................... 51

Figure 2.36: DSC thermograms of control epoxy, PS-*b*-PCL-*b*-PBA and different wt-% of their nanostructured blends…………………… 52

Figure 2.37: Force-indentation plots of 10 wt.-% of 22 mol.-% eSB50 (2) having mol. wt. 80 000 g/mol with epoxy, inside (1, solid line) and outside of the vesicles (2, dashed line). Inset shows AFM phase image ……………………………................................ 54

Figure 2.38: Tapering mode–AFM height micrographs of: a) 1 wt % Al_2O_3 with 48 mol.-% eSBS and b) 3 wt % Al_2O_3 with 44 mol.-% eSBS. Inset showing the phase image…………………………… 56

Figure 3.1: Scheme of polystyrene-*block*-polybutadiene-*block*-polystyrene (SBS) triblock copolymer; a and b are degrees of polymerization of polystyrene and polybutadiene, respectively………………… 58

Figure 3.2: Schematic structure of a) star block copolymer $(SB)_{X,}$ b) linear triblock copolymer (SBS) and c) diblock copolymer (SB); the outer solid lines represent the polystyrene chains………………... 59

Figure 3.3: Structures of a) 3-metacholoroperoxybenzoic acid, b) performic acid, c) peracetic acid and d) hexafluoro isopropanol and phenylarsonic acid, which were used for the epoxidation of the copolymers……………………………………………………….. 59

Figure 3.4: Structures of a) diglycidyl ether of bisphenol-A (DGEBA) and b) methylene dianiline (MDA); the components used to prepare epoxy resin systems……………………………………………… 59

Figure 3.5: The molecular structure of; a) boehmite nanofiller, b) alkyl benzenesulphonic acid boehmite surfactant c) layered silicate (Nanofil 5) and d) layered silicate surfactant…………………….. 60

Figure 3.6: Epoxidation reaction of an SBS triblock copolymer; the C=C

double bonds were changed into the epoxide groups, ***a*** and ***b*** represent the degrees of polymerization of styrene and butadiene unit respectively in SBS and eSBS molecules............................... 61

Figure 3.7: Scheme of epoxidation reaction of butadiene units in the block copolymer; the C=C double bonds were changed into the epoxide groups in presence of peroxide.. 62

Figure 3.8: Scheme showing the formation of diglycidyl ether of bisphenol-A (DGEBA) by the reaction between epichlorohydin and bisphenol-A in presence of NaOH……………………………….. 64

Figure 3.9: Scheme showing the reaction of diglycidyl ether of bisphenol-A (DGEBA) with methylene dianiline (MDA) leading to cross-linked structure…………………………………………………… 64

Figure 3.10: Scheme showing the reaction of diglycidyl ether of bisphenol-A(DGEBA) with methylene dianiline (MDA) and epoxidized block copolymer (eSBS)………………………………………… 65

Figure 3.11: Schematic representation of thermogaravemetric analysis (TGA) curves of mass loss and differential thermogram………………... 68

Figure 3.12: Schematic represents the measurements of glass transition temperature of the specimens…………………………………….. 69

Figure 3.13: Schematic representation of Load (P)-indentation depth (h) diagram of the microindentation measurements…………………… 70

Figure 3.14: Schematic plot of a microindentation load–indentation depth curve. Plasticity is calculated as OA/OB=plastic work/ (plastic work + elastic work)…………………………………………... 72

Figure 4.1: FTIR spectra of copolymers epoxidized to different degrees: black line = $(SB)_X$, red line = $e(SB)_X$-25, blue line = $e(SB)_X$-50 and purple line = $e(SB)_X$-100 materials; the figures after $e(SB)_X$ denote the weight-% of butadiene units that have been epoxidized... 74

Figure 4.2: FTIR spectra of styrene/butadiene block copolymers samples having different molecular architectures; black line = $(SB)_X$, red line = SBS and blue line = SB…………………………………… 75

Figure 4.3: FTIR spectra of epoxidized styrene/butadiene of block

copolymers having different molecular architectures; black line = SBS, red line = eSBS-100, green line = eSB-100 and blue line = e(SB)$_X$-100, with 100 wt.-% degree of epoxidation…………….. 76

Figure 4.4: FTIR spectra of (SB)$_X$ copolymer compared with that of its epoxidized analogues modified by different methods; black line = (SB)$_X$, green line = MCPBA, blue line = PAA, pink line = HFIP and red line = PFA with 50% degree of epoxidation……… 77

Figure 4.5: FTIR spectra of epoxidized copolymer, neat epoxy resin and EP/e(SB)$_X$-50 blend; black line = e(SB)$_X$-50, blue line = neat epoxy resin (EP) and red line = EP/e(SB)$_X$-50 blend…………… 78

Figure 4.6: a) SEM micrograph of fracture surface morphology of EP/(SB)$_X$ blend, b) optical image of EP/(SB)$_X$ blend and c) TEM image of neat (SB)$_X$.. 81

Figure 4.7: Left lower and right higher magnification of TEM images of blend of; a) epoxy resin/e(SB)$_X$-25, b) epoxy resin/e(SB)$_X$-50 and c) epoxy resin/e(SB)$_X$-100. Inset; histogram of measurement of thickness of; a) polystyrene, and b) and c) epoxy phase in nm.. 83

Figure 4.8: Left lower and right higher magnification of TEM images of blend of; a) epoxy resin/eSBS-100 and b) epoxy resin/eSB-100. Inset; histogram of measurement of thickness of epoxy phase in nm... 86

Figure 4.9: Left lower and right higher magnification of TEM images of blend of; a) EP/e(SB)$_X$-50 (85/15), b) EP/e(SB)$_X$-50 (55/45) and c) EP/e(SB)$_X$-50 (40/60). Inset; histogram of measurement of thickness of epoxy phase in nm.. 88

Figure 4.10: TEM images of; a) EP/OS, b) EP/LS, c) EP/eSB)$_X$-50/OS, d) EP/e(SB)$_X$-100/OS nanocomposite at without staining of Os_2O_4.. 90

Figure 4.11: a) Variation of specimen mass with temperature and b) the DTG curves for epoxy resin/e(SB)$_X$ blends using e(SB)$_X$ having different degree of epoxidation; pink line = pure (SB)$_X$, black line = epoxy resin, red line = EP/e(SB)$_x$-25, green line = EP/e(SB)$_X$-50 and blue line = EP/e(SB)$_X$-100.............................. 93

Figure 4.12: a) Variation of specimen mass with temperature and b) the DTG curves for epoxy resin/epoxidized different architecture of copolymer blends; black line = pure $(SB)_X$, red line = epoxy resin, blue line = EP/e$(SB)_X$-100, purple line = EP/eSBS-100 and pink line = EP/eSB-100.. 96

Figure 4.13: Thermograms of the blends of epoxy resin with modified star block copolymer epoxidized to 50% using different methods a) Variation of specimen mass with temperature and b) the DTG curves of mass loss rate against temperature; pink line = pure $(SB)_X$, black line = epoxy resin, purple line = EP/e$(SB)_X$-50 (MCPBA), red line = EP/e$(SB)_X$-50 (PFA) and blue line = EP/e$(SB)_X$-50 (HFIP)... 98

Figure 4.14: a) Variation of specimen mass with temperature and b) the DTG curves for epoxy resin/e$(SB)_X$ blends using e$(SB)_X$ having different weight fraction; black line = pure $(SB)_X$, red line = epoxy resin, blue line = EP/e$(SB)_X$-50 (85/15), purple line = EP/e$(SB)_X$-50 (55/45), pink line = EP/e$(SB)_X$-50 (70/30), green line = EP/e$(SB)_X$-50 (40/60) and dark blue line = e$(SB)_X$-50......... 100

Figure 4.15: A Plots of ln(dα/dt) versus 1/T according to Arrehinus equation method for the EP/e$(SB)_X$-25 blend... 102

Figure 4.16: Bar diagram of activation energy of decomposition of epoxidation degree variation blends of epoxy resin/e$(SB)_X$........... 103

Figure 4.17: Bar diagram of activation energy of decomposition of epoxidation method variation blends of epoxy resin/e$(SB)_X$…….. 104

Figure 4.18: DSC traces of epoxy resin (EP) and EP/e$(SB)_X$ blends of epoxidation degree variation; black line = EP, red line = EP/e$(SB)_X$-25, blue line = EP/e$(SB)_X$-50 and purple line = EP/e$(SB)_X$-100, the blends comprising 70% by wt. of EP and 30% by wt. of e$(SB)_X$…………………………………………….. 106

Figure 4.19: A plot of T_g versus degree of epoxidation of copolymer in EP/e$(SB)_X$ blends... 107

Figure 4.20: A plot of specific heat capacity of epoxy resin (EP) and degree of epoxidation of copolymer in EP/e$(SB)_X$ blends………………….. 108

Figure 4.21: A plots of ΔT_g of epoxy resin (EP) and degree of epoxidation degree of copolymer in EP/e(SB)$_X$ blends……………………….. 109

Figure 4.22: DSC traces of EP/e(SB)$_X$-100, EP/eSBS-100 and EP/eSB-100 blends compared with epoxy resin (EP); black line = EP, red line = EP/e(SB)$_X$-100, blue line = EP/eSBS-100 and purple line = EP/eSB-100, the blends comprise 70% by wt. of EP and 30% by wt. of each architecture of copolymer……………………………. 109

Figure 4.23: A plot of T_g of epoxy resin (EP) and various architecture of copolymer blends.. 110

Figure 4.24: A plot of ΔC_p of EP and architecture variation of copolymer blends.. 111

Figure 4.25: A plot of ΔT_g of EP and architecture of copolymer blends........... 111

Figure 4.26: A plot of T_g of EP/e(SB)$_X$-50 (85/15), EP/e(SB)$_X$-50 (70/30), EP/e(SB)$_X$-50 (55/45), EP/e(SB)$_X$-50 (40/60) weight fraction blends……………………………………………………………….. 113

Figure 4.27: A plot of ΔC_p of EP/e(SB)$_X$-50 (85/15), EP/e(SB)$_X$-50 (70/30), EP/e(SB)$_X$-50 (55/45), EP/e(SB)$_X$-50 (40/60) weight fraction blends……………………………………………………………….. 114

Figure 4.28: A plot ΔT_g of EP/e(SB)$_X$-50 (85/15), EP/e(SB)$_X$-50 (70/30), EP/e(SB)$_X$-50 (55/45), EP/e(SB)$_X$-50 (40/60) weight fraction blends.. 115

Figure 4.29: Load (P)-indentation depth (h) diagrams of loading and unloading curves of five different specimens of EP/e(SB)$_X$-25 blends; pink coloured curve is the average of five different curves……………………………………………………………….. 116

Figure 4.30: Load (P)–indentation depth (h) diagrams of the epoxy resin (EP) compared with its blends containing 30% by weight of e(SB)$_X$ epoxidized to different degrees as indicated and neat (SB)$_X$ block copolymer; black line = EP, red line = neat (SB)$_X$, blue line = EP/e(SB)$_X$-25, dark green line = EP/e(SB)$_X$-50 and purple line = EP/e(SB)$_X$-100………………………………………………………… 116

Figure 4.31: Microhardness value of epoxy resin (EP) compared with EP/e(SB)$_X$ (70/30) blends with variation of epoxidation degree

$e(SB)_X$ and neat $(SB)_X$ ………………………………………….. 118

Figure 4.32: HM bar diagrams of epoxy resin blend with epoxidized block copolymers ($e(SB)_X$-100, eSBS-100 and eSB-100) compared with that of epoxy resin and neat $(SB)_X$ …………………………. 120

Figure 4.33: HM bar diagrams of epoxy resin and EP/$e(SB)_X$-25 composite of boehmite/layer silicate nanofillers compared with that of neat $(SB)_X$ and epoxy resin …………………………………………… 121

Figure 4.34: Energy bar diagram of EP and EP/$e(SB)_X$ blends with epoxidation degree variation and pure $(SB)_X$; composition of epoxy resin and $e(SB)_X$ in blend is 70/30..................................... 123

Figure 4.35: Deformation energy diagram plot of $(SB)_X$, epoxy resin (EP) and the epoxidation degree variation of epoxy resin/ BCP blends.. 124

Figure 4.36: Secondary electron mode SEM images of different magnifications of blend between epoxy resin and $(SB)_X$ block copolymer in 70/30 composition; a) lower and b) higher magnification.. 126

Figure 4.37: Secondary electron mode of left lower and right higher magnification SEM images of; a) an epoxy resin, b) EP/$e(SB)_X$-50 (70/30 composition by weight) blend and c) EP/$e(SB)_X$-50/OS (70/27/3 composition by weight) composite................................. 128

Figure 4.38: Schematic representation of the morphology developed by the investigated epoxy resin/BCP system of the epoxidation degree variation... 131

Figure 4.39: Scheme showing morphology-deformation behaviour correlation in the blends of epoxy resin and functionalized block copolymer; the corresponding morphology and deformation structures are sketched above each bar daigram... 131

TABLE OF CONTENTS

Page No.

Title Page i
Declaration ii
Recommendation iii
Certificate of Approval iv
Acknowledgements v
Abstract vi
List of Acronyms/Abbreviations viii
List of Symbols x
List of Tables xi
List of Figures xiii

CHAPTER - 1 ………..……………………………………….......................... 1
1. INTRODUCTION AND OBJECTIVES ….. 1
1.1 Introduction and Rationale….……………………………………………… 1
1.2 Objectives ………………………………………………………………… 6

CHAPTER - 2 ……………………………………………………………….. 7
2. LITERATURE SURVEY……………………………………………… 7
2.1 Structure-Properties Correlation in Polymers ……………………………….. 7
  2.1.1 Phase behaviour and morphology of multi-component polymers……... 7
  2.1.2 Phase behaviour and morphology of block copolymers ………………. 12
  2.1.3 Mechanical properties and deformation behaviour……………………. 17
2.2 Epoxy Resins and Their Synthetic Methods…………………………………. 20
2.3 Blends of Epoxy Resin with Other Polymers……………………………...... 25
2.4 Morphology and Different Physical Properties of Epoxy Resin System……. 29
2.5 Toughness Enhancing Mechanisms in Polymers and Thermosets…………... 36
2.6 Morphological Aspects of Toughening……………………………………… 38
  2.6.1 Thermoplastic and thermoplastic elastomer toughening ……………... 40
  2.6.2 Ester/ether containing compound/curing agents toughening ………… 42

2.6.3 Toughening by nanofillers and ionomers …………………………….. 43
2.7 Nanostructured Epoxy Resins ………………………………………………. 46
2.7.1 Overview on nanostructured resins …………………………………... 46
2.7.2 Using block copolymers as nanostructuring templates ………………. 49

CHAPTER – 3 ……………………………………………………...................... 58
3. MATERIALS AND METHODS………………………………………… 58
3.1 Materials ………………………………………………………………….. 58
3.1.1 Block copolymers……………………………………………………… 58
3.1.2 Epoxidizing agents…………………………………………………….. 59
3.1.3 Epoxy resin systems…………………………………………………… 59
3.1.4 Other chemicals ……………………………………………………….. 60
3.1.5 Nanofillers ……………………………………………………………... 60
3.2 Functionalization of Styrene/Butadiene Copolymers ……………………….. 61
3.2.1 Preparation of epoxidized copolymer………..………………………….. 61
3.2.2 Estimation of degree of epoxidation……………………………........ 63
3.2.3 Fabrication of epoxy resin/e(SB)$_X$ Blends………………………........ 64
3.3 Characterization Techniques ………………………………………………... 66
3.3.1 Fourier transforms infrared (FTIR) spectroscopy................................. 66
3.3.2 Electron microscopy.. 67
3.3.3 Thermal methods.. 67
3.3.4 Mechanical properties……………………………………………….. 70

CHAPTER – 4 ……………………………………………………...................... 73
4. RESULTS AND DISCUSSION ……………………………………….... 73
4.1 Spectroscopic Analyses...…………………………………………………… 73
4.1.1 Effect of degree of epoxidation of (SB)$_X$ copolymer ………………….. 73
4.1.2 Effect of block copolymer architectures... 75
4.1.3 Effect of (SB)$_X$ epoxidized with different methods................................ 77
4.1.4 Epoxy blends analysis………………………………………………… 78
4.2 Morphological Analyses……………………………………………………... 80
4.2.1 Morphological analysis by transmission electron microscopy............ 81
4.2.1.1 Effect of degree of epoxidation of (SB)$_X$ copolymer…………… 81

4.2.1.2 Effect of block copolymer architecture...................................... 85
4.2.1.3 Effect of e(SB)$_X$ copolymer weight fraction 87
4.2.1.4 Nanocomposites with boehmite and layered silicate.................. 90
4.3 Thermal Characterization... 92
4.3.1 Thermogravimetric Analysis (TGA).. 92
4.3.1.1 Effect of different parameters: degree of epoxidation, block copolymer architecture, and method of epoxidation……….......... 92
4.3.1.2 Effect of e(SB)$_X$ copolymer weight fraction..…………………. 99
4.3.2 Calorimetric Investigations.. 105
4.3.2.1 Effect of different parameters: degree of epoxidation, block copolymer architecture, and method of epoxidation………..… 106
4.3.2.2 Effect of e(SB)$_X$ copolymer weight fraction 112
4.3 Mechanical Properties and Deformation Behaviour………………........... 115
4.4.1 Effect of degree of epoxidation of (SB)$_X$ copolymer………………….. 116
4.4.2 Effect of block copolymer architecture... 119
4.4.3 Effect of nanoparticles in blends... 120
4.4.4 Toughness and deformation behaviour.. 122
4.4.5 Fracture surface analysis by SEM……………………………………... 126
4.5 Scheme of Structure-Properties Correlations ……………………………….. 130

CHAPTER – 5 ……………………………………………………...................... 133
5. CONCLUSION AND RECOMMENDATION…………………………… 133

CHAPTER – 6……………………………………………………………………... 136
6. SUMMARY……………………………………………………………………... 136

REFERENCES

APPENDICES

Lists of Published Papers

Lists of Scientific Presentations

CHAPTER – 1

1. INTRODUCTION AND OBJECTIVES

1.1 Introduction and Rationale

Polymers, often called plastics, form indispensible part of our daily life. Although, many people consider polymers simply as the packaging materials used for household objects, they are truly a diverse group of natural and synthetic compounds ranging from rubber to thermoforming materials and thermosets. The opportunity of fine–tuning both the soft and the rigid nature of these materials has provided them with wide varieties of applications from soft fabrics, medical devices to aircraft, along with non-plastic products such as silicon, paper etc. Thus the notion of refereeing polymers only to packaging plastics is just the tip of the iceberg [1].

Broadly, plastics can be classified as thermoplastics (TPs), thermoplastic elastomers (TPEs) and thermosets, based on their structure; processability and mechanical behavior. Thermoplastics soften on heating and harden on cooling while thermosets form cross-linked rigid networks that do not further soften at elevated temperature. In contrast, TPEs possess both properties of thermoplastics and rubbers [2]. Typical combinations of both rubbery and plastic material in thermoplastic elastomers offer advantages over thermosoftening and thermosetting plastics. Particularly the nano-sized domain formed during the assembly of rigid thermoplastics with soft elastomeric part as matrix provides an excellent model of nanostructure-properties relationship [3].

Thermoplastic elastomers (TPEs), a class of copolymers or block copolymer, are synthesized by joining thermoplastic chains with the elastomeric ones with covalent bonds. Styrenic block copolymer, an amorphous copolymer, based on A-B or A-B-A architectures, one of the commercially relevant copolymers (where A and B represent different polymers). Polystyrene-*block*-polybutadiene-*block*-polystyrene (SBS), polystyrene-*block*-polyisoprene-*block*-polystyrene (SIS) and polystyrene-*block*–poly(ethylene/1-butene)-*block*-polystyrene (SEBS) block copolymers are main practical applications of the nanostructured TPEs. The molecular chains of these copolymers undergo intramolecular phase segregation to form well defined periodic nanostructures [4,5]. In recent years, many studies on microphase separation of block copolymers have attracted both scientific and commercial interest owing to their capability to self-assemble into microdomains of controlled morphology at nanoscale [4-7]. Several experimental and theoretical studies have shown that the morphological variation of the block copolymer mainly depends on the degree of polymerization (N), composition or volume fraction (f_A), molecular architecture, processing history and Flory-Huggins interaction paramertes (χ) [5-8].

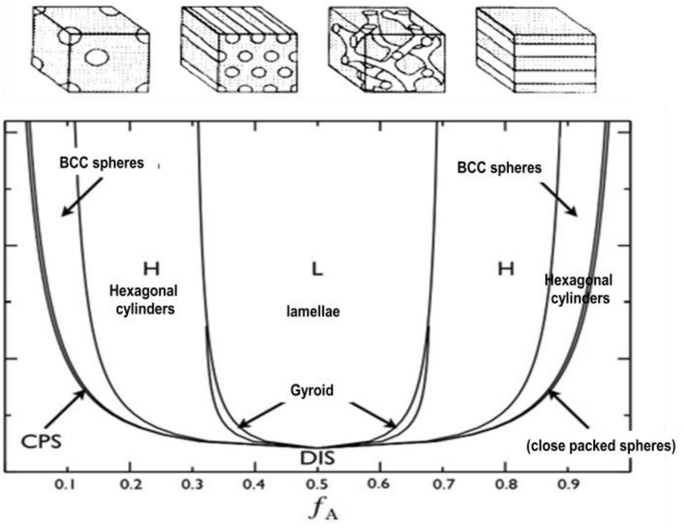

Figure 1.1: Theoretical phase diagram of diblock copolymer morphology; close packed sphere (CPS), body centred cube (BCC), sphere, hexagonal cylinder (H), gyroid (G) and lamellar (L) structure [8].

As depicted in Figure 1.1, change in volume fraction (f_A) of one of the polymers (i.e. A) and product χN results in variable morphological structures under equilibrium condition. For example, very low f_A even with higher χN would result none of the morphologies. With increase in f_A and χN, closed packed spheres (CPS) and then body centre cubic (BCC) spheres will be formed. Further increase in f_A and χN causes morphological shift to hexagonal (H) cylinders and then gyroid (G) and lamellar (L) phases. Finally the morphologies in reversed order appear [5-8].

The interaction parameter (χ) in turn depends on the temperature (T) as shown in equation (1.1).

$$\chi \propto \frac{1}{\mathrm{T}} \quad \ldots\ldots\ldots\ldots\ldots\ldots\ldots\ldots\ldots\ldots\ldots\ldots.. \quad (1.1)$$

At high temperatures, i.e. at low value of χ the chains are mixed homogeneously as each polymer undergoes melting. As the temperature is reduced, the tendency for the blocks to segregate is enhanced, i.e. the enthalpic process of demixing is favoured.

However, this is necessarily accompanied by a reduction in entropy as the chain configuration becomes more constrained [8].

The morphology of SBS, SIS, SEBS, common example of the block copolymer thermoplastic elastomers, is formed by microphase separation of the polystyrene end blocks and polydiene or ethylene-butylene (EB) copolymer mid-block where the glassy polystyrene domains are embedded in the elastomeric matrix. However, these non-polar polymers sometimes need to increase their polarity to comply with suitable functional group. Moreover, the anionic polymerization technique, commonly used to synthesize these copolymers, is not suitable for inserting polar monomers. Thus, post-synthetic chemical modification in order to generate polar groups on the block copolymer is an effective approach [9-13].

The modification in block copolymers is crucial to make them compatible with other polymers such as thermosets. The method of chemical modification has been in the limelight for many years as evidenced by enormous amount of research in this field [9-15]. Such modifications in styrenic block copolymer have particularly attracted the interest of materials scientists because of the self organized, nanophase-separated structures because these polymers can be used as templates to generate nanostructured thermosets [15-19].

Thermosetting plastics, which are resistant to higher temperature compared to thermoplastics (TPs) and thermoplastic elastomers (TPEs), cannot be remolded once solidified due to heavily cross-linked structures [20]. Epoxy resins (such as diglycidyl ether of bisphenol-A, DGEBA), the common example of thermosets, are the double epoxy ring containing polymers. These are widely used as adhesives and coatings because of their high mechanical moduli, good chemical resistance, and good adhesive properties to various materials [21]. Their brittleness can be reduced by blending with other polymers such as rubbers and thermoplastics (TPs). Thus, improved epoxy resin blends could replace the conventional structural materials such as wood, steel etc. [22].

During the past decades, many researchers have employed various strategies in an effort to enhance the toughness of epoxy resins [22-27]. As an example, the morphological results from the studies by Ratna *et al.* [28] have been presented in Figure 1.2. They studied carboxyl-terminated poly(2-ethyl hexyl acrylate) (CTPEHA), cross-linked with diethyl toluene diamine (DETDA) as curing agent. A significant improvement in toughness was observed for the blends cured at 140 ^{o}C which was attributed to the formation of phase-segregated structure (see Figure 1.2a). On the other hand, homogeneous morphology was observed (i.e. without phase separation) for the blends cured at 180 ^{o}C (Figure 1.2b). The disparity in curing temperature was generated different phase morphologies during the processing. This difference in Figure 1.2 a and b was due to the fact that at a higher temperature the curing reaction was so fast that was immediately reached to the geletion and the dissolved rubber did not get enough time to undergo phase separation. As a result, poor impact resistance was noticed for such blends [28].

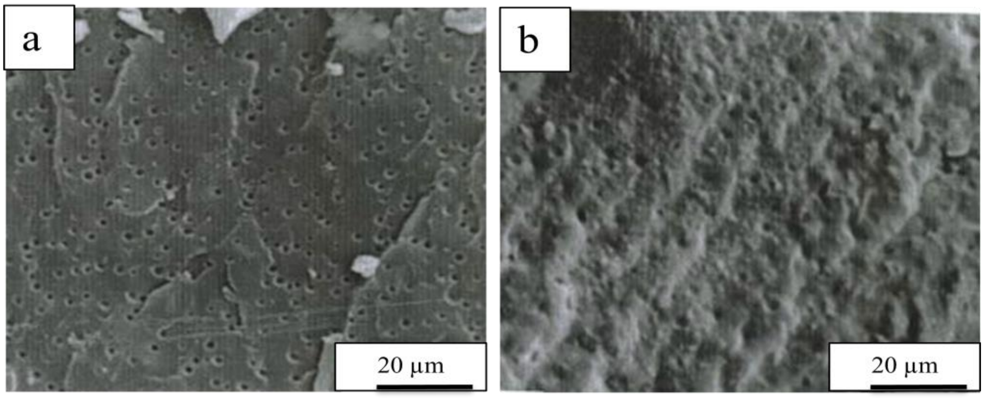

Figure 1.2: Scanning electron micrographs of fracture surfaces of epoxy/DETDA/ CTPEHA systems cured at; a) 140 °C and b) 180 °C, the amount of CTPEHA was 10 phr [28].

The toughness of epoxy resin has also been improved by using several modifiers including polysiloxane, reactive butadiene-acrylonitrile solid, carboxyl terminated copolymer of butadiene and acrylonitrile (CTBN) liquid rubbers [29-31]. Other researchers used thermoplastics such as polyphenylene oxide (PPO) to toughen the epoxy system by nanostructure production [32,33]. Such treatment resulted in heterogeneous two phase morphology in the epoxy resins (see Figure 1.3).

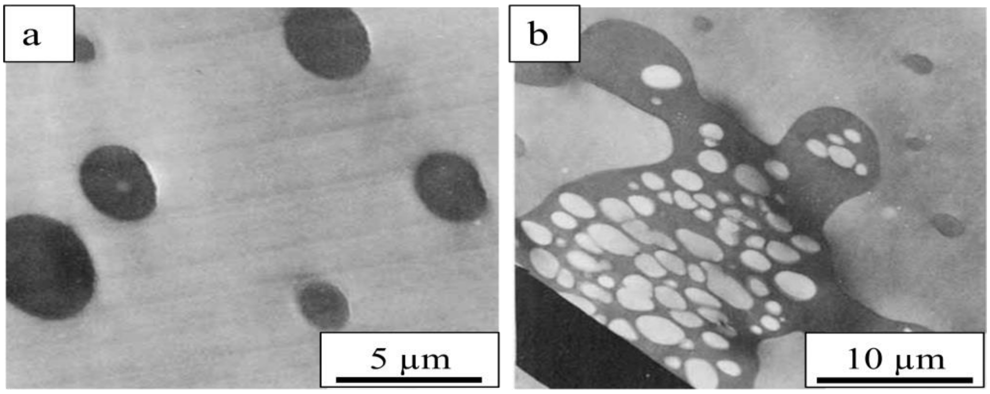

Figure 1.3: Transmission electron micrographs of DGEBA/Pip/PPO stained with RuO_4 shows; a) the presence of small 2 μm PPO particles; b) the large PPO particles contain epoxy inclusions [33].

The piperidine (Pip) cured epoxy resin/PPO blends showed the presence of PPO particle, approximately 2 μm in diameter, with fine dispersion into the epoxy matrix

(Figure 1.3a). On the other hand, the dispersion of PPO was heterogeneous with large size in which epoxy resin distributed in numerous sizes as white particle in PPO (Figure 1.3b). It has been concluded that certain degree of phase-segregation is necessary for improvement in toughness, but there is a risk of the products being translucent and opaque. The above mentioned methods used to improve the toughness of the epoxy resins have the drawbacks of macro-phase separation thus leading to opaque texture. The techniques of blending of epoxy resin with block copolymer offer advantages of both toughening and maintaining transparency with the formation of nanostructure in the blends [33,34].

One of the strategies involves direct mixing of block copolymers. The directly miscible block copolymers such as poly(ethyleneoxide)–*block*-poly(propyleneoxide) –*block*-poly(ethyleneoxide) (PEO-*b*-PPO-*b*-PEO), poly(ethyleneoxide)-poly(ethylene-*alt*-propylene) (PEO-PEP) block copolymer etc., have been added to epoxy resin to induce microphase separation. However, the direct combination is not only insufficient to improve the mechanical properties including fracture toughness, but also unable to utilize the block copolymer nanostructure as a template to create completely nanostructured epoxy resin [34,35].

In the recent years, another strategy of functional modification of block copolymer to improve compatibility and miscibility with epoxy resin has been reported [16,36-38]. Serrano *et al.* [16] have recently reported that elastomeric modification of epoxy resin is more effective to obtain better microphase separation before and after curing [16]. They used epoxidized block copolymers based on styrene and butadiene and also identified that ordered and/or disordered nanostructures can be formed through reaction-induced phase separation leading to the blends with improved fracture toughness and thermal properties [16,38,39].

Several studies have been reported about the synthesis and characterization of nanostructured epoxy blends focusing on the effect of chemical modification of copolymer on morphology, thermal and mechanical properties [36-40]. However, the structure-property correlation of such blends with particular attention to their deformation behaviour has not been completely understood.

Thus, the present study has been designed to understand the structure–property relationships (particularly correlation between the morphological, thermal and deformation behaviour) of the blends of epoxy resin with polystyrene/polybutadiene based block copolymers. The effect of variation in degree of epoxidation, chemical modification methods and molecular architecture of the copolymer to the nanostructure formation in epoxy resin/epoxidized block copolymer blends will be studied. Furthermore, it is expected that the findings of this study may provide guidelines to the industries for the efficient use of nanostructured resins with enhanced commercial values.

1.2 Objectives

Styrenic block copolymers (such as those using polystyrene as glassy component and polybutadiene or polyisoprene as rubbery component) are well known for their nanostructured morphology, toughness and transparency. On the other hand, epoxy resin, a thermosetting material, has wide applications as coating, sealants, adhesives etc., but their brittle nature limits their mechanical properties. Thus, this study has been aimed at exploring the use of those block copolymer after chemical modification as a blend component with epoxy resin thereby generating nanostructures responsible for enhanced toughness and maintained optical transparency.

The objective of this work is to fabricate nanostructured, toughened and transparent epoxy resin blends using polystyrene/polybutadiene based block copolymers as template, as the later possess the highly ordered nanostructures with periodicity in the range of 20-50 nm.

The specific objectives of the present study are listed below.

1) Synthesis of epoxidized block copolymer through variation in degree and methods of chemical modification,
2) Preparation of cured epoxy resin blends of variable compositions with chemically modified copolymers,
3) Preparation of composites of layer silicate and boehmite nanofillers with selected blends,
4) Characterization of the materials hence produced by Fourier transform infrared (FTIR) spectroscopy, electron microscopy (such as transmission electron microscopy (TEM) and scanning electron microscopy (SEM)), thermal methods (such as thermogravimetic analysis (TGA) and differential scanning calorimetry (DSC)) and microhardness analyses, and
5) Formulation of structure-properties correlation in the nanostructured epoxy resin blends and composites.

CHAPTER – 2

2. LETRATURE SURVEY

2.1 Structure-Properties Correlation in Polymers

Thermoplastic polymers consist of linear or branched molecular chains linked together by strong intramolecular as well as weak intermolecular bonds. Application of heat and pressure can reshape these polymers. However, this may cause some alternation in their properties. The structure of these polymers may be in semi-crystalline or amorphous forms. Some examples of thermoplastics are polystyrene (PS), polyethylene (PE), polyamides (PA), polyvinyl chloride (PVC), polyesters, polycarbonates (PC) and polyacetals [1-4,41].

Another type of polymers having elastic and plastic nature is thermoplastic elastomers (TPEs). TPEs comprise a thermoplastic rigid component and rubbery elastomeric component. Block copolymers are thermoplastic elastomers having both the hard and soft blocks that combine one after another by covalent bonding. They can further be divided into two subdivisions: copolymers with amorphous rigid segments such as styrenic block copolymers and those with crystalline rigid segments, such as polyurethanes, copolyesters, copolyamides etc. [2-5].

In this way, different types of polymers have different properties which may depend upon their processing conditions as reflected by differences in the internal organization of microstructures of the polymer. The internal organization is the morphology of the polymer studied primarily by microscopy and complimented by other techniques. The later helps to establish the structure-property relationship of polymers [42].

2.1.1 Phase behavior and morphology of multi-component polymers

Multicomponent polymeric materials consist of polymer blends, composites or combinations of both. A polymer blend has the combination of two or more polymers. When two polymers are mixed, the most frequent result is a system that exhibits almost total phase separation. A phase diagram of polymer blends is shown in Figure 2.1. When two polymers mutually dissolve, they generally phase-separate at some higher temperature rather than at some lower temperature which is known as lower critical solution temperature (LCST) (see Figure 2.1, upper portion). Because of the low entropy of mixing, high-molecular-weight polymer blends exhibit the LCST phenomenon. If the polymer chains are short, an upper critical solution temperature (UCST) may be seen (see Figure 2.1, lower portion). This remarkable result can be interpreted by considering the unusual features of the mixing process. At the critical point, the heat of mixing should balance the entropy of mixing times absolute temperature [43]. Only nucleation and growth occurs in the metastable region. Further, spinodal decomposition is best observed by crossing through the critical point into the unstable region without crossing the metastable region. In some cases, however, the spinodal decomposition might result if the metastable region is rapidly crossed such that the nucleation of phase separation do not occur [44].

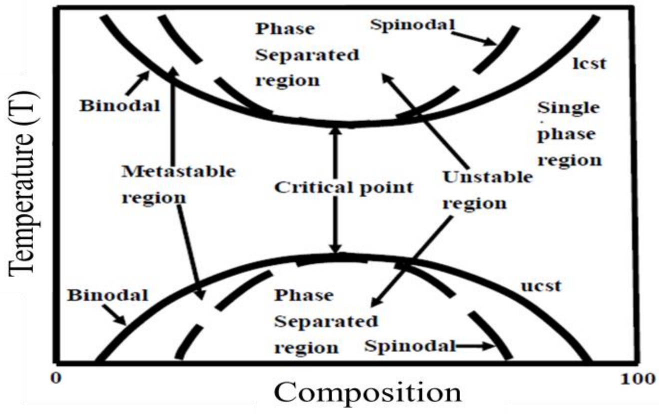

Figure 2.1: Phase diagram for a polymer blend showing an upper critical solution temperature, UCST (apex of lower curve), and a lower critical solution temperature, LCST (apex of upper curve) [44].

Based on the theoretical phase diagram depicted in Figure 2.1, one of the first commercial miscible blends obtained was polyvinylchloride with butadiene-acrylonitrile copolymers. After that, several commercial blends such as cross-linked phenol-formaldehyde resins with natural rubber, poly(2,6-dimethyl-1,4-phenylene oxide) (PPO) and high impact polystyrene (HIPS), Poly(butylene terephthalate)/polycarbonate (PBT/PC), poly(ethylene terephthalate)/polycarbonate (PET/PC)/polypropylene (PP), and ethylene-propylene-diene monomer rubber (EPDM) etc. were prepared for better property profile than neat polymers [44].

In the frame of phase behavior and morphology of multicomponent polymers, the morphologies of polymer blends and composites are widely investigated by both the X-ray and the neutron scattering techniques as well as by the electron microscopy. A series of interpenetrating networks (IPNs) morphologies with varying degrees of phase continuity is shown in Figure 2.2.

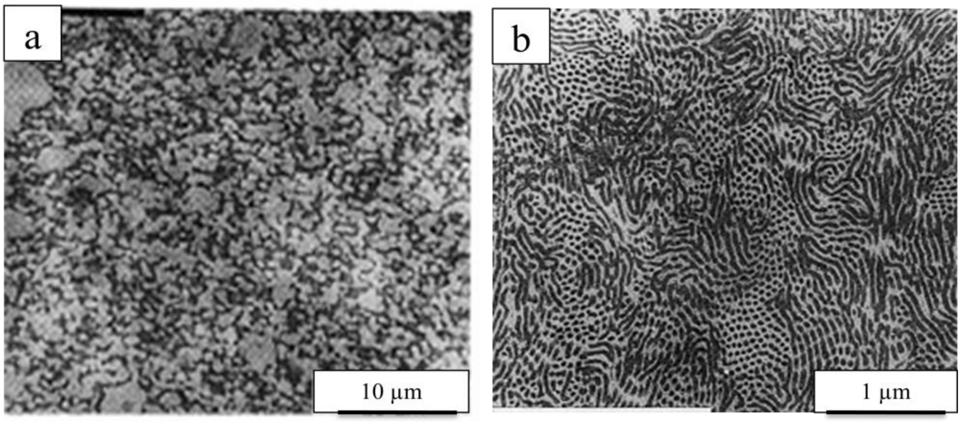

Figure 2.2: TEM images of phase morphology of a) graft copolymers and IPNs of SBR rubber and polystyrene b) polystyrene–*block*–polybutadiene–*block*–polystyrene (40% butadiene), illustrating the existence of the cylindrical structures [43].

In these polymer blends, grafting tends to lower the interfacial tension and binds the two phases together. Mainly, due to very small entropy of mixing and usually positive heat of mixing, two polymers will be immiscible unless some strong interaction (such as hydrogen bonding) exists between them. The morphology of IPNs based on styrene–butadiene rubber (SBR) and polystyrene is illustrated in Figure 2.2a. Various morphologies such as cylinders, spheres, and lamellae are seen; and hence their succeeding physical and mechanical properties are controlled, depending upon the chain length, by cross-linking and/or mixing. The SBR phase, stained dark in Figure 2.2, toughens the brittle polystyrene. Apart from this, some other important properties of the rubber phase include its low glass transition temperature, small domain size, and extent of grafting of the polystyrene phase [43].

The morphology of phases changes from sphere to cylinder and to alternating lamella depending upon the relative chain length of the two blocks. Spheres contain short chain blocks which are formed within the continuous phase of the longer chain blocks. Alternating lamellae form when the blocks are about the same length. Figure 2.2b shows the morphology of a block copolymer which is also based on the polystyrene and polybutadiene with planar oriented cylinders [43].

In this context, one of the early efforts to make toughened plastics was with the development of high impact polystyrene (HIPS) [43]. The synthesis starts with the solution polymerization of styrene in presence of butadiene that leads to the grafting of chains. The HIPS bears spherical domains (see Figure 2.3) which shows the phase-within-a-phase-within-phase morphology. This complex morphology results primarily from the spinodal decomposition within the rubber domains although the nucleation and growth kinetics are sometimes important. As described in Figure 2.1, nucleation and growth results in spheroidal domains while spinodal decomposition often results in interconnected cylinders. After their appearance, the rubber cellular domain structures are sometimes called *Salami* structure. The toughness obtained in such materials is related to the rubber phase volume which is the rubber volume plus the occluded polystyrene cellular domain volume [43].

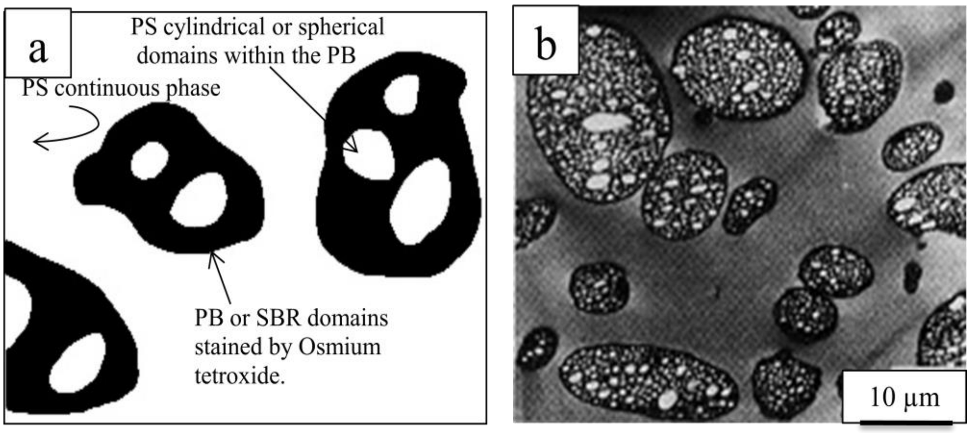

Figure 2.3: a) Illustration of high impact polystyrene (HIPS) morphology showing a phase-within-a-phase-within-a-phase organization, with polystyrene being the continuous phase, b) TEM image of phase morphology of HIPS [43].

Similarly, for the thermosetting/thermoplastic elastomer blend, Lipic group [35] performed an inclusive analysis involving various weight fractions of a poly(ethylene oxide)-poly(ethylene-alt-propylene) (PEO–PEP) diblock (f_{PEO} = 0.51, M_n = 2700 g/mol) in an epoxy system cured with aromatic amine. A phase diagram similar to that envisaged by self-consistent field theory [45] for a mixture of diblock copolymer with PEO homopolymer was obtained. An increase in principal d-spacing was seen as an effect of the increased epoxy molecular weight. These results were found to be consistent with the swelling of PEO blocks by epoxy resin. The connectivity of PEO–PEP blocks and the requirements to maintain constant density and minimize chain stretching lead to the improved interfacial curvature with the increase in concentration of resin. Figure 2.4a shows the phase diagram obtained without hardener where the phase behavior of block copolymer/epoxy blends is similar to model block copolymer/homopolymer blends and vary with changes in the blend composition and temperature. The morphologies in Figure 2.4a are observed with increasing epoxy concentration: lamellar, cubic bicontinuous, hexagonally packed cylinders, body-centered cubic packed spheres, and disordered micelles. As the molecular weight of epoxy compound increases, the PEO block segregates from the epoxy matrix which is indicated by an increase in the principal d spacing of the ordered structures and occurrence of the order-order phase transitions at certain compositions as shown in Figure 2.4b. Close inspection of the data showing d-spacing against cure time indicated that the swelling continues to occur long after the gel-point. This is attributed to the fact that the gel-point is a property of the bulk sample and do not necessarily coincide with the restriction of local mobility on the nanometer scale [35,46]

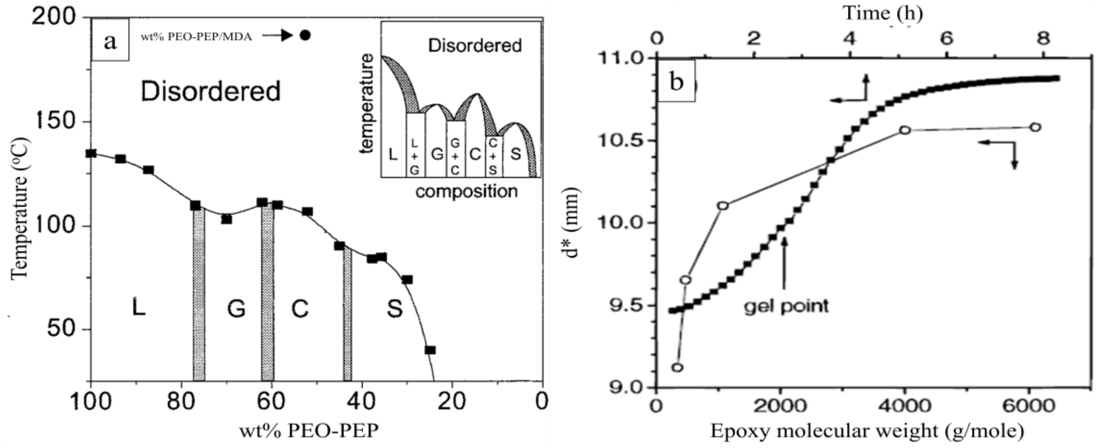

Figure 2.4: a) Phase diagram of epoxy resin/PEO–PEP diblock without hardener. The inset shows the implication of how the complete diagram may look like (L = lamellar, G = gyroid, C = hexagonally packed cylinders, S = spheres). b) Variation of principal d spacing in the 52 wt% diblock system with increasing epoxy molecular weight (open circles) and with cure (filled squares) [35].

Likewise, the phase behavior, crystallization, and nanoscale structures are investigated in the block copolymer/thermosetting resin blends. The phase behavior is found to be greatly dependent on the curing conditions and dispersion of materials in Epoxy/SB blends with three different phases, such as PS microphase, epoxy rich phase and PB microphase [47]. The amphiphilic PEO-PPO-PEO block copolymer/epoxy blends show the macroscopic phase separation and composition-dependent nanostructures which may be spherical and bicontinuous domain structures ranging from 20 to 100 nm [48]. Similarly, the amphiphilic star block copolymer/epoxy blend also forms the similar macroscopic phase separation with composition-dependent nanostructures in the order of 10-30 nm. Further, the blend displays a combined morphology of worm-like micelles and spherical micelles with characteristic of a bicontinuous microphase structure [49].

2.1.2 Phase behavior and morphology of block copolymers

Styrenic block copolymers comprise two distinct monomers, A and B, with various architectures. Generally, these architectures are based on diblock (AB), triblock (ABA) or (ABC), multiblock or segmented (AB)n, pentablock (ABABA), and star diblocks (AB)nX copolymers in block structure, where, A and B are the hard plastic phase and soft elastomer phase, respectively. These block copolymers are synthesized in laboratory by anionic polymerization [50]. In these copolymers, the elastomeric B phase is the main constituent which can tune the properties of the block copolymer. The wide range of properties observed in block copolymer is either due to the variation in parameters such as morphology, composition with respect to the volume fractions of the blocks, f_A (for block A) or f_B (for block B), their architecture, molecular weight, total degree of polymerization (N), and Flory-Huggins interaction parameter (χ) between those blocks. The thermodynamic interaction between any two dissimilar blocks is given by the dimensionless interaction parameter (χ) which is inversely proportional to the temperature as shown in the equation 1.1 (see section 1.1) [5-8,42].

On the basis of these parameters, the morphology of block copolymer varies from body centered cube (BCC), hexagonal packed cylinder (Hex), and gyroid (G) to lamellar (L) structures. These morphological structures are formed by the microphase separation between the two phases, A and B. The microphase separation between the copolymers can create nanoscale domains due to the tendency for segregation on lowering the temperature where separation is well-defined periodic microdomains of controlled morphology on the nanoscale. The ordered nanostructures in block copolymer are self-assembled in solid state, melt as well as in the solution. [5-8].

In concern to microphase separation, Leibler gave a theory of microphase separation in block copolymers [6] which explained the microscopic statistical theory of phase equilibria in noncrystalline block copolymers of type AB. This shows that the microphase separation transition (MST) appears due to a specific unstable mode which emerges in the homogeneous copolymer melt under certain critical conditions. Besides, a BCC mesophase is expected to be a metastable phase for a large range of compositions. A hexagonal and lamellar mesophase may be stable near the MST.

Moreover, Lohse and Hadjichristidis [7] performed an extensive study on microphase separation in block copolymer with nonlinear chain architecture, linear terpolymers with three chemically different blocks, and mixtures of linear diblocks with molecular weight or compositional differences.

Further, transmission electron microscopy (TEM) was used for the study of microphase separation in block copolymer. It critically corroborates the theoretical treatment of microphase separation in which a complete separation of microphases with sharp boundaries between them and also the effect of the later is completely overlooked [7].

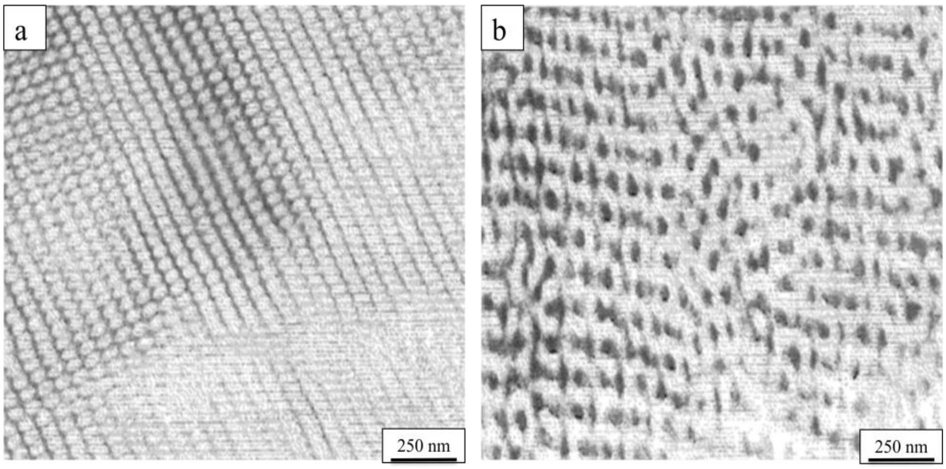

Figure 2.5: Transmission electron micrographs of: a) $(PI)_2PS$ and b) $(PI)_3PS$ miktoarm polymers with approximately 50 volume % PS [7].

TEM micrographs (Figure 2.5) of a) $(polyisoprene)_2$ /polystyrene [$(PI)_2PS$] and b) $(PI)_3PS$ miktoarm polymers (having approximately 50 vol.-% of PS) are used as an example to explain the morphology of the block copolymers that can exhibit interesting morphological features either by moving the borders of the classical morphology map or by forming new morphological structures. In Figure 2.5, the micrographs of; a) $(PI)_2PS$ miktoarm has hexagonally packed cylinders whereas b) $(PI)_3PS$ miktoarm forms a bicontinuous structure. At the same volume fraction, a linear diblock (PI/PS) would give a lamellar morphology [7].

The phase separation behavior of block copolymers has been further studied by several research groups [5-7, 50-52]. They explained the location and characterization of the order-disorder transition (ODT) as a function of temperature and the observation of thermally accessible order-order transitions (OOT) between phases. Furthermore, the study also showed that the richness of the phase diagram in the surrounding area of ODT includes the presence of an additional phase along with the bicontinuous and rheological signatures of the various transitions [50]. Also, the accuracy of theoretical predictions of order-disorder transition temperature (T_t) was studied; and it was found to depend upon the accuracy of the temperature and both the interaction parameter and specific volumes of the constituent components in a block copolymer [51]. Similarly, ordering phenomena in thin block copolymer films was studied by Dijk and Berg [52] using atomic force microscopy (AFM). They explained the cylindrical mesophase formation in thin films of a commercial styrene-butadiene-styrene (SBS) block copolymer. Furthermore, a complex ordering phenomenon occurred during annealing. They also found that the orientation of polystyrene cylinders depends upon the film thickness [52].

Recently, the progress in polymer chemistry has exposed unique opportunities to prepare tailored block copolymers at rational cost. More than two decade of rigorous academic research and formulation of influential statistical theories and computational methods have facilitate the study of equilibrium and even non-equilibrium behavior of copolymers and their blends with other polymers. The gap between realistic nanostructured plastics and block copolymer self-assembly with still-unexplored blends of properties is going to lessen [53]. Therefore, as one of the major classes of synthetic systems, amphiphilic block copolymers are host tools for constructing self-assembled nanostructures. It is feasible to create nanostructures either in pure melt or in solution by controlling the architecture of individual molecules. Wide varieties of the morphologies from discrete micelles and vesicles to continuous network structure are obtained by the modification of ordered nanostructures. These block copolymer micelles, vesicles, and mesophases have several application areas that range from nanocomposites to biomedical devices [54].

In this context, self-assembled smectic phases in rod-coil block copolymers were investigated by Chen *et al.* [55] in which they found that the rod-coils formed smectic C-like and 0-like morphologies with domain size ranging from 10 nm to almost 1 µm. Moreover, Self-assembly of polyethylene glycol (PEG) based block copolymers for biomedical applications is studied by Otsuka *et al.* [56] where PEG-functionalized surface are present in brush form or in micelle form. Zhang and co-workers [57] have investigated the self-assembly behavior of amphiphilic block copolymer/nanoparticle mixture in dilute solution by self-consistent-field theory/density functional theory. They recorded that the aggregate morphologies of amphiphilic block copolymer/nanoparticle mixture can experience, with the increase in particle radius and/or particle volume fraction, a transition from vesicles to the mixture of circle and rod like micelles as shown in Figure 2.6 [57].

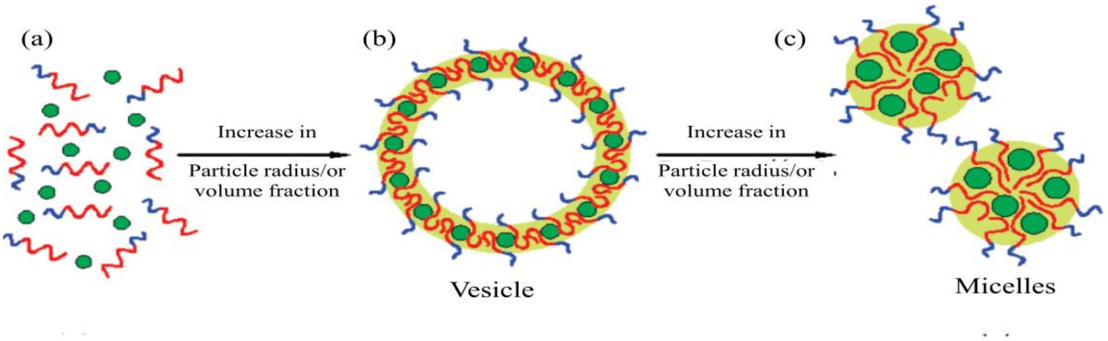

Figure 2.6: Schematic representations of: a) disorder state, b) vesicle, and c) micelles for the amphiphilic diblock copolymer nanocomposite. The red lines = hydrophobic blocks, blue lines = hydrophilic blocks, and circles filled with green color = nanoparticles [57].

In the Figure 2.6, red lines, blue lines, and circles filled with green color represent the hydrophobic blocks, hydrophilic blocks, and nanoparticles, respectively. The phase diagram presented in Figure 2.6 contains a disorder state at small values of particle radius and/or particle volume fraction. The hydrophobic nanoparticles and amphiphilic block copolymers were uniformly dispersed in solution (Figure 2.6a). With increasing the particle radius and/or particle volume fraction, the diblock copolymer chains and particles join together to form vesicles (Figure 2.6b). The transition from vesicles to mixture of spherical and rod like micelles was triggered by a further increase in particle radius and/or particle volume fraction. The nanoparticles were distributed in the cores of micelles (Figure 2.6c). Likewise, Thompson *et al*. [58] prepared the block copolymer-directed assembly of nanoparticles which formed mesoscopically ordered hybrid materials. Apart from this, Mulligan *et al.* [59] synthesized self assembled ZnO nanostructures at room temperature using a microphase separated diblock copolymer as a template.

On the other hand, polymer blends can be defined as the mixing of a polymer with the other polymers by different methods, such as solution casting, melt mixing etc. They may contain homopolymer or block copolymer. In the blends of two or more homopolymers with block copolymer, there is interplay between the macrophase separation of the blend constituents. Its effect depends upon the relative lengths of the polymers and also on the composition of the blend. Segregation or miscibility of the block copolymer in the blend can be determined by small angle x-ray scattering technique (SAXS) or TEM [8]. Phase behavior of block copolymer/homopolymer blends have been investigated which shows that the blends of AB diblock copolymer and A homopolymer with similar degrees of polymerization are weakly segregated [45]. Thomann *et al.* [60] investigated the gradient interfaces in SBS and SBS/PS blends and their influence on the development of a substantial "PS softening" effect which preferentially forms elongated PB lamellar morphologies and lead to an improved mechanical ductility.

Furthermore, the phase behavior of block copolymer (BCP) supramolecules is studied by hydrogen bonding of various carboxyl and phenol containing azo compounds to the poly(4-vinylpyridine) blocks of polystyrene-*block*-poly(4-vinylpyridine) (PS-*b*-P4VP) [61].

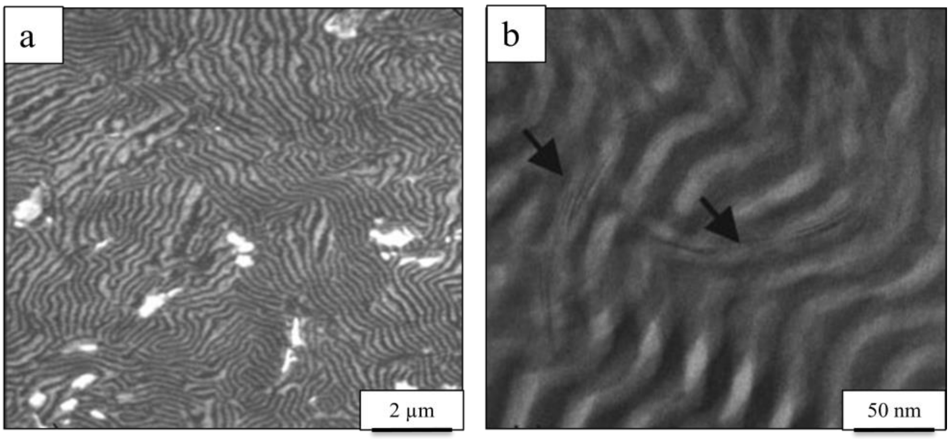

Figure 2.7: a) Tapering mode-AFM image of intercalated SBS/CLO-BDHA nanocomposite for 2 phr content and b) Height-magnifications TEM image showing intercalation of OMMT in SBS lamella [62].

Additionally, nanocomposites based on organically modified montmorillonites (OMMTs) and sodium montmorillonite (CLO-Na^+) with poly(styrene-*b*-butadiene-*b*-styrene) (SBS) diblock copolymer in presence of intercalated tactoids of surfactants (*i.e.* CLO- dioctadecyl dimethylammonium bromide (DMOcA) and CLO- hexadecyl benzyl dimethylammonium chloride (BDHA)) at low contents explains the well dispersion of the OMMT than others in matrix. Consequently, the structure perfection of block copolymer is observed to decrease and the lamellae width is found to increase slightly by intercalated OMMT [62]. This can be seen in Figure 2.7a which shows an example of tapering mode-AFM of SBS/CLO-BDHA nanocomposite for 2 phr content. Figure 2.7b is the height-magnifications TEM image which also shows a slight increase of lamellae width by intercalated OMMT and decrease of structure perfection in block copolymer [62].

2.1.3 Mechanical properties and deformation behavior

Mechanical properties and deformation behavior of polymers are crucial in material science research since these properties limit the use of polymeric materials in wide applications. The mechanical properties such as stiffness, strength, elongation at break, and toughness or fracture toughness etc. provide information related to the material's durability, strength, and effectiveness for the proper use. These mechanical properties of the polymer can be investigated by tensile test, microhardness test, fracture impact test and many more. The deformation behavior of a material is a non-reversible shape change in reaction to the applied force on it. This mechanism can be studied by the electron microscopy and X-ray diffraction techniques [42]. Crystalline polymers are complicated systems with an amorphous phase interlaying with crystalline lamellae and with most of the macromolecular chains engaged in both phases. The mechanical properties such as strength and toughness of the polymer crystalline systems are interdependent due to several affecting phenomena such as crystal plasticity, cavitation, and molecular orientation. High toughness and high resistance are the most desired property of the material to exhibit large plastic deformability and an impact without failure, respectively. The ductility is expressed by decreasing the stress-strain curve at yield stress which may be caused either by shear yielding or by multiple crazes. Shear yielding can be seen in a wide range of temperature however only if the critical shear yielding is lower than the stress required initiating and propagating crazes. Crazing occurs mostly in amorphous polymers though it has been also seen in crystalline polymer where crazes are propagated between lamellae through spherulite centers as well as through the materials between spherulite [42].

The semicrystalline polymers exhibit a hierarchical morphology with structures ranging from nanometer to millimeter scale. Various electron microscopic techniques are applied to obtain the typical structural unit images, such as crystalline blocks, lamellae, spherulites, and fibrils. The most common example of the semicrystalline polymers is polyethylene (PE) and polypropylene (PP). Additional examples include polyamides, polyurethanes, fluoropolymers, biomedical polyesters etc. The mechanical properties such as tensile strength, ductility, brittleness etc. are related to the micromechanical phenomena, such as crazing, chevron formation, fibrillation, and shear band formation. The range of mechanical properties of semicrystalline polymers extend from brittle to highly ductile behavior which comprise necking, cold drawing, and strain hardening in the stress-strain curves [63].

Moreover, the amorphous polymers form a large group of materials which include glassy, brittle polymers (PS, SAN, PMMA etc.) and ductile polymers (PC and PVC). The structure, morphology, and mechanical properties were linked by the micromechanical processes of fracture deformation behavior. Weak domain like or globular structures can exist in amorphous polymer which are often visible only by using the staining induced contrast enhancement in TEM. The micromechanical behavior is linked to the formation of localized deformation zones, such as crazes, shear bands or deformation bands. A typical type of deformation seen in amorphous brittle polymers is craze [63]. The mechanical properties and deformation behaviors of the polymer blends depend on the nature of polymer, polymer blend composition, and the morphology they formed *via* macro to nanophase separation. Only the mechanical properties and deformation behaviors of block copolymers, their blends, and nanocomposites have been explained in this section [8].

Two major experiments to evaluate the deformation and fracture energy of polymer blends are tensile stress–strain test and impact resistance test. In a tensile stress–strain experiment, the sample is elongated until it breaks; and the stress is recorded as a function of extension. On the other hand, impact resistance test is used to measure the material's resistance to a sharp blow. In both the stress–strain and impact resistance studies, energy is absorbed within the sample by a viscoelastic deformation of polymer chains and finally by the creation of new surface areas. Energy may be absorbed by shear yielding, crazing, or cracking [43,64].

In this context, the variety in mechanical properties spans from brittle fracture to highly ductile behavior and rubber elasticity depending upon the polymer used. Three important types of stress–strain curves are illustrated in Figure 2.8.

i) The brittle plastic stress–strain curves are linear up to fracture at about 1% to 2% elongation. Typical stresses at break are of the order of about 6 MPa.

ii) A tough plastic is polyethylene which is semicrystalline with the amorphous portions above T_g. Young's modulus of a tough plastic is somewhat lower than that of the brittle, glassy plastic (see Figure 2.8). Characteristically, this class of polymer exhibits a yield point followed by extensive elongation at almost constant stress. This is called the plastic flow region and is clearly a region of nonlinear viscoelasticity. Extension at constant stress in the plastic flow region is often referred to as cold drawing. Finally, the polymer strain hardens and then ruptures. Many tough plastics break at about 50% elongation.

iii) The third type of stress–strain curve is that exhibited by elastomers. The equation of state for rubber elasticity governs here with its peculiar nonlinear curve. The deformation may be elastic and recoverable or permanent (irreversible deformation). Elastic energy is stored in the sample in terms of energy per unit volume. Because of the development of crazes – which are microscopic voids – within the strained material, the volume of the sample may increase and sometimes by several percent [43,64].

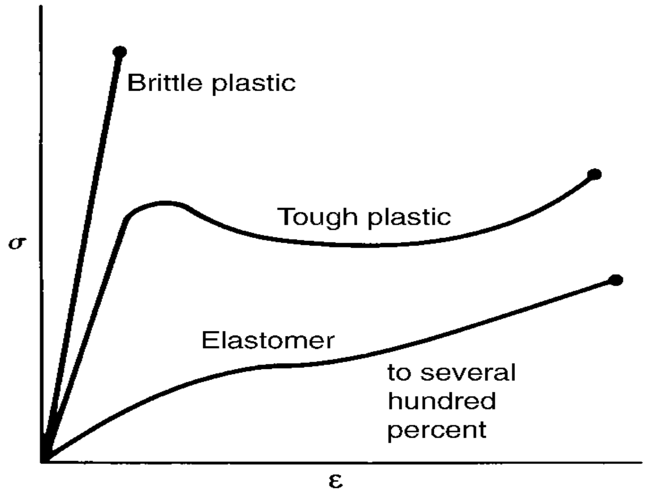

Figure 2.8: Stress–strain (σ/ε) curve of different types of polymeric materials [43].

Yet, a heterogeneous deformation is evident in polymers with pronounced morphology, such as semicrystalline and amorphous, in block copolymers, blends or composites having mechanically distinguishable parts. However, in polymer materials without such apparent morphology, the deformation at a smaller scale is also heterogeneous. Above the linear part of the stress- strain curve (Figure 2.8) up to a possible yield point or onset of fracture, localized heterogeneous deformation mechanisms appear [64].

Depending on the chemical structure and entanglement, molecular weight of the polymer, and the deformation conditions; three types of heterogeneous deformation are recorded, *i.e.* crazes, deformation zones and shear bands. Crazes are localized bands of plastically deformed polymer material which appeared perpendicular to the stretching direction. These are constituted by polymer fibrils of about 5-15 nm diameter which in turn are stretched in loading direction and separated by elongated voids with diameters up to about 50 nm (see Figure 2.9a).

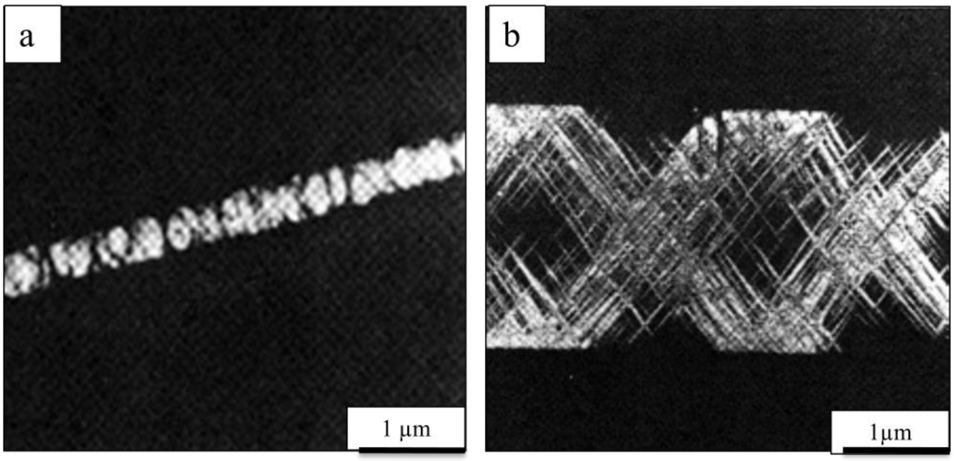

Figure 2.9: TEM images of; a) fibrillar structures spanning the craze in polystyrene, b) shear bands structures of section of polystyrene deformed at 60°C, observed between crossed polarizers [43].

Deformation zones possess the same orientation as crazes and are the result of shear processes. On the other hand, shear yielding involves molecular slip, usually at 45°, to the applied stress assuming an uniaxial stress–strain relationship (see Figure 2.9b) [43,64]. The thermosets are almost always amorphous. Therefore, their tensile strength is similar to the amorphous plastic, however the epoxy resin shows high tensile strength and elongation at break is 90 MPa and 2.5% respectively [43].

On contrary, other thermosets such as phenol-formaldehyde and unsaturated polyester have confirmed the tensile strength of 55-60 MPa and elongation at break of 1-3%. Hence, these thermosets also exhibit the deformation behavior similar to thermoplastics. In epoxy resin/thermoplastic elastomers blend, toughness can be increased with the advancement in tensile properties and the deformation behavior might be like the rubber toughened blends [43].

Thus, the structure-property correlation of polymers provides an idea of rapid progress in the field of polymer such as block copolymers which helps in innovations of sophisticated materials applications. A variety of persistent challenges are identified that stand between block copolymers nanostructures that found widespread successes in the novel applications with processing [50].

2.2 Epoxy Resins and Their Synthetic Methods

Thermosetting plastics are rigid and heavily cross-linked materials which are made up of lines of molecules and are resistant to higher temperature in contrast to the ordinary thermoplastics. These materials cannot be remolded once solidified by the cross-linking process. The common examples are epoxy resins, aminoplastics, phenolics, unsaturated polyester resins, silicones etc. These materials are generally brittle and can be toughened by blending with rubbers, copolymers, fibers, and so on. [20, 21].

Thermosetting resins are formed by covalently cross-linked, thermally stable networks which are infusible in heat and insoluble in solvent. These resins are prepared by the formation of long chain molecules and the application of heat or the addition of curatives for the formation of chain growth molecules and the production of complex cross-linked resin, respectively. Sometimes, the cross-linking may also be carried by ultraviolet (UV) irradiation [20, 21, 28].

Epoxy resins are commercially prepared by the reaction between bisphenol-A (BPA) and epichlorohydrin (ECD) (Figure 2.10**)** in presence of sodium hydroxide. They contain more than one 1, 2 epoxide groups per molecule and are known as diglycidyl ether of bisphenol-A (DGEBA) [20, 21, 28]. They are oxirane containing oligomers, which cure through the reaction of epoxide groups with a suitable curing agent.

Epoxy resins are distinctive among all the thermoset resins due to several characteristic features, such as minimum pressure for fabrication, low cure shrinkage, and high degree of cross linking with temperature [65]. Because of these distinctive characteristics and useful properties of the network polymers, epoxy resins are broadly used in structural adhesives, surface coatings, engineering composites, and electrical laminates [20, 21, 28].

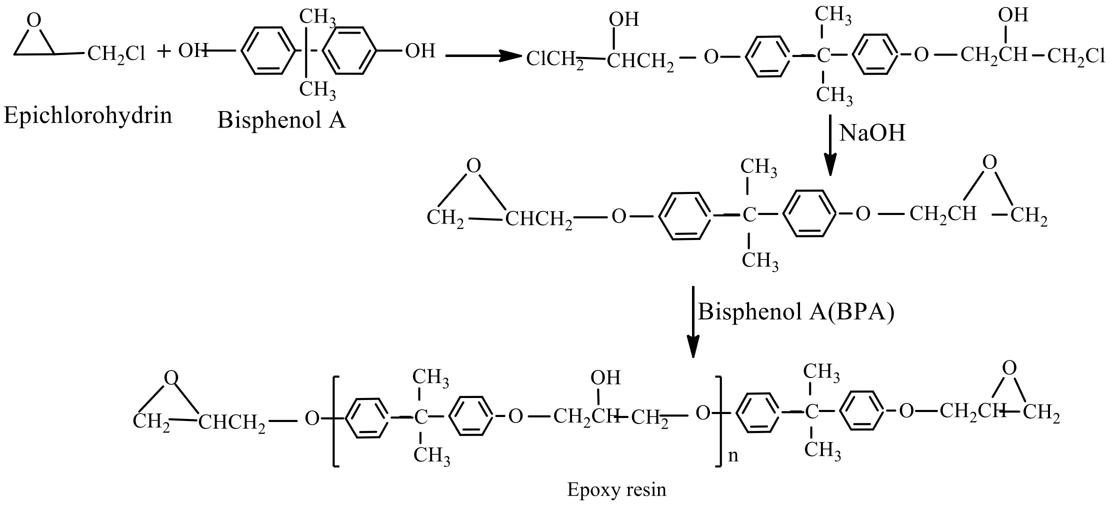

Figure 2.10: Reaction scheme for the synthesis of DGEBA epoxy resin [28].

While talking about their relevance in composite materials, most of the applications utilize conventional difunctional epoxy as a matrix. However, for many high performance purposes, such as aerospace and critical defense applications, incorporation of epoxies of higher functionality, known as multifunctional epoxies, is required. Epoxies of higher functionality which are available commercially include tri- and tetra-functional epoxy resins [28,66]. In the following paragraphs, however, preparation of some other types of resins other than the epoxies is described.

2.2.1 Novolac

Novolac is formed by the reaction of formaldehyde with an excess amount of phenol/ phenol derivative in the presence of an acid catalyst as shown in Figure 2.11.

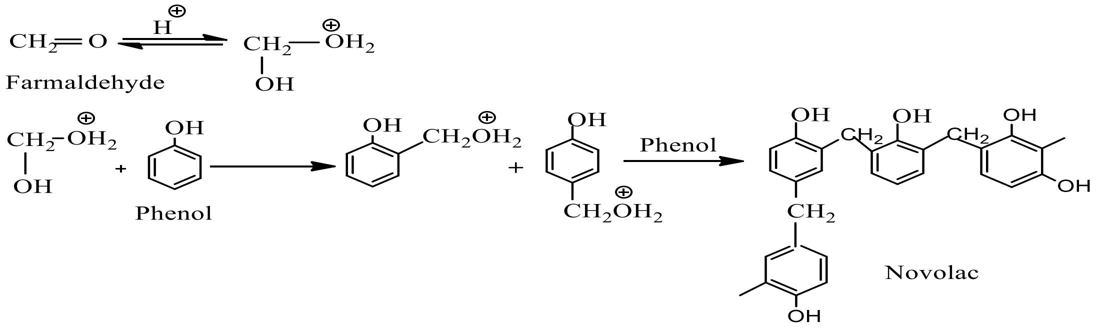

Figure 2.11: Reaction scheme for the synthesis of novolac phenolic resin [28].

The reaction ratio of phenol to formaldehyde used is in the range 1.49 to 1.72 in acid medium. Further, the reaction involves initial protonation of hydrated formaldehyde followed by electrophilic substitutions in the *ortho* and *para* position. At low temperature, the addition of formaldehyde to phenol forms the product of *o*- or *p*-methylol phenols. At higher temperature, the condensation reactions take place between methylol phenol and phenol or methylol phenol to produce a prepolymer and the desired resin [28, 66].

2.2.2 Resole

Resole is produced by the reaction between phenol or phenol derivative and an excess amount of formaldehyde in presence of a base catalyst. The reaction takes place in the basic medium through the addition of formaldehyde with phenoxide ion; hence it leads to the formation of *o*- or *p*-monomethylol phenol along with some di- or trimethylol phenol. The reaction scheme for the synthesis of resole is shown in Figure 2.12 [28,66]

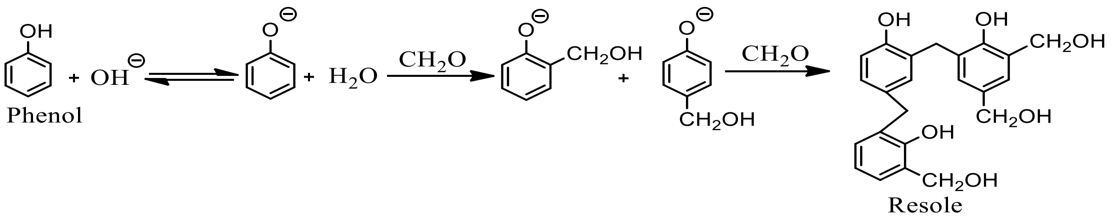

Figure 2.12: Reaction mechanisms for the formation of resole phenolic resin [28]

2.2.3 *Amino Resins*

Amino resins are prepared by reacting amino group-containing compounds with formaldehyde. Urea-formaldehyde (UF) and melamine-formaldehyde (MF) resins are the most popular amino resins. UF and MF resins are the product of formaldehyde with urea and melamine, respectively. The general reaction scheme for the synthesis of UF resins is given in Figure 2.13 [28,66].

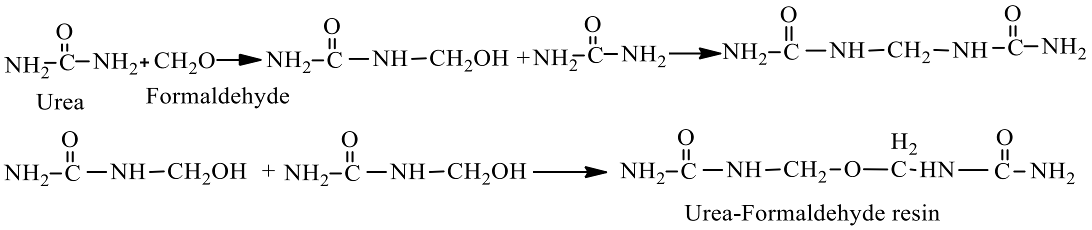

Figure 2.13: Reaction steps for synthesis of urea-formaldehyde resin [28].

2.2.4 *Furan Resins*

Furan resins are prepared by the reaction between phenol and furan compounds, such as furfural, furfuryl alcohol, and furan. They are used as supplements to the phenolic resins. For instance, furan compounds can be used instead of formaldehyde in the conventional fabrication of phenolic resins. The most popular and viable furan resins are produced from furfuryl alcohol (FFA) which undergoes homopolymerization through an addition reaction in the acidic medium (Figure 2.14) [28,66].

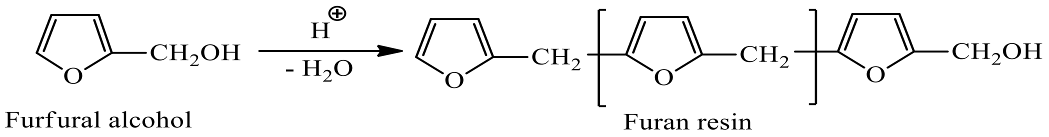

Figure 2.14: Reaction step for the synthesis of furan resin [28].

2.2.5 *Polyester resins*

A large number of commercially available polyester resins are employed to develop new materials. These resins can be conveniently classified into unsaturated polyesters, vinyl esters, alkyds, allyl resins, and so on.

Unsaturated polyester (UPE) resins consist of unsaturated polyester as a monomer and p-benzoquinone (or hydroquinone and phenothiazine) as an inhibitor. In addition to saturated acid, maleic anhydride or fumeric acid is used to make unsaturated polyesters. In fact, unsaturated polyester resins are made by reacting a diacid or dianhydride with a dihydroxy compound (diols). The chemical reaction for the synthesis of UPE is shown in Figure 2.15 [28, 66].

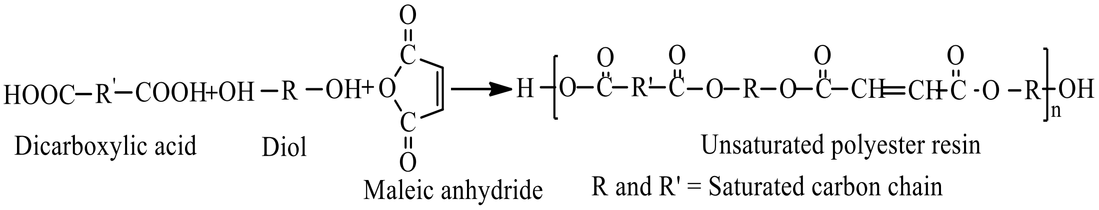

Figure 2.15: Reaction for the synthesis of unsaturated polyester resin [28].

2.2.6 Curing Agents

Due to the versatility of epoxy resins towards a wide variety of chemical reactions, they can be cured using a variety of curing agents, also known as ‘hardeners’, with different conditions. The choice of curing agent depends upon the appropriate curing conditions and the final application of the resin. Epoxies can be cured with amines, thiols, and alcohols. The reaction occurs through the cleavage of an oxirane ring *via* a nucleophillic addition reaction. Due to the involvement of an addition reaction, no volatile by-products are anticipated during the curing process. Amines are widely used as hardeners. The chemical structures of some commonly used amine curing agents for epoxy resins are shown in Figure 2.16 [28,35,66].

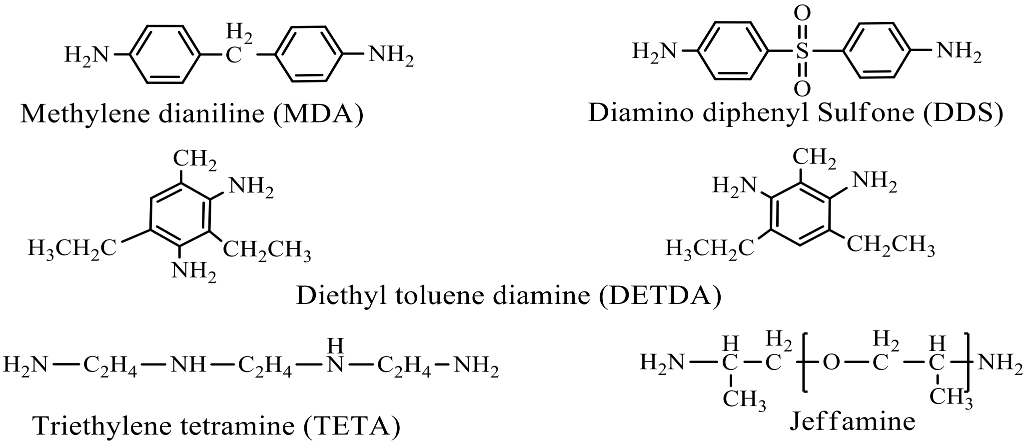

Figure 2.16: Molecular structures of commonly used amine curing agents [28,35,66].

During the curing reaction, two epoxy rings react with a primary amine. The first step involves the combination of primary amine hydrogen with the epoxy group. It is followed by the second step in which a reaction between the secondary amine hydrogen with another epoxy occurs. Amines used for curing epoxy resins can be grouped into three categories, namely aliphatic, cycloaliphatic, and aromatic. The reactivity of the amine increases with its nucleophilic character, *i.e.* aliphatic > cycloaliphatic > aromatic. Thus, appropriate temperatures and catalysts must be employed for curing [28].

2.3 Blends of Epoxy Resin with Other Polymers

In the frame of epoxy resin based polymer blends, Gallucci and Going [67] studied the preparation and reactions of epoxy modified polyethylene. The epoxy-modified polyolefins were prepared by the radical grafting of glycidyl methacrylate to polymer melts. Reactions of these materials with amines and carboxylic acids were also studied which showed that the modified polymers undergo typical epoxide reactions [67].

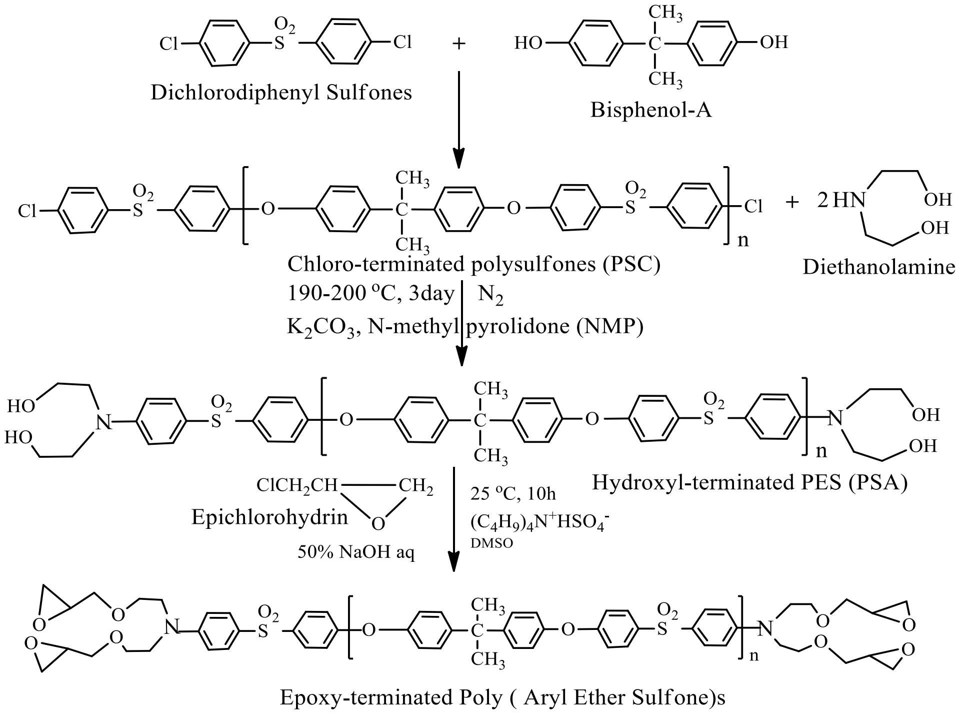

Figure 2.17: Reaction scheme of the epoxy-terminated poly (aryl ether sulphone)s [68].

Further, Iijima *et al.* [68] prepared epoxy-terminated poly(aryl ether sulfone) (PSE) by the reaction of epichlorohydrin with hydroxyethyl-terminated polysulfones.

Hydroxyethyl-terminated polysulfones were prepared from the reaction between chloro-terminated polysulfones (PSC) and diethanolamine, whereas PSC was obtained by the reaction of dichlorodiphenyl sulfones with bisphenol-A. Both PSE and PSC were used as modifiers for toughening of epoxy resin cured with *p,p'*-diaminodiphenyl sulfone as shown in Figure 2.17. Similarly, siliconized epoxy matrix resin can be developed by reacting diglycidyl ethers of bisphenol A (DGEBA) based epoxy resin with hydroxyl terminated polydimethylsiloxane (silicone) modifier [69]. Aminopropyltriethoxysilane is used as crosslinker and dibutyltindilaurate is employed as catalyst. The siliconized epoxy resin can be cured with 4, 4-diamino diphenyl methane (DDM), 1,6-hexane diamine (HDA), and bis (4-aminophenyl) phenyl phosphate (BAPP). A reaction scheme showing the formation of siliconized epoxy hydroxyl-terminated polydimethylsiloxane is depicted in Figure 2.18.

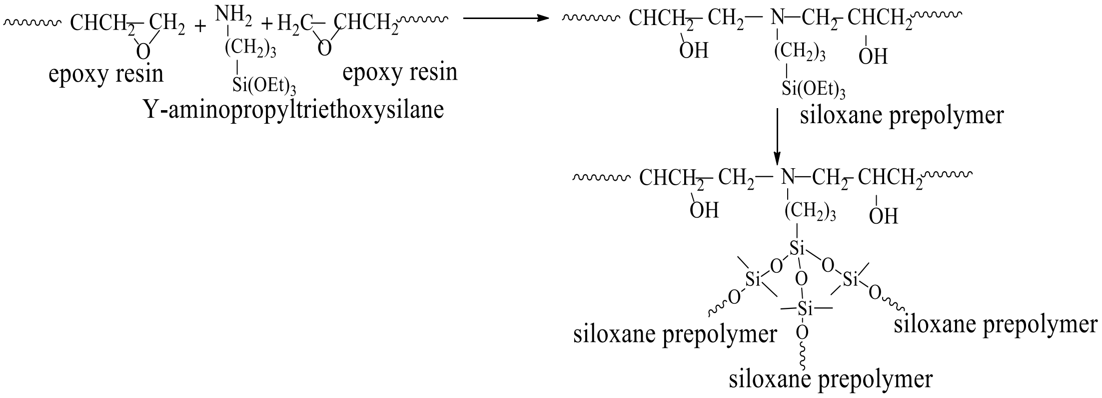

Figure 2.18: Reaction scheme of the Formation of siliconized epoxy hydroxyl-terminated polydimethylsiloxane structure [69].

Also, the polypropylene (PP)/recycled acrylonitrile butadiene rubber (NBR)/ epoxy blends are prepared by using epoxy resin as compatibilizing agent indicating the better processibility and enhanced mechanical properties [70]. An illustration of proposed reaction for epoxy resin with NBR is given in Figure 2.19.

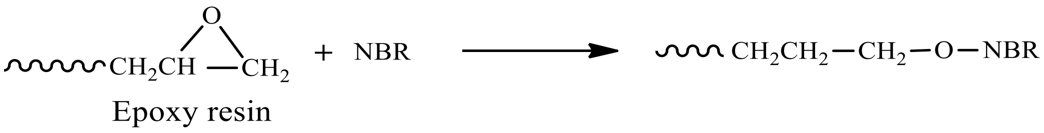

Figure 2.19 A proposed reaction scheme for epoxy resin with NBR [70].

Zhang *et al.* [71] prepared modified polysulfide sealants with lower compression set by a simple method of introducing the DGEBA epoxy resin into sealants. The investigation on reactivity analysis and gel faction test verified that the incorporation of epoxy resin in sealants is just a blending process rather than copolyaddition with polysulfide resin [71]. Furthermore, the poly(sily ether) with pendant chloromethyl groups (PSE) can be synthesized by the polyaddition of dichloromethylsilane (DCM) and DGEBA with tetra butylammonium chloride (TBAC) as a catalyst. The blends of epoxy resin with PSE are prepared through *in situ* curing reaction of DGEBA and 4,4-diaminodiphenylmethane (DDM) in the presence of PSE [72]. Tri-functional epoxy resins are synthesized from the condensation of 4-hydroxybenzaldehyde with phenol followed by epoxidation with halohydrin; and they are modified with silicon rubber to reduce stress [29].

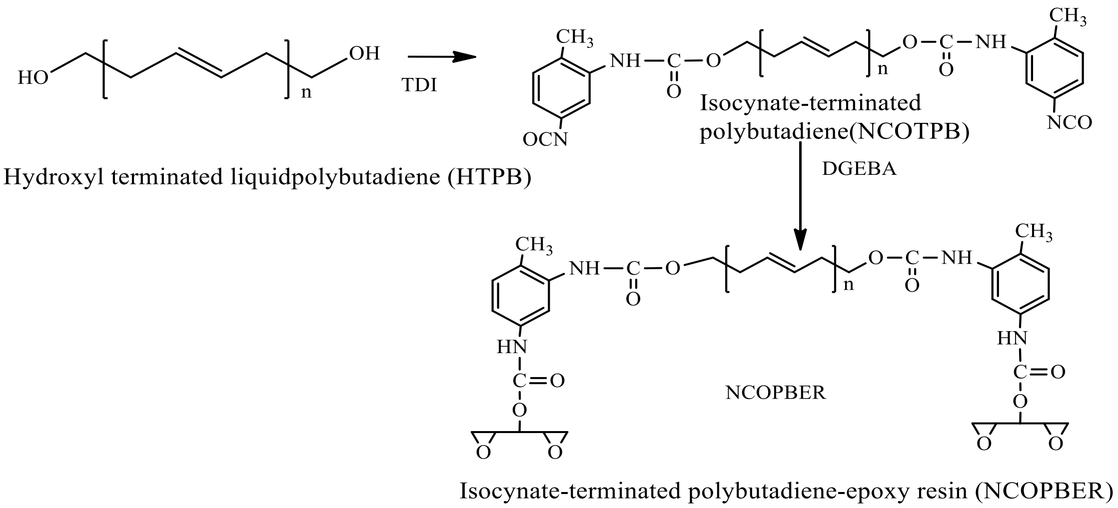

Figure 2.20: Reaction schemes involved in the preparation of polybutadiene-epoxy resin block copolymer from isocyanate-terminated polybutadiene (NCOTPB) [30].

On the other hand, DGEBA based epoxy resins modified with block copolymer of polybutadiene are prepared from isocyanate-terminated polybutadiene (NCOPBER) and carboxyl-terminated polybutadiene (CPBER) [30].

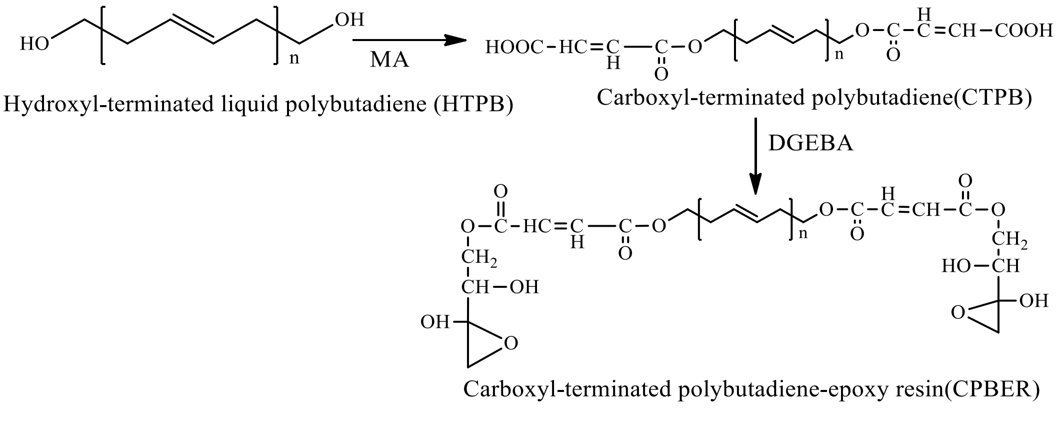

Figure 2.21: Reaction schemes involved in the preparation of polybutadiene-epoxy resin block copolymer from carboxyl-terminated polybutadiene (CTPB) [30].

Use of NCOPBER has resulted cured transparent epoxy network, whereas the CPBER has formed opaque network. The reaction of preparation of NCOPBER and CPBER are given in Figure 2.20 and 2.21, respectively.

Moreover, the study has also been extended to the bio based epoxy resins. Bio based epoxy resins are also synthesized for the development of new materials in polymer composite application. Bisphenol A and liquefied bamboo (*i.e.* liquefied in phenol or in polyethylene glycol/glycerol co-solvent with H_2SO_4 as a catalyst) are reacted with epichlorohydrin to form liquefied bamboo-epoxy resins blend by the addition of triethylene tetramine (TETA) [73]. On the other hand, an inexpensive, alternative epoxy resin system based on soybean oil has also been developed for polymer composite applications. Epoxidized methyl soyate (EMS) and epoxidized allyl soyate (EAS) were synthesized by Zhu *et al.* [74]. These materials consist of mixtures of epoxidized fatty acid esters. The epoxidized soy-based resins provide better intermolecular crosslinking and yield materials that are stronger than materials obtained from commercially available epoxidized soybean oil (ESO) [74]. Similarly, for the preparation of epoxy or unsaturated ester group containing polymers, fatty acid waste can be recycled as raw material and utilized in the radical polymerization between the styrene and itaconic acid. Glycidyl ester of styrene-itaconic acid copolymer can be prepared by esterification reaction with epichlorohydrin (Figure 2.22). The effects of polymer structure and incorporation of different polymers are used in the preparation of composites which have shown the pronounced improvement of thermal and mechanical properties [75]. An example of the chemical reaction of the preparation of glycidyl ester of styrene-itaconic acid copolymer is shown in Figure 2.22.

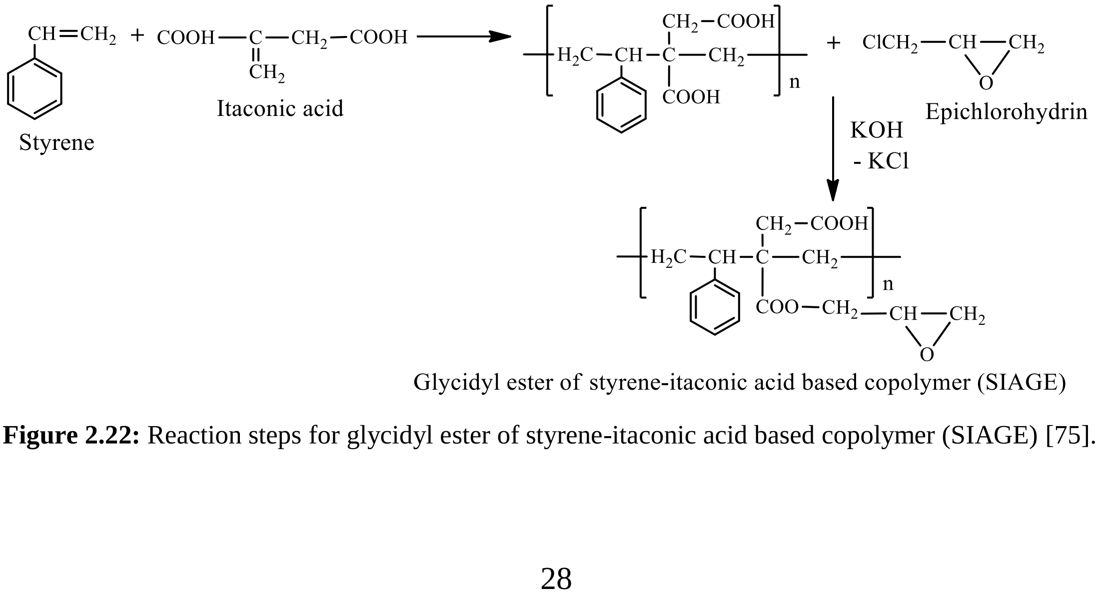

Figure 2.22: Reaction steps for glycidyl ester of styrene-itaconic acid based copolymer (SIAGE) [75].

2.4 Morphology and Different Physical Properties of Epoxy Resin System

Epoxy resin bears brittle nature of glassy thermosetting materials. The phase morphology of epoxy resin has been developed by blending with different polymers. Firstly, an emulsifying agent was added to improve the morphology of thermoplastic modified epoxies. Zheng *et al.* [72] have studied epoxy resin (ER)/Poly(sily ether) (PSE) blends. Based on the blend composition, it can display PSE- or epoxy-dispersed and heterogeneous morphologies. However, poly(ε-caprolactone) (PCL) toughened epoxy network has shown the ordered morphology which is distinct and well known from thermoplastic block copolymers in thermosetting polymers [76]. On the other hand, the morphology of poly(phenylene oxide) (PPO)-DGEBA and epoxy resin/ poly(ether sulfone) (PES) thermoplastic blends are not uniform and numerous large, occluded PPO and PES particles can be seen in their respective blends. Yet, both blends show the formation co-continuous morphologies [33,77]; and it is possible in PPO-DGEBA blend only by the addition of a styrene-maleic anhydride copolymer [33].

The rubber-modified resin would be more durable than the epoxy cardanol-based epoxy network modified with CTBN. The former would display a two phase separated morphology with dispersed rubber globules in the matrix resin. [78] Fluorine containing methacrylic ester copolymers are used for the surface modification of epoxy resin. The amount of fluorine in the modified resin surface layer increased with increasing the modifier content. It shows that these copolymers are good surface modifiers to improve oil and water repellency [79].

Different morphologies of the bends of thermosetting resin and thermoplastic elastomers are developed for alternating the mechanical properties and toughness of the materials. In the epoxy resin based blends of amphiphilic poly(n-butylene oxide)-*b*-poly(ethylene oxide) (PBO–PEO) diblock copolymers, the copolymers form well-defined microstructures that persist upon curing of the epoxy. Figure 2.23 shows three representative images, obtained from blends with PBO–PEO-2, -4, and -6 where the PBO core appears as dark inclusions dispersed within a gray matrix. Three distinct morphologies are evident in these micrographs. PBO–PEO-2 (f_{EO} = 0.11) produces bilayer vesicles ranging in diameter from about 100 to 500 nm. Increasing PEO content leads to the micelle formation with a worm-like cylindrical geometry at PBO–PEO-4 (f_{EO} = 0.18) and a spherical micelles geometry at PBO–PEO-6 (f_{EO} = 0.25).

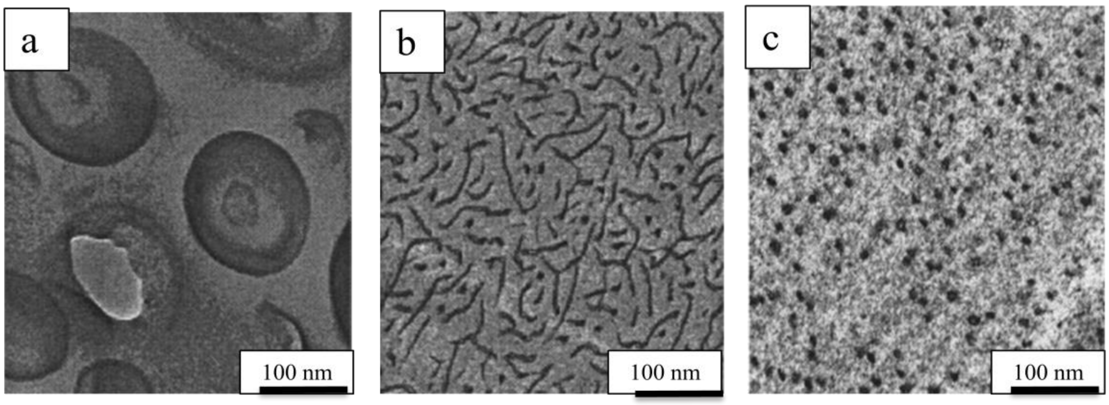

Figure 2.23: TEM images of cured epoxy novolac (DER383/PN) containing 5% by weight of a) PBO–PEO-2 vesicles, b) PBO–PEO-4 worm-like micelles, and c) PBO–PEO-6 spherical micelles [80].

Addition of 5% by weight of these block copolymers has improved the fracture toughness of the epoxy by as much as 19 times with relatively small reduction in the elastic modulus [80]. Similarly, DGEBA/DDM cured with PEO–PPO–PEO block copolymers blend also showed the PPO block self-assembled into nanoscopic entities which are similar to the morphologies of diblock copolymer epoxy resin blends as shown in Figure 2.23. This can be stabilized as micelles by their physical interactions thus avoiding their coalescence and, consequently, the macrophase separation process [34]. Based on the composition, polystyrene-*b*-polybutadiene (SB) varies from 100 nm to 300 nm in which micelles are formed within SB surrounded phase in epoxy resin matrix. At higher composition of SB, the blend morphology bears microphase separated, regular, long, unchanged lamellar structure in SB phase [47]. Furthermore, novolac blended with poly(2-vinylpyridine)-*block*-poly(isoprene) (P2VP-*block*-PI) in presence of hexamethyltetramine (HMTA) curing agent is also able to form microphase-separated domains. By tailoring the block lengths; lamellar, cylindrical, and spherical cross-linked phase-morphologies have been formed in the blend [81].

The phase morphology developed by the blends of epoxy resin with the liquid rubber alternates the mechanical properties and toughness of the material. Barcia *et al.* [30] studied the epoxy system modified with hydroxyl-terminated polybutadiene (HTPB) and carboxyl-terminated polybutadiene (CPBER) which indicates the presence of heterogeneous and two-phase morphology in both systems. Likewise, poly(styrene-co-acrylonitrile) (SAN) modified epoxy resin blend/glass fibre composites provide two glass transition temperature (T_g) that correspond to the epoxy rich and poly(styrene-co-acrylonitrile) (SAN) rich phases, and hence confirms the two-phase morphology of the blend [82]. Figure 2.24 a) and b) represent the SEM images of fracture surface of the pure epoxy and carboxyl-terminated poly(butadiene-co-acrylonitrile) (CTBN) modified epoxy matrix, respectively.

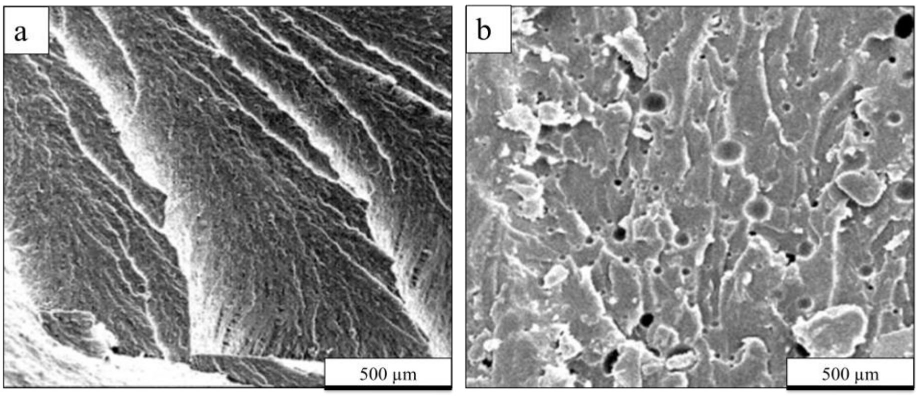

Figure 2.24: SEM images of prepared samples a) epoxy and b) CTBN modified epoxy [78].

Compared to the pure epoxy resin, blend shows better properties in terms of increase in impact strength and elongation-at-break of the casting and gloss, scratch hardness, adhesion, and flexibility of the film. SEM of the CTBN modified system shows improvement in these properties which indicates that the rubber-modified resin would be more durable than the pure epoxy. Cardanol based epoxy network modified with CTBN displays two-phase separated morphology with dispersed rubber globules in the matrix resin [78]. Furthermore, carboxyl-randomized poly(2-ethyl hexyl acrylate) (CRPEHA) and epoxy-randomized poly(2-ethylhexyl acrylate) (ERPEHA) liquid rubbers are evaluated as toughening agents for the epoxy resin with respect to their thermal properties, impact and adhesive joint strength of the modified networks [26].

On the other hand, aggregated structure and mechanical properties of the liquid silicone rubber, polyurethane (PU), and epoxy (EP) blends were investigated by Chiu *et al.* [83]. From the relationship between the intermolecular interaction and mechanical properties, they found that the aggregation structure of the three-phase blends was influenced by the reaction between silicone and PU, silicone and EP, and PU and EP. Consequently, a change in the cross linking density and appearance of the interpenetrating polymer network structure was observed [83].

Moreover, Katsoulis and co-workers [84] studied the effect of layered silicate nanoclays, nano-silica and double-walled carbon nanotubes (DWNTs) with the tetra-functional and bi-functional epoxy resins on the thermal stability and flame retardant properties. The morphology of the polymer/clay nanocomposites showed intercalated and somewheres exfoliated structure [85]. However, DWNTs have an adverse effect on the properties due to their poor dispersion in the matrix [84].

Several studies have been carried out regarding the thermal properties of epoxy resin based polymer blends [47,73,84]. Wu and Lee [73] investigated the effects of amount and structure of polymer on the physico-mechanical and thermal properties of epoxy. The copolymer epoxy resins prepared with phenol liquefied bamboo also have better thermal stability, lower thermal weight loss rate, and higher residual char content [73]. Moreover, Lützen and co-workers [76] explained the TGA curves (see Figure 2.25 a) of neat epoxy resin and epoxy resin with poly(e-caprolactone) (PCL4000). It was found that the initial degradation temperature depends strongly on the molecular weight of poly(e-caprolactone). Above 400 °C, both curves accounted for nearly the same characteristics with a plateau between 440 and 500 °C as a second degradation step. The derivation of weight loss gave a maximum thermal degradation at 409 °C for the neat epoxy polymer and 407 °C for the PCL4000 containing sample. This indicates that the excellent thermal stability of the neat epoxy polymer is essentially maintained on adding poly(e-caprolactone) (PCL4000) [76]. Similarly, the alkoxysilane functionalized polycaprolactone/polysilaxane modified epoxy resin composites also showed an improved thermal stability and good hydrophobicity. Therefore, it was believed that this modified epoxy appears promising as new high performance and highly functional materials [86].

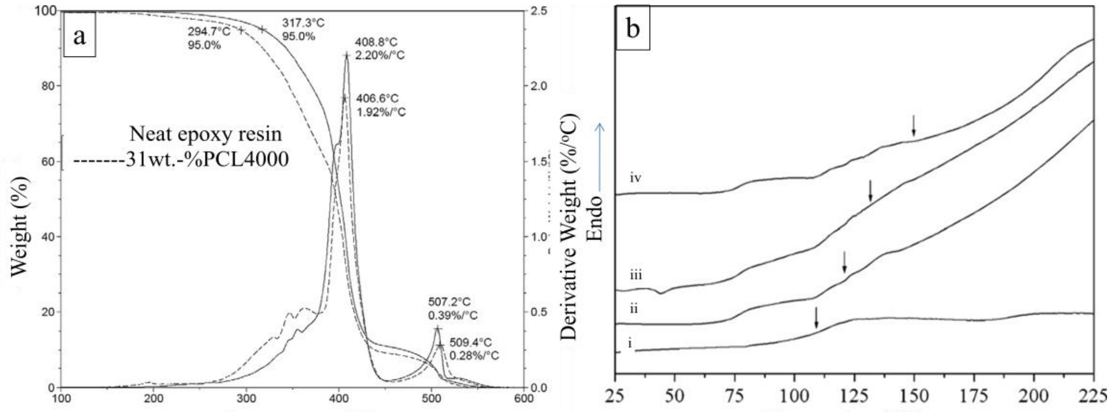

Figure 2.25: a) TGA of neat epoxy and 31 wt.% PCL4000 containing epoxy in air with 10 K/min heating rate [76] and b) DSC thermograms of EP/PFR composites containing i) 0, ii) 5, iii) 10, and iv) 15 wt% PFR contents [87].

The results show that the glass transition temperatures (T_g) of the EP/PFR composites are higher than that of pure epoxy resin (EP). In addition, the value of T_g increases upon increasing the PFR content which is shown as a, b, c, and d in Figure 2.25b. The bulky, aromatic, DOPO containing pendant, which hinders the mobility of molecular chains, may be responsible for the higher T_g characteristic [87]. Thermosetting materials with moderate T_g's and good thermal stabilities are obtained in all cases. The thermal stability and flame retardant properties of the cured epoxy resins are improved by the incorporation of both silicone and phosphorus moieties. The presence of phosphorus increased the limiting oxygen index (LOI) values leading to polymers with enhanced flame retardant property when the phosphorus content is reached to a value of 1.0 wt.-%. Also, the LOI reaches more than 35.6. This may be due to the nitrogen-phosphorus synergistic effect [88]. The synergistic effect of silicone and phosphorus enhanced the flame retardency and LOIs, which was also observed for siliconized epoxy resins cured with phosphorus containing diamine compound [69]. Similarly, earlier studies have reported that the combination of silsesquioxane and 10-[2',5'-bis(9-oxiranyl-nonayloxy)phenyl]-9,10-dihydro-9-oxa-10-phosphaphenanthrene-10-oxide (DOPO) have increased both the quantity and thermal stability of the char which also have accounted for the improvement of the flame retardancy of EPs [87, 88, 89, 90].

The mechanical properties such as surface hardness, tensile strength, elongation at break, and stress at maximum load were also studied in epoxy resin and its composites. These properties were obtained higher in composites than pure epoxy resin. The composites reinforced with bio-based polymers showed about 74.55–243% increase in elastic modulus over the pure epoxy matrix. Young's modulus values were obtained higher for composites with styrene-based polymers [91].

However, tensile strength and Young's modulus were found to decrease with an increase in the amount of epoxide groups in epoxidized natural rubber (ENR) and also with an increase in the amount of ENR in the blends as shown in Figure 2.26 (a and b). Meanwhile, percent elongation at break slightly increased when ENR content was not greater than 5 phr [92]. Figure 2.26a shows that the rubber possessed lower tensile strength compared to epoxy resin, and thus the tensile strength of blended resins were lower compared to epoxy resin. It can also be pointed out that, as the amount of ENRs in the blends increased, the tensile strength is decreased. The lowering effect was more significant in case of ENR with higher epoxide groups such as ENR60. The increment of double bonds in the structure prohibited strain crystallization during testing. Figure 2.26b shows impact strength of epoxy resin and blended resins.

Further, it has been shown that the addition of natural rubber (NR) in epoxy resin have clearly improved the impact strength of epoxy resin. Rubber globular nodules might have contributed to this toughening effect. Although the amount of NR was 10 phr, the impact strength was found to be lower. For epoxy/ENR blends, when the amount of ENRs in the blends was not higher than 10 phr, the impact strength of blend samples was higher than that of the epoxy resin [92].

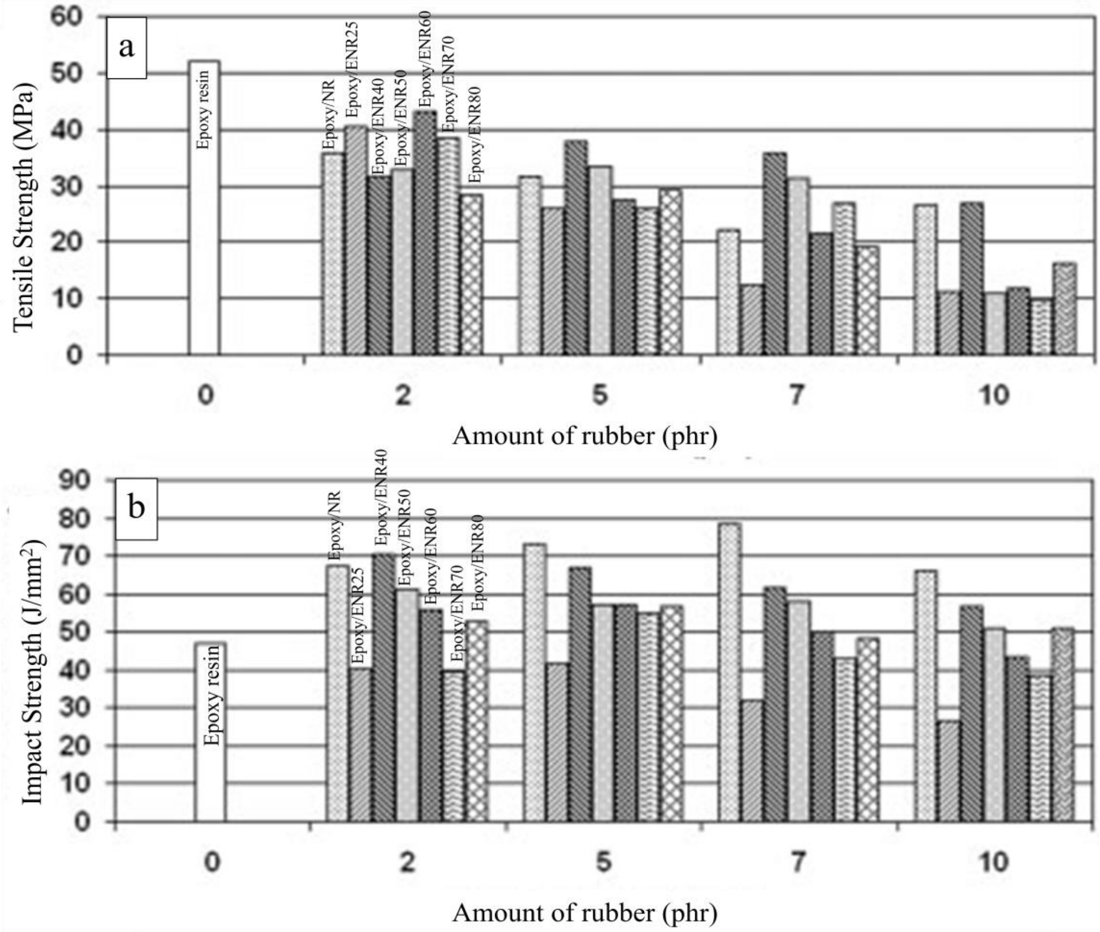

Figure 2.26: a) Tensile strength and b) impact strength of epoxy resin, epoxy/NR blend, and epoxy/ENR blends [92].

On the other hand, the tensile modulus, yield strength, and impact strength of PA6/PC 75/25 blend have also been improved considerably on increasing the epoxy content, where epoxy resin acted as a compatibilizer [93]. Moreover, the improvement of tensile and impact strength has a close relationship with the dispersion of nanotubes. This was observed in the novel epoxy-group modified phosphazene-containing nanotubes (EPPZTs)/epoxy resin composites [94].

Further, studies have confirmed that the best mechanical performance in terms of flexural and tensile properties was achieved with the block copolymer derived from carboxyl terminated polybutadiene (CPBER), whereas a more flexible material has been obtained with isocyanate-terminated polybutadiene (NCOPBER) block copolymer modified network [30]. Likewise, the tensile and flexural properties (strength and modulus) of modified epoxy resins (EPs) were found to be lower than those of the unmodified EP and decrease with an increase in the carboxyl-terminated poly(butadiene-co-acrylonitrile) (CTBN) content. On the other hand, an increase in the tensile strain with the incorporation of CTBN was also noticed [95]. Tensile properties and oil resistance of polypropylene (PP)/recycled acrylonitrile butadiene rubber (NBRr)-epoxy resin (EP) blends were superior to those of PP/NBRr blends [70]. Stress-strain behavior during compression revealed that the epoxy resin could reduce the compression stress when the sealants were loaded to a certain strain which effectively pointed out the crosslink breakages and benefited to compression resistance. The incorporation of 2 phr epoxy resin sets in a slightly higher T_g and distinctly reduced compression of polysulfide sealant from 28.3% to 11.2% after it is compressed to 25% at 23 ^oC for 1 day [71].

Similarly, most of the enhanced mechanical and thermal properties such as tensile, flexibility, dynamic viscoelastic, dynamic mechanical strength, impact strength, and toughness when compared to the parent epoxy resin are studied in chloro-terminated polysulfones (PSC) and epoxy-terminated poly (aryl ether sulfone)s (PSE) [68], soy-based epoxy resin system [74], epoxy/poly(e-caprolactone) (PCL) [76], and epoxy/jute composites [96].

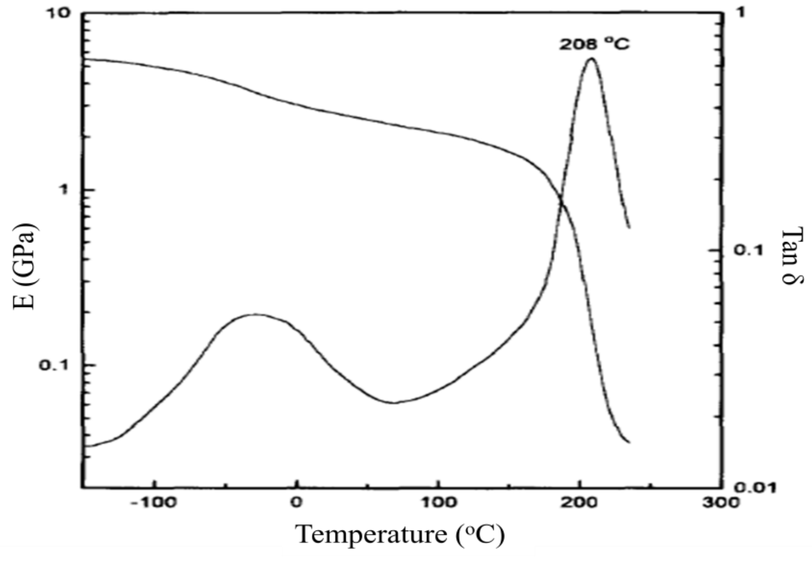

Figure 2.27: Dynamic mechanical spectrum of 88/12 DDM cured epoxy resin/PEK-C blends [97].

Mechanical measurements showed that incorporation of phenolphthalein poly(ether ether ketone) (PEK-C) have slightly decreased both the fracture toughness (K_{ic} and G_{IC}) and the flexural properties, apparently, due to the reduced cross-link density of the epoxy network [97]. The dynamic mechanical spectrum of the 88/12 DDM cured ER/PEK-C blend is presented in Figure 2.27. The figure clearly displays a maximum at 208°C on the tan δ versus T curve which corresponds to the T_g of the cured blend. This result further shows that no phase separation occurred in the blend during the curing process. It was concluded that all the DDM cured ER/PEK-C blends obtained were homogeneous with single phase [97].

2.5 Toughness Enhancing Mechanisms in Polymers and Thermosets

To overcome the brittle properties of epoxy resin, several toughness enhancing mechanisms were employed. The general consequences can be used for toughening of different polymers including amorphous and semicrystalline polymers or nanocomposites. The main effects of toughening, including many microscopic or nanoscopic highly localized events of energy absorption, appear together in a large material volume with large total energy absorption. This effect was possible only in a heterogeneous material with a particular morphology. Some applicable mechanisms are explained in the order of their increasing toughening efficiency.

Multiple microcrack and void formation mechanism occurs by debonding of microparticles/fibers which creates new surfaces and microcracks. The energy absorption is limited due to the surface energy. Only very brittle materials, such as epoxy resin, can be toughened by this effect; and such effect is known from brittle inorganic materials (e.g. ceramics) [64].

Bridging mechanisms are applicable in a brittle matrix by dispersing the ductile particles. The particles were stretched bridging both the crack boundaries in front of a propagating crack. The volume content of bridged particles was low. This mechanism has an effect only in brittle materials in which crack is stopped by the soft particles.

Multiple initiations of crazes/shear band mechanisms were performed by the soft particles which acted as stress concentrators and initiated small crazes or shear bands in the equatorial zones or between the particles. This mechanism can be seen in the rubber toughened thermoplastics [64].

Nanovoid formation with yielding fibrillation mechanisms are appeared by debonding of nanoparticles which is created by nanovoids, stress concentrations and yielding fibrillation of the nanosized matrix strands between the voids. The advantages of this mechanism are an enhancement of stiffness due to the hard filler and an increase in toughness due to the plastic yielding of matrix between the nanovoids. All these toughening mechanism were based on well dispersed particles in the matrix [64].

To get the desired thermomechanical properties, it is necessary to maintain a high crosslink density of the thermoset resin network. Unfortunately, these highly crosslinked glassy networks suffer from poor fracture resistance [28]. Thermoset resins are characterized by a crosslinking reaction as a result of which the modifier undergoes a macro-phase separation. Moreover, accumulation of free liquid plasticizer molecules at the fiber surface can act as a weak boundary layer and cause a substantial reduction in the mechanical performance of a composite [28]. Traditionally, toughening (*i.e.* resistance to the propagation of a sharp crack) was achieved using rubbery modifiers which were either thoroughly immiscible with the epoxy or undergo reaction induced macrophase separation [98- 103]. In recent years, theoretical understanding regarding the toughening mechanisms has been advanced. Several theories have been proposed to depict the toughening effect of rubber particles on the brittle thermoset matrix. These were based on the fractographic features and fracture properties of rubber-toughened thermoset networks. Some of the mechanisms to explain the impact behavior of rubber and other polymers (thermoplastic, thermoplastic elastomer) toughened epoxy are explained with an example as shown in Figure 2.28 [32].

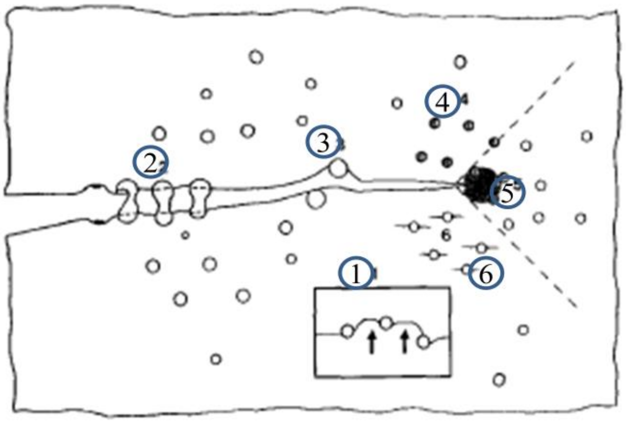

Figure 2.28: Schematic diagram of toughening mechanisms proposed for thermoplastic-modified epoxies: 1) crack pinning, 2) particle bridging, 3) crack path deflection, 4) particle yielding, 5) particle-yielding induced shear banding, and 6) microcracking [32].

Shear yielding [32,46, 98-103] was a major mechanism proposed for second phase modified polymers especially when the fillers were of a rubbery nature. It involved matrix deformation and cavitations of the particles in response to the stresses near the crack tip. In addition, there was shear yielding between the holes formed by the cavitated rubber particles. Plastic deformation blunts the crack tips, and consequently the local stress concentration was reduced allowing the material to support higher loads before failure occurred. For this reason the major energy absorption mechanism was suggested to be the plastic deformation of the matrix. In the particle bridging mechanism [32], rigid or flexible particles played two roles: a) they acted as bridging particles granting compressive grip in the crack path and b) the ductile particles deformed plastically in the material surrounding the crack tip providing additional crack shielding. The particle bridging was held to be responsible for most of the improvements in toughness (Figure 2.28).

A crack-pinning mechanism [32] propose that, as a crack propagated through the resin, the crack front bent out between the second phase dispersion and remained pinned at the positions where it has encountered the particles (Figure 2.28).

The microcracking mechanism [98-103] supposed that incorporation of rubber into polymers generate microcracks caused by the presence of fillers (Figure 2.28). Such microcracks provided improved toughness and originate tensile yielding and thus a large tensile deformation. Voids result when the microcracks open and permit large strains. Debonding effectively lowers the modulus in the frontal zone around the crack tip therefore reducing the stress intensity there. All the toughening mechanisms proposed above have their attractive features but none are compelling in their wide applicability.

2.6 Morphological Aspects of Toughening

Phase morphology is a main issue for the effective rubber toughening, other resins toughening, block copolymer toughening, and particulate toughening. These toughening provide the nature of post-yield deformation mechanism of matrix materials that can be generated by rubber, resins, polymers etc. These particles are more effective in crazing, cavitation, shear yielding, and pinning which are the major energy dissipating mechanisms for brittle polymer.

Further, the toughening mechanism has been initiated by the rubber. Its particles cavitate and fracture, the resultant voids in the matrix grow and coalesce, and finally, the matrix also forms shear bands where cavitations and shear banding are deduced as the two major deformation mechanisms [99,100]. In this method, liquid rubber is blended with thermoset resins. First the epoxy resin is toughened by using the rubber to improve morphological and mechanical character for the development of the new materials. The toughener should be miscible with the resin at the beginning and undergo phase separation after the curing which directs to the formation of a two-phase microstructure. The researchers have used different kinds of the toughener to toughen the epoxy resin, such as carboxyl-terminated polybutadiene (CPBER), hydroxyl-terminated polybutadiene (HPBER) [30], and carboxyl terminated copolymers of butadiene-acrylonitrile (CTBN) liquid rubber [95,99, 100].

Bussi and Ishida [104] investigated the blends of epoxy resin and hydroxyl terminated, internally epoxidized polybutadiene rubber for the study of the mechanical properties. The fracture toughness properties of the blends did not show any significant improvement due to the existence of only weak chemical bonding between the rubber particles and the epoxy matrix. The behaviour of epoxy resin blended with epoxidized natural rubber (ENR) showed the toughening of epoxy resin. The fracture surface morphology suggested that toughening was induced by the presence of ENR globular nodules attached to the epoxy matrix [92]. Likewise**,** Saleh and coworkers [95] showed an improvement of the fracture toughness of the epoxy resin (EP) with the presence of carbonyl-terminated butadiene acrylonitrile copolymer (CTBN) liquid rubber. The fracture surface demonstrated the presence of two-phase morphology [95]. Addition of the aramid-CTBN block copolymer was due to the increase in the area of damage zone caused by the formation of the fine CTBN phase which indicated the toughness improvement [105].

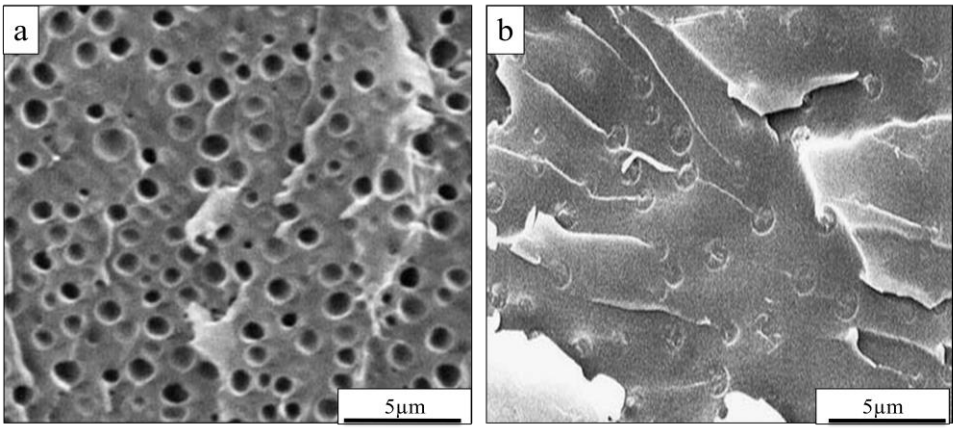

Figure 2.29: Scanning electron micrographs of the fracture surfaces of; a) 20 phr CTBN-modified epoxy resin [95] b) 15 phr DGEBA/PEEKMOH blends [106].

One of the example shows that in the case of 20 phr of CTBN-modified epoxy (Figure 2.29 a), excess of CTBN loading leads to some agglomeration of cavitated rubber particles throughout the epoxy with an increase of the cavitated rubber particles size (1.40 μm) [95,99,100,105]. The domain size and size distribution were reliant on the molecular weight and concentration of PEEKMOH in the blends which provided substantial improvement in fracture toughness. Another example is presented in Figure 2.29b, where the surface seems to be smooth and the cracks are propagated uninterrupted showing ridge patterns and river marks [106].

2.6.1 Thermoplastic and thermoplastic elastomer toughening

The essential mechanisms responsible for the toughening of block copolymer modified thermoset epoxies are not completely understood. A current theory suggests cavitation of the rubbery cores in dispersed micelles as the key event that triggers shear yielding thus resulting in enhanced toughness [64]. In the frame of elastomer toughening study, Pearson and Yee [32] investigated piperidine cured epoxy resin modified with poly(phenylene oxide) (PPO). It was shown that the fracture toughness improved with PPO content in a linear fashion. The micromechanical mechanism responsible for the improvement in toughness was found to consist of crack bifurcation and microcracking. Some evidence of particle bridging was also observed; and it was considered that the particle bridging may play an important role in the formation of a microcracked damage zone [32]. Besides, Kuan and co-workers [107] studied a reactive polymer for toughening epoxy resin. 5 wt % polyurea was adopted as fracture toughener to significantly toughen the piperidine/epoxy.

Furthermore, Declet-Perez and co-workers [108] have prepared spherical micelles forming block copolymers with rubbery cores (prone to cavitation) and glassy cores (unable to cavitate). Unexpectedly, both systems have shown to enhance the fracture toughness although the rubbery core micelles outperform the glassy core counterparts. They noticed that the mechanism invoked matrix shear yielding, activated by cavitation of the nanoscale rubber domains, as the primary energy absorbing process. The sequence of events in the proposed toughening mechanism was based on the hypothesis that rubber cavitation reduced the triaxial constraint of the network allowing plastic deformation to occur [27,108]. Likewise, Thio *et al.*[109] investigated epoxy toughening using low molecular weight poly(hexylene oxide)-poly(ethylene oxide) diblock copolymers in which the fracture surfaces of each blend exhibited distinct traits related to the mechanisms of crack propagation. The blend containing small spherical micelles appeared flat with no significant deformation of the matrix prior to fracture. In contrast, the presence of the larger worm-like micelles and bilayer vesicles increased the surface roughness, although, with different characteristics which indicated some small-scale plastic deformation matrix [109].

Moreover, an amphiphilic poly(ethylene-alt-propylene)-*b*-poly(ethylene oxide) (PEP-PEO) block copolymer (BCP) blended with epoxy resin formulation [110] and amphiphilic poly(n-butylene oxide)-*b*-poly(ethylene oxide) (PBO–PEO) diblock copolymers of various compositions with epoxy resins [34] showed self-assembled, wormlike micelle structures. On the other hand, an anhydride cured epoxy resin was modified using two poly(styrene)-*b*-1,4-poly(butadiene)-*b*-poly(methyl methacrylate) (SBM) block copolymers which showed spherical micelles and became increasingly interconnected into a network with the increase in concentration of modifier [111]. For toughening mechanism, worm-like, spherical, and elongated cylindrical micelles produce improved toughness. This can be interpreted on the basis of a combination of mechanisms including crack tip blunting, cavitation, particle debonding, limited shear yielding, and crack bridging [34,110,111]. An example of the crack tip double-notch four-point-bending (DN-4PB) specimen of BCP-toughened epoxy: evidence of wormlike structure cavitation or fragmentation after severe stretching as is shown in Figure 2.30.

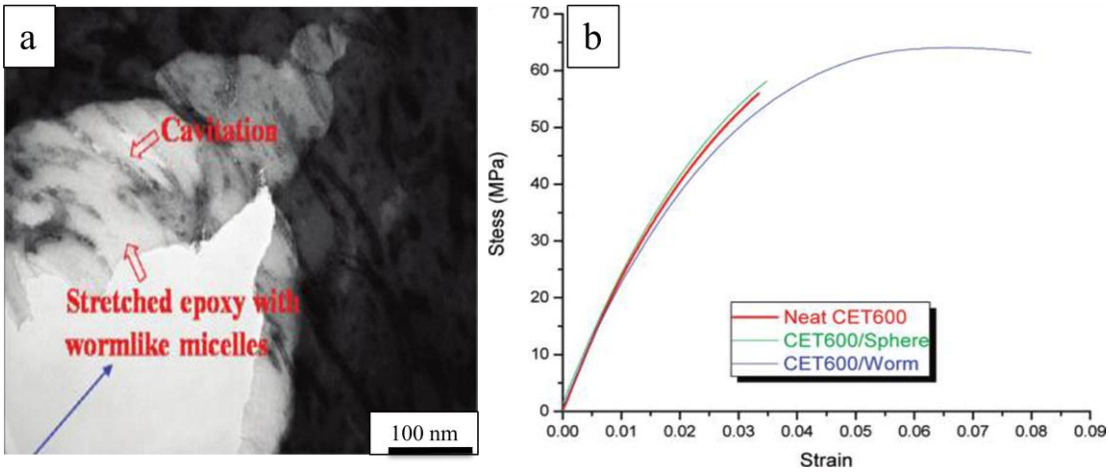

Figure 2.30: a) TEM images of the crack tip DN-4PB specimen of BCP-toughened epoxy; wormlike structure cavitation or fragmentation after severe stretching, and b) Representative engineering stress-strain curves of CET600, CET600/sphere, and CET600/worm [110].

As shown in Figure 2.30a, a higher magnification observation at the crack tip region further reveals the morphology of the stretched, thinned epoxy matrix that contain wormlike micelles at the edge of the crack This was indicative of the high ductility of the BCP worm-like micelle modified epoxy. This enhanced matrix ductility was consistent with the tensile behavior of the epoxy system. Careful investigation of the micrographs reveals cavitation of the soft rubber inside the worm-like micelles in the stretched epoxy region [110]. The neat epoxy, BCP worm-like micelle modified epoxy, and BCP spherical micelle modified epoxy are designated as CET600, CET600/worm, and CET/sphere, respectively. Representative engineering stress-strain curves of CET600, CET600/sphere, and CET600/worm are given in Figure 2.30b.

The presence of worm-like micelles results in a prominent increase in the tensile strength and elongation at break. These enhancements are not observed to the same extent with the spherical micelle modified epoxy. Upon evaluation with CET600 and CET600/sphere, it is clear that the CET600/worm material exhibits a remarkably improved ductility and toughness along with a slight increase in strength. This tensile property enhancement is likely to be caused by the presence of the worm-like micelles and the surrounding epoxy network that might be modified by the corona PEO blocks [110].

2.6.2 Ester/ether containing compound/curing agents toughening

Various toughening mechanisms like crack pinning, crack path deflection, ductile nature of crack, and plastic deformation of the matrix are responsible for the increase in fracture toughness of the blends [64]. To address these mechanisms, several studies have been useful for the enhancement of toughness by different types of esters containing compounds and curing agents.

Toughening and curing agents are prepared by the reactions of epoxidized oleic methyl ester and epoxidized oleic capryl ester, respectively, with curing agent. Toughness enhancement is attributed to the flexibility of the end carbon chains and ester carbon chains of the oleic esters in the toughening curing agents [112]. Poly(ether esters) thermoplastic elastomers with polyoxytetramethylene soft segments and poly(hexamethyleneterephthalate) hard segments are used to toughen anhydride cured epoxy resins. The compatibility between resin and toughener and also the mechanical properties of the modified resin depends upon the ratio between the hard and soft segments [113]. An example of the scanning electron microscopy (SEM) image of epoxy/poly(ether ester) blend containing 80 wt.% soft segment content

(SSC); and a comparison plots of tensile modulus and fracture toughness of epoxy resins modified with 10 wt % polyetherester as functions of modifier composition are given in Figure 2.31.

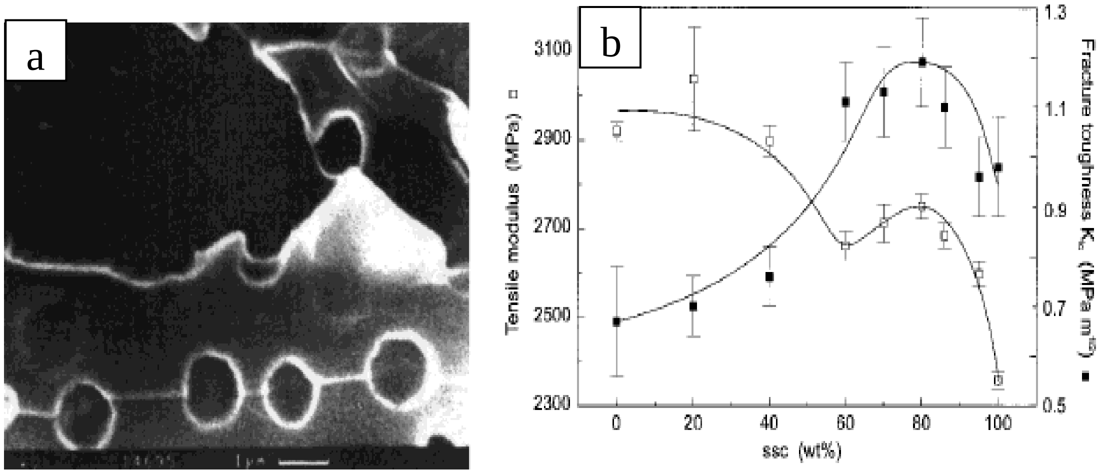

Figure 2.31: a) SEM image of fracture surfaces of epoxy/10 wt.% poly(ether ester) blend containing 80 wt % soft-segment content (SSC), b) Comparison plots of tensile modulus and fracture toughness of epoxy resins/10 wt % poly(ether ester) (PEE) as functions of modifier composition [113].

SEM image (Figure 2.31a) shows holes that are surrounded by the deformation rings appearing in the samples modified with polyether ester containing 80 wt % SSC. Epoxy resins blended with 10 wt % of the poly(ether ester) exhibits an increase in toughness by 50–150% while the strength and modulus decreases by 20% or less as shown in Figure 2.31b.There was a special composition in the range of about 70–90 wt % where the soft segments in the polyether ester showed a synergetic increase in both the toughness and tensile properties. An increase in fracture toughness and elastic modulus (as well as tensile strength) leads to the peak values of these properties for the same modifier composition as shown in Figure 2.31b [113].

2.6.3 Toughening by nanofillers and ionomers

For the toughening mechanism, various nanomaterials have been used for the enhancement of the thermal and mechanical properties. Several works have been carried out by using the nanomertrials in different blends of epoxy matrix for the toughness enhancement. The toughening mechanisms such as crack pinning, crack deflection, and immobilized polymer are common which can be fulfilled by nanofillers and ionomers. The electron microscopy put forward an evidence of the toughening mechanisms including crack deflection, debonding, and plastic deformation of the debonded matrix (plastic void growth) for both untreated and treated nanocomposites. However, further crack deflection and microcracking is the mechanisms distinctively observed for the treated nanocomposites [99,102,114].

Wu *et al.* [114] used the block ionomer complexes, based on sulfonated polystyrene-*block*-poly(ethylene-ran-butylene)-*block*-polystyrene (SSEBS) and a tertiary amine-terminated poly(ε-caprolactone) or (SSEBS-c-PCL), to toughen epoxy resin [114].

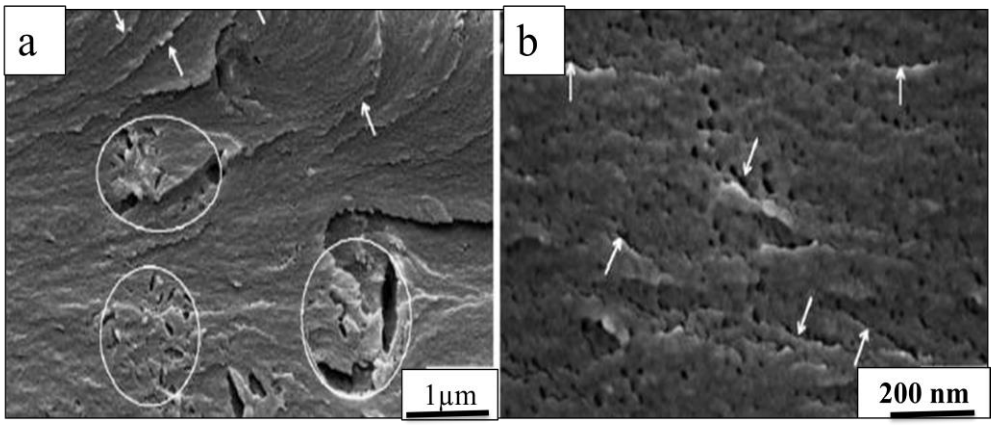

Figure 2.32: Different magnifications of scanning electron micrographs of fracture surfaces of epoxy blends with 10 wt % SSEBS-c-PCL containing 2.4 wt % PCL [114].

According to them, the damaged regions (circled areas in Figure 2.32a) are caused by the debonded spherical micelles ahead of the crack front which coalesce forming large and small areas of detached epoxy. When the main crack passed them, tails are left behind similar to those due to crack pinning. However, there is no real crack pinning so that the toughness contribution cannot be significant. Crests of matrix tearing on different crack planes can be observed in these two figures implying the presence of plastic shear deformation (see arrows in Figure 2.32a); but they do not come from crack deflection which would have introduced a high fracture surface roughness. Higher magnification of the fracture surface in Figure 2.32b also reveals many small holes caused by pullout of debonded spherical domains. Nanocavitation of particles cannot be verified. However, careful observation also indicated the existence of lines of holes that are expanded, elongated, and coalesced to form arrays of tiny cracks along the main crack growth direction (see arrows in Figure 2.32b) [114].

The similar toughening mechanism was also followed by anhydride cured epoxy resin modified by the addition of silica nanoparticles. The well-dispersed phase of nanosilica particles is in good agreement with the measured modulus with theoretical models [115]. On the other hand, multicomponent nanocomposite materials based on a high performance epoxy system and single walled carbon nanotubes (SWNTs) were prepared for the noncovalent wrapping of nitric acid treated SWNTs with a PEO based amphiphilic block copolymer. This leads to highly disaggregated filler with a boosted miscibility in the epoxy matrix allowing its dispersion without organic solvents which also followed the toughening mechanism [116]. Conversely, improvement in stiffness of the high-functionality epoxy resins was comparable with those achieved for the bifunctional (DGEBA) resin system. Although it was often found that the improvement in the modulus sacrifices toughness of the material, both toughness and stiffness could be improved through the incorporation of organoclay. The improved modulus and toughness makes the nanocomposite strategy an attractive alternative to the commonly used micron-sized fillers [117]. Ni *et al*. [118] prepared a new inorganic/organic hybrid material containing polyhedral oligosilsesquioxane (POSS) with n-butyl glycidyl ether (nBGE) and 1,4-butanediol diglycidyl ether (BDGE). The toughening and the thermal properties of the cured epoxy resin were greatly improved by the addition of the hybrid. The enhancement was approved to nano-scale effect of the POSS structure and the formation of anchor structure in the cured network. This indicated the diffuse shear yielding near a growing crack combined with a large concentration of small local plastic deformation events [101,118].

Similarly, the tensile properties of well-dispersed non-treated alumina (NT-Al_2O_3) and 3-amino propyl triethoxysilane treated alumina (APTES–Al_2O_3)/ epoxy nanocomposites were measured with different nanoparticle loadings. APTES–Al_2O_3 nanoparticle filled epoxy showed significant increase in the strain-to-break (39% at 10 phr particle loading), while it exhibited an increase in modulus and maintained the strength. The fracture toughness, fatigue crack propagation (FCP) rate, and tensile test of the material indicate that the crack deflection, debonding and plastic deformation of the debonded matrix (plastic void growth) implies for the untreated particles with a relatively weak interface. However, a stronger interface led to enhanced crack deflection and microcracking [119, 120]. Experimental data of EP/Al_2O_3 and EP/TiO_2 nanocomposites plotted for Fracture toughness against nanoparticles' volume content and fracture toughness increase *versus* diameter to distance ratio of the filler are compared with the corresponding theoretical data for crack pinning theory in Figure 2.33 [121].

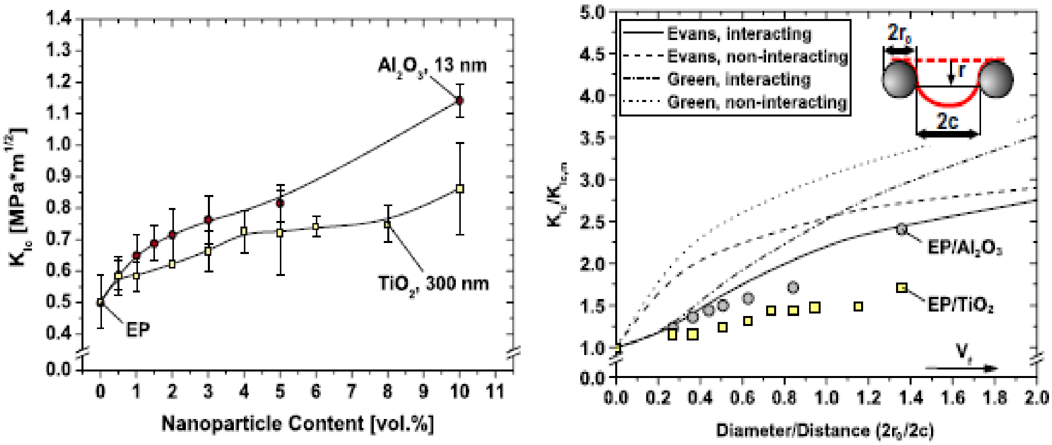

Figure 2.33: Fracture toughness against nanoparticles volume content plots for EP/Al_2O_3 and EP/TiO_2 nanocomposites and the fracture toughness increase with increasing diameter to distance ratio ($2r_0/2c$) curves of the fillers [121].

A comprehensive study, particularly with regard to fracture and toughening mechanisms, was carried out on series of nanocomposites containing varying amounts of nanoparticles either titanium dioxide (TiO_2) or aluminium oxide (Al_2O_3). These nanocomposites were systematically produced by applying high (shear) energy during a controlled dispersion process in order to reduce the size of agglomerates and to gain a homogeneous distribution of individual nanoparticles within the epoxy resin. It was found that the presence of nanoparticles in epoxy induces various fracture mechanisms – for example, crack deflection, plastic deformation, and crack pinning. At the same time, nanoparticles can overcome the drawbacks of traditional tougheners (e.g. glass beads or rubber particles) by simultaneously improving the stiffness, strength, and toughness of epoxy without sacrificing the thermo-mechanical properties [121].

2.7 Nanostructured Epoxy Resins

2.7.1 Overview on nanostructured resins

In material science, researchers are looking forward to developing the nanostructured materials for the advancement in their properties. For this reason, recent researches have been focused on the nanostructured thermosetting materials [16,122]. This initiative has already been started since 1990s where the well defined ordered nanostructures in thermosetting epoxy or phenolic resins based on the self assembling capability of block copolymers are being widely studied [16,39,122]. The first work was carried out by the Hillmyer groups by blending the block copolymer with epoxy resin [122]. In general, amphiphilic block copolymers that have more than two blocks in which only one of the block is miscible with the thermosetting matrix were used as structure directing agents [122]. Yet, there might be different ways to generate the self assembled nanostructure in thermosets. One of the pragmatic ways is to use the concept of chemical compatibility by introducing specific groups in one of the blocks and inserting the reactive block in the synthesized block copolymers. In fact, epoxidized polyisoprene-polybutadiene block copolymer [123] as well as glycidyl methacrylate [124] and methacrylic acid-based copolymers [125] have been synthesized to generate nanostructured thermosetting materials which have wide applications in the present context.

Further, block copolymer modified epoxy resins have created major interest, since it was established that the blend could lead to a self assembled nanostructure thermosets. Over moderate to high polymer concentration, the system behaves as expected for the block copolymer in a solvent selective for one block. Two types of non reactive and reactive modifiers copolymers are studied. The enhancement in the mechanical properties of the modified thermoset depends upon the morphology adopted by the polymer. Besides improving the mechanical properties, the morphology was also found to have an effect on the glass transition and the block copolymers used to fabricate nanostructured epoxy resins [46].

The nanostructured thermosets have been synthesized by several investigators for their prominent application. The general route to prepare such materials is a templating scheme where a solution containing an amphiphilic compound and a reactive compound self assemble to form lamellar, hexagonally packed cylindrical or cubic structures with dimensions around 1-30 nm [35].

The effect of miscible rubber are clearly seen in the rubber modified epoxies (RME’s) which are formulated by blending a reactive epoxy system. This shows a macroscopic phase separation of the rubber. The process is often referred to as “polymerization-induced phase separation” [28]. Apart from this, researchers have also introduced a method of creating nanostructured thermosets using direct miscibility of an amphiphilic block copolymer like polycaprolactone (PCL) [126], poly(propylene oxides) (PPO) [33], and poly(ethylene oxide) poly(ethylene-*alt*-propylene) (PEO-PEP) [35] in which a reactive epoxy resin selectively mixes with the oxides containing block. When hardener is added and the epoxy cures, a highly cross-linked thermoset matrix is formed. However, PEO shows the disorder heterogeneous morphology [33]. A summary of epoxy resin/block copolymer blend systems are given in Table 2.1

Table 2.1: A summary of epoxy resin/block copolymer blend systems investigated in the literatures

Resin	Blend component	Remarks	Ref.
DGEBA	SB star block	self assemble nanostructure in uncured state	16
DGEBA	SB diblock + MCDEA	self-organized structures with the microphases fixed *via* a curing reaction. RIMS	17, 40
DGEBA	PEO-PEP + PN	parameters that control the microphase morphology	18
DGEBA	PS-*b*-PMMA + DDM	self assemble PS block formed spherical micelles or spherical/worm-like domain	19
DGEBA	PEO-PEP + MDA PEO-PEE +MDA	templating an ordered structure on the nanometer scale, nanoscopic core/shell-like morphologies	35, 122
Novolac	PEO-*b*-PPO-*b*-PEO + HMTA	reaction induced microphase separation (RIMS)	23
DGEBA	SBS + DDM	nanostructured morphologies	36
DGEBA	SBS + MCDEA	miscibility increment at low content of SBS	37
DGEBA	SB star block + MCDEA	tailoring interactions between DGEBA and immiscible block copolymers	38, 39
DGEBA	SBG and SBMG + DDS	network formation	124, 125
DGEBA	PCL + HHPA	display two-phase systems	126
DGEBA	PEO-*b*-PPO-*b*-PEO + DDM	Increase the miscibility of the system	127
Phenolic	PEO-*b*-PCL + HMTA	variety of composition-dependent nanostructures	128
DGEBA	PEO-*b*-PCL-*b*-PS + DDS	tandem reaction-induced microphase separation	129
Novolac	PS-*b*-PEO + HMTA	intermolecular hydrogen-bonding interactions	130
Dicyclopentadiene	PNS-PLA + Grubbs catalyst	reaction-induced phase separation (RIPS)	131

Recently, Serrano and co-workers [16,17,38,39] have established an another method for developing the nanostructured thermosetting materials using functionalized block copolymer. The functionalized block copolymer was made compatible with the epoxy resin for generating nanostructures in the blend. Likewise, Feng *et al*. [23] and Ocando *et al*. [40] have also studied the reaction induced microphase separation (RIMS) of PS block in poly(styrene-b-butadiene) with thermosetting mixtures.

2.7.2 Using block copolymers as nanostructuring templates

Block copolymer modified epoxy resins have engendered significant interest, since it was established that the combination could guide to nanostructured thermosets through self assembly. Morphologies such as copolymer vesicle and spherical/wormlike micelles can be shaped under the suitable conditions. The improvement in mechanical properties of the modified epoxy resins depend upon the morphology adopted by the polymers. In addition to improving the mechanical properties, the morphology is also found to have an effect on the glass transition in nanostructured thermosets systems. The block copolymers are exploited to fabricate nanostructured epoxy resins and their properties [46]. Previously, Grubbs *et al*. [132] observed that the nonreactive poly(ethylethylene)-*b*-poly-(ethylene oxide) (PEE-*b*-PEO) copolymers, reactive poly(epoxyisoprene)-*b*-polybutadiene (BIx*n*) copolymers, and poly(methyl acrylate-*co*-glycidyl methacrylate)-*b*-polyisoprene (MG-I) copolymers form ordered microstructures in the blends with epoxy.

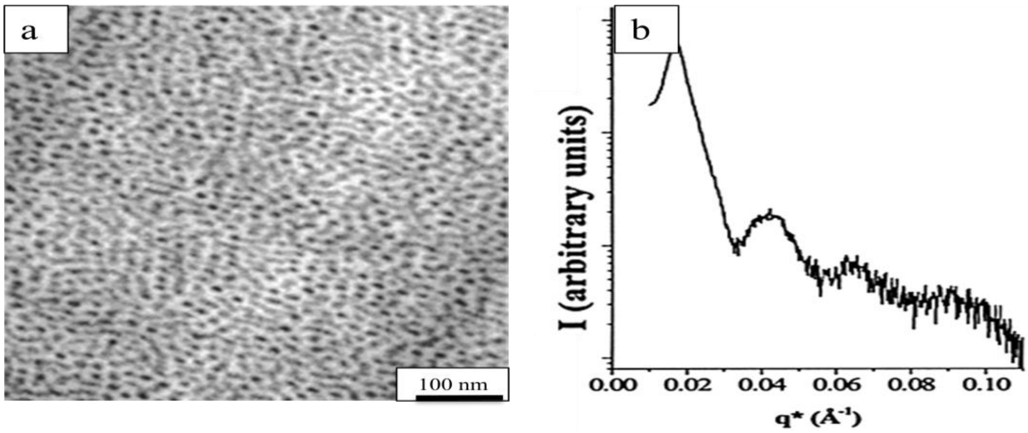

Figure 2.34: TEM micrograph and SAXS pattern for cured 20 wt- % MG-I/epoxy blends [132].

As an example, a TEM image and small angle x-ray scattering (SAXS) pattern of 20 wt - % of MG-I/epoxy blend are shown in Figure 2.34 which confirm that the spherical micelles become more densely packed at higher copolymer concentrations. TEM images and SAXS patterns of the cured composites demonstrated that the MG-I block copolymers within a curing epoxy resin cured without macrophase separation of the block copolymer (Figure 2.34).

In fact, capability of these types of copolymers to template epoxy resin is expected to arise from the combination of proper miscibility of one block of a block copolymer with epoxy components by the curing process. The energy barriers to the nucleation and growth the of copolymer rich regions in the epoxy matrix occurs as network formation and varies with the molecular weight of epoxy [132]. Besides, Guo *et al.* [133] prepared nanostructured blends of MDA cured epoxy resin with a low molecular weight amphiphilic polyethylene-block-poly-(ethylene oxide) (PE-b-PEO) symmetric copolymer. In their study, three morphological systems were identified corresponding, precisely, to the three systems of crystallization kinetics of PE blocks. This new phenomenon was explained on the basis of homogeneous nucleation controlled crystallization within the nanoscale confined environments in the block copolymer/thermoset blends [133]. In the same way, Larrañaga *et al*. [34] have also prepared a rational design of thermosetting epoxy matrices structured at nanoscale that can be obtained by controlling molar ratio and molecular weight of PEO–PPO–PEO block copolymers and the cure conditions. Moreover, potential applications of optically transparent nanoporous materials based on epoxy matrices could be developed through the use of these systems [34].

Ritzenthaler *et al.* [125] have investigated the epoxy thermoset blended with polystyrene-*block*-polybutadiene-*block*-poly (methyl methacrylate) (PS-*b*-PB-*b*-PMMA) triblock copolymers before and after the epoxy-amine reaction. Before reaction, the three blocks self organized on a nanometer scale in PS spheres surrounded by the PB nodules while the PMMA blocks were solubilized with the epoxy precursors forming a swollen corona [125]. Likewise, their another similar study has found that the copolymer amounts increased from 10 to 50 wt % induces a morphology change to either “spheres on spheres” or “core-shell” structure depending upon the PB content in the triblock. For higher than 50 wt % copolymer concentration, an organization with long-range order similar to the neat block copolymer morphology was formed which strongly depends on the processing technique used [134]. Further, Rebizant *et al*. [124] have synthesized epoxy resin modified by polystyrene-*block*-polybutadiene-*block*-poly(methylmethacrylate)-*block*-poly(glycidyl methacrylate) (SBMG) copolymers. The resulting blend finely tuned the morphology of nanostructured materials in epoxy-amine networks. They found an interesting insight into the problem of factors governing the expulsion of the methacrylic block out of the epoxy-amine phase during network formation [124].

A new family of templates for generating nanostructured epoxy matrices at cured and uncured state with long range order in the bulk is controlled by the degree of epoxidation of butadiene block in polystyrene-*block*-polybutadiene star copolymer.

These nanostructured thermosetting materials are prepared by the modification of an epoxy resin with 30 wt.-% epoxidized polystyrene-*block*-polybutadiene copolymer (PS-b-PepB) [16,17,37-40]. Similarly, epoxidation of a commercial, cheap SB star block copolymer beyond 40 mol % epoxidation degree can be considered as an effective way for the preparation of novel nanostructured materials based on thermosetting matrices with potentially advanced mechanical properties and retention of the optical transparency of the epoxy matrix. The copolymer self assemblies have formed the morphology into a well defined hexagonal nano ordered structure of about 30 nm diameter; and, consequently, this has established its use as a structure directing agent to generate the nanostructured thermosetting materials as shown in Figure 2.35. It can be easily observed from Figure 2.35 that hexagonally nano ordered structure consists of PS cylinders arranged in the epoxy rich phase. With respect to the location of epoxidized and non-epoxidized butadiene segments (PB and PepB units), a higher magnification of TEM images of these systems (Figure 2.35 a and b) show the presence of PB units in both the epoxy-rich phase and near to the PS cylinders.

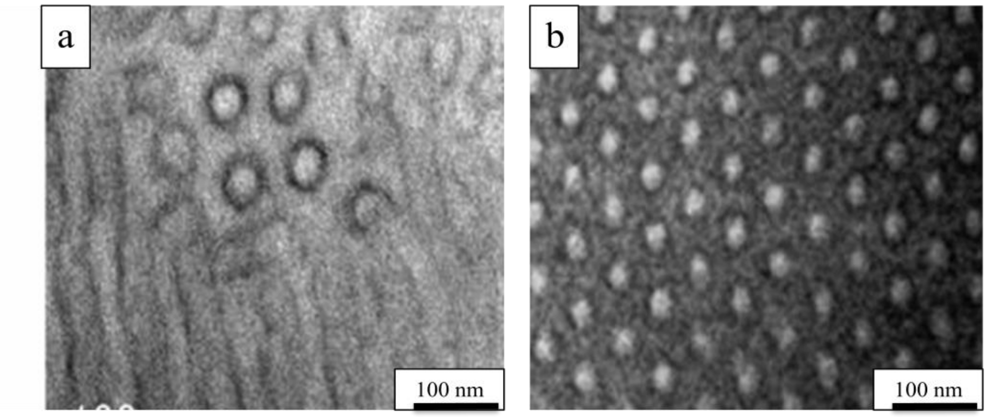

Figure 2.35: Higher magnification transmission electron micrographs for DGEBA/MCDEA blends containing 30 wt % of; a) 40 mol.-% SepB and b) 61 mol.-% SepB modified systems [39].

Furthermore, other morphologies could also be generated by using PS-b-PB copolymers with different PS/PB ratios. Nevertheless, at higher epoxidation, the epoxy rich phase become the matrix in the nanostructured thermosetting blends [38,39]. Ramos *et al.* [135] studied the gradient on block copolymer concentration through the film thickness and the effects of casting solvents used on the nanostructuring of a thermosetting epoxy coating modified with an epoxidized poly(styrene-*b*-butadiene-*b*-styrene) (SBS) triblock copolymer. The observed result was the conversion of small micelles into larger micellar domains in the case of low block copolymer content [135]. Likewise, the synthesis and characterization of optically active epoxy based nanostructured thermosets obtained using epoxidized poly(styrene-*b*-butadiene-*b*-styrene) (SBS) as templating agent and modified with azo-benzene groups were also studied for the development of multifunctional advanced thermosetting materials with distinct optical properties [136].

Similarly, the polystyrene-*block*-poly(ε-caprolactone)-*block*-poly-(n-butyl acrylate) (PS-*b*-PCL-*b*-PBA) triblock copolymer is also used as templates for the nanostructured epoxy resins by a double reaction induced microphase separation mechanism involving PBA and PS blocks. Depending on the concentration of the triblock copolymer, several types of nanophases are formed in the thermosets. At higher content of the triblock copolymer, these nanophases are found to be arranged in the lamellar lattice. Thermal analysis have shown that the formation of nanostructures in the thermosets have caused a part of poly(ε-caprolactone) sub-chains to demix from the epoxy matrix with the occurrence of curing reaction. The fractions of demixed PCL blocks can be estimated according to the T_g-composition relation of the model binary blends of epoxy and PCL [137]. For instance, DSC thermograms of the control epoxy, PS-*b*-PCL-*b*-PBA, and their thermosetting blends are shown in Figure 2.36.

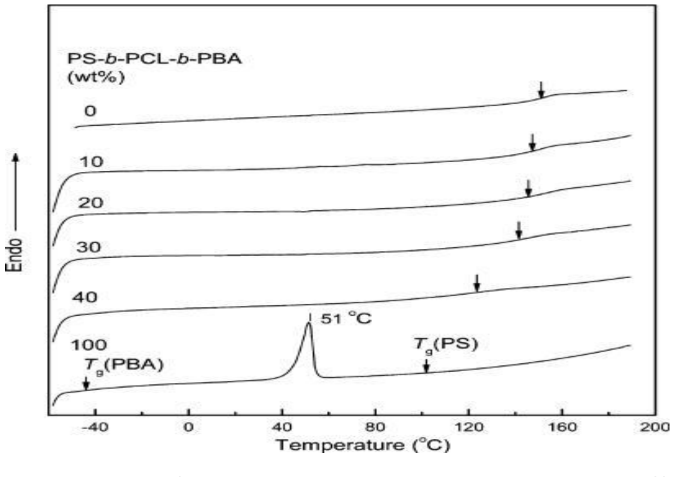

Figure 2.36: DSC thermograms of control epoxy, PS-*b*-PCL-*b*-PBA and different wt-% of their nanostructured blends [137].

The glass transition temperature (T_g) of the control epoxy is about 151 ^{o}C. In the DSC curve of PS-*b*-PCL-*b*-PBA triblock copolymer, a sharp melting transition at ~51 ^{o}C and two glass transitions are displayed at about -60 and 90 ^{o}C, respectively. The melting transition was attributed to the crystalline PCL block, whereas the glass transitions are responsible for the PBA and PS blocks, respectively [137]. The fact that the melting transition of PCL block appeared prior to the glass transition of PS block indicates that the triblock copolymer is microphase separated. It can also be noted that all the thermosets investigated do not exhibit the melting transition of PCL block which suggests the PCL blocks to be trapped in the epoxy networks and become no longer crystalline, *i.e.* the PCL block are miscible with the epoxy networks. The miscibility is further substantiated by the depression in the glass transition temperatures (T_gs) of epoxy rich phases (Figure 2.36). The T_g value of epoxy matrix can be employed to evaluate the mixing status of the PCL block with epoxy matrix [137].

On the contrary, the formation of the nanostructures follows the mechanism of self assembly. The static contact angle measurements have indicated that the nanostructured thermosets containing poly(2,2,2-trifluoroethyl acrylate)-*block*-poly(ethylene oxide) (PTFEA-*b*-PEO) diblock copolymer can display a significant enhancement in surface hydrophobicity as well as a reduction in the surface free energy. The improvement in surface properties can be recognized as the enrichment of fluorine containing sub chain (*i.e.*, PTFEA block) of amphiphilic diblock copolymer on the surface of nanostructured thermosets [138]. Also, Hu and Zheng [139] have reported the epoxy thermosets containing polysulfone-*block*-polydimethylsiloxane (PSF-*b*-PDMS) multiblock copolymer that possesses the microphase separated morphological structures. Depending on the content of the PSF-*b*-PDMS multiblock copolymer, the spherical particles with the size of 50–200 nm in diameter were dispersed into the continuous epoxy matrices which have shown to improve the thermomechanical properties and surface hydrophobicity [139]. Additionally, Zhang *et al.* [140] have also investigated the reaction induced phase separation of epoxy/4,4-diaminodiphenyl sulfone (DDS)/polysulfone (PSF) blend. At the higher glass transition temperature and higher molecular weight, PSF behaved as a slow dynamic component during the phase separation process. Interestingly, they explained the asymmetric properties and dynamically asymmetric phase separation mechanism between the components at elevated temperature [140]. In another way, Ocando and co-workers [40] also showed the different mechanisms involved through morphology development depending on the content of epoxidized polybutadiene (PBep) in the initial mixture and improvement in the thermomechanical properties.

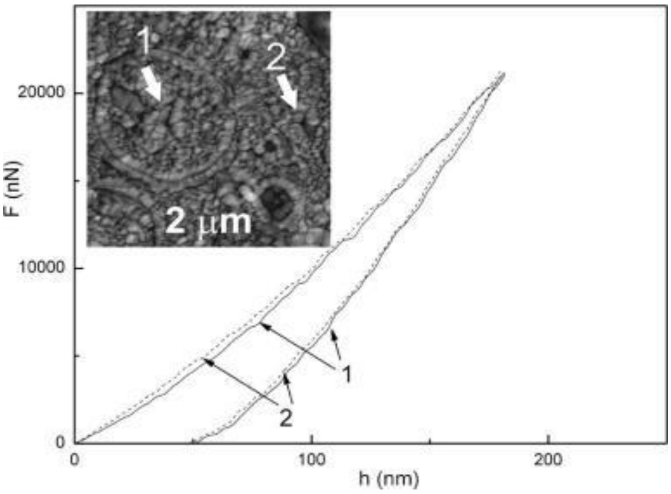

Figure 2.37: Force-indentation plots of 10 wt.-% of 22 mol.-% eSB50 (2) having mol. wt. 80 000 g/mol with epoxy, inside (1, solid line) and outside of the vesicles (2, dashed line). Inset shows AFM phase image [40].

Figure 2.37 shows a nanoindentation analysis using the AFM technique which was carried out on both inner and outer (1, solid line and 2, dashed line in Figure 2.37) regions of a vesicle shell for the 10 wt% SB50(2) (mol. wt. = 80000 g/mol.) and epoxidation degree of 22 mol.-% with the epoxy mixture. The force-indentation curves of both the phases shows similar stiffness which has confirmed their similar composition based on epoxy matrix [40].

Furthermore, Akiyama *et al.* [141] have investigated the phase behavior of poly(styrene-*b*-isoprene-*b*-styrene) (SIS)/tackifier resin blends by thermal analysis, morphological observation, and cloud point measurements. It was found that the blends showed lower critical solution temperature (LCST) phase transition and upper critical solution temperature (UCST) phase transition and the properties of pressure sensitive adhesion [141]. Further explanation of LCST and UCST are also given in the phase diagram for polymer blends earlier in the section 2.1. In addition, Soares and coworkers [142] used the liquid polybutadiene functionalized with isocyanate groups to develop a nanostructured epoxy network. It is important to note the unique combination of toughening properties and higher Young's modulus achieved in these modified thermosets without affecting the T_g. These results open several possibilities for the applications in important fields that require thermoset materials with a combination of toughness, stiffness, and high glass-rubber transition temperature [142]. A summary of morphology of epoxy resin/block copolymer blend systems are given in Table 2.2

Table 2.2: A summary of morphology of epoxy resin/block copolymer blend systems investigated in the literatures

Basic polymer	Hardener	Morphology	Ref
SSEBS-c-PCL	MDA	core−shell model	114
BIx*n* and MG-I	MDA	hexagonal cylindrical morphologies	132
PE-*b*-PEO	MDA	spherical micellar phasemorphology	133
PS-*b*-PB-*b*-PMMA	MCEDA	spheres on spheres"morphology and core- shell	125, 134
SBS	N-aminoethylpiperazine	larger micellar	135
SBS	MCDEA	spherical micellar morphology	136
PS-*b*-PCL-*b*-PBA	4,4'-Methylenebis(2-chloroaniline) (MOCA)	worm-like to well-defined lamellar based on increase in composition	137
PTFEA-*b*-PEO	MOCA	microphase-separated morphology i.e., the nanostructures	138
PSF-*b*-PDMS	DDM	spherical particles	139
PSE	DDS	layered structure formation	140
liquid polybutadiene	triethylene-tetramine (TETA)	nanoscopic structure	142
PEO-PPO and PEO-PPO-PEO	MDA	nanoscopic phase separation	143

In the same way, molecular dynamics and morphology were further investigated by Mojivic *et al.* [143] in epoxy blend with poly(ethylene glycol-co-propylene glycol) (PEO-PPO) and poly(ethylene glycol)-*block*-poly-(propylene glycol)-*block*-poly(ethylene glycol) (PEO-PPO-PEO). Also, a similar study was carried out by Serrano *et al.* [144] in epoxy resin modified with an epoxidized poly(styrene-*b*-butadiene) (SepB) linear block copolymer.

A nanostructure-mechanical property correlation in toughening epoxy with block ionomer complexes was explained by Wu and coworkers [114]. They established the correlations between nanostructure parameters and fracture toughness which have provided a fundamental understanding of nanostructure toughening of thermosets *via* an innovative strategy based on block ionomer complexes [114].

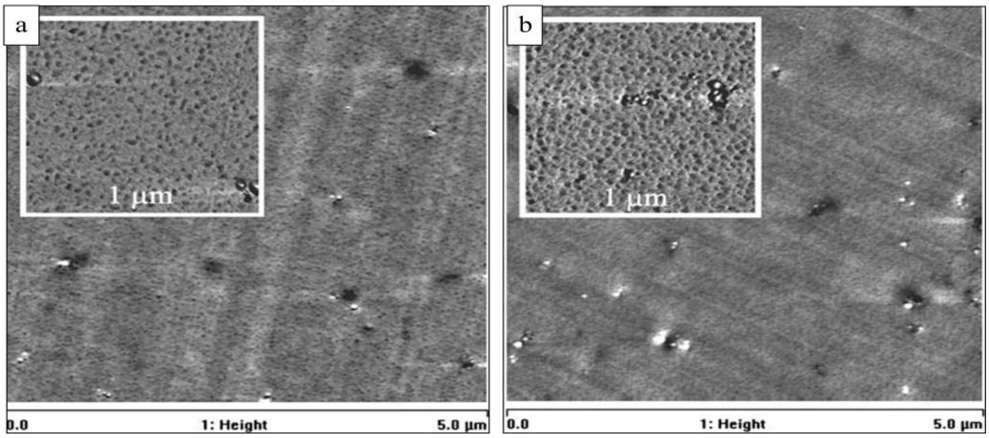

Figure 2.38: Tapering mode–AFM height micrographs of: a) 1 wt % Al_2O_3 with 48 mol.-% eSBS and b) 3 wt % Al_2O_3 with 44 mol.-% eSBS. Inset showing the phase image [145].

In addition, Ocando *et al.* [145] have studied the effect of addition of (1 wt.-% and 3 wt.-%) alumina nanoparticles (Al_2O_3) to epoxy modified by poly(styrene-*b*-butadiene-*b*-styrene) (SBS) epoxidized triblock copolymer. Homogeneous dispersion of Al_2O_3 nanoparticles in the epoxy matrix containing polystyrene (PS) microphase separated nanodomains are shown by composites of TM-AFM image in Figure 2.38. Though the Al_2O_3 nanoparticles were added in the epoxy blend, it did not affect the glass transition temperature. Well dispersed Al_2O_3 nanoparticles in the nanostructured epoxy systems based on epoxidized SBS triblock copolymer allowed an increase in the fracture toughness though maintaining the transparency and stiffness of the neat epoxy [145]. Tercjak and coworkers [146] have prepared and characterized microphase separated epoxy-based materials modified with an amphiphilic poly(styrene-*b*-ethylene oxide) diblock copolymer (PS-*b*-PEO). The microphase separated materials for a high range of PS-*b*-PEO contents showed the morphologies changing from spherical micelles to long wormlike micelles on passing through vesicles upon increasing the copolymer amounts. In the case of 20 wt.% inorganic/organic epoxy-based materials, location of nanoparticles in PEO-block/epoxy-rich phase confined between the two microphase separated PS-block-rich phases and thus designed a highly transparent multiphase materials possessing interesting specific properties, such as high UV shielding efficiency and high water repellence [146].

Similarly, Kosmidou *et al.* [147] have studied the structural, mechanical, and electrical characterization of epoxy-amine/carbon black nanocomposites in which the low dielectric constant below the filler content of 1% w/w indicates clearly that no cluster formation takes place; and this filler content separates, in fact, the dispersed and the agglomerated state of nanoparticles. Song *et al.* [148] investigated the enhanced thermal conductivity of epoxy–graphene composites by using non-oxidized graphene flakes with non-covalent functionalization. Similarly, Teng *et al.* [149] showed the thermal conductivity and structure of non covalent functionalized graphene/epoxy composites. Moreover, Tang *et al*. [150] have investigated the effect of graphene dispersion on the mechanical properties of graphene/epoxy composites.

CHAPTER - 3

3. MATERIALS AND METHODS

3.1. Materials

3.1.1 Block copolymers

Polystyrene-*block*-polybutadiene-*block*-polystyrene (SBS) block copolymers having different molecular architectures (triblock and star block copolymers) and polystyrene-*block*-polybutadiene (SB) diblock copolymer were used as the materials for the entire research. Figure 3.1 presents the general structure of the SBS triblock copolymer.

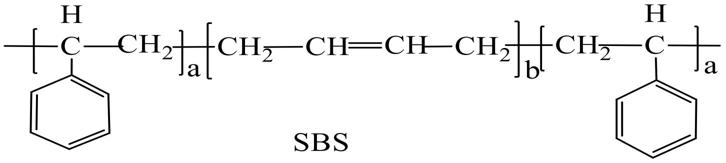

Figure 3.1: Scheme of polystyrene-*block*-polybutadiene-*block*-polystyrene (SBS) triblock copolymer; ***a*** and ***b*** are degrees of polymerization of polystyrene and polybutadiene, respectively.

The block copolymers were received from R. Bening, Kraton Polymers, Houston, TX (USA). The characteristics of each block copolymer along with their notations are presented in Table 3.1.

Table 3.1: Characteristics of block copolymers sample code, architecture, butadiene content in wt.-% and molar mass (g/mol)

Sample code	Architecture	Butadiene (wt.-%) *	Molar mass (g/mol)**	M_w/M_n^{ϕ}
$(SB)_X$	Star block	70	120,000	1.01
SBS	Triblock	50	91,000	1.01
SB	Diblock	52	56,000	1.01

* Butadiene content (wt-%) determined by Weij's titration

** Number average molar mass determined by gel permeation chromatography by polystyrene standard

$^{\phi}$ Polydispersity index where M_w and M_n are weight-average molecular weight and number-average molecular weight

The structures of each block copolymer used in experiment are given in Figure 3.2.

Figure 3.2: Schematic structure of a) star block copolymer $(SB)_X$, b) linear triblock copolymer (SBS) and c) diblock copolymer (SB); the outer solid lines represent the polystyrene chains.

3.1.2 Epoxidizing agents

The block copolymers indexed in Table 3.1 were subjected to epoxidation reaction using different reagents such as 3-metacholoperoxy benzoic acid (MCPBA), performic acid (PFA), peracetic acid (PAA) and hexafluoro isopropanol (HFIP) with phenyl arsonic acid (catalyst) as sketched in Figure 3.3

a) 3-metachloroperoxy benzoic acid

b) Performic acid

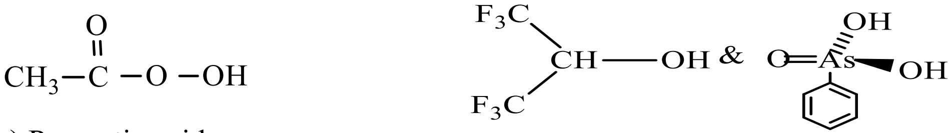

c) Peracetic acid

d) Hexafluoroisopropanol Phenylarsonic acid

Figure 3.3: Structures of a) 3-metacholoroperoxybenzoic acid, b) performic acid, c) peracetic acid and d) hexafluoro isopropanol and phenylarsonic acid, which were used for the epoxidation of the copolymers.

3.1.3 Epoxy resin systems

The chemicals used for preparing epoxy resin systems were, diglycidyl ether of bisphenol-A (DGEBA) resin and methylene dianiline (MDA) as hardener. The structure of these chemicals used is shown in the Figure 3.4.

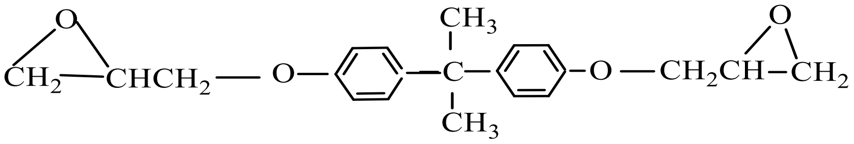

a) Diglycidyl ether of bisphenol-A (DGEBA)

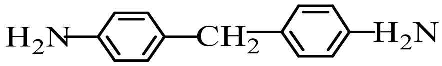

b) Methylene dianiline (MDA)

Figure 3.4: Structures of a) diglycidyl ether of bisphenol-A (DGEBA) and b) methylene dianiline (MDA); the components used to prepare epoxy resin systems.

The molecular weight and epoxy value of the DGEBA was 340.41 g/mol and 170.20 respectively, as per information from the data sheet of the supplier (Sigma Aldrich Ltd. Germany). Likewise, the molecular weight of MDA was 198.27 g/mol.

3.1.4 Other chemicals

Dicholoromethane (99%), sodium bicarbonate ($NaHCO_3$), sodium sulphate (Na_2SO_4), potassium iodide/starch paper, toluene (99%), formic acid (85%), polyethelene glycol (PEG-400), hydrogen peroxide (30%-w/v), methanol (99.5%), and chloroform (99%) were used. Unless otherwise mentioned, all the chemicals were purchased from Sigma-Aldrich Ltd., Germany and were used without further purification.

3.1.5 Nanofillers

The nanoparticles - boehmite (Disperal OS2) and layered silicate (Nanofil 5) - were supplied by Sasol Chemicals (Hamburg, Germany) and Süd-Chemie (Munich, Germany) respectively. The general chemical formula of boehmite is γ- AlO(OH) and layered silicate is $(Ca,Na,H)(Al,Mg,Fe,Zn)_2(Si,Al)_4O_{10}(OH)_2.nH_2O$ which were organically modified. The molecular structures of boehmite and layer silicate and their corresponding surfactants are sketched in Figure 3.5.

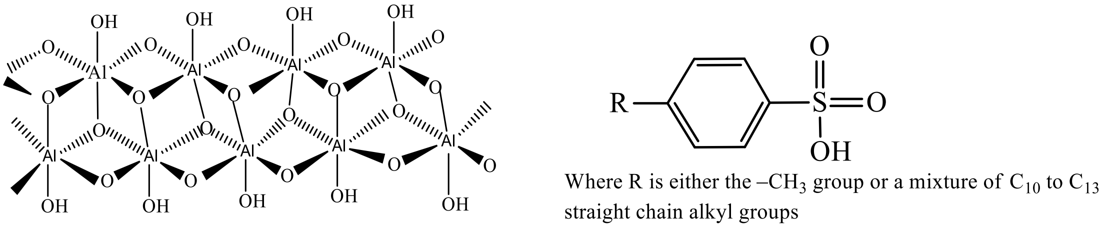

Where R is either the $-CH_3$ group or a mixture of C_{10} to C_{13} straight chain alkyl groups

a) Boehmite nanofiller structure

b) Alkyl benzenesulphonic acid

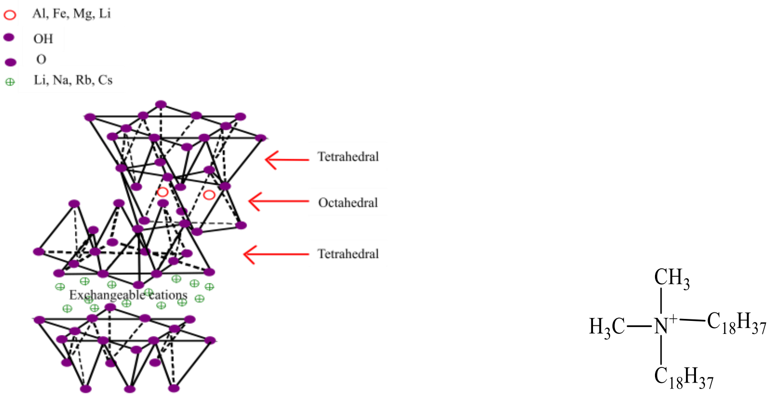

c) Structure of layered silicate (Nanofil 5) [151] d) Dimethyl dioctadecyl ammonium ion

Figure 3.5: The molecular structure of; a) boehmite nanofiller, b) alkyl benzenesulphonic acid boehmite surfactant c) layered silicate (Nanofil 5) and d) layered silicate surfactant.

3.2 Functionalization of Styrene/Butadiene Copolymers

The Styrene/butadiene copolymers, having double bonds in butadiene units, can be modified by different methods such as epoxidation, sulphonation, acrylation so as to introduce reactive functional groups into the polymer chain. For instance, the oxarine or epoxy group is introduced into the chain replacing the butadiene unit during epoxidation reaction which is the main technique of chemical functionalization employed in this work.

3.2.1 Preparation of epoxidized copolymer

The epoxidation of the styrene/butadiene copolymer was carried out by a) variation in degree of epoxidation, b) architecture of the copolymers and c) by utilizing different methods. The star block copolymers (namely $(SB)_X$, see Table 3.1) was epoxidized to various degrees following the standard procedure discussed in literatures [9,14,16].In a typical experiment, one gram of the $(SB)_X$ was dissolved in 25 mL dichloromethane and equivalent amount of 3-metachloroperoxy benzoic acid (MCPBA) was added slowly to solution at a temperature of 0 ^oC. The mixture was stirred thouroghly for one and half hour under argon atmosphere. The completion of the reaction was tested by the potassium iodide/starch paper. After the completion of the reaction, the mixture was filtered. The filtrate was extracted with saturated aqueous solution of sodium bicarbonate ($NaHCO_3$) and then dried with sodium sulphate (Na_2SO_4) solution and filtered. The organic portion of the solution was separated and the epoxidized copolymer was recovered by removing solvent in a rotary evaporator. Hence, the residue was dried. The epoxidation reaction is sketched in Figure 3.6. (detail of reaction mechanism in Appendix -1).

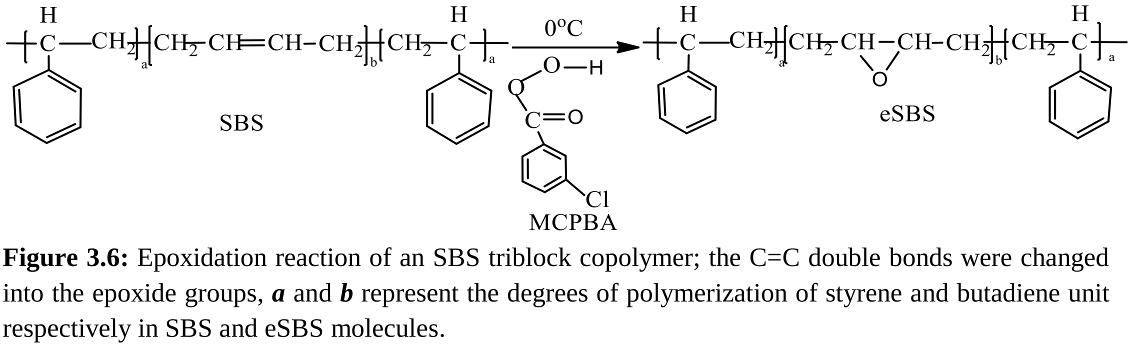

Figure 3.6: Epoxidation reaction of an SBS triblock copolymer; the C=C double bonds were changed into the epoxide groups, ***a*** and ***b*** represent the degrees of polymerization of styrene and butadiene unit respectively in SBS and eSBS molecules.

Further the star block copolymer $(SB)_X$ was epoxidized by using other methods *viz.*

using 3-metachloroperoxy benzoic acid (MCPBA), performic acid (PFA), peracetic acid (PAA) and hexafluoro isopropanol (HFIP) method in order to find the optimum method of chemical modification of the polymer. All these method use to common principle of the reaction between the butadiene units and peroxide (see Figure 3.7).

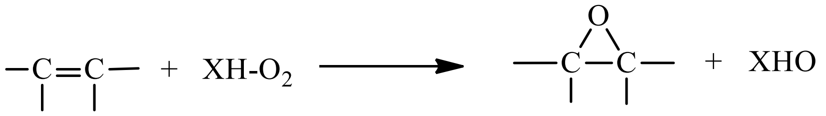

Figure 3.7: Scheme of epoxidation reaction of butadiene units in the block copolymer; the C=C double bonds were changed into the epoxide groups in presence of peroxide.

The steps involved in epoxidation using PFA and HFIP are illustrated in Appendix -2 and 3. The relevant samples prepared those ways are indexed in Table 3.2

Table 3.2: List of epoxidized copolymers prepared by different methods

S. N.	Sample Code	*Epoxidation degree (wt.-%)	Remarks
1	e$(SB)_X$-25	25	$(SB)_X$ star block copolymer epoxidized by MCPBA method to different degrees
2	e$(SB)_X$-50	50	
3	e$(SB)_X$-100	100	
4	e$(SB)_X$-50 (PFA)	50	$(SB)_X$ copolymer epoxidized by PFA method to 50 wt.-% epoxidation degree
5	e$(SB)_X$-50 (PAA)	50	$(SB)_X$ copolymer epoxidized by PAA method to 50 wt.-% epoxidation degree
6	e$(SB)_X$-50 (HFIP)	50	$(SB)_X$ copolymer epoxidized by HFIP method to 50 wt.-% epoxidation degree
7	e(SBS)-100	100	SBS linear triblock copolymer epoxidized by MCPBA method to 100 wt.-% epoxidation degree
8	e(SB)-100	100	SB diblock copolymer epoxidized by MCPBA method to 100 wt.-% epoxidation degree

*Targetted epoxidation degree is in terms of weight percent of butadiene chains present in parent block copolymer $(SB)_X$.

The epoxidized samples are denoted by adding suffix ‘e’ in each sample notation. For instance, epoxidized versions of $(SB)_X$ with the epoxidation degree of 25, 50 and 100 wt.-% of total polybutadiene will be denoted by e$(SB)_X$-25, e$(SB)_X$-50 and e$(SB)_X$-

100 respectively. The PFA, PAA and HFIP methods of epoxidation to $(SB)_X$ in 50 wt.-% epoxidation degree will be represented by $e(SB)_X$-50 (PFA), $e(SB)_X$-50 (PAA) and $e(SB)_X$-50 (HFIP) respectively. Similarly, for the copolymer of architecture variation, the epoxidized sample of $(SB)_X$ star block, SBS triblock and SB diblock in 100 wt.-% epoxidation degree will be denoted by $e(SB)_X$-100, e(SBS)-100 and e(SB)-100, respectively (see Table 3.2).

The analysis of the epoxidation samples prepared by the different methods revealed that MCPBA worked as the best reagent for the targetted chemical modification. Hence, the method was extended to two linear architectures of block copolymers *viz* SB diblock and SBS triblock copolymers. The copolymers were epoxidized to 100% by MCPBA method; also indexed in Table 3.2.

3.2.2 Estimation of degree of epoxidation

The fraction of epoxy groups of selected epoxidized styrene/butadiene $e(SB)_X$ block copolymer was determined by the HCl-acetone (1:80 ratio by volume) method using direct titration method as per procedure described by Xie *et al.* [152]. The results are given in Table 3.3

Table 3.3: Determination of epoxy value by titration method [168]

Sample Code	Targetted epoxidation degree (%)	Epoxy value	Experimental epoxidation degree (%)
$(SB)_X$	00	0.00	-
$e(SB)_X$-25	25	0.185	18.5
$e(SB)_X$-50	50	0.355	35.5

The sample was prepared by the performic acid (PFA) method and the epoxy value was calculated by the equation:

$$E = \frac{(V_0 - V_1)\,X\,N}{10W} \quad \ldots\ldots\ldots\ldots\ldots\ldots\ldots.(3.1)$$

where, V_0 is the volume consumed by the blank solution during the titration and V_1 is the volume consumed by the $e(SB)_X$ sample solution, N is the strength of the methanolic NaOH solution, and W is the weight of the $e(SB)_X$ sample [152]. The real experimental value was less than the targetted epoxidation degree of block copolymer. It implies that the chemical used in the reaction could not epoxidize at the targetted level due to formation of the reduced amount of performic acid *in situ* preparation.

3.2.3 Fabrication of epoxy resin/e(SB)$_X$ blends

Diglycidyl ether of bisphenol-A (DGEBA) is a copolymer of thermosetting polymer and can be synthesized by the reaction of epichlorohydin and bisphenol-A as shown in Figure 3.8.

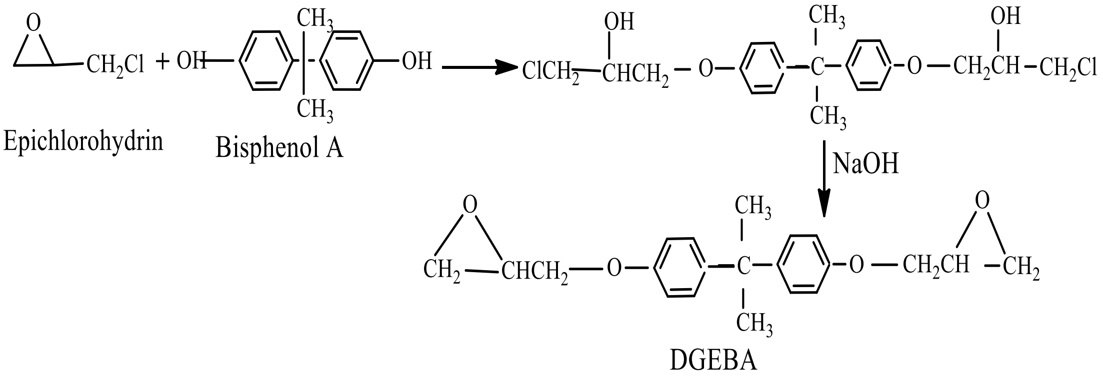

Figure 3.8: Scheme showing the formation of diglycidyl ether of bisphenol-A (DGEBA) by the reaction between epichlorohydin and bisphenol-A in presence of NaOH.

The epoxy system (EP) was a mixture consisting of diglycidyl ether of bisphenol-A (DGEBA) and methylene dianiline (MDA) as the aromatic amine hardener. Epoxy resins and hardener were mixed in stoichiometric amounts (2 mol of epoxy resin: 1 mol of hardener). In a typical experiment, 0.77 g of DGEBA was mixed with 0.23 g MDA to get 1 g cured product. The general reaction involved is given in Figure 3.9.

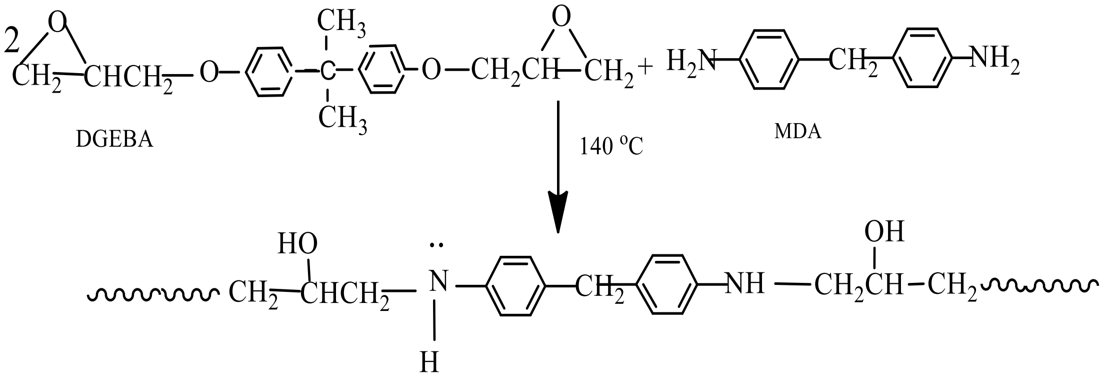

Figure 3.9: Scheme showing the reaction of diglycidyl ether of bisphenol-A (DGEBA) with methylene dianiline (MDA) leading to cross-linked structure.

The content comprising pure epoxy resin and methylene dianiline was poured into cylindrical Teflon molds and pre-cured at 80 °C for 12 hours followed by post-curing at 140 °C for another 12 hours.

The blends of epoxy system (EP) with epoxidized block copolymers were prepared. The epoxy resin/e$(SB)_X$ were prepared with different compositions. For instance, the EP/e$(SB)_X$ blends with weight ratio of 70/30, the following procedure was adopted. First, 0.54 g of DGEBA and 0.3 g e$(SB)_X$ components were dissolved separately in 25 mL of toluene. Then, both the solutions were mixed and the mixture wass heated to 110 °C for complete evaporation of the solvent. The residue was mixed together with 0.16 g of MDA and stirred well. As a result, highly cross-linked network-structured thermosetting blends were formed.

The content of the blends was poured into cylindrical Teflon molds (see Appendix-4) and pre-cured and post-cured as stated above. The reactions involved are illustrated in Figure 3.10. It should be, however, noted that the reactions presented are only schematic as the reactions of different epoxy groups and amine groups have random character.

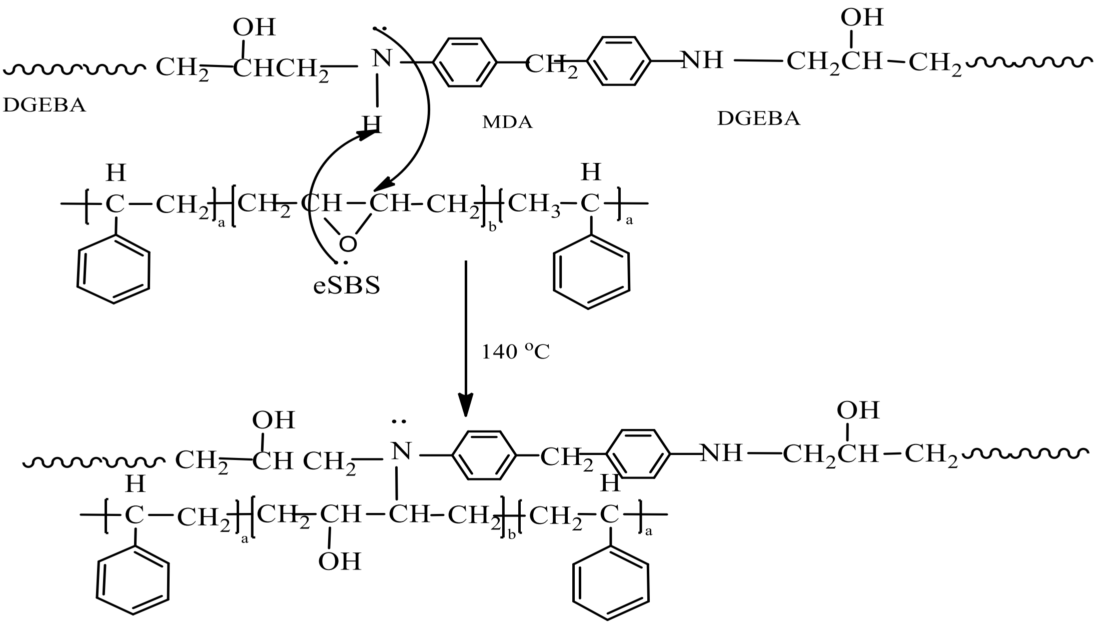

Figure 3.10: Scheme showing the reaction of diglycidyl ether of bisphenol-A(DGEBA) with methylene dianiline (MDA) and epoxidized block copolymer (eSBS).

For the preparation of nanocomposites, same procedure was repeated by adding 3 % by weight of boehmite (named as Disperal OS2) and layered silicate (Nanofil 5) separately to the mixture in the required proportion. The nanocomposites were also pre-cured in the vacuum oven at 80 °C for 12 hours followed by post curing at 140 °C for additional 12 hours. The samples prepared using above mentioned procedures are listed in Table 3.4.

Table 3.4: List of epoxy resin blends and nanocomposites; all cured at 80 ^{o}C and 140 ^{o}C for 12 hr and 24 hr respectively

S.N.	Sample Code	EP (wt.-%)	e(SB)$_X$ (wt.-%)	Disperal (wt.-%)	Nanofil 5 (wt.-%)
1	EP	-	-	-	-
2	EP/e(SB)$_X$-25 [70/30]	70	30	-	-
3	EP/e(SB)$_X$-50 [70/30]	70	30	-	-
4	EP/e(SB)$_X$-50 [85/15]	85	15	-	-
5	EP/e(SB)$_X$-50 [55/45]	55	45	-	-
6	EP/e(SB)$_X$-50 [40/60]	40	60	-	-
	Different architecture of copolymer				
7	EP/e(SB)$_X$-100 [70/30]	70	30	-	-
8	EP/e(SBS)-100 [70/30]	70	30	-	-
9	EP/e(SB)-100 [70/30]	70	30	-	-
	Different method of epoxidation				
10	EP/e(SB)$_X$-50 (PFA) [70/30]	70	30	-	-
11	EP/e(SB)$_X$-50 (HFIP) [70/30]	70	30	-	-
	Nanocomposites				
12	EP/OS	97	-	3	-
13	EP/LS	97	-	-	3
14	EP/e(SB)$_X$-25/OS [70/27/3]	70	27	3	-
15	EP/e(SB)$_X$-25/LS [70/27/3]	70	27	-	3
16	EP/e(SB)$_X$-50/OS [70/27/3]	70	27	3	-
17	EP/e(SB)$_X$-100/OS [70/27/3]	70	27	3	-

3.3 Characterization Techniques

3.3.1 Fourier transforms infrared (FTIR) spectroscopy

FTIR spectroscopy gives the information about the functional groups present in materials. The interactions of the molecules having different functional groups with the infrared radiation is displyed as the IR spectrum.

The FTIR spectra of the samples were recorded using a FTIR Affinity 2500, Schimadzu, Singapore, spectrometer in attenuated total reflectance (ATR) mode. The spectra were recorded in the range of 400-4000 cm^{-1} with a resolution of 20 cm^{-1}. This experiment was performed in University of Cologne, Cologne, Germany.

3.3.2 Electron microscopy

Both, the scanning electron microscopy (SEM) and transmission electron microscopy (TEM) were carried out in the Institute of Physics, Martin Luther University, Halle-Wittenberg, Halle, Germany.

Scanning electron microscopy

Scanning electron microscopy was used for the study of morphological features and deformation behaviour of the materials. For specimen preparation for SEM, a small notch was introduced into each specimen using a sharp blade. Then, sample was cooled under liquid nitrogen followed by fracture in the frozen state. Afterwards, each fracture surface was sputter coated with approximately 20-50 nm thin film of gold film. The thin film has two functions: avoid surface charging and irradiation damage.
The experiments were carried out by using scanning electron microscopy (JSM 6300, JEOL) employing secondary electrons (SE) mode.

Transmission electron microscopy

Transmission electron microscopy (TEM) was used to investigate the phase morphology of the specimens. The specimens from the bulk samples for transmission electron microscopy analysis were prepared by ultramicrotomy using a Leica UCT ultramicrotome equipped with diamond knife with cutting edge of 45^{o}. The ultrathin sections of approximately 70 nm thickness were prepared at a temperature of -100 ^{o}C. The sections were studied using a LEO912 TEM, operating at an acceleration voltage of 120 kV. Selective staining of butadiene phase of the sample was performed by osmium tetroxide (OsO_4) vapor.

3.3.3 Thermal methods

The materials were characterized by thermogravimetric analysis (TGA) and differential scanning calorimetry (DSC) techniques.

Thermogravimetric analysis

Thermogravimetric analysis (TGA) was used primarily for determining thermal stability of polymers. It was a technique for measuring the mass variation in a sample as a function of temperature under a controlled nitrogen atmosphere. The typical TGA curves are schematically given in Figure 3.11.

Mass loss against temperature of the TGA curve gives the information about the thermal stability of substance and maintains its properties as nearly unchanged as possible on heating. It also helps to determine the procedural decomposition temperature. Similarly, arepresentative DTG curve is also shown in Figure 3.11. For the sample preparation, a small piece of sample was cut by the blade. About 10-15 mg of the sample was kept in the aluminium trioxide (Al_2O_3) crucible for the measurement.

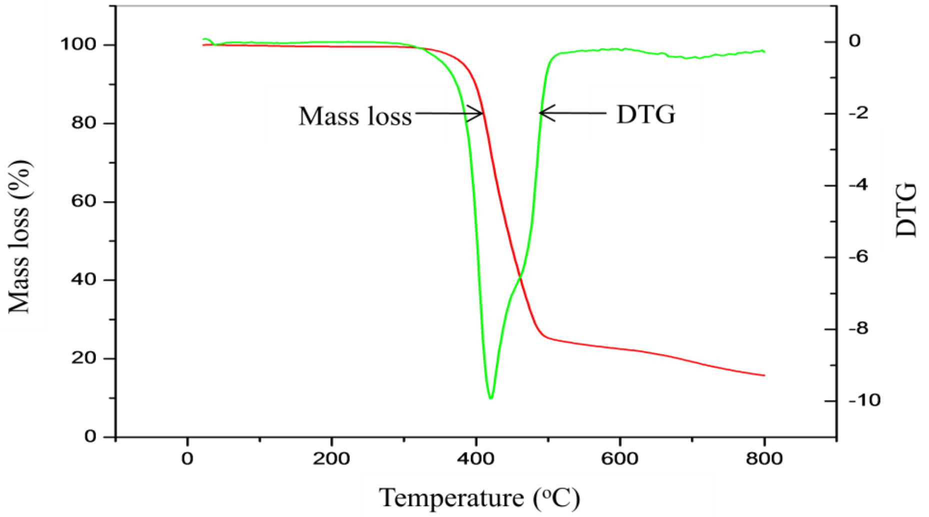

Figure 3.11: Schematic representation of thermogaravemetric analysis (TGA) curves of mass loss and differential thermogram (DTG).

In this study, thermogravimetric measurements of the samples were performed by using Netzsch TG 209 balance (Germany) under nitrogen atmosphere from 80 °C to 800 °C at a heating rate of 10 °C/min. The sample was ignited under nitrogen gas flow in 2 ml/min. This experiment was performed in University of Rouen, France.

Differential scanning calorimetry

Differential scanning calorimetry (DSC) was used to study the glass transition temperatures (T_g) of the samples which gives information about interaction among the blend composites components.

About 10 mg specimens were weighed in a Mettler Toledo MX5 precision balance to resolution of 0.001 mg and reproducibility of ± 0.003 mg. The samples were crimped into aluminum pan/lid with an average mass of 45 mg.

TA DSC Q100 was used to perform these calorimetric analyser tests. This DSC measured the relative heat flow through the crimped sample pan with respect to an empty reference pan. For this experiment, only one calibration temperature was performed by using the melting temperature of Indium and the heating rate was 20 ^{o}C/min. For the study of glass transition temperature (T_g) and specific heat capacity (ΔCp) of the blends and composite, specimens were heated in two heating run from 20 to 200 ^{o}C. The DSC thermogram analysis was done by taking the second heating run temperature.This experiment was partially carried out in University of Rouen, France.

Further, the Glass Transition Temperature is a temperature taken to represent the temperature range over which the glass transition takes place. For the determination of the glass transition temperature (T_g), the midpoint temperature (T_m) of the plot represent the T_g as shown in Figure 3.12.

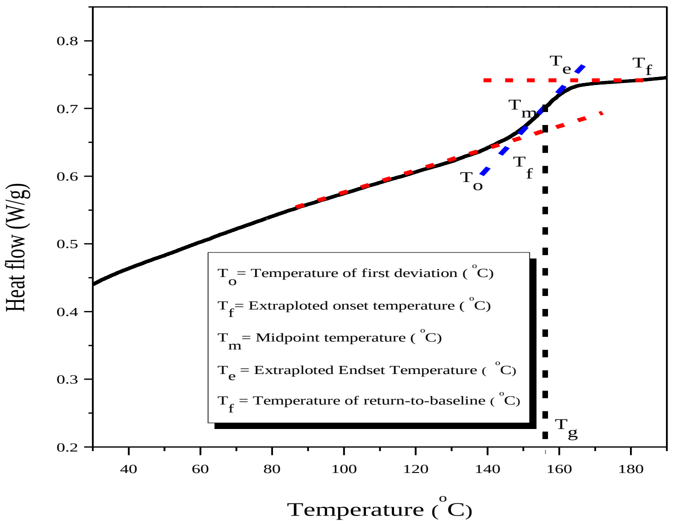

Figure 3.12: Schematic represents the measurements of glass transition temperature of the specimens.

After the calculation of T_g in a DSC experiment, heat capacity is measured as the absolute value of the heat flow, divided by the heating rate, and multiplied by a calibration constant.

Using the equation (2), the heat capacity can be calculated as:

$$^{dH}/_{dt} = Cp\left(^{dT}/_{dt}\right) \quad \text{or}$$

$$Cp = \left[\frac{dH/dt}{dT/dt}\right] x\, K \ldots\ldots\ldots\ldots\ldots\ldots\ldots\ldots\ldots\ldots\ldots\ldots\ldots..(3.2)$$

where K = calibration constant

3.3.4 Mechanical properties

The microhardness measurements were performed at 25 °C on a Fischerscope H100C recording microhardness testing machine (Helmuth Fischer Co., Germany) equipped with a pyramidal Vickers diamond indenter. The indenter was penetrated into the sample with the application of force up to 1000 mN. This technique comprises the continuous measurement of the load applied by an indenter as a function of its penetration depth. This measurement was done in Centre for Engineering Sciences, Martin Luther University, Halle-Wittenberg, Halle, Germany.

Load (*P*)–indentation depth (*h*) diagrams were measured at different locations on the samples up to a maximum load (P_{max}) of 1 N with a constant small loading rate of 50 mN/s similar to the unloading rate while applying the load (P) on the sample the indentation depth may reach up to given maximum depth (h_{max}). The meaning of the parameters measured to calculate the hardness and modulus can be found schematic representation of a P-h diagram (see Figure 3.13).

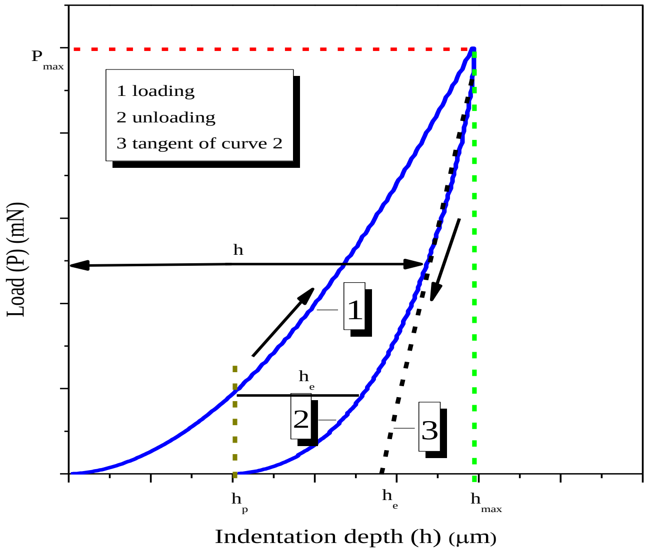

Figure 3.13: Schematic representation of Load (P)-indentation depth (h) diagram of the microindentation measurements [154].

The evaluation of these curves permits the determination of both plastic (W_{pl}) and elastic works (W_{el}) of deformation, different hardness parameters (such as Martens hardness, Vickers hardness, etc.) and the indentation modulus E_{IT} of the samples [153,154] (see Figure 3.13). In the Figure 3.13, the number 1, 2 and 3 represent the loading, unloading and tangent of curve respectively. For the determination of Martens hardness (HM), it is defined as:

$$\mathrm{HM} = {}^{\mathrm{F(h)}}\!/_{\mathrm{A_s(h)}} = {}^{\mathrm{F(h)}}\!/_{26.43\mathrm{h}^2} \quad \ldots\ldots\ldots\ldots\ldots\ldots (3.3)$$

where, $A_s(h)$ is the surface area of the indenter penetrating beyond the zero-point of the contact (force (F) in N, h in mm and HM in Nmm^{-2}). The corrected values of h corresponding to real shape of the indenter have been used to determine the Martens hardness (HM).

The elastic properties i.e. the values of the indentation modulus E_{IT} were determined using the equation (4).

$$\mathrm{E_{IT}} = \frac{1-\mathrm{v}^2}{0.5\sqrt{\frac{24.5}{\pi}\left(\frac{\mathrm{dh}}{\mathrm{dF}}\right)_{\mathrm{F_{max}}}\left(4\mathrm{h_{max}}-3\mathrm{F_{max}}\left(\frac{\mathrm{dh}}{\mathrm{dF}}\right)_{\mathrm{F_{max}}}\right)-8.73\times10^{-13}\,\mathrm{Pa}^{-1}}} \quad \ldots\ldots\ldots\ldots\ldots\ldots\ldots (3.4)$$

The term $8.73\mathrm{x}10^{-13}$ Pa^{-1} in equation (2) is the effective compliance of diamond. For the exact determination of the indentation modulus E_{IT}, one has to knowledge of the magnitude of Poission's ratio *v* of the material.

Furthermore, the elastic and plastic energy of deformation, U_{el} and U_{pl}, and the total energy of deformation $U_t=U_{el}+U_{pl}$ have been determined from the F–h diagrams (Figure 3.13).

Indentation plasticity

Indentation plasticity and scratch toughness or "load-bearing capacity" are, due to their operational simplicity, the two most widely used qualitative methods for determining the toughness. [155].

In a related approach, Fox-Rabinovich *et al.* [156] proposed the "microhardness dissipation parameter (MDP)" (see Figure 3.14) to express the plasticity in terms of he mechanical work done during different stages of indentation measurement, *i.e.*

$$\text{MDP} = \frac{\text{Plastic work}}{(\text{Plastic work} + \text{Elastic work})} \dots\dots\dots\dots\dots\dots\dots\dots..(3.5)$$

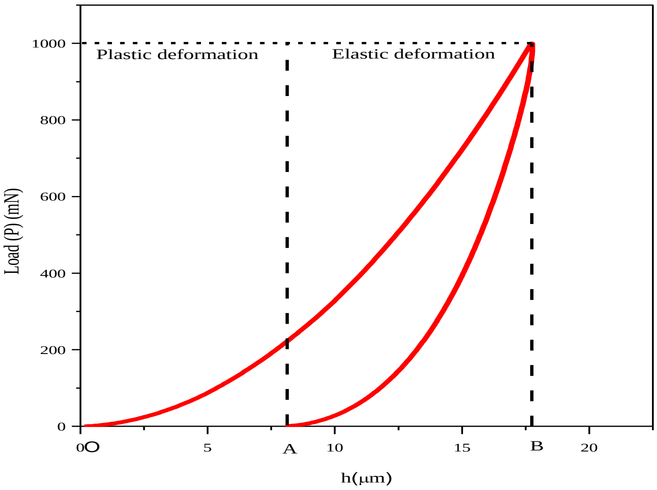

Figure 3.14: Schematic plot of a microindentation load–indentation depth curve. Plasticity is calculated as OA/OB=plastic work/ (plastic work + elastic work) [155].

However, plasticity is not toughness. Plasticity is the capacity to resist plastic deformation, while toughness measures the ability of a material to resist crack propagation. It is defined as the ratio of the plastic displacement divided by the total displacement in the load (P)–displacement (h) curve of a microindentation measurement. Mathematically, plasticity can be defined as:

$$\text{Plasticity} = \frac{\varepsilon_p}{\varepsilon} \dots\dots\dots\dots\dots\dots\dots\dots\dots\dots\dots\dots\dots\dots\dots\dots\dots\dots (3.6)$$

where, ε_p is the plastic deformation and ε is the total deformation [155].

CHAPTER – 4

4. RESULTS AND DISCUSSION

In this section, the overall characterization and analysis of the materials by applying the different techniques are discussed. Functionalization of block copolymers and functional group of blends are analyzed through Fourier transform infrared (FTIR) spectroscopy. The bulk morphologies of the specimens are studied *via* transmission electron microscopy (TEM). Similarly, the mechanical properties of the specimens are investigated by microindentation hardness technique. Further, the fracture surface morphology and deformation behavior are established using scanning electron microscopy (SEM). Besides, the discussion is mainly concentrated on the effect of degree of epoxidation of $(SB)_X$ copolymer, block copolymer's architectures, and methods of epoxidation of the block copolymers.

4.1 Spectroscopic Analyses

The first step in this work is based on the chemical modification of different kinds of block copolymers so that those could be compatible to the epoxy resin and generate nanostructures. The chemical functionalization of the block copolymer was first studied by FTIR spectroscopic analysis.

4.1.1 Effect of degree of epoxidation of $(SB)_X$ copolymer

As explained in the experimental section (section 3.2.1), the star block copolymer $(SB)_X$ was epoxidized to different extent.

Fourier transform infrared (FTIR) spectra of $(SB)_X$ compared to the chemically modified specimens with different extent of epoxidation (*i.e.* 25%, 50%, and 100%) are evaluated in Figure 4.1. The FTIR analyses of pure $(SB)_X$ and those treated to various degree of epoxidation demonstrated significant differences in their spectra. In Figure 4.1 (including the graphs in other figures also), the spectra have been shifted to make the comparison possible between $(SB)_X$ copolymers and epoxidized $(SB)_X$ copolymer in different degree of epoxidation, methods, and architecture of copolymers with their respective epoxidized specimens. Thus, the transmittance has been expressed in arbitrary unit (a.u.).

For the pure $(SB)_X$ copolymer, characteristic peaks centered at 966 cm^{-1} and 910 cm^{-1} can be clearly observed. These peaks correspond to the C-H bending vibrations of vinyl side chain (CH_2=CH-) and trans-1,4-polybutadiene, respectively [16].

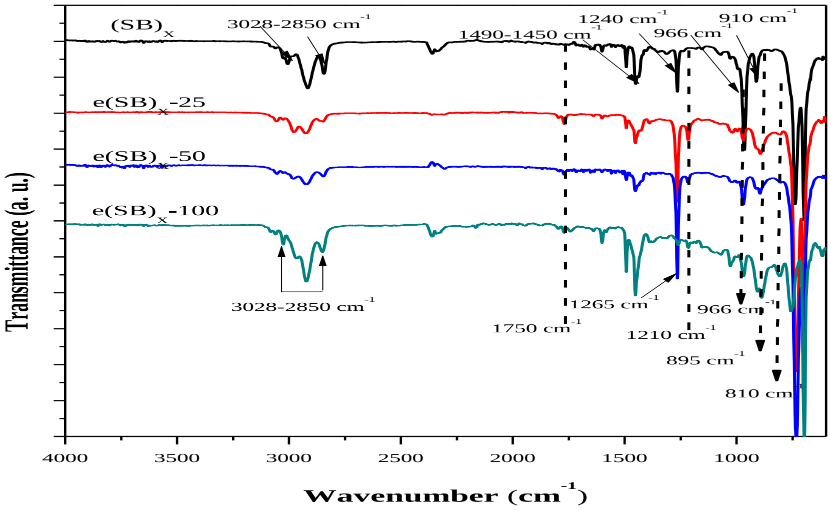

Figure 4.1: FTIR spectra of copolymers epoxidized to different degrees: black line = $(SB)_X$, red line = $e(SB)_X$-25, blue line = $e(SB)_X$ 50 and purple line = $e(SB)_X$-100 materials; the figures after $e(SB)_X$ denote the weight-% of butadiene units that have been epoxidized.

Further, the peak at 1240 cm^{-1} represents the in-plane bending of aromatic C-H bonds. Similarly, the peaks around 1450 cm^{-1} and 1490 cm^{-1} represent the C-H bending vibrations of CH_2 groups whereas those at 2850–3028 cm^{-1} correspond to the C-H stretching vibrations of CH_2 and CH_3 groups.

In addition, within the observed spectra of the specimens epoxidized to various degrees $e(SB)_X$, the peaks centered at around 810 cm^{-1}, 895 cm^{-1}, 1210 cm^{-1}, and 1265 cm^{-1} confirm the occurrence of epoxidation reaction. This is in agreement with the published data [9-11] where the peaks at 810 cm^{-1}, 895 cm^{-1}, and 1265 cm^{-1} have been assigned to the half stretching and whole stretching of epoxy rings, respectively. As expected, the intensity of those peaks increases with an increase in the degree of epoxidation implying that there is insertion of more and more epoxide groups to the doubly bonded C=C locations in the butadiene rich chains (see Figure 4.1). Furthermore, FTIR spectra of $e(SB)_X$ in the range of 800–1300 cm^{-1} reveals some interesting observations. The intensity of the peak around 966 cm^{-1} (corresponding to the C=C bond with *cis* conformation) decreases with increase in the degree of epoxidation which demonstrates that the epoxidation reaction is preferred at the *cis* position of the double bond. On the other hand, the intensity of the peak at 910 cm^{-1}

has completely disappeared indicating that the reaction is also favoured to the trans-double bond. Additionally, the peak centered at around 1210 cm^{-1} in epoxidized samples exhibits the formation of ether (-O-) linkages which is in accordance with the earlier studies [9-11, 156]. Likewise, the presence of absorption peak at 1750 cm^{-1} in the FTIR spectra of thus prepared $e(SB)_X$ samples implies the occurrence of side reactions leading to the formation of carbonyl (-CO) group.

Thus, from the above results, it is concluded that the $(SB)_X$ star block copolymers are easy to epoxidize to different degrees of epoxidation that complement the targeted yield. The peak intensity at 810 cm^{-1} and 895 cm^{-1} increases with increase in the degree of epoxidation. Further, the intensity of the peak at around 966 cm^{-1}, corresponding to the *cis* conformation of C=C double bond, decreases with increase in epoxidation thus indicating that the epoxidation reaction favoured at *cis* position of the double bond. The peak around at 910 cm^{-1} has completely disappeared which represents that the reaction is also preferred to the trans-double bond.

4.1.2 Effect of block copolymer architectures

It was also a matter of interest to investigate whether the block copolymer chain architecture has any influence on the morphology and properties of blends with epoxy resin. Thus, the Fourier transform infrared (FTIR) spectra of $(SB)_X$ star block copolymer are compared with SBS triblock copolymer and SB diblock copolymer. The results are presented in Figure 4.2.

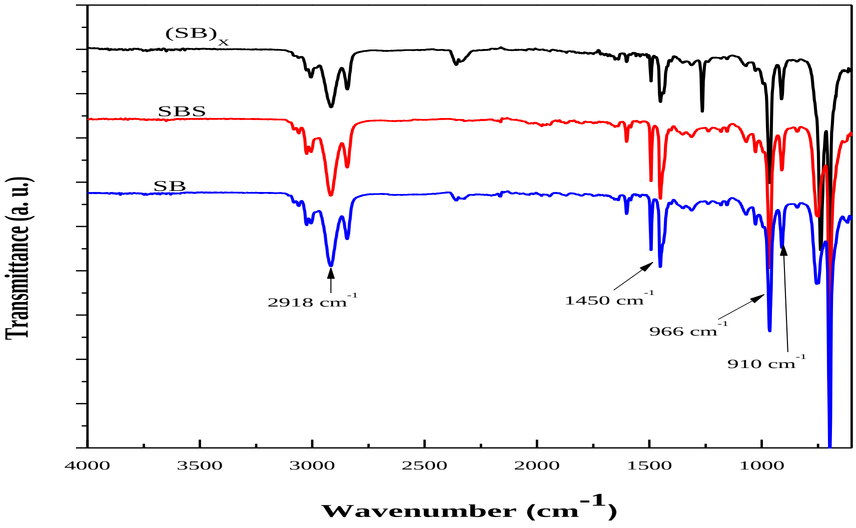

Figure 4.2: FTIR spectra of styrene/butadiene block copolymers samples having different molecular architectures; black line = $(SB)_X$, red line = SBS and blue line = SB.

The peaks around 910 cm^{-1}, 966 cm^{-1}, 1450 cm^{-1} and 2918 cm^{-1} which are typical of pure (SB)$_X$ (as mentioned in above section 4.1.1) are also observed in all the architectures of copolymers studied (see in Figure 4.2).

Further, it should be noted that the linear block copolymers like SBS and SB contains approximately 50% by weight of polybutadiene whereas (SB)$_X$ bears 70% (see Table 3.1). In Figure 4.3, the FTIR spectra of epoxidized (SB)$_X$, SBS, and SB copolymers are compared with those of the pure (SB)$_X$ star block copolymer.

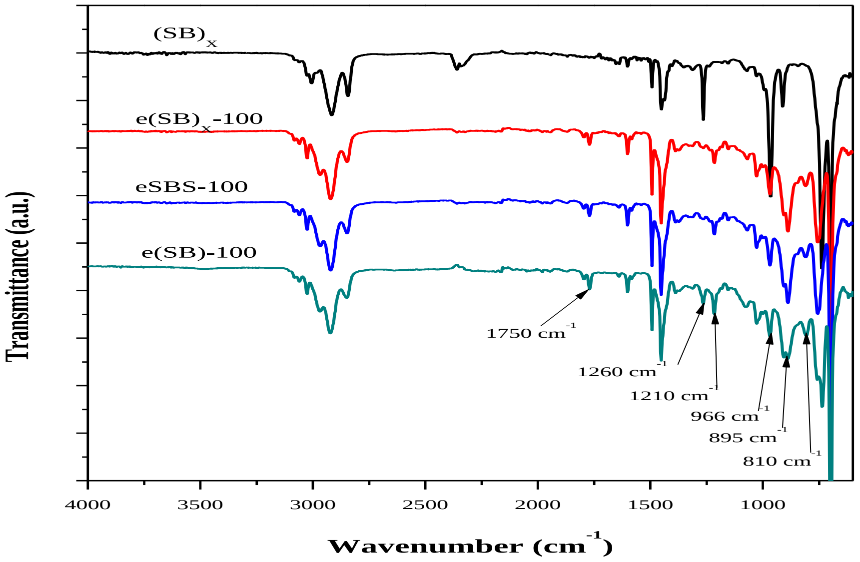

Figure 4.3: FTIR spectra of epoxidized styrene/butadiene of block copolymers having different molecular architectures; black line = SBS, red line = eSBS-100, green line = eSB-100 and blue line = e(SB)$_X$-100, with 100 wt.-% degree of epoxidation.

The epoxidized (SB)$_X$, SBS, and SB copolymers have been named as e(SB)$_X$-100, eSBS-100, and eSB-100, respectively. Besides the typical IR peaks for pristine (SB)$_X$, these epoxidized analogues show some new peaks as well; whereas some typical peaks have been disappeared too. The peaks centered around 810 cm^{-1} and 895 cm^{-1} are designated to the half epoxy group stretching whereas those around 1210 cm^{-1} and 1260 cm^{-1} are assigned to the whole epoxy ring stretching. Further, the peak around 1750 cm^{-1} is allocated for the carbonyl group (C=O) vibration. The results are further supported by the literatures [157-159]. For instance, earlier studies have shown that the peaks due to epoxy absorption are found at 810 cm^{-1}, 880 cm^{-1}, 1270 cm^{-1} and 1380 cm^{-1}. In addition, the absorption of carbonyl (C=O) group at about 1700–1740 cm^{-1} and hydroxyl (-OH) group at about 3200–3700 cm^{-1} are also reported. Similar results are also delineated by other studies as well [157-159]. These studies also outlined the presence of weak absorption peaks at 1725 cm^{-1} and 3500 cm^{-1} that correspond to the carbonyl group (C=O) and hydroxyl group (-OH), respectively. In fact, these observations imply the occurrence of side reactions during the epoxidation of block copolymers.

In summary, all the copolymer architectures were successfully epoxidized. It should also be noted that, as expected, the block copolymer architectures played no role in the chemical functionalization of block copolymer.

4.1.3 Effect of $(SB)_X$ epoxidized with different methods

The FTIR spectra of block copolymers epoxidized in different ways are compared with that of pure $(SB)_X$ polymer in Figure 4.4. The epoxidized copolymers (*i.e.* the $e(SB)_X$ samples) prepared by different methods such as *meta*-chloroperoxy benzoic acid (MCPBA), peracetic acid (PAA), hexaflouro isopropanol (HFIP), and performic acid (PFA) in 50% epoxidation degree are discussed.

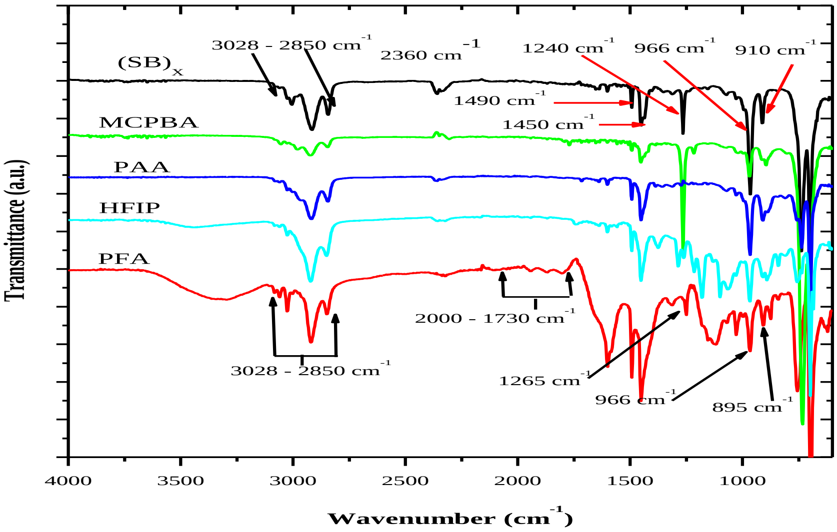

Figure 4.4: FTIR spectra of $(SB)_X$ copolymer compared with that of its epoxidized analogues modified by different methods; black line = $(SB)_X$, green line = MCPBA, blue line = PAA, pink line = HFIP and red line = PFA with 50% degree of epoxidation.

In the Figure 4.4, all the $(SB)_X$ copolymers epoxidized by different methods show similar remarkable peaks as indicated for the epoxidation that are previously shown in the FTIR spectra of Figure 4.1. Thus, the presence of these peaks confirms the success of the epoxidation of the block copolymer by different methods. However, it should be noted that the peak assignments to different functional groups are rather qualitative because they are not normalized for the quantitative comparison of the relative degree of epoxidation by different methods. Though, a quantitative study on epoxidation was carried out by Antonietti *et al.* [14] using FTIR spectroscopy in which better results were obtained for MCPBA in toluene.

On the whole, all the methods introduced in the experimental section were found to be suitable for the epoxidation of block copolymers. The HFIP method is noted to be the most time-effective whereas the PFA method the most cost-effective methods. However, the presence of some strange peaks around 950–1400 cm^{-1} range in the e(SB)$_X$ samples prepared by PFA and HFIP methods might account for the occurrence of side reactions. Thus, these methods are not quite optimal for the epoxidation of styrene/butadiene block copolymers. Yet, the MCPBA method was found to be the most suitable one in terms of time, cost, and ease of controlling reaction conditions.

4.1.4 *Epoxy blends analysis*

Fourier transform infrared (FTIR) spectra of epoxy resin (EP)/epoxidized block copolymers (EP/e(SB)$_X$-50) blends and neat epoxy resin are presented in Figure 4.5. Further, they are also compared with the FTIR spectra of epoxidized block copolymer, *i.e.* the (SB)$_X$ copolymer targeted to 50% epoxidation.

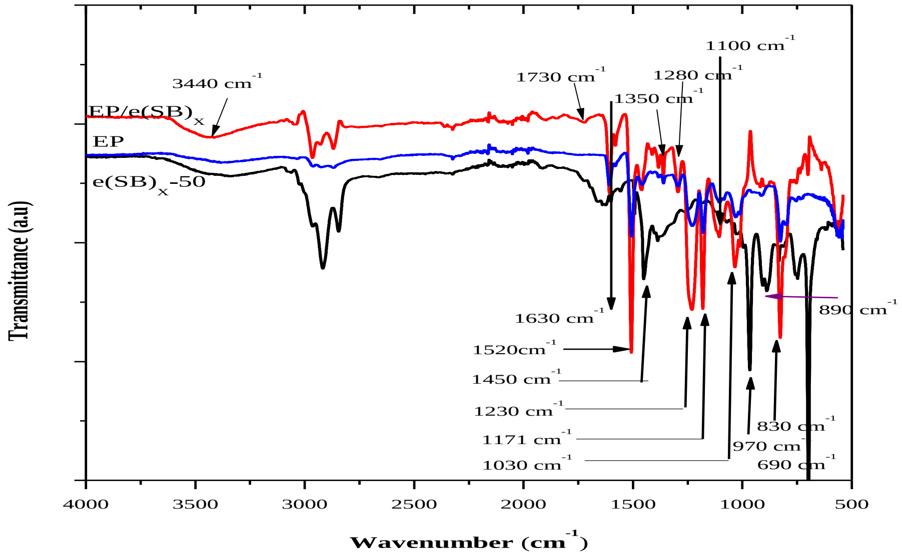

Figure 4.5: FTIR spectra of epoxidized copolymer, neat epoxy resin and EP/e(SB)$_X$-50 blend; black line = e(SB)$_X$-50, blue line = neat epoxy resin (EP) and red line = EP/e(SB)$_X$-50 blend.

In the FTIR spectra of epoxy resin, weak absorption signals in the range of 2864–2984 cm^{-1} (specific to the vibration of CH, CH_2, and terminal methyl groups) and 825–843 cm^{-1} can be attributed to the epoxy ring. The infrared (IR) bands characteristics of ester groups are located at 1280 cm^{-1}, 1230 cm^{-1}, 1170 cm^{-1}, and 1030 cm^{-1} which correspond to the stretching of C-O-C bond. On the other hand, a weak absorption peak at 1630 cm^{-1} observed in the cured epoxy resin is characteristic of non-conjugated double bonds of aromatic rings.

As it can be seen in the Figure 4.5, the absorption band belonging to the epoxide ring (970 cm^{-1} and 890 cm^{-1}) in e$(SB)_X$-50 almost disappears in the epoxy resin and EP/e$(SB)_X$-50 blend while the absorption band at 830 cm^{-1} is still present in both. This indicates that the epoxidized $(SB)_X$-50 reacts with methylene dianiline (MDA) and diglycidyl ether of bisphenol-A (DGEBA).

On the other hand, new bands with higher intensity appears in EP/e$(SB)_X$-50 blend in the range of 1030–1280 cm^{-1} and is assigned to the stretching of –C-O-C- group. Similarly, another broad peak appears at 3440 cm^{-1} which is characteristic of secondary OH and NH groups. Hence, the thus obtained results are the consequences of all the chemical reactions of the epoxy ring with amino groups. Similarly, a peak at 1350 cm^{-1} is assigned for the N–H bending and that at 1650-1500 cm^{-1} is for the N-H deformation in primary amines. However, in secondary amines, it is shifted towards lower wave numbers (1580- 1490 cm^{-1}) and is usually weak [159]. Also, a new signal typical of the carbonyl groups is present at 1730 cm^{-1} in the blend. Similar results were also reported in literatures [160-161]. According to some earlier studies [160-161], the peak around 830 cm^{-1} represents the stretching of C-O-C in oxarine group and that at 1030 cm^{-1}, 1170 cm^{-1}, 1230 cm^{-1}, and 1280 cm^{-1} corresponds to the stretching of C-O-C in ethers. Likewise, the IR band at 1350 cm^{-1} is assigned to N–H bending, and those at 1520 cm^{-1} and 1630 cm^{-1} are allocated to the stretching of carbon-carbon single (C-C) and double (C=C) bonds in aromatic rings, respectively. Also, some literatures have reported a signal at 830 cm^{-1} that is attributed to the aromatic ring of para-substituted benzene [160].

Thus, the peak intensity at around 1030–1280 cm^{-1} is accredited to the stretching of –C-O-C- group and that at 3440 cm^{-1}, appeared as a broad band, is assigned to the secondary OH and NH groups. Similarly, the IR band at 1350 cm^{-1} corresponds to the stretching of N–H bending and that in the range of 1650-1500 cm^{-1} is for N-H deformation in primary amines of the blend. This result is an effect of all the chemical reactions of epoxy ring with amino groups during the blend formation. Consequently, it provides an additional support for the proper cross-linking between the epoxy ring and the amino group in the blend.

To sum up, $(SB)_X$ star block copolymer is successfully epoxidized to their different degree of epoxidation. Fourier transform infrared (FTIR) spectroscopic study reveals a half stretching and full stretching of the oxarine group. Further, the study also indicated that the epoxidation reaction was favoured at *cis* position of the double bond.

Besides, all the architectures of block copolymers are also epoxidized successfully. However, it should also be noted that the copolymer architectures do not affect the epoxidation of block copolymer. Though all the methods were viable for the epoxidation of star block copolymers, the MCPBA method was found to be the most selective one in terms of time, cost and ease of controlling reaction conditions.

Similarly, the blends have also shown a good cross-linking between the epoxy ring and amino group. This result also indicates the effects of all the chemical reactions of epoxy ring with amino groups in the blend formation.

4.2 Morphological Analyses

After a successful epoxidation, the copolymers were used to prepare the blends for further analyses. In particular, bulk morphologies of the blends and some nanocomposites were investigated by transmission electron microscopy (TEM).

To begin with, the morphology of the blend of epoxy resin (EP) with pristine $(SB)_X$ copolymer is presented in Figure 4.6 with the help of optical and scanning electron micrographs. The EP/$(SB)_X$ composition of the blend was 70/30 by weight.

In the figure, the blend shows two phase morphology with segregation of the components into distinct layers. On the surface film, the $(SB)_X$ particles have diameter of approximately 5 µm as shown in Figure 4.6 (a). Similarly, in the bulk, the blend shows the phase morphology with widely separated structure of EP resin and $(SB)_X$ copolymer. In the observed micrograph (see Figure 4.6 a), there is a large region covered only with the EP resin and spherical $(SB)_X$ particles which are 2.5 µm to 5 µm in diameter.

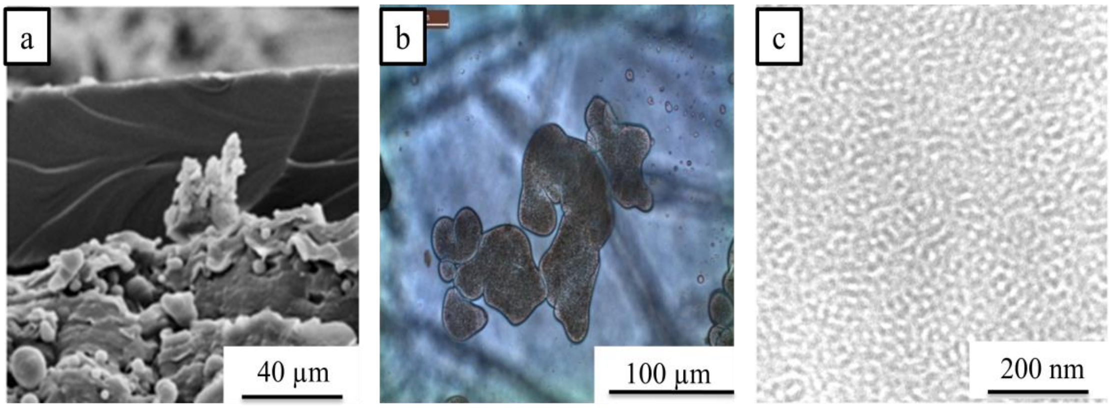

Figure 4.6: a) SEM micrograph of fracture surface morphology of EP/(SB)$_X$ blend, b) optical image of EP/(SB)$_X$ blend and c) TEM image of neat (SB)$_X$.

It is clear that the blend components in the observed samples are highly incompatible; a representative example of the incompatible polymer blends [47]. Thus, the strategy of modifying the block copolymer by chemical functionalization of the butadiene unit was adopted.

The surface of the blends shows incompatibility and phase segregation between the components (Figure 4.6a and b). This can also be observed in the optical micrograph in the Figure 4.6b which shows the phase separation of the epoxy resin and (SB)$_X$ block copolymer. Further, the TEM image of pure (SB)$_X$ shows the periodic nanostructure with cylindrical polystyrene (PS) (Figure 4.6c). This structure can be introduced into the epoxy resin as a template to generate nanostructure. For this reason, block copolymer can be chemically modified to enhance compatiblility and generate nanostructures in epoxy resin.

4.2.1 Morphological analysis by transmission electron microscopy

Transmission electron microscopy (TEM) was used to study the morphology of EP/block copolymer blends in detail. The sample preparation has been explained in section 3.3.2. Due to the selective staining of polybutadiene containing phase by OsO_4, it appears dark in TEM images while others remains bright.

4.2.1.1 Effect of degree of epoxidation of (SB)$_X$ copolymer

The TEM results obtained for blends of EP with (SB)$_X$ epoxidized to 25%, 50%, and 100% by weight of total butadiene in the copolymer (named as e(SB)$_X$-25, e(SB)$_X$-50 and e(SB)$_X$-100, respectively) have been discussed in this section. The EP/e(SB)$_X$ composition was set to 70/30 by weight. The reason for choosing a 70/30 composition is given below.

First, we were interested in investigating the maintained stiffness and enhanced toughness on the nanostructuring of the epoxy matrix; and, to the best of our knowledge, this ratio will able to maintain these properties. Second, our goal is to use low amount of toughening agent because most of the literatures deal with similar epoxy/toughner weight ratio [16,37-40]. The TEM images of a blend containing 70% by weight of EP and 30% by weight of: e(SB)$_X$-25, e(SB)$_X$-50, and e(SB)$_X$-100 are shown in Figure 4.7 a, b, and c, respectively.

In Figure 4.7a, the macrophase separation (*i.e.* the segregation of components in domains and several microns in diameter) can be seen distinctly in which 30 wt.-% of e(SB)$_X$-25 (the block copolymer was partially oxidized) acts as the matrix, whereas the 70 wt.-% of epoxy resin is embedded in it as large spherical particles whose diameter ranges from 2.5 µm to 6.5 µm (see Table 4.1). It is interesting to note that the inverted morphology is formed in the blend even at high content of epoxy resin; and it forms a dispersed phase in continuous copolymer matrix.

Further, the spherical and worm-like domains, approximately 25 nm in diameter as shown by histogram in Figure 4.7a (higher magnification), are polystyrene domains of the (SB)$_X$ block copolymer. Some of the particles are more than 30 nm thick which might be the droplets formed by epoxy resin (EP) and epoxidized block copolymer. It can be concluded that, even at low degree of epoxidation of the block copolymer (SB)$_{X,}$ there is a good compatibility between the block copolymer and the epoxy resin as demonstrated by the formation of dispersed phase by the majority component (*i.e.* epoxy resin) and appearance of polydisperse domains in the matrix.

Nevertheless, the compatibility was not sufficient for inducing nanostructures to the epoxy resin. As expected, the blend represented by morphology, depicted in Figure 4.7a, is translucent owing to the large size of the particles; much larger than the wavelength of visible light (λ = 400 nm to 600 nm).

On the other hand, alternation in the blend morphology changes the inverted phase for e(SB)$_X$-25-modified system to dominant microphase separation for e(SB)$_X$-50-modified system which seems to be in contrast with the increase of miscibility between epoxy resin and block copolymers with increase in the epoxidation reaction. Let us examine how the change in degree of epoxidation affects the morphology of the blends.

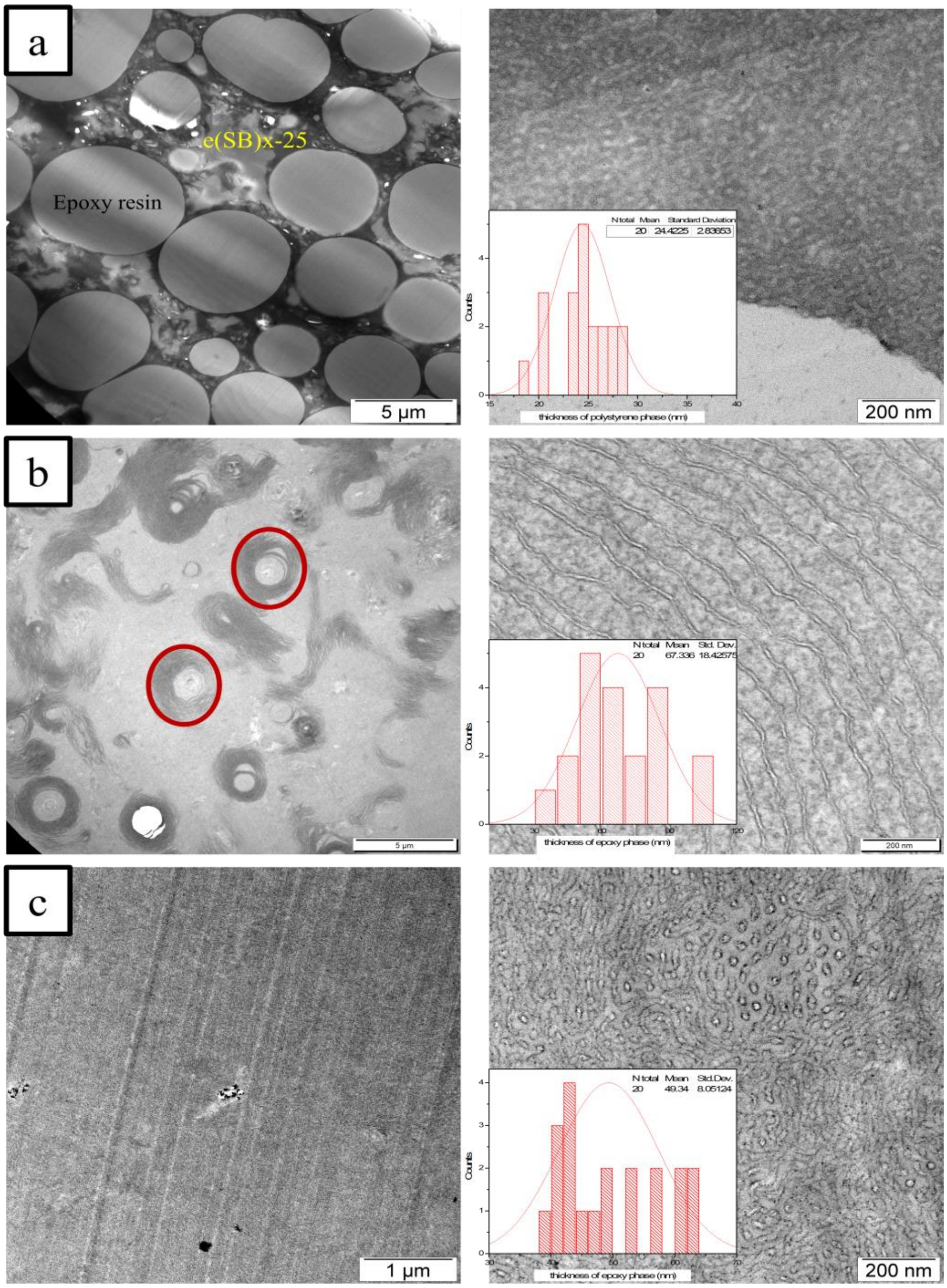

Figure 4.7: Left lower and right higher magnification of TEM images of blend of; a) epoxy resin/e(SB)$_X$-25, b) epoxy resin/e(SB)$_X$-50 and c) epoxy resin/e(SB)$_X$-100. Insets are the histogram of measurement of thickness of: a) polystyrene, and b) and c) epoxy phase in nm.

Here, Figure 4.7b represents the morphology of epoxy resin/e(SB)$_X$-50 blend in which the block copolymers were epoxidized to 50 wt.-% of the total polybutadiene. The morphology seems to change almost to the nanostructure at higher epoxidation level of the star block copolymer (SB)$_X$. Closer examination of the micrographs reveals that the blend has a nanostructured morphology over a large area (see low magnification TEM image of Figure 4.7b). The morphology resembles cylindrical morphology of the block copolymer [39]. Occasionally, lamella-like structure characterized by the onion-like patterns (shown by circles in Figure 4.7b) can also be observed.

Further, the cylindrical polystyrene (PS) microdomains of the block copolymer, which appear as thinnest layers in Figure 4.7b (higher magnification), are embeeded between the dark appearing layers of polybutadiene (PB) and epoxidized PB (ePB) layers. The PS and PB layers are approximately 15 nm and 10 nm, respectively (see Table 4.1). Also, the thickness of the PS layers (actually the PS cylinders) is in close agreement with that of the PS-domain of the block copolymer. There are much thicker (approximately 90 nm thick) layers of epoxy resin compatibilized by the epoxidized block copolymer. The thickness of these strands is approximately 70 nm (Table 4.1). Similar results were recorded by Serrano *et. al*. [38, 39] and Guo *et al*. [133] on their efforts to prepare nanostructured thermosetting systems using block copolymers.

On further increasing the degree of epoxidation of butadiene chain of the block copolymer, it is anticipated that the compatibility of the copolymer with the EP resin will be enhanced [16,33]. The block copolymer was fully epoxidized (i.e. to 100% by weight of butadiene) and blended with the epoxy resin with the same ratio to e(SB)$_X$ copolymer composition. For highest epoxidation degrees, the corresponding blends were transparent thus signifying the possibility of microphase separation and nanostructuring. The epoxidation of PB block improves the miscibility of the synthesized copolymers and the epoxy resin thus leading to nearly ordered nanostructures in blends. TEM images (see Figure 4.7c) clearly show how the morphology modifies to complete nanostructured blend at highest epoxidation level of the star block copolymer (SB)$_X$. The morphology appears to be PS cylinders as well as co-contineous like structure dispersed in epoxy matrix in the blend (see lower magnification TEM image of Figure 4.7c). The average diameter data of PS cylinders and thickness of epoxy phase are given in Table 4.1

Table 4.1: The average diameter of PS cylinders and thickness of epoxy phase in blend of EP/e(SB)x-25, EP/e(SB)x-50 and EP/e(SB)x-100

Sample code	Diameter of PS cylinders	Thickness of Epoxy phase
EP/e(SB)$_X$-25	25 nm	4.5 µm
EP/e(SB)$_X$-50	15 nm/10 nm PB phase	70 nm
EP/e(SB)$_X$-100	32 nm	50 nm

Moreover, the cylindrical polystyrene (PS) domains of the block copolymer, which appear as white clear cylindrical structure in Figure 4.7c (higher magnification), are found in dispersed phase in epoxy resin. Actually, the PS cylinders have approximately 32 nm in average diameter (see Table 4.1). The epoxy resin thickness (approximately 50 nm) in nanostructured EP/e(SB)$_X$-100 blend is almost similar to the copolymer domain in which epoxy resin is completely compatibilized by the epoxidized block copolymer. Similar results were reported by Serrano *et. al*. [16, 38, 39] and Occando *et al*. [37,40] on their work to prepare nanostructured thermosetting systems using block copolymers. It can be expected that such morphology plays a significant role to modify the thermal and mechanical properties of the blends (see in section 4.3).

Thus, it is clear from the above discussion that epoxidation level of the block copolymer is a key factor to generate nanostructures in epoxy resin. Higher the degree of epoxidation of the block copolymer, higher is the ease of formation of epoxide group (which are compatible to epoxy resin) and hence higher will be the degree of nanostructuring.

4.2.1.2 Effect of block copolymer architecture

After the discussion of the effects of degree of epoxidation on the morphology, we examined how the change in architecture of block copolymer affects the morphology of the blends. The blends of EP with various architecture of copolymers, namely (SB)$_X$, SBS, and SB epoxidized to 100% (by weight of total butadiene), is labelled as e(SB)$_X$-100, eSBS-100, and eSB-100, respectively. The result of EP/e(SB)$_X$-100 blend has been explained in the above section 4.2.1.1 (Figure 4.7c). Hence, only the results of EP/eSBS-100 and EP/eSB-100 blends are presented in this section.

In the frame of studying the effect of block copolymer architecture, TEM images of EP/eSBS-100 and EP/eSB-100 blends prepared by linear architecture of tri- and di-block copolymers are shown in Figure 4.8 (a and b). The morphology of the blends is found to be completely changed in their nanostructure at the highest epoxidation level of the linear tri- and di-block copolymer. Comprehensive study of the micrographs presented in Figure 4.8a exhibits that the morphology of the blend looks like lamellar structures in dark surface of epoxy phase (low magnification TEM image of Figure 4.8a). On the other hand, the TEM image of EP/eSB-100 blend in Figure 4.8b (lower magnification) shows the PS cylinders dispersed in epoxy phase. The morphology appears cylindrical with different length in both the blends.

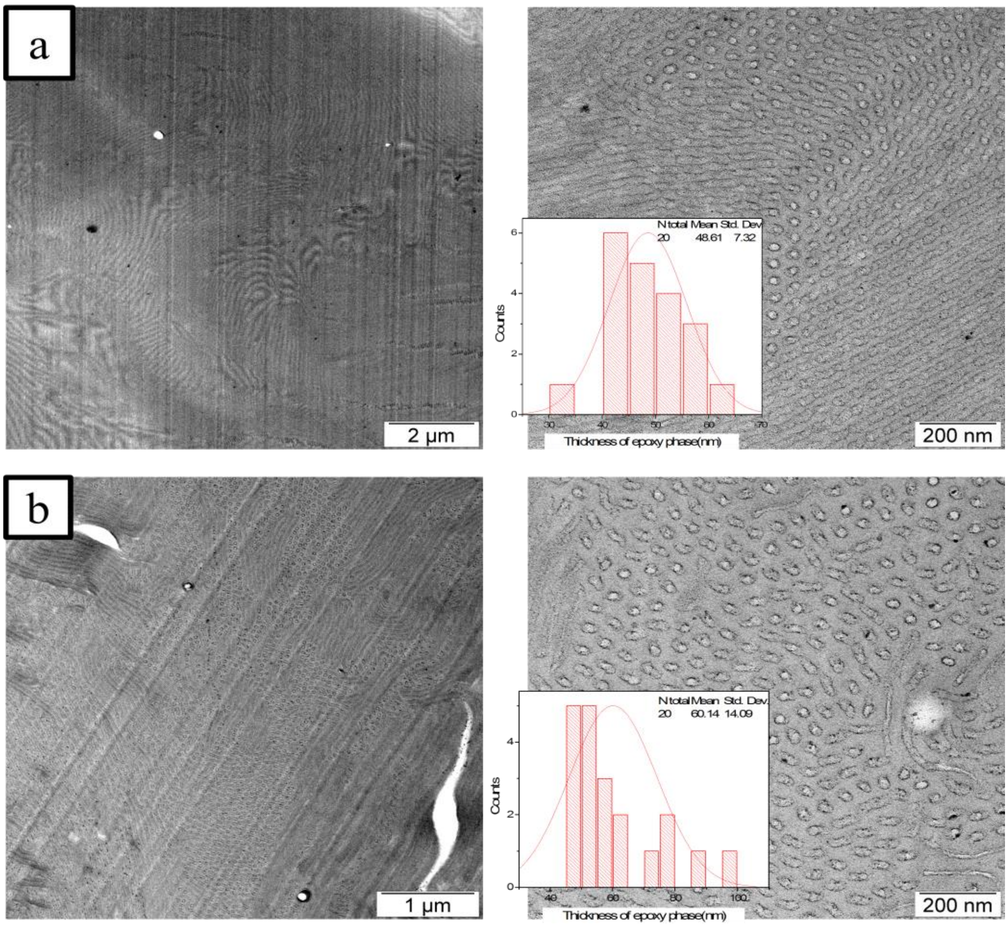

Figure 4.8: Left lower and right higher magnification of TEM images of blend of; a) epoxy resin/eSBS-100 and b) epoxy resin/eSB-100. Insets showing the histogram of measurement of thickness of epoxy phase in nm.

Further, for the highest epoxidation degree, a long-ordered cylindrical structure, similar to that shown for the EP/e(SB)$_X$-100 blend, can be clearly observed in EP/eSBS-100 and EP/eSB-100 blends (see higher magnification of Figure 4.8a and b). In general, the polystyrene (PS) domains size and thickness of the epoxy phase remains almost similar in all the architectures of the blend. However, the thickness of epoxy phase is slightly lower in both the EP/e(SB)$_X$-100 and EP/eSBS-100 blends compared to the EP/eSB-100 (see Table 4.2).

The observed result might be due to the diblock structure in architecture of SB copolymer. Moreover, at highest epoxidation degree, the PS domain size increases compared to that of the lower epoxidation degree. Similar findings were also reported in earlier studies [37-40], where the cylindrical PS domain size was about 33 nm in the highest epoxidation degree and distributed in a regular manner. These nanostructures of the blends also influence the thermal and mechanical properties which are discussed in the later section 4.3.

The average size of PS cylinders and thickness of epoxy phase are given in Table 4.2.

Table 4.2: The average size of PS cylinders and thickness of epoxy phase in different architecture of copolymer epoxy blends of EP/e(SB)x-100, EP/eSBS-100 and EP/eSB-100

Sample code	Diameter of PS cylinders	Thickness of Epoxy phase
EP/e(SB)$_X$-100	32 nm	50 nm
EP/eSBS-100	34 nm	49 nm
EP/eSB-100	33 nm	60 nm

All in all, the morphology of the blend completely turns into nanostructures by changing the architecture of block copolymer at fully epoxidized butadiene phase of the block copolymer. Only the nature of the nanostructures is moderately altered with the change in architecture of copolymer. It can be concluded that the copolymer architecture has slightly influenced the morphology of the blends with EP resin.

4.2.1.3 Effect of e(SB)$_X$ copolymer weight fraction

After the examination of the effect of architecture variation of block copolymer on the morphology of blends, we studied how the change in composition of e(SB)$_X$ affected the morphology of the blends. For this purpose, the block copolymer was epoxidized to 50% by weight of total butadiene. The EP/e(SB)$_X$-50 composition set to 85/15, 70/30, 55/45, and 40/60 by weight (labelled as EP/e(SB)$_X$-50 (85/15), EP/e(SB)$_X$-50 (70/30), EP/e(SB)$_X$-50 (55/45), and EP/e(SB)$_X$-50 (40/60), respectively) is discussed in this section.

Transmission electron micrographs of EP/e(SB)$_X$-50 blends in different compositions at higher and lower magnifications are presented in Figure 4.9 along with the corresponding histograms of thickness distribution of epoxy phase.

In EP/e(SB)$_X$-50 (85/15) blend, the macrophase separation morphology can be distinctly seen in between epoxy resin and e(SB)$_X$-50. Only 15 wt.% of e(SB)$_X$-50 is present in the blend which dispersed as matrix (Figure 4.9a). Epoxy resin (EP) is distributed in large spherical shaped structure in e(SB)$_X$-50; and few EP resins are also embedded in the nanosized structure in copolymer matrix (see higher magnification Figure 4.9a). The size of the EP phase in blend is ranging from approximately 350-1950 nm (see histogram of higher magnification in Figure 4.9a).

This size of EP phase indicates that the epoxy resins dispersed in various sizes are unable to form the ordered nanostructures.

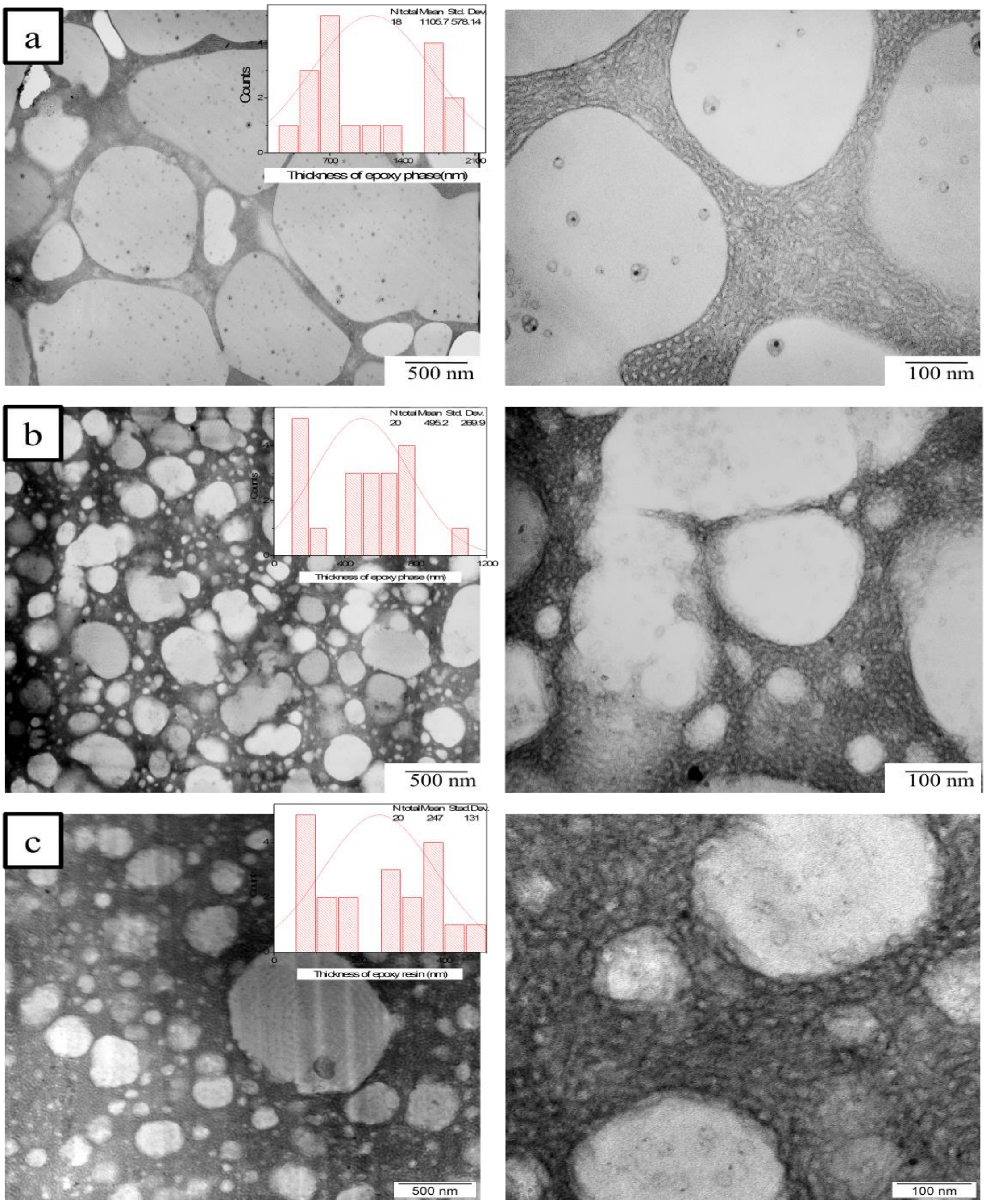

Figure 4.9: Left lower and right higher magnification of TEM images of blend of; a) EP/e(SB)$_X$-50 (85/15), b) EP/e(SB)$_X$-50 (55/45) and c) EP/e(SB)$_X$-50 (40/60). Insets presenting histogram of measurement of thickness of epoxy phase in nm.

Similarly, the EP/e(SB)$_X$-50 (55/45) blend (Figure 4.9b) also shows similar macrophase separation morphology. The dispersion of epoxy resin in blend is smaller in size when compared to the EP/e(SB)$_X$-50 (85/15). The size of EP phase is also about 100-1100 nm in the blend.

Also, similar phase behaviour is observed in the case of EP/e$(SB)_X$-50 (40/60) blend (see Figure 4.9c) too. However, the dispersion of the epoxy resin, in this case, is smaller than EP/e(SB)x-50 (55/45) blend. The size of epoxy resin in the blend ranges from 75-450 nm. Remarkably, a single large spherical EP resin is observed in this blend; and its size is about 1050 nm. These results indicate that the size of epoxy resin depends on the weight fraction where decrease in weight fraction of epoxy resin results the decrease in dispersed size of the EP phase.

However, the blend morphology is largely turned in microphase separated nanostructure in EP/e$(SB)_X$-50 (70/30) as explained in the previous section (Figure 4.7b). Besides, the another phase in the blends is polystyrene (PS) which remains in the cylindrical form dispersed approximately 15 nm in diameter similar as the $(SB)_X$ copolymer in all blends (higher magnification of Figure 4.9). The mean thickness of the epoxy phase of each blends are given in Table 4.3.

Table 4.3: Mean thickness of epoxy phase in composition variations blends EP/e$(SB)_X$-50 (85/15), EP/e$(SB)_X$-50 (55/45) and EP/e$(SB)_X$-50 (40/60)

Sample code	Thickness of Epoxy phase
EP/e$(SB)_X$-50 (85/15)	1106 nm
EP/e$(SB)_X$-50 (55/45)	495 nm
EP/e$(SB)_X$-50 (40/60)	247 nm

Thus, it can be concluded that, even at low composition of the block copolymer $(SB)_{X,}$ there is a good compatibility between the block copolymer and the epoxy resin as demonstrated by the formation of dispersed phase by the majority components (*i.e.* epoxy resin) and appearance of polydisperse domains in the matrix. Nevertheless, the compatibility was not sufficient for inducing nanostructures to the epoxy resin. Yet, the heterogeneous morphology with microphase separation at microscale as well as nanoscale was observed in all the cases. Similar type of composition variation study of epoxy resin (EP)/polyethylene-*block*-poly-(ethylene oxide) (EEO) blend was also carried out by Guo *et al.* [56,56,133]. They found that the morphology of the cured blends have changed gradually with increasing EEO content. The 90/10, 80/20, and 70/30 EP/EEO blends also gave rise to a similar morphology [133]. The effect of such type of morphology can be seen in the thermogravimetric analysis (see section 4.3.1).

From now, it can be summarized that the effect of composition variation is distinctly observed in the morphology of blends. The various size spherical structures of epoxy resin are also formed in most of the blends. The nature of the formation of various morphologies is similar in all the blends.

4.2.1.4 Nanocomposites with boehmite and layered silicate

In this section, we briefly investigate the effect of nanoparticles on the morphology of the blends. Two kinds of nanoparticles are used: boehmite and layered silicate coated with alkyl benzene sulphonic acid and dimethyl dioctadecyl ammonium ion surfactant, respectively. The amount of nanofillers in each composite is 3 parts by weight. Transmission electron micrographs of the neat epoxy resin/boehmite (EP/OS), EP/layered silicate (LS), EP/e(SB)$_X$-50/OS and EP/e(SB)$_X$-100/OS nanocomposite are presented in Figure 4.10a, 4.10b, 4.10c and 4.10d respectively.

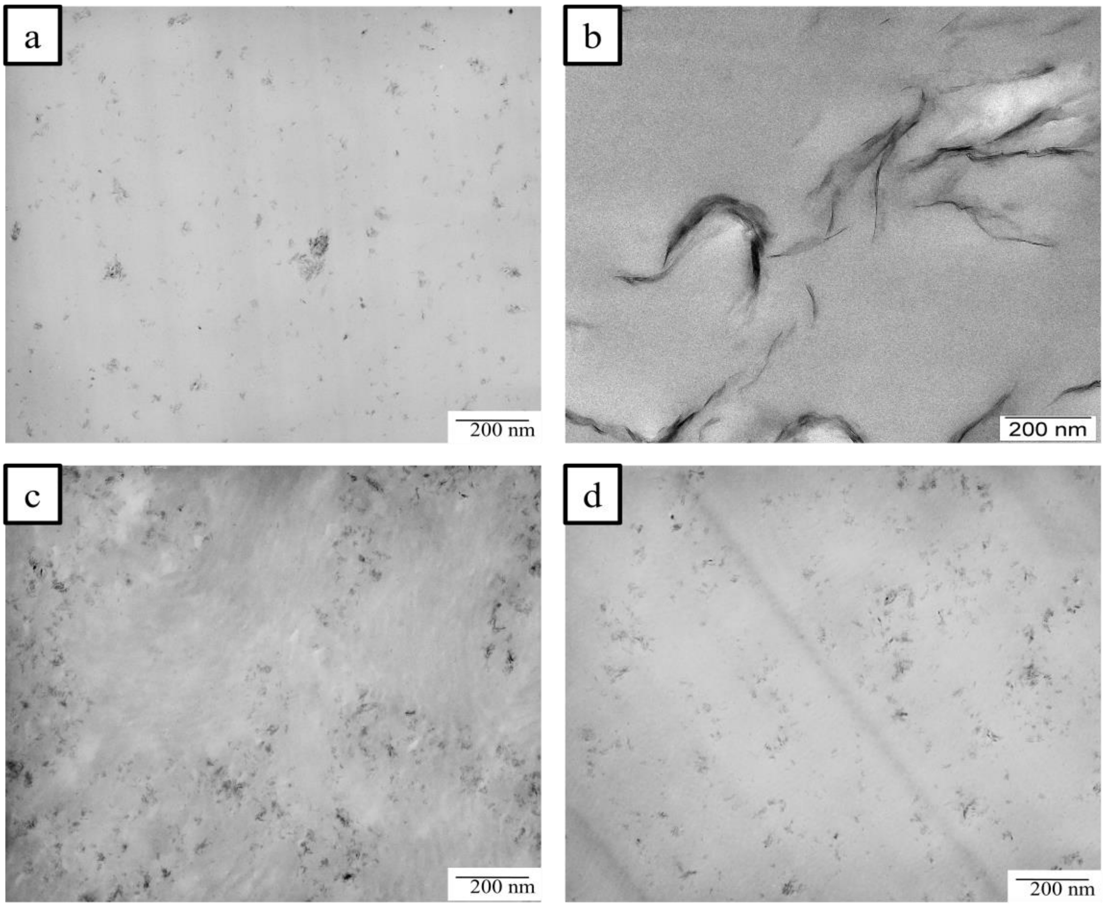

Figure 4.10: TEM images of; a) EP/OS, b) EP/LS, c) EP/eSB)$_X$-50/OS, and d) EP/e(SB)$_X$-100/OS nanocomposite at without staining of Os$_2$O$_4$.

The TEM images (see Figure 4.10a) of epoxy resin nanocomposite show the dispersion of boehmite nanoparticles in dark in the gray coloured epoxy resin matrix. It can also be observed that the boehmite nanoparticles are homogeneously dispersed in the epoxy resin. Each boehmite nanofillers are spherical and have the size of 10 nm. The dispersion of boehmite nanofiller are observed to be agglomerated (average size of 55 nm) along with some exfoliation.

In our study, only the effect of dispersion of layered silicate nanoparticles in epoxy resin has been observed. The layered silicates (LS) have two dimensional structure whose dispersion in the epoxy resin (EP) looks like thread structure. In this study, the dispersion of LS in epoxy is distinguished in TEM image (Figure 4.10b) by three different ways – exfoliation, intercalation, and aggregation. The layered silicate nanoparticles are dispersed with exfoliation in small dark thread like structures with approximately 22 nm in size. Somewhere, it can be observed in the intercalated and agglomerated form also.

Likewise, the micrographs of EP/e(SB)$_X$-50/OS and EP/e(SB)$_X$-100/OS nanocomposite without staining condition of Os_2O_4 vapour (see Figure 4.10c and d), distinctly showed the uniform dispersion of boehmite nanoparticles in the blend matrix. The size of the boehmite nanofiller dispersion, approximately 57 nm in epoxy matrix, in EP/e(SB)$_X$-50/OS composite is nearly same to EP/e(SB)$_X$-100/OS; yet somewhere larger size particles (62.5 nm) can also be seen in the later. Compared to the EP/OS composite, the size of agglomerated boehmite nanofiller in blend composite is slightly higher. This might be due to the effect of formation of nanostructures in the blends. The average size of the nanofillers dispersion in epoxy resin and blends composite are given in Table 4.4.

Table 4.4: The average size of dispersion of nanofillers in epoxy resin and blend composites of EP/OS, EP/LS, EP/e(SB)$_X$-50/OS, EP/e(SB)$_X$-100/OS

Sample code	Size of dispersion of nanofillers
EP/OS (boehmite)	55 nm
EP/e(SB)$_X$-50/OS	57.5 nm
EP/e(SB)$_X$-100/OS	62.5 nm
EP/LS (nanofil 5)	22 nm

Similar result was noticed by Occando *et al.* [145] and Tercjak *et al.* [146] on their work to explain the low degree of epoxidation of block copolymer epoxy resin blend nanocomposite by using Al_2O_3.

Hence, it can be concluded that the surfactant coated nanoparticles can be incorporated uniformly into the epoxy resin and its blends with block copolymer. This might be due to the functionalization of nanoparticles with their respective surfactants. The nanoparticles showed good adhesion with the block copolymers. Therefore, the fillers can affect the mechanical properties of the blends by compensating the stiffness of the later (discussed in section 4.4). In this study, we are limited only to the 3wt.-% of nanofillers in the preparation of the blend, since our motive is to use fewer amount of nanofillers and hence develop a cost effective method for the improvement in the mechanical properties of the blends.

4.3 Thermal Characterization

4.3.1 Thermogravimetric Analysis

Thermogravimetric analysis (TGA) was performed to obtain the information on the thermostability of epoxy resin based polymer blends. In brief, the mass loss of the samples was determined as a function of temperature ranging from the 25 to 800 ^{o}C at heating rate of 10 ^{o}C/min under nitrogen atmosphere [162].

4.3.1.1 Effect of different parameters: degree of epoxidation, block copolymer architecture, and method of epoxidation

Thermogravimetric analysis (TGA) curves (mass *versus* temperature) and the corresponding derivative thermogravimetric (DTG) curves (mass loss rate *versus* temperature) for neat $(SB)_{X,}$ epoxy resin and their blends (*i.e.* EP/e$(SB)_X$-25, EP/e$(SB)_X$-50, and EP/e$(SB)_X$-100) are shown in Figure 4.11. Only a portion of the plots has been converted to DTG in 4.11b.

As indicated in Figure 4.11a, the degradation of pure epoxy resin (black coloured curve) begins at about 150 oC with a complete degradation at 466 oC. This shows that the epoxy resin (EP) remains no longer thermally stable above 150 oC. Similar result of degrdation of epoxy resin was found in the literature [162].

The residual mass (found in the term of char) (see Table 4.4) left in the TGA measurements was recorded after the completion of the experiment. It has been found that about 19% char of epoxy resin (EP) left over at the end of the experiment while this amount is lower in all the blends. It implies that the strong cross-linked network structure might lead to the formation of stable char of the resin under nitrogen atmosphere. Thus, the network strength might have been diminished in the blends.

On the other hand, pure $(SB)_X$ copolymer (pink coloured curve in Figure 4.11a) shows an initial mass loss of about 2% most probably due to the removal of trapped moisture; and it begin s to degrade at 390 °C and complete at 514 °C. This implies that the $(SB)_X$ copolymer is more stable than the resin due to the presence of polystyrene (PS) in which the resonance structure of benzene rings contributes for the higher degradation temperature [163].

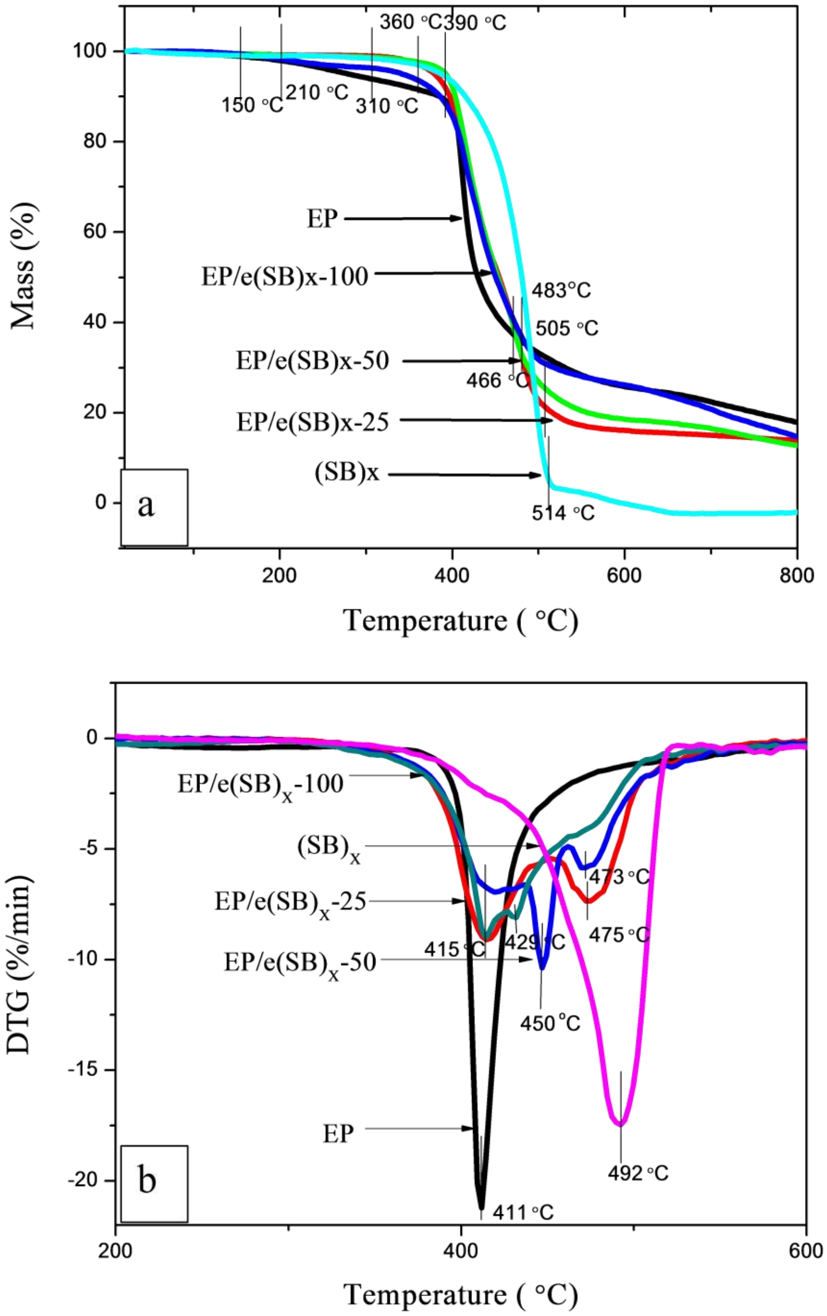

Figure 4.11: a) Variation of specimen mass with temperature and b) the DTG curves for epoxy resin/$e(SB)_X$ blends using $e(SB)_X$ having different degree of epoxidation; pink line = pure $(SB)_X$, black line = epoxy resin, red line = $EP/e(SB)_x$-25, green line = $EP/e(SB)_X$-50 and blue line = $EP/e(SB)_X$-100.

The mass of all the $EP/e(SB)_X$ blends (see Figure 4.11a) remain constant up to 200

^{o}C. Afterwards, the EP/e(SB)$_X$-25 blend (red coloured curve) starts to degrade from about 360 ^{o}C and complete at about 505 ^{o}C. Similarly, EP/e(SB)$_X$-50 blend (green colored curve) begins to degrade from about 310 ^{o}C and complete at 505 ^{o}C. Furthermore, EP/e(SB)$_X$-100 blend (blue coloured curve) shows initial degradation starting from 210 ^{o}C and completing at 483 ^{o}C. These results indicate that the thermostability has been improved in all the blends when compared to the epoxy resin (EP).The results further point out that the initial degradation temperature decrease with increase in the degree of epoxidation. This also shows that the miscibility of epoxy and copolymer increases with the increase in the degree of epoxidation. The characteristic data extracted from the TGA curves of epoxidation degree variations are given in Table 4.5. Moreover, the limiting oxygen index (LOI) parameter, though presented in the table, will be discussed shortly.

Table 4.5: Characteristics data extracted from the TGA curves of epoxidation degree variations

Sample code	Residual mass (%)	*T_i ^{o}C	*T_1 ^{o}C	*T_2 ^{o}C	*T_3 ^{o}C	*T_f ^{o}C	LOI (%)
(SB)$_X$	1	390	492			514	
EP	19	150	411			466	26.36
EP/e(SB)$_X$-25	14	360	415	475		505	23.85
EP/e(SB)$_X$-50	12	310	415	450	473	505	22.88
EP/e(SB)$_X$-100	14	210	415			483	23.84

*T_i = initial degradation temperature, *T_1 = First degeradation temperature, *T_2 = Second degeradation temperature and *T_3 = Third degeradation temperature, *T_f = final degradation temperature,
LOI = Limiting oxygen index

The analysis of DTG curves of the blends and pure polymers (Figure 4.11b) reveals that there are at least two sharp degradation steps represented by the temperature T_1 and T_2 for each blend. This implies the presence of at least two degradation phenomena in the blends. Nevertheless, epoxy resin/propyl ester phosphazene blend has shown to have one-stage thermal degradation reaction [164]. Epoxy resin (EP) (black colored curve, Figure 4.11b) shows a sharp degradation peak temperature (T_1) at 411 ^{o}C which indicates the presence of only one epoxy phase. Similarly, neat (SB)$_X$ (pink colored curve, Figure 4.11b) shows a sharp degradation peak temperature (T_1) at 492 ^{o}C. This temperature indicates the polystyrene (PS) phase degradation. A small broad degradation peak can also be seen at around 425 ^{o}C which corresponds to the polybutadiene phase degradation.

Besides, the EP/e(SB)$_X$-25 blend (red colored curve, Figure 4.11b) shows two sharp degradation temperatures T_1 and T_2 at 415 ^oC and 475 ^oC, respectively. The first degradation temperature (T_1= 415 ^oC) corresponds to the degradation of epoxy phase in the blend. On the other hand, the second degradation temperature (T_2) at 475 ^oC represents the degradation of PS phase of $(SB)_X$ block copolymer. The second degradation peak in this case is larger than that in other blends which indicates the presence of large amount of unmodified $(SB)_X$. The results, however, show the improvement in thermostability of the blends when compared to the epoxy resin. This might be due to the formation of macrophase separated morphology with spherical epoxy resin domains dispersed in $(SB)_X$ copolymer (refer to Figure 4.7a).

In addition, EP/e$(SB)_X$-50 and EP/e$(SB)_X$-100 blends also show similar degradation behavior as of EP/e$(SB)_X$-25 blend. However, there are three degradation peak temperatures located at 415 ^oC, 450 ^oC and 473 ^oC. The first degradation peak temperature (T_1 = 415 ^oC) represents the sharp mass loss of the epoxy phase which is near to the degradation temperature of epoxy resin (EP). Though, the second degradation peak temperature (T_2 = 450 ^oC) is strange in our result. This might be due to the degradation of unmodified polybutadiene (PB) phase (as indicated by TEM results in Figure 4.7b). The third one (T_3 = 473 ^oC) might be related to the degradation of polystyrene (PS) phase which is near to the degradation temperature of pure $(SB)_X$. Thus, these results suggest advancing the thermostability of blends which could be due to the reasons of forming a barrier protection layer of PB and PS in epoxy resin blends.

Moreover, EP/e$(SB)_X$-100 blend (blue colored curve in Figure 4.11b) exhibits the first degradation peak temperature (T_1) at 415 ^oC which corresponds to the epoxy phase of the blend. A broad peak near 470 ^oC can also be seen in the DTG curve (see Figure 4.11b) which indicates the degradation of PS cylinders as explained earlier in the formation of nanostructure morphology of the blend (Figure 4.7c).

Hence, it can be concluded that the epoxidation degree variation shows the improvement in thermostability of blends. The initial degradation temperature is higher in lower degree of epoxidation compared to the higher degree.

Also, the thermogravimetric analysis (TGA) and derivative thermogravimetric analysis (DTG) curves for neat $(SB)_{X,}$ epoxy resin and their blends using block copolymer having different architectures (i.e. EP/e$(SB)_X$-100, EP/eSBS-100 and EP/eSB-100) are shown in Figure 4.12.

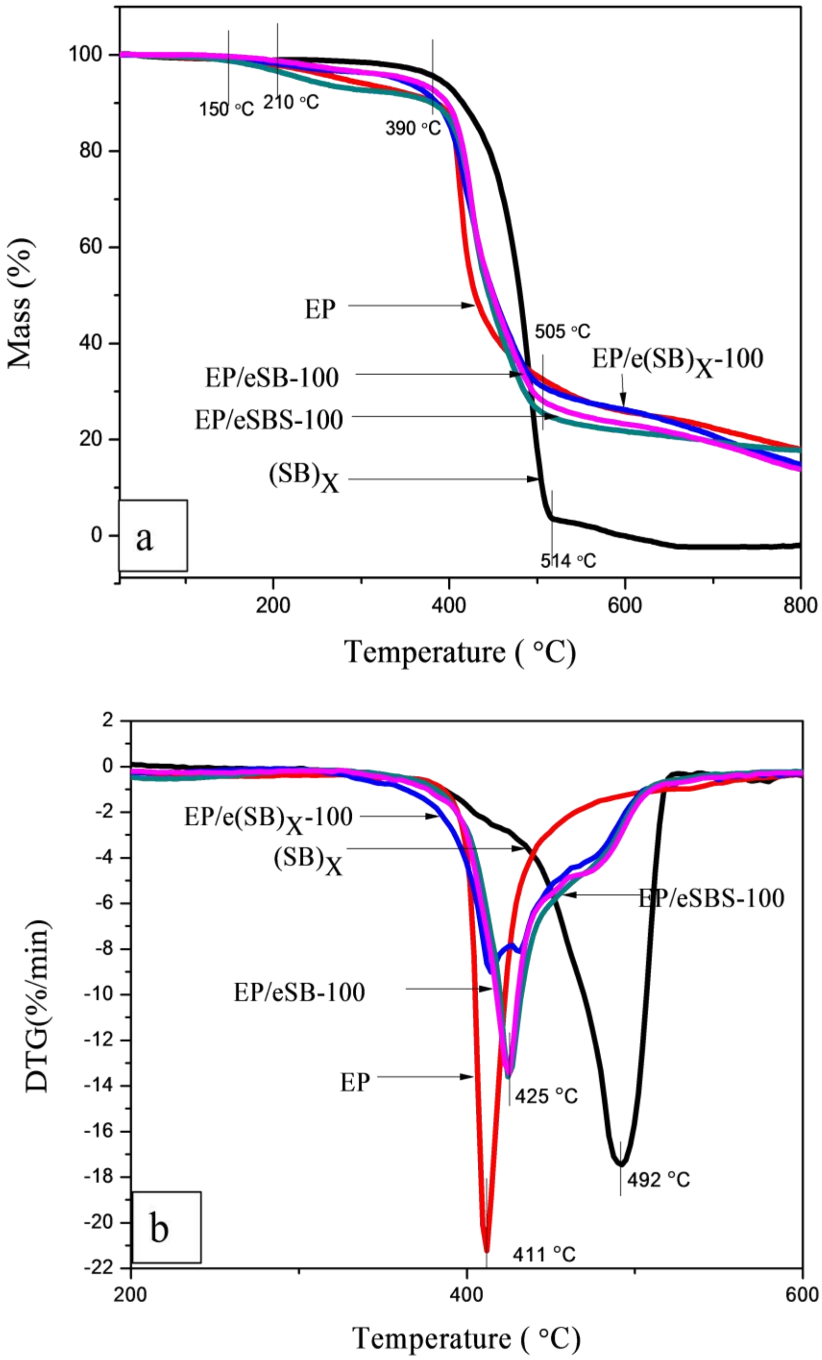

Figure 4.12: a) Variation of specimen mass with temperature and b) the DTG curves for epoxy resin/epoxidized different architecture of copolymer blends; black line = pure $(SB)_X$, red line = epoxy resin, blue line = EP/e$(SB)_x$-100, purple line = EP/eSBS-100 and pink line = EP/eSB-100.

The TGA curves show that all the curve s of the blends lie in between the neat epoxy resin and neat $(SB)_X$ (see Figure 4.12a). The blends have the similar nature of degradation behaviour as explained earlier in Figure 4.11. Some characteristic data obtained from these curves are listed in Table 4.6.

Table 4.6: The data obtained from the TGA curves of various architectures of copolymer

Sample code	Residual mass (%)	T_i °C	T_1 °C	T_f °C	LOI (%)
$(SB)_X$	1	390	492	514	
EP	19	150	411	466	26.88
EP/e$(SB)_X$-100	14	210	415	483	23.84
EP/eSBS-100	18	210	425	505	25.77
EP/eSB-100	14	210	424	505	23.69

The EP/eSBS-100 and EP/eSB-100 blends have similar nature of TGA and DTG curves (see Figure 4.12). The mass loss curves in Figure 4.12a show that these two blends also begin to degrade at 210 ^{o}C and complete at 505 ^{o}C. The DTG curves analysis of these blends shows the occurrence of only one sharp degradation peak temperature at around 425 ^{o}C. This temperature represents the epoxy phase degradation as in the previous case. A broad and short peak at 470 ^{o}C (Figure 4.12b) also account for the complete miscibility of block copolymer with epoxy resin since no traces of unmodified copolymers are left and all the PS cylinders (according to the electron microscopy studies in section 4.2.1.1, Figure 4.8) degrade at this temperature. This indicates that the thermostability remains same in all blends whatever is the architecture of copolymer used in the blend. The degradation temperature of PS phase is lower in the blend than that of pure block copolymer.

Thus, it can be summarized that the architectures of copolymers do not show significant effect in thermostability of the blends.

Further, TGA and DTG curves of the blends, prepared by different methods namely EP/e$(SB)_X$-50 (MCPBA), EP/e$(SB)_X$-50 (PFA) and EP/e$(SB)_X$-50 (HFIP), are shown in Figure 4.13.

The mass loss curves (Figure 4.13a) show the higher initial degradation temperature (T_i) of blends than EP. The EP/e$(SB)_X$-50 (HFIP) blend has the initial degradation temperature shifted to 210 ^{o}C and completes at 505 ^{o}C. However, other two blends begin to degrade at 310 ^{o}C and ends at 505 ^{o}C. The thermostability of EP/e$(SB)_X$-50 (PFA) and EP/e$(SB)_X$-50 (MCPBA) blend has been improved than that of the EP/e$(SB)_X$-50 (HFIP) blend. From the mass loss curves, it is clear that the EP/e$(SB)_X$-50 (HFIP) blend could not show a significant improvement in the degradation properties compared to other two blends. The DTG curves (Figure 4.13b) analysis of the blends indicates that the epoxy phase sharply degrades above 415 ^{o}C; and the another temperature at 470 ^{o}C corresponds to the PS phase degradation as in the previous case.

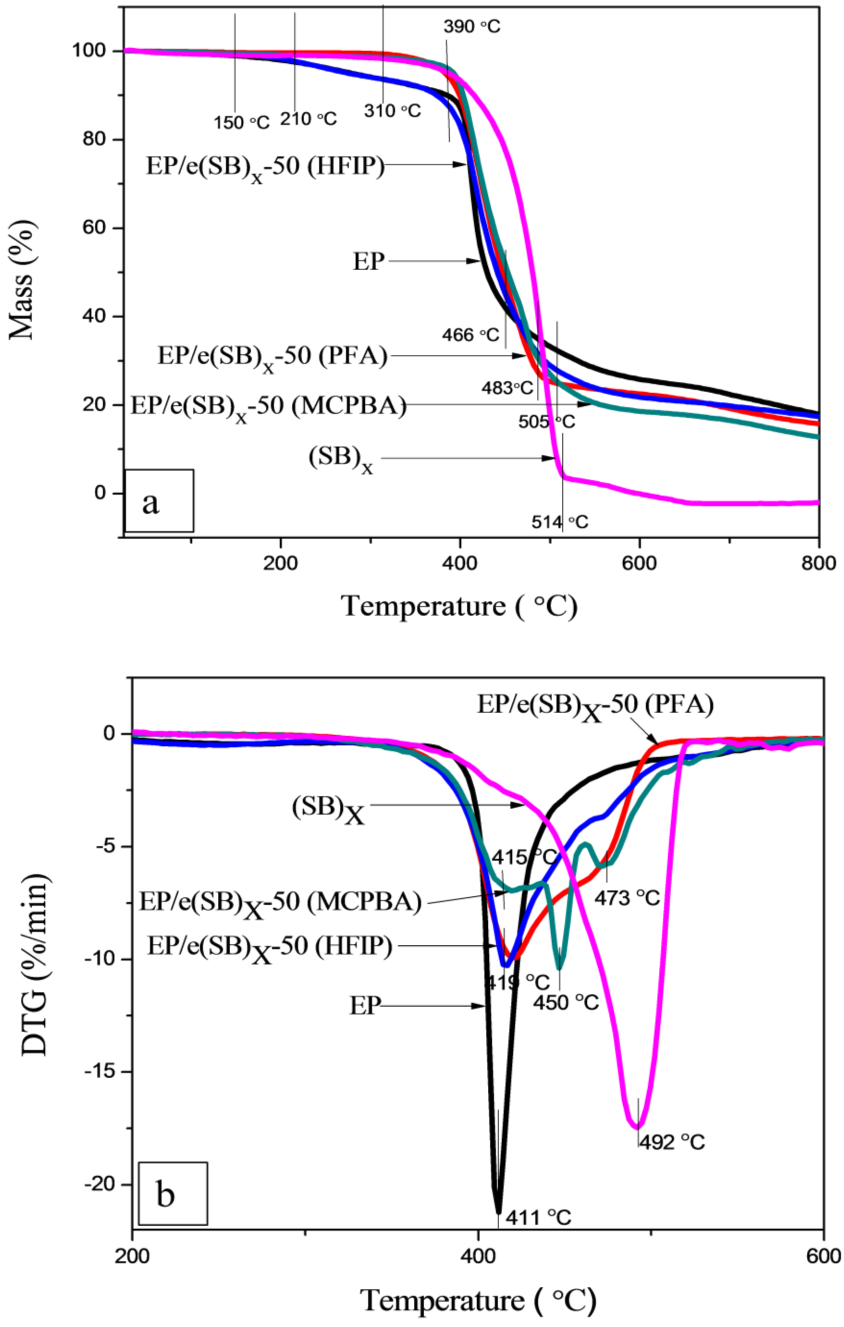

Figure 4.13: Thermograms of the blends of epoxy resin with modified star block copolymer epoxidized to 50% using different methods a) Variation of specimen mass with temperature and b) the DTG curves of mass loss rate against temperature; pink line = pure (SB)$_X$, black line = epoxy resin, purple line = EP/e(SB)$_x$-50 (MCPBA), red line = EP/e(SB)$_X$-50 (PFA) and blue line = EP/e(SB)$_X$-50 (HFIP).

The data extracted from these curves are listed in Table 4.7.

Table 4.7: Characteristics data received from the TGA curves of method variations

Sample code	Residual mass (%)	T_i °C	T_1 °C	T_2 °C	T_3 °C	T_f °C	LOI (%)
EP	19	150	411			466	26
EP/e(SB)$_X$-50 (MCPBA)	12	310	415	450	473	505	23
EP/e(SB)$_X$-50 (PFA)	16	310	419			505	25
EP/e(SB)$_X$-50 (HFIP)	17	210	416			505	26

In summary, the observed general trends in the thermostability of the blends are independent of the methods of epoxidation. However, the MCPBA and PFA methods are significant for thermostability of the blend

4.3.1.2 Effect of e(SB)$_X$ copolymer weight fraction

Thermogravimetric analysis (TGA) and the corresponding derivative (DTG) curves for neat (SB)$_{X,}$ epoxy resin (EP), and their weight fraction blends are presented in Figure 4.14; and they are thoroughly discussed in this section. Epoxidised (SB)$_X$ copolymer having 50% degree of epoxidation by weight of total polybutadiene (e(SB)$_X$-50) are studied. The compositions of blend of epoxy resin (EP) with e(SB)$_X$-50 by weight were set to be 85/15, 70/30, 55/45, and 40/60.

The mass loss curves (see Figure 4.14a) show a gradual degradation of pure (SB)$_X$ and e(SB)$_X$ that begins from 390 °C and complete at 514 °C. Similarly, most of the blends have initial degradation temperature (T_i) at 284 °C except EP/e(SB)$_X$-50 (70/30) blend. The probable reason for this has already been explained earlier in the section 4.3.1.1. Yet, all the blends have same final degradation temperature (T_f) at 505 °C. The DTG curve of e(SB)$_X$-50 (Figure 4.14b) clearly confirms two degradation temperature: first at 414 °C and second 484 °C. The first degradation temperature (414 °C) indicates that the epoxy ring present in the epoxidized (SB)$_X$ degrades near to the epoxy phase. The second degradation temperature (484 °C) shows PS phase degradation as similar to the pure (SB)$_X$.

The DTG plots (Figure 4.14b) corresponding to the first degradation temperature (T_1) of the blends shows a gradual upward shift which indicates the degraded epoxy phase and also accounts for the decrease in the amount of epoxy resin with change in the weight fraction. The higher amount of epoxy resin in EP/e(SB)$_X$-85/15 blend (which contains 85% by weight of epoxy resin) and lower amount of epoxy resin in EP/e(SB)$_X$-50 (40/60) blend (containing 40% by weight of epoxy resin) shows the higher and lower peak intensities, respectively. This confirms that the amount of epoxy group decreases with the decrease in epoxy resin in blends.

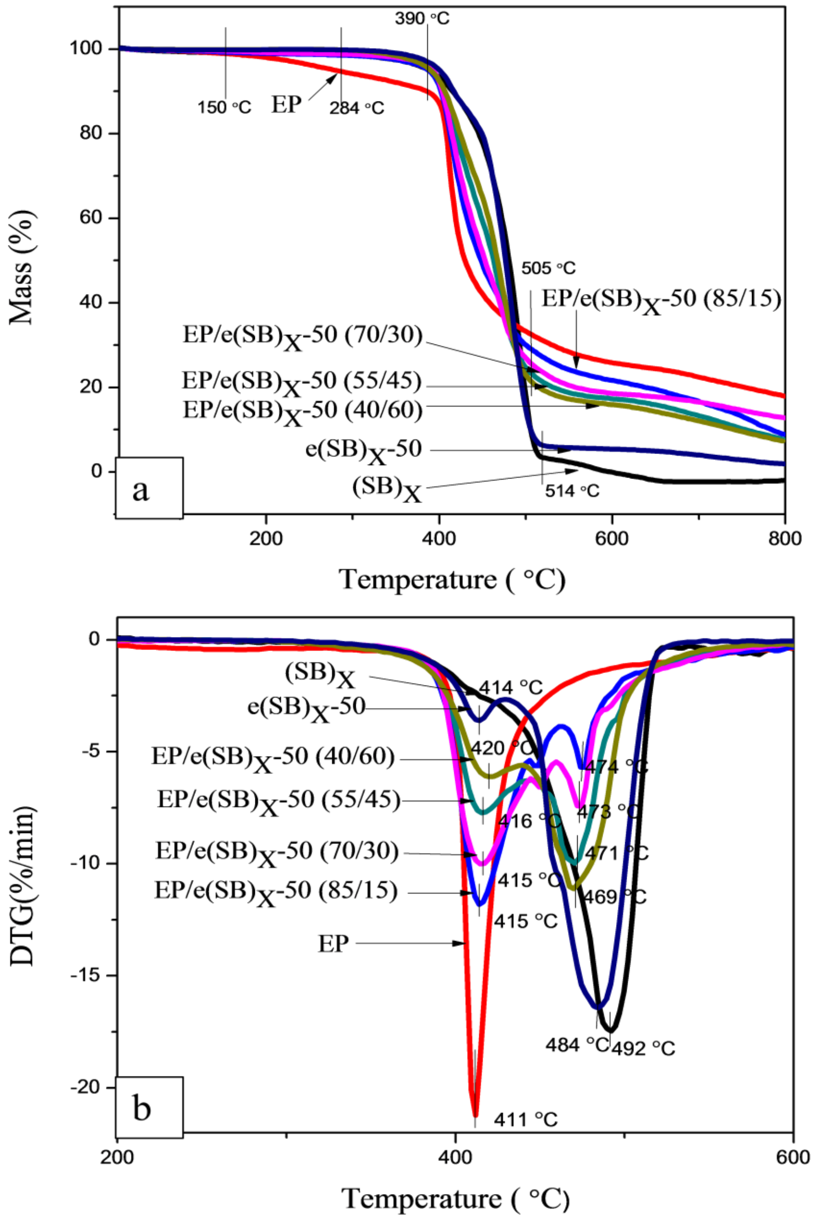

Figure 4.14: a) Variation of specimen mass with temperature and b) the DTG curves for epoxy resin/e(SB)$_X$ blends using e(SB)$_X$ having different weight fraction; black line = pure (SB)$_X$, red line = epoxy resin, blue line = EP/e(SB)$_x$-50 (85/15), purple line = EP/e(SB)$_X$-50 (55/45), pink line = EP/e(SB)$_X$-50 (70/30), green line = EP/e(SB)$_X$-50 (40/60) and dark blue line = e(SB)$_X$-50.

On the other hand, second degradation temperature (T_2) DTG curves are also shifted upward gradually one after another due to the decrease in the amount of e(SB)$_X$. The improvement in thermostability of the materials is also correlated to the resulting nanostructured morphology of the blends in which the PS phase from the block copolymer forms the potential layer [163]. Typical data obtained from these curves are listed in Table 4.8.

Table 4.8: Characteristics data extracted from the TGA curves of composition variations

Sample code	Residual mass (%)	T_i °C	T_1 °C	T_2 °C	T_3 °C	T_f °C	LOI (%)
EP	19	150	411			466	26.36
e(SB)$_X$-50	2	390	414	484		514	17.83
EP/e(SB)$_X$-50 (85/15)	9	284	415	448	474	505	21.33
EP/e(SB)$_X$-50 (70/30)	12	310	415	450	473	505	22.88
EP/e(SB)$_X$-50 (55/45)	8	284	416	471		505	20.67
EP/e(SB)$_X$-50 (40/60)	7	284	420	469		505	20.49

Residual mass percentage of each blend is presented in above Table 4.8. The residual mass is comparatively lower than the neat epoxy while increasing the composition of e(SB)$_X$.

Therefore, it can be concluded that the weight fraction blends show improvement in their thermostability particularly in their initial degradation temperature. Further, the composition variation in blends does not play any significant role to increase the thermostability.

Limiting Oxygen Index (LOI)

Limiting oxygen index (LOI) is another suitable parameter that measures the flame retardancy based on the char yield. A higher char residual material can be said to be more fire resistant. Char yield was previously correlated to LOI by Gracik and Long [164] using the equation:

$$\mathrm{LOI} = 16.9 + 0.5\ (\mathrm{Char\ wt.\%, 800\ °C\ in\ N_2}) \ldots\ldots\ldots\ldots\ldots\ldots\ldots..(4.1)$$

The calculated LOI values of epoxy resin and blends are presented in the Table 4.5-4.8. The LOI value is found to be decreased from 26% (EP) to 23% (EP/e(SB)$_X$-50), 24% (EP/e(SB)$_X$-25), and 24% (EP/e(SB)$_X$-100). Similarly, other blends also show the almost similar value of LOI. These values indicate that the blends have low flame retardant property as compared to the epoxy resin. Yet, some earlier studies have shown that the chemically modified epoxy resins bear good flame retardant properties [165, 166]

Activation energy of decomposition

Activation energy for decomposition is the amount of energy required to decompose the cross linked network of thermosetting polymers. It is found to be dependent upon the structure of network.

Theoretically, all kinetic studies start with the basic equation that relates the rate of mass loss at a constant temperature to the fractional decomposition [167], *i.e.*

$$\frac{\mathrm{d}\alpha}{\mathrm{dt}} = \mathrm{k}\,\mathrm{f}(\alpha) \ldots\ldots\ldots\ldots\ldots\ldots\ldots\ldots\ldots.. (4.2)$$

where, dα/dt is the rate of mass loss, α is the fractional decomposition at any time, and k is the rate constant. The term *f*(α) is a function of α given by:

$$f(\alpha) = (1-\alpha)^n \ldots\ldots\ldots\ldots\ldots\ldots\ldots.. (4.3)$$

The activation energy of decomposition is calculated using the model of Arrhenius equation [168]. The rate constant is dependent on the reaction temperature according to the Arrhenius equation:

$$\mathrm{K} = \mathrm{A}\,\mathrm{e}^{-\mathrm{E_d}/\mathrm{RT}} \ldots\ldots\ldots\ldots\ldots\ldots\ldots\ldots\ldots (4.4)$$

where, E_d is the activation energy, A is a pre-exponential factor, R is the gas constant, and T is the reaction temperature. Combining equations 4.2-4.4 [168], we can write:

$$\frac{\mathrm{d}\alpha}{\mathrm{dt}} = \mathrm{A}(1-\alpha)^n\left(\mathrm{e}^{-\frac{\mathrm{E_d}}{\mathrm{RT}}}\right) \ldots\ldots\ldots\ldots\ldots (4.5)$$

Activation energy (E_d) of the blends can also be determined using the method of Arrhenius equation from the linear fitting of ln(dα/dt) *versus* 1/T. For example, the activation energy of decomposition of EP/e(SB)$_X$-25 blend is calculated using the corresponding ln(dα/dt) *versus* 1/T plots as given in Figure 4.16.

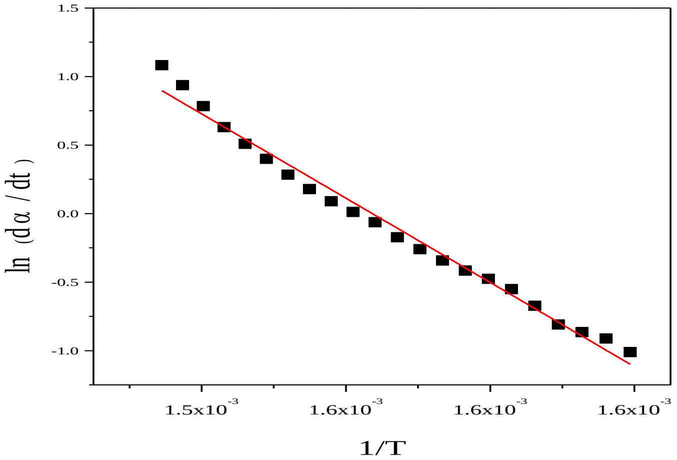

Figure 4.15: A Plots of ln(dα/dt) versus 1/T according to Arrehinus equation method for the EP/e(SB)$_X$-25 blend.

In all the samples, activation energy was calculated in the temperature range of 337 to 420 ± 5 °C. The amount of energy obtained during the thermal degradation is given in Table 4.9.

Table 4.9: Activation energy values for the thermal decomposition of epoxy resin, $(SB)_X$ and their blends

Sample code	Temperature range (°C)	Activation energy (E) KJ/mol
Epoxy resin	337-410	143
(SB)x	337-415	106
EP/e$(SB)_X$-25	337-415	156
EP/e$(SB)_X$-50	344-415	138
EP/e$(SB)_X$-100	337-415	125
EP/eSBS-100	337-425	164
EP/eSB-100	337-425	152
EP/e$(SB)_X$-50 (PFA)	337-415	157
EP/e$(SB)_X$-50 (HFIP)	337-415	147
EP/e$(SB)_X$-50 (85/15)	337-422	137
EP/e$(SB)_X$-50 (70/30)	337-420	196
EP/e$(SB)_X$-50 (55/45)	338-421	162
EP/e$(SB)_X$-50 (40/60)	337-425	136

Similarly, for the variation of epoxidation degree, the activation energy of the degradation of epoxy resin and blends are presented in Figure 4.16.

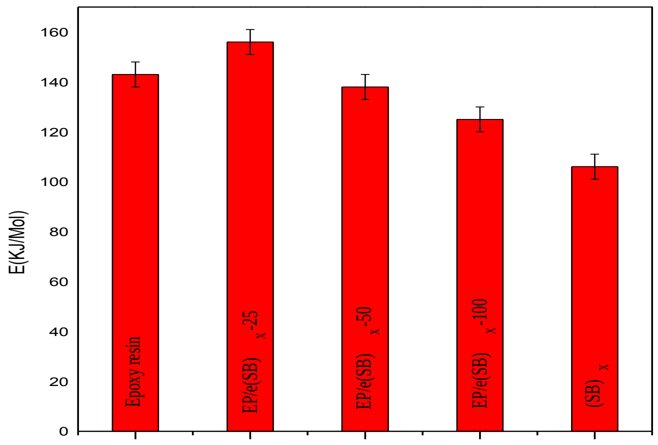

Figure 4.16: Bar diagram of activation energy of decomposition of epoxidation degree variation blends of epoxy resin/e(SB)x.

It can be seen that, compared to other blends, the activation energy of EP/e(SB)$_X$-25 blend is higher. This blend shows strange behaviour which might be due to the microphase separation morphology. Further, the activation energy of decomposition of epoxy resins EP/e(SB)$_X$-50 and EP/e(SB)$_X$-100 have almost similar values. This indicates that there is the occurrence of similar cross linking reaction in them. Also, the similar cross linked density, but higher than neat (SB)x, in them signifies that there is cross linking between epoxy and copolymer to form nanostructures (Figure 4.16). The curing reaction itself is a complex function of energy of reactive molecules as well as relative configuration of the reactant molecules that changes during the reaction process

Similarly, in architecture varied blends, we could not observe any large differences in the amount of activation energy of decomposition between the epoxy resins (EP) and the blends. Moreover, in the method varied blends, activation energy of decomposition shows the similar trends as explained in case of epoxidation degree varied and architecture varied blends (see Figure 4.17). Furthermore, in composition varied blends, the variation in observed activation energy of decomposition is irrespective of the change in weight fraction ratio of epoxy resin (EP) to epoxidised block copolymer (e(SB)x) (see Table 4.9). The cross linking density is higher in 70/30 composition, *i.e.* EP/e(SB)$_X$-50 (70/30). Other blends have similar activation energy of decomposition. This indicates that the cross-linking density and the curing reaction are almost similar in the blends in addition to their similar thermal stability.

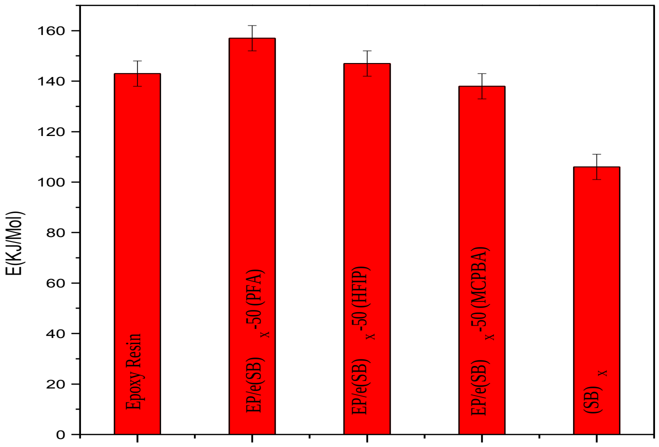

Figure 4.17: Bar diagram of activation energy of decomposition of epoxidation method variation blends of epoxy resin/e(SB)x.

Similarly, many other studies have also been carried out to investigate the activation energy of decomposition in other systems as well [169-172]. Tripathi and Srivastava [169] have reported that the activation energy increases with the addition of liquid elastomer in the glycidyl and non-glycidyl epoxy resin with carboxyl terminated butadiene acrylonitrile (CTBN) blends. On the other hand, Lee et al. [170] have found the constant activation energy of decomposition in the epoxy resin/liquid rubber blends. Similarly, Sharma et al. [171] have studied the thermal degradation kinetic of ultraviolet-visible (UV) cured epoxy acrylate resins in which activation energy was calculated in two different steps. Higher activation energy of decomposition was recorded due to the higher esterification of blends. Likewise, Shukla and Srivastava [172] also found that the activation energy increased with decrease in the resole content from 100 to zero weight percent in the epoxy/resole blends.

In summary, it can be concluded that the thermostability of the blends has been influenced by the degree of epoxidation, architecture of block copolymer, and method and composition variation during epoxidation. While the thermostability is improved by the increment in the epoxidation degree and composition of e(SB)X-50 in blends, the architecture variation have almost no effect. Likewise, all the methods are good enough to epoxidize the sample for the improvement of the thermostability. However, the blend of HFIP method shows thermostability near to the epoxy resin. Further, the weight fraction blends confirm the improvement of thermostability by showing a high initial degradation temperature. Thus, the blending of e(SB)X offers the possibility to increase, besides imparting an enhanced toughness, the thermostability of the materials. Yet a lowering of flame retradant property is observed among the blends compared to the neat epoxy resin. Moreover, increase in activation energy of decomposition of the blends when compared to epoxy resin has also shown high thermal degradation. According to our study, the block copolymer is one of the best ingredients to improve the thermostability in epoxy resin blends whatever the processing technique is applied.

4.3.2 Calorimetric Investigations

Differential scanning calorimetry (DSC) was used to study the glass transition temperature (Tg) and specific heat capacity (ΔCp) of EP/block copolymer blends and composites in detail. For the sake of simplicity, the study has been divided into following subsections:

4.3.2.1 Effect of different parameters: degree of epoxidation, block copolymer architecture, and method of epoxidation

The differential scanning calorimetric (DSC) plots of the pure epoxy resin (EP) and its blends with e(SB)$_X$-25, e(SB)$_X$-50, and e(SB)$_X$-100 are presented in Figure 4.18. In each blend, the weight fraction of each e(SB)$_X$ is maintained at 30%.

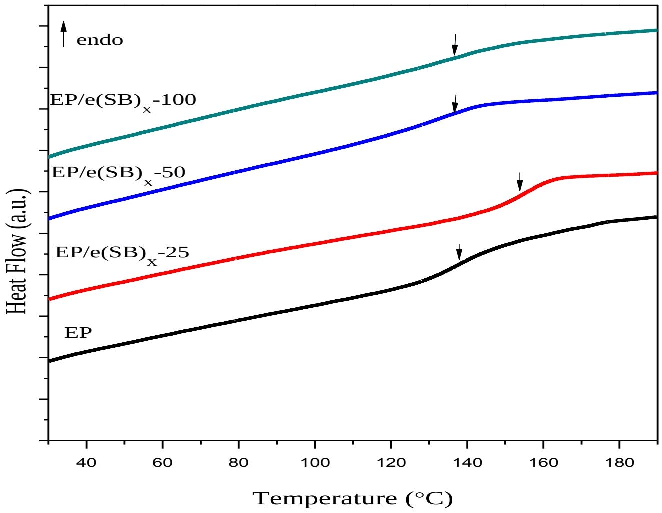

Figure 4.18: DSC traces of epoxy resin (EP) and EP/e(SB)$_X$ blends of epoxidation degree variation; black line = EP, red line = EP/e(SB)$_X$-25, blue line = EP/e(SB)$_X$-50 and purple line = EP/e(SB)$_X$-100, the blends comprising 70% by wt. of EP and 30% by wt. of e(SB)$_X$.

By evaluating the curves, basically, the glass transition temperatures (T_g) and specific heat capacities (ΔC_p) of the samples were determined. The magnitude of T_g provided the information about reversible change of the amorphous region in a polymer from a viscous or rubbery condition to a hard and relatively brittle one and *vice-versa*. Likewise, ΔC_p refers to a specific mass and temperature change for the material (J/g°C). It is the thermodynamic property of a material which gives the information about the molecular mobility (or disorderness of the molecules) and also provides useful information about the physical properties of the material as a function of temperature. The effects of ΔC_p on the crystalline polymers contain more order and thus fewer degrees of molecular motion. Less molecular motion results in lower specific heat capacity. ΔT_g also gives the information of time distribution or structure distribution of the molecule chain in the region of phase change in the DSC plot. It is measured by the change in extrapolated endset temperature (T_e) to extrapolated onset temperature (T_f) in DSC thermograms, *i.e.* $\Delta T_g = T_e - T_f$. In other words, It is measured by the change in temperature of the point where the dynamics of the chain cease (vitrify) to that of the point where the dynamics of chain begins (movement). The values thus obtained are collectively presented in Table 4.10.

Table 4.10: The characteristics T_g and ΔC_p data obtained from the DSC thermograms of EP and EP/e(SB)$_X$ blends of epoxidation degree variation

Sample code	T_g (°C)	ΔT_g (°C)	ΔC_p (J/g°C)
EP	138	21	0.18
EP/e(SB)$_X$-25	154	13	0.20
EP/e(SB)$_X$-50	138	15	0.12
EP/e(SB)$_X$-100	138	23	0.11

The T_g of epoxy resin (EP) was measured at 138 °C. This temperature is close to the curing temperature (T_c) of EP resin.Thus, it implies that the resin has been completely cured. The T_g of EP/e(SB)$_X$-50 and EP/e(SB)$_X$-100 blends is similar to that of the EP resin as expected, but it is slightly higher in EP/e(SB)x-25 blend (Figure 4.19).

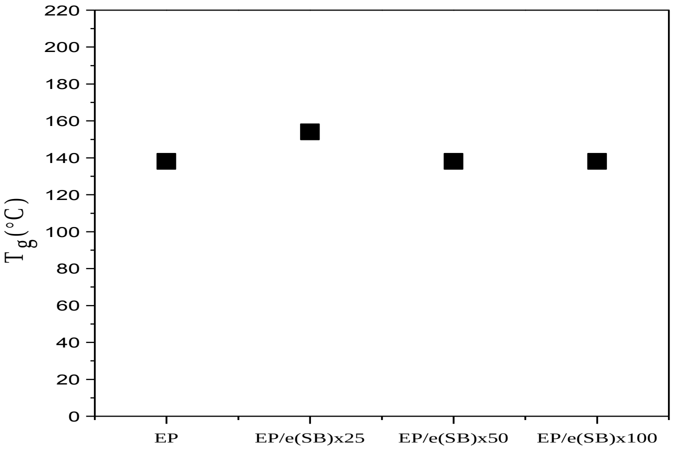

Figure 4.19: A plot of T_g versus degree of epoxidation of copolymer in EP/e(SB)x blends.

This further supports for the complete curing of the blends. However, the higher T_g of EP/e(SB)x-25 blend is not well understood. This might be the effect of morphology formed in the blends which shows the macroscopic phase separation, the inverted phase of matrix where epoxy resin is dispersed in spherical structure, and the formation of a largely dimixed system. Similar results were also reported by Serrano *et al.* [39] and Gupta and his co-worker [173] in their works, where the T_g of the epoxy phase was more or less near to the curing temperature (such as 140 °C and 150

^{o}C) of epoxy resin and blends.

Similarly, epoxy resin (EP) shows a measured value of ΔC_p to be 0.18 J/g^{o}C where the epoxy resin was present in 100%. In the blend, 70% is epoxy resin and the corresponding ΔC_p value is calculated to be 0.26 J/g^{o}C.This value indicates that the system is cross-linked with the curing agent; and the mobility of the chain is decreased. According to the literature, the reported value of ΔC_p for epoxy resin was1.06 J/g^{o}C at T_g of 145.66 ^{o}C [174]. Similarly, in contrast to the calculated value for EP/e(SB)x-25 blend is 0.20 J/g^{o}C where epoxy contain 70% by weight, the expected value of ΔC_p, considering 100% epoxy resin, is 0.28 J/g^{o}C. This indicates that the blend system shows dramatic change due to the demixing of the epoxy and (SB)$_x$ copolymer. The disorderness of the EP phase in blend is also increased because of the higher value of ΔC_p as compared to ΔC_p value of pure EP (Figure 4.20). The measured value of ΔC_p is lower than the expected value which tells us that the few amount of e(SB)$_x$ interacts with EP. In this blends, both T_g and ΔC_p are higher than the pure EP indicating that the system is complex and it needs further investigation.

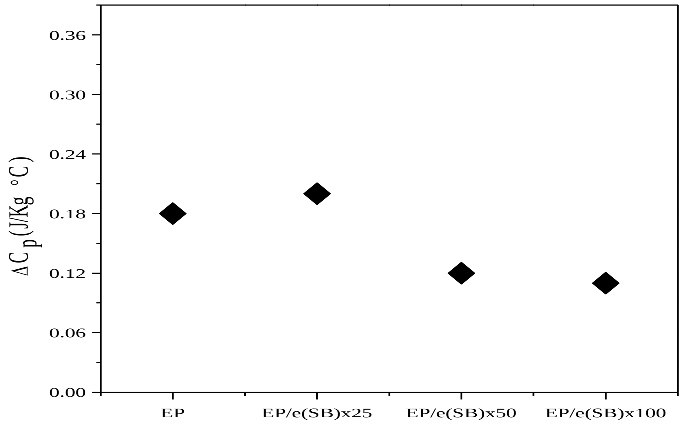

Figure 4.20: A plot of specific heat capacity of epoxy resin (EP) and degree of epoxidation of copolymer in EP/e(SB)x blends.

In the EP/e(SB)$_X$-50 blend, the measured value of ΔC_p was 0.12 J/g^{o}C, however, an expected value was 0.17J/g^{o}C. This indicates that the disorderness of the EP molecules decrease with good interaction between the EP and (SB)$_X$ molecules. Similarly, in the EP/e(SB)$_X$-100 blend, the measured value of ΔC_p was 0.11 J/g^{o}C, though, an expected value was 0.16 J/g^{o}C. This means that the mobility of the molecules decrease at higher degree of epoxidation which confirms the better interaction of the EP and e(SB)$_X$ molecules.

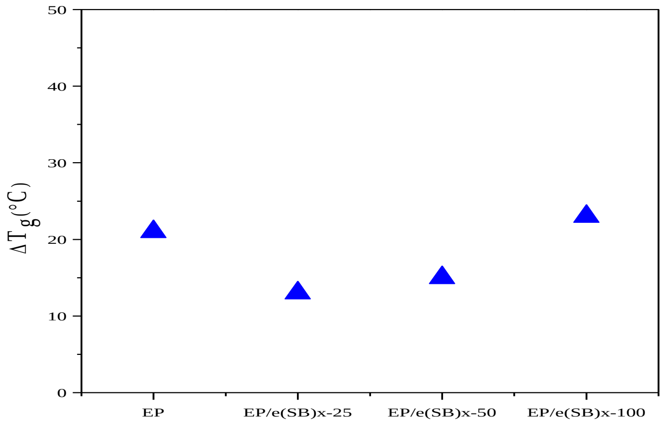

Figure 4.21: A plots of ΔT_g of epoxy resin (EP) and degree of epoxidation degree of copolymer in EP/e(SB)x blends.

ΔT_g values (Figure 4.21) of all the blends and EP have a range between 13 ^oC to 23 ^oC. Therefore, the structure distribution is almost similar. The dynamic of molecular chain begin to vitrify in this temperature range which is low in EP/e(SB)x-25 blend where, for other blends and EP, it is high. In a previous study [175], it has been reported that the ΔT_g was also used to judge polymer-polymer miscibility and to measure the breadth of the glass transition region. The width of the transition may be indicative of the presence of microphase separation and of the interfaces [175].

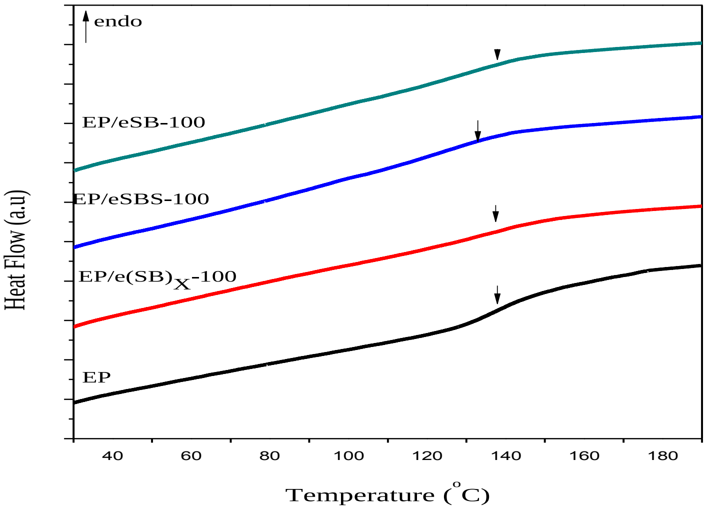

Figure 4.22: DSC traces of EP/e(SB)$_X$-100, EP/eSBS-100 and EP/eSB-100 blends compared with epoxy resin (EP); black line = EP, red line = EP/e(SB)$_X$-100, blue line = EP/eSBS-100 and purple line = EP/eSB-100, the blends comprise 70% by wt. of EP and 30% by wt. of each architecture of copolymer.

Likewise, DSC plots of the pure epoxy resin and its blends with e(SB)$_X$-100, eSBS-100, and eSB-100 are presented in Figure 4.22. In these blends, the weight fraction of epoxy resin and epoxidized block copolymer is 70/30.

The T_g of EP/e(SB)x-100 and EP/eSB-100 blends was 138 ^oC and EP/eSBS-100 was 134 ^oC. The expected T_g value in these blends were 140 ^oC which is the curing temperature of our system. The EP/e(SB)x-100 and EP/eSB-100 blends have same T_g value as we expected, however, T_g of EP/eSBS-100 blend is slightly lower than expected (Figure 4.23). This is also not far from the curing temperature (T_c). This indicates that the blend samples are fully cured. The values thus obtained are collected in Table 4.11.

Table 4.11: Characteristics T_g and ΔC_p data obtained from the DSC thermograms of epoxy resin and epoxy resin/block copolymer blends

Sample code	T_g (^oC)	ΔT_g	ΔC_p (J/g^{o}C)
EP	138	21	0.18
EP/e(SB)$_X$-100	138	23	0.11
EP/eSBS-100	134	27	0.12
EP/eSB-100	138	21	0.10

The specific heat capacity (ΔC_p) of blends is presented in Figure 4.24. According to our calculation, an expected ΔC_p value of EP/eSB-100 is 0.14 J/g^{o}C, however, the measured value is 0.10 J/g^{o}C.

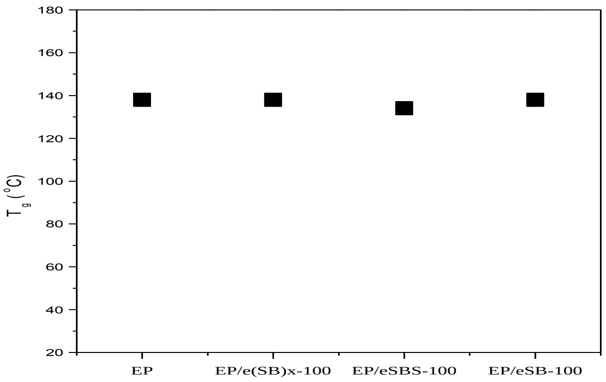

Figure 4.23: A plot of T_g of epoxy resin (EP) and various architecture of copolymer blends.

This indicates that the disorderness of the molecules are also decreased as compared to the EP/e(SB)$_X$-100 blend. This also confirms the better interaction of the EP and

SB molecules. Similarly, EP/eSBS-100 blend shows slightly higher value of ΔC_p (see Table 4.11). However, an expected ΔC_p value is 0.19 J/g^{o}C and measured value is 0.12 J/g^{o}C. The mobility of EP phase is more than the other blends.

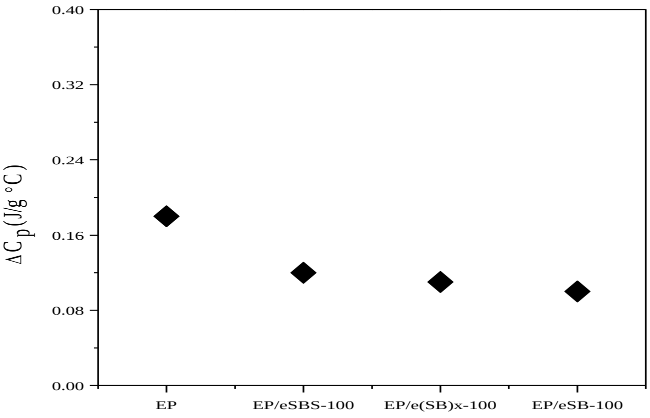

Figure 4.24: A plot of ΔC_p of EP and architecture variation of copolymer blends.

Likewise, the ΔT_g values (Figure 4.25) are almost similar in all blends which indicate that the time distribution of the reaction is almost similar. This further verifies that the miscibility is also homogeneous [174].

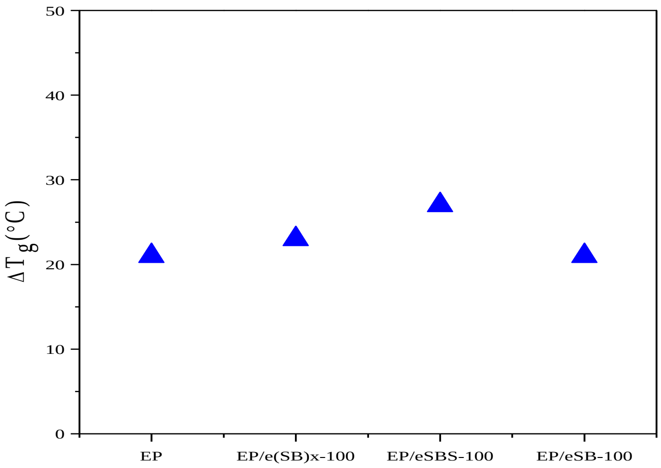

Figure 4.25: A plot of ΔT_g of EP and architecture of copolymer blends.

On the other hand, the values of glass transition temperature (T_g) and specific heat capacity (ΔC_p) of epoxy resin and the blends prepared by different methods EP/e(SB)$_X$-50 (MCPBA), EP/e(SB)$_X$-50 (PFA) and EP/e(SB)$_X$-50 (HFIP) are summarized in the Table 4.12.

Table 4.12: Characteristics T_g and ΔC_p data obtained from the DSC thermograms of epoxy resin and EP/e(SB)$_X$ blends prepared by different method

Sample code	T_g (^oC)	ΔT_g (^oC)	ΔC_p (J/g^oC)
EP	138	21	0.18
EP/e(SB)$_X$-50 (MCPBA)	138	15	0.12
EP/e(SB)$_X$-50 (PFA)	139	16	0.17
EP/e(SB)$_X$-50 (HFIP)	114	50	0.35

The glass transition temperature (T_g) of EP/e(SB)$_X$-50 (MCPBA) and EP/e(SB)$_X$-50 (PFA) blends is similar to the curing temperature (T_c). These T_g values indicate that the complete curing and cross linking reaction is also sufficient at that temperature. However, T_g of EP/e(SB)$_X$-50 (HFIP) blend was 114 ^oC which is lower value than that of EP/e(SB)$_X$-50 (PFA) and EP/e(SB)$_X$-50 (MCPBA) blends. The T_g of EP/e(SB)$_X$-50 (HFIP) blend represents the differences in cross-linking reaction between epoxy with e(SB)$_X$.

According to the data obtained, an expected specific heat capacity (ΔCp) of the EP/e(SB)$_X$-50 (HFIP) is 0.5 J/g^oC but measured value is 0.35 J/g^oC. This value is higher than other blends which also signify that the mobility of the EP phase is higher. This might be due to the side reaction in e(SB)$_X$ prepared by HFIP method which indicate the poor cross-linking reaction between epoxy and copolymer.

Similar results were also obtained for ΔT_g. The ΔT_g value of the EP/e(SB)$_X$-50 (MCPBA) and EP/e(SB)$_X$-50 (PFA) are similar to the epoxy resin but higher in EP/e(SB)$_X$-50 (HFIP) blend. This result indicates that the dynamics of molecular chain begin and vitrify at the same temperature range, whereas, it is longer in EP/e(SB)$_X$-50 (HFIP) blend. This is due to a broad transition region which indicates the partial miscibility. The width of the transition indicates the presence of microphase separation in the blend morphology [175].

4.3.2.2 Effect of e(SB)$_X$ copolymer weight fraction

Differential scanning calorimetry (DSC) thermograms of EP/e(SB)$_X$-50 blends with weight fractions (85/15, 70/30, 55/45 and 40/60) are explained in this section. The values thus obtained from each blends are presented in Table 4.13.

Table 4.13: The characteristics of T_g and ΔC_p value extracted from the DSC thermograms of epoxy resin and EP/e(SB)$_X$ blends with composition variation

Sample code	T_g (°C)	ΔT_g(°C)	ΔC_p (J/g°C)
EP/ e(SB)$_X$-50 (85/15)	139	17	0.16
EP/ e(SB)$_X$-50 (70/30)	138	15	0.15
EP/e(SB)$_X$-50 (55/45)	132	19	0.11
EP/ e(SB)$_X$-50 (40/60)	115	43	0.09

The T_g of EP/e(SB)$_X$-50 (85/15) was 139 °C which near to curing temperature. According to the published reports [39,174,175], the T_g of the cured epoxy phase showed the range from 120 °C to 330 °C depending on the curing condition and indicating the good cross-linking reaction in the blends. Based on these reports, our T_g values are also similar to our curing temperature (T_c). The epoxy resin and its blends show similar T_g which also demostrating the cross-linking reaction beteween epoxy resin and epoxidized copolymers in presence of methylene dianiline.

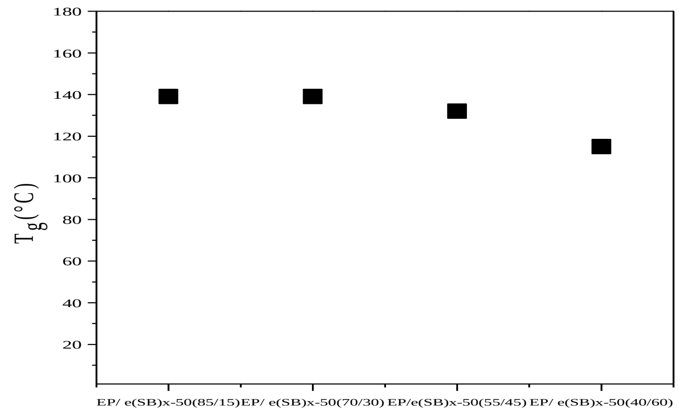

Figure 4.26: A plot of T_g of EP/e(SB)$_X$-50 (85/15), EP/e(SB)$_X$-50 (70/30), EP/e(SB)$_X$-50 (55/45), EP/e(SB)$_X$-50 (40/60) weight fraction blends.

However, T_g of EP/e(SB)$_X$-50 (60/40) blend was 115 °C (Figure 4.26) which shows the low value with compared to the other blends. This might be the effect of higher amount of copolymer containing with polystyrene and polybutadiene phase and these both phase have low T_g value.

Similarly, an expected the specific heat capacity (ΔC_p) of EP/e(SB)$_X$-50 (85/15) is 0.23 J/g°C, whereas, calculated value is 0.16 J/g°C (Figure 4.27). This ΔC_p value decreases gradually with increase in composition of copolymer. This indicates that molecular mobility of the EP phase is higher in EP/e(SB)$_X$-50 (85/15) blend and gradually decreases disorderness of EP phase in other blends with the increase in composition of copolymer . In contrast, ΔC_p of blends decreases with increase in composition of e(SB)$_X$ which indicate that the mobility of the EP chains seem to decrease with increase in e(SB)$_X$-50 composition. However, the mobility of the EP chains appear to relax with addition of higher amount of e(SB)$_X$. This is due to the fact that the amount of block copolymer increases which reduces the mobility of epoxy phase. It might be due to the fact that the higher amount of block copolymer chains restricted the mobility of EP phase.

T_g is also correlated to the nanostructure of the oriented material with different phases such as crystalline to amorphous which also emphasize attractive applications of the microindentation method to the study of the mechanical properties of polymer surfaces [176]. Saiter *et al.* [175] also found that the low value of ΔC_p at T_g considered as thermodynamically strong and kinetically fragile in melamine formaldehyde resin system. Our system is also low ΔC_p which is thermodynamically stromg and less fragile. This means that epoxy resin is toughened by copolymer which decreased the fragility of epoxy blends.

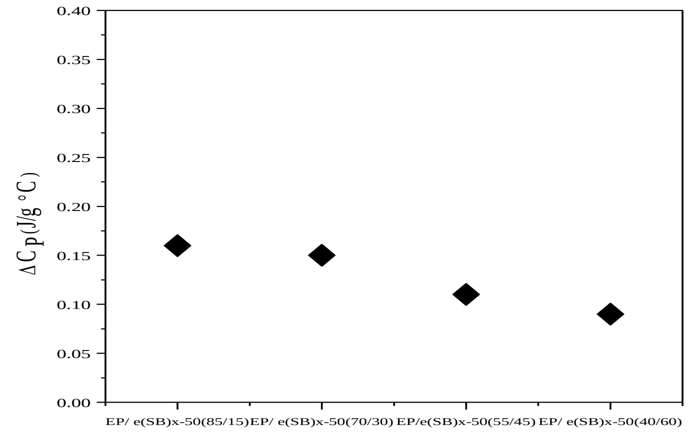

Figure 4.27: A plot of ΔC_p of EP/e(SB)$_X$-50 (85/15), EP/e(SB)$_X$-50 (70/30), EP/e(SB)$_X$-50 (55/45), EP/e(SB)$_X$-50 (40/60) weight fraction blends.

The ΔT_g of the composition variation blends are presented in Figure 4.28. The values are similar in all blends except 40/60 composition blend. This indicates that struture distribution is almost similar to all bends however, the 40/60 composition blend shows the wider range of structure distribution. This is due to the presence of large amount of copolymer which took the maximun time of relaxation [175]. This result also indicates the miscibility of the EP and copolymer is similar in almost blends.

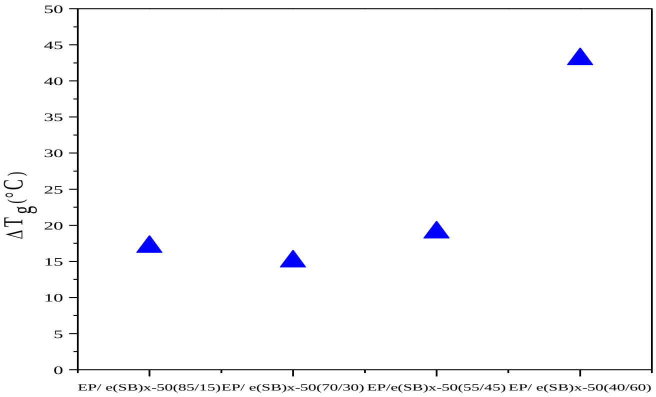

Figure 4.28: A plot ΔT_g of EP/e(SB)$_X$-50 (85/15), EP/e(SB)$_X$-50 (70/30), EP/e(SB)$_X$-50 (55/45), EP/e(SB)$_X$-50 (40/60) weight fraction blends.

In conclusion, the glass transition temperature (T_g) and specific heat capacity remains almost same as epoxy resin in all parameter. The glass transition temperature (T_g) of the EP and blends conclude that they were completely cured at that curing temperature. The values of ΔC_p also indicate that the mobility of the EP phase decrease in blends due to the miscibility of two different component.

4.4.1 Mechanical Properties and Deformation Behaviour

The mechanical properties and deformation behavior of the blends and composites have been studied by the microindentation method. Those measurements provide the information about stiffness of the samples as well as plastic and elastic components of deformation. In this section, the microhardness behaviour of the blends and composites studied are discussed

Each sample was tested five times to obtain the resonable statistical data. For example, the load (*P*)-indentation depth (*h*) curves of the EP/e(SB)$_X$-25 blends obtained for five different specimens are presented in Figure 4.29.

It can be seen that the indenter penetrates into the sample untill the predefined load of 1000 mN is reached. The maximum reached indentation depth lies between 16 µm and 19 µm. Using the suitable mathematical treatment, the average curve can be calculated which is shown bya blue line in Figure 4.29.

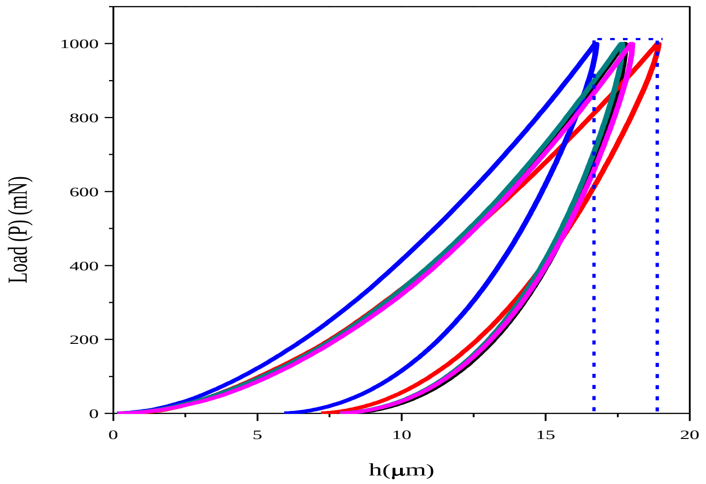

Figure 4.29: Load (P)-indentation depth (h) diagrams of loading and unloading curves of five different specimens of EP/e(SB)$_X$-25 blends; pink coloured curve is the average of five different curves.

For further evaluation of the properties of the materials, the average of five different curvess were taken. Using these curves, different parameters such as Martens hardness (HM), indentation modulus (E_{IT}), universal hardness (MH) etc. can be determined (as described in the procedure in section 3.5).

4.4.2 *Effect of degree of epoxidation of (SB)$_X$ copolymer*

The load (*P*)–indentation depth (*h*) diagrams of some of the epoxidation degree variation blends (comprising 30 % by weight of e(SB)$_X$ and 70 % by weight of the EP) are present in Figure 4.30.

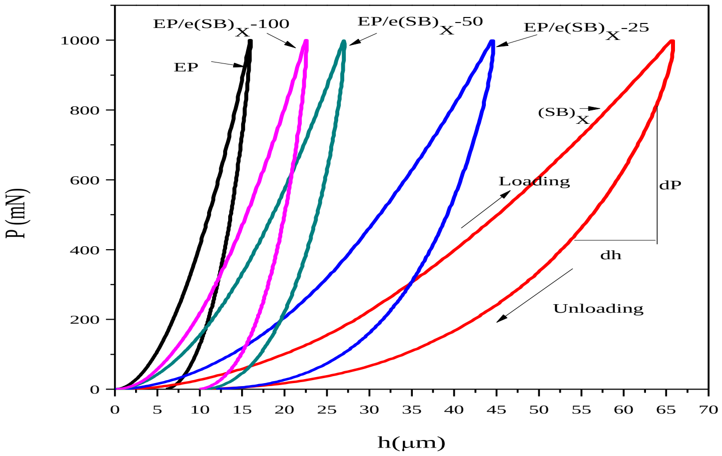

Figure 4.30: Load (P)–indentation depth (h) diagrams of the epoxy resin (EP) compared with its blends containing 30% by weight of e(SB)$_X$ epoxidized to different degrees as indicated and neat (SB)$_X$ block copolymer; black line = EP, red line = neat (SB)$_X$, blue line = EP/e(SB)$_X$-25, dark green line = EP/e(SB)$_X$-50 and purple line = EP/e(SB)$_X$-100.

For the sake of comparison, the curves of the neat copolymer alone and the cured resin are also included in Figure 4.30. For all the samples, the maximum load of 1000 mN was used. Figure 4.30 shows that the pure $(SB)_X$ has the flattest curve along all the materials, with highest value of indentation depth *i.e.* 65 µm, an observation expected for a soft elastomeric material. At first glance, it can be observed that the area under the curve is maximum for $(SB)_X$ compared with that for other materials (Figure 4.30). When 30% by weight of the epoxidized copolymers $e(SB)_X$ is added to the resin the maximum indentation depth (h_{max}), the area under the curves, decrease progressively with the maximum for the pure EP resin. At the same time, the slopes of initial part of unloading curves progressively increase.

As introduced in section 3.5, the indentation modulus was determined from the slope of initial part of the unloading curve (see figure 4.30 indicated by dP/dh for sample SBS for instance). The lower the magnitude of the slope, the lower will be the value of the indentation modulus, E_{IT} (as well as the hardness value) of the sample. Thus, careful inspection of Figure 4.30 reveals that the sample $(SB)_X$, being the softest material, has the lowest value of E_{IT}. The largest value of E_{IT} (i.e. 3097 MPa) is possessed by the epoxy resin (see Table 4.14). The values have been collected in Table 4.14.

Table 4.14: The characteristics data of HM and E_{IT} of $(SB)_X$, epoxy resin (EP) and their epoxy resin/$e(SB)_X$ blends

Sample code	HM(MPa)	E_{IT} (MPa)	W_t (nJ)	h_{max} (µm)
$(SB)_X$	8.42 ± 0.45	170 ± 13	21952 ± 686	64
$EP/e(SB)_X$-25	16.76 ± 1.56	406 ± 46	15454 ± 925	45
$EP/e(SB)_X$-50	54.88 ± 2.32	1434 ± 57	8822 ± 183	25
$EP/e(SB)_X$-100	68.07 ± 3.62	1760 ± 143	7892 ± 264	22
EP	135.36 ± 6.56	3097 ± 157	5536 ± 203	16

The indentation moduli and the hardness values of the blends of epoxidized block copolymer and epoxy resin, which are hence not identical, lie between the values of $(SB)_X$ and EP resin. Among the blends, the modulus value of the blend of resin with $e(SB)_X$-25 is the lowest (*i.e.* 406 MPa), which can be attributed to the largest rubbery polybutadiene content of the $(SB)_X$ block copolymer which remains unepoxidized.

The blends ($EP/e(SB)_X$-50) and ($EP/e(SB)_X$-100) have comparable slopes in their unloading curves and hence have comparable moduli (*i.e.*1400-1800 MPa) and hardness values (*i.e.* 55-68 MPa).

It can be observed that the HM value of EP resin reduces drastically on addition of 30% by weight of e(SB)$_X$ copolymer. The Marten’s hardness of the EP resin is about 140 MPa. The unmodified block copolymer (BCP) is the softest material with HM value of 8 MPa. Addition of BCP (SB)$_X$ epoxidized to 25% to the epoxy resin (EP), it shows least value of HM (*i.e.*18 MPa). This should be noted that it has macrophase separated structure (see Figure 4.31). However, the epoxy resin (EP)/50% epoxidized (SB)$_X$ blends shows 55 MPa value of HM. This increment is due to the formation of partially nanostructured (Figure 4.31). Similarly, the EP/e(SB)$_X$-100 blend performs about 70 MPa valueof HM which shows that the complete nanostructured blend gives 50% Marten’s hardness with compared to epoxy resin (Figure 4.31). The Martens hardness (HM) of the samples presented in Table 4.14 are plotted as bar diagrams in Figure 4.31.

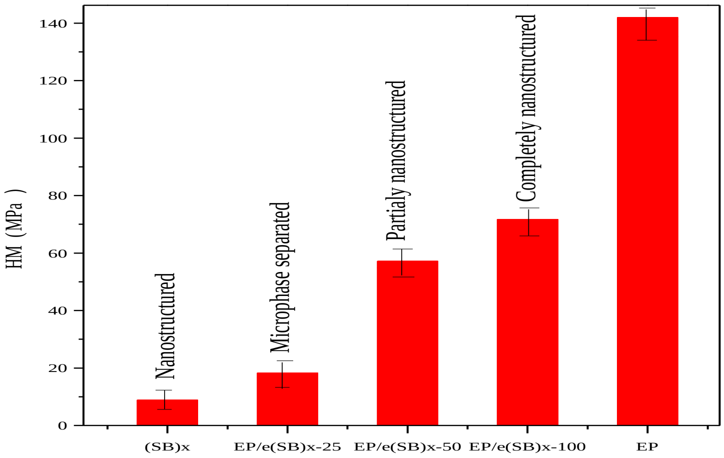

Figure 4.31: Microhardness value of epoxy resin (EP) compared with EP/e(SB)$_X$ (70/30) blends with variation of epoxidation degree e(SB)$_X$ and neat (SB)$_X$.

Among the blends the completely nanostructured blends have the best HM and E_{IT} values. The Martens hardness depends strongly on the phase morphology [36] which is completely changed in the blend as shown in TEM images (Figure 4.7). It can be concluded that the blending with block copolymer make the resin significantly softer.

Now, we discuss the maximum indentation depth (h_{max}) and area (W_t) under the loading and unloading curve to correlate the stiffness and toughness of the blends. The value of and h_{max} (see Table 4.14) of the pure (SB)$_X$ is higher than the blends and epoxy resin which shows the material used in the experiment is very tough. The value of h_{max} decreases with blends to EP which indicates that the stiffness increases to EP. Likewise, the value of area (W_t) also decreases from blends to EP. This also indicates that the toughness decreases. We found that the toughness is higher EP/e(SB)x-25 blend which have lower epoxidation degree of $(SB)_X$. We should attempt to find an optimum stiffness and toughness in higher epoxidation level which will be great challenge.

In summary, the hardness and, hence, the elasticity modulus of the blends increases in epoxidation degree of the star block copolymer. An optimum required in HM and E_{IT} is achieved when the blends have nanostructured morphology.

4.4.2 Effect of block copolymer architecture

In Figure 4.30, the load (*P*)–indentation depth (*h*) diagrams of some of the blends (comprising 30 % by weight of epoxidized copolymer and 70 % by weight of the resin) are presented for the explanation of mechanical properties. The curves of the neat star copolymer and the cured EP resin are also included for the comparison with blends. The discussion of the microindentation properties are presented here only qualitatively. First, the hardness (of any kind such as Vickers hardness, Martens hardness, etc.) and indentation modulus are generally correlated; the increase in one property has the consequence of increase of the other [42,176]. In other words, the hardness and indentation modulus increase or decrease in parallel way. Before further discussion, the amount of elastomeric phase in parent block copolymers is worth to mention. The samples SBS, SB and $(SB)_X$ have 50%, 52% and 70% by weight of elastomeric polybutadiene phase (see Table 3.1 in section 3.1.1).

The indentation moduli (and thence the hardness values) of the blends are similar (Table 4.15) and fall intermediate between the values of the two samples. Amongst the blends, the modulus value for the blend of resin with $e(SB)_X$ is the lowest, which can be attributed to the largest rubbery polybutadiene content of the block copolymer $(SB)_X$ (see Table 3.1).

Table 4.15: The characteristics data of HM and E_{IT} of epoxy/architecture of copolymer blends

Sample code	HM(MPa)	E_{IT}(MPa)	Wt (nJ)	h_{max} (μm)
EP	135 ± 6	3097 ± 157	5536 ± 203	16
EP/e$(SB)_X$-100	68 ± 3	1760 ± 143	7892±264	22
EP/eSBS-100	76 ± 4	1995 ± 110	7336±224	21
EP/eSB-100	62 ± 33	1643 ± 721	7678±816	29

It can be seen that the HM value of EP resin also decreases almost 50% on addition of 30% by weight of different architecture of copolymers. The EP/e(SB)$_X$-100 blends is the one having fairly low HM and E_{IT} compared to other blends. This may be due to highest content of polybutadiene. In all the cases, HM value decreases from about 140 MPa to 90 Mpa; and the blends are completely nanostructured with best HM and E_{IT} values. The HM value of the samples presented in Table 4.15 are plotted as bar diagrams in Figure 4.32.

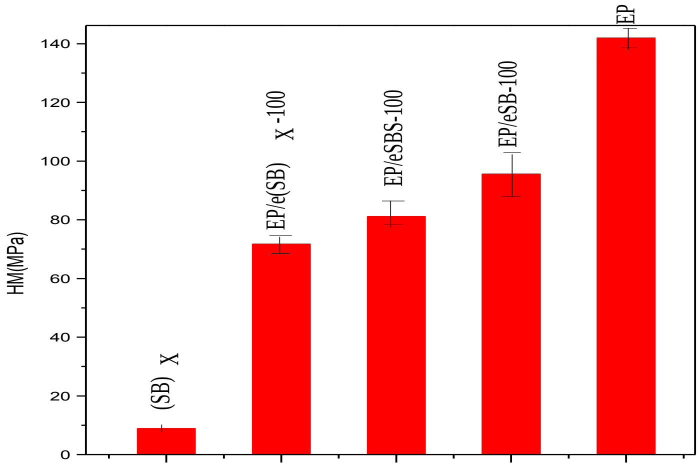

Figure 4.32: HM bar diagrams of epoxy resin blend with epoxidized block copolymers (e(SB)$_X$-100, eSBS-100 and eSB-100) compared with that of epoxy resin and neat (SB)$_X$.

Likewise, the value of area (W_t) under loading and unloading curve and indentation depth (h_{max}) (see Table 4.14) are almost similar in all the blends.

It can be concluded that the architecture of the block copolymers does not play significant role in the mechanical properties of the blends.

4.4.3 Effect of nanoparticles in blends

The composition of epoxy resin/nanoparticle was 97/3 by weight. For the blend nanocomposite, the resin/e(SB)X/nanoparticles was 70/27/3 by weight. The HM bar diagram (see Figure 4.33) of the epoxy resin/boehmite (OS) composite shows the highest value of microhardness than the epoxy resin whereas the composite of layered silicate (LS) gives the lower microhardness value than the epoxy resin. This might be due to the effect of dimensionality of the nanofillers where boehmite and layered silicate nanofillers are three and two dimensional structures, respectively. The effect of nanoparticles on blends composite increases the hardness and indentation modulus in similar way.

One can see that the addition of 3% by weight of boehmite nanofiller causes a significant increase in HM bar diagram of the resin (Figure 4.33). Similarly, the bar diagrams for the block copolymer modified resins and composite are also decreased. Thus, the loss of the modulii and hardness caused by addition of block copolymer is compensated by the addition of small amount of nanofiller.

In case of the composites comprising layered silicate (LS) nanofiller, some abnormal phenomena are observed (Figure 4.33). For instance, the HM bar diagram of the resin with filler is found to decrease, *i.e.* a loss in modulus and hardness values, which is a surprising observation because generally an expectation is to increase in hardness and indentation modulus due to the addition of inorganic filler. Similar results are obtained for the EP/e(SB)$_X$-25/LS composites containing layered silicate (see Figure 4.33).

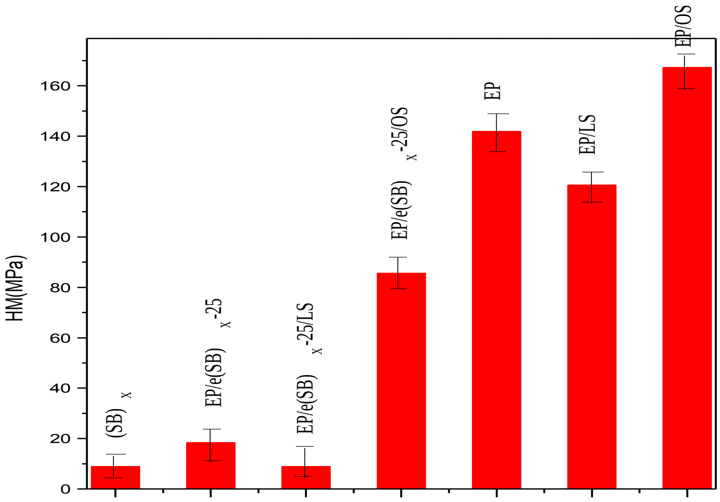

Figure 4.33: HM bar diagrams of epoxy resin and EP/e(SB)$_X$-25 composite of boehmite/layer silicate nanofillers compared with that of neat (SB)$_X$ and epoxy resin.

It seems that the curing properties of the resin might have been suppressed by the addition of LS leading to the worsening in surface mechanical properties. All the blends and composites (at higher degree of epoxidation) are optically transparent implying the existence of predominantly nanostructured morphology. It is found that the surface mechanical properties of the blends as determined by microindentation measurements generally enhance by the incorporation of nanoparticles.

The epoxidized $(SB)_X$ contributed to increase the toughness of the resin while the nanoparticles contributed to increase their hardness. The nanostructured morphology of the blends and composites has been confirmed by electron microscopic studies in section 4.2.2. This result indicates that the blend nanocomposites enhance the toughness and compensate for the loss of the stiffness caused in the resin by the addition of block copolymer.

The result of microhardness, indentation modulus, area under the curve (W_t), and maximum indentation depth (h_{max}) are presented in Table 4.16 which confirms that the blend composite has higher value than others.

Table 4.16: The characteristics data of HM, E_{IT}, W_t and h_{max} of epoxy resin (EP), epoxy resin/e$(SB)_X$-25 blends and thier nanocomposites

Sample code	HM(MPa)	E_{IT} (MPA)	W_t (nJ)	h_{max}(μm)
EP	135 ± 6	3097 ± 157	5536 ± 203	16
$(SB)_X$	8.42 ± 0.45	170 ± 13	21952 ± 686	64
EP/OS	165 ± 1	4412 ± 60	4926 ± 10	14
EP/LS	110 ± 9	2672 ± 350	6245 ± 385	18
EP/e$(SB)_X$-25	16 ± 1	406 ± 46	15454 ± 925	45
EP/e$(SB)_X$-25/OS	48 ±37	955 ± 698	11874 ± 4205	34
EP/e$(SB)_X$-25/LS	7 ±1	177 ± 26	31899 ± 14364	71

Thus, the result shows that the value of HM and E_{IT} are higher in blend nanocomposite which concludes that the nanoparticles compensate the stiffness in tough blend materials.

4.4.4 Toughness and deformation behaviour

One of the prime objects of the present study is to characterize the deformation behaviour of the nanostructured blends in attentation to the toughness enhancement. Toughness is an important property of the materials which is generally accessed by high speed mechanical testing evaluating precisely the total plastic deformation energy [119,120,176]. However, due to the lack of large amount of specimens needed for macroscopic testing, the classical evaluation of toughness was not possible. Alternatively, the energy absorbed during microindentation can be regarded as a parameter related to toughness of the blends [176]. The load (*P*)-indentation depth (*h*) diagram of each sample can be evaluated to calculate the total energy absorbed during the indentation process. Further, the indentation depth (h_{max}) and residual depth (h_{res})

can be correlated with the ease of plastic and elastic deformation of the material.

The deformation energy determined from the area under each curve has been indexed in Table 4.17 for some of the samples. The total energy has been split into plastic (U_{pl}) and elastic (U_{el}) energies.

Table 4.17: Characteristic plastic (U_{pl}) and elastic (U_{el}) energies data obtained from the microhardness measurements of the epoxy resin (EP) and EP/e(SB)$_X$ blend with epoxidation degree variation

Sample code	U_{pl} (nJ)	U_{el} (nJ)
EP	2634	2897
EP/e(SB)$_X$-100	4481	3418
EP/e(SB)$_X$-50	5094	3729
EP/e(SB)$_X$-25	8003	7451
(SB)$_X$	9582	12370

The results for the blends with constant composition (*i.e.* EP/e(SB)$_X$ weight ratio =70/30) and variable degree of epoxidation are compared with that of EP and pure block copolymer (SB)$_X$ in Table 4.16 and also presented in Figure 4.34.

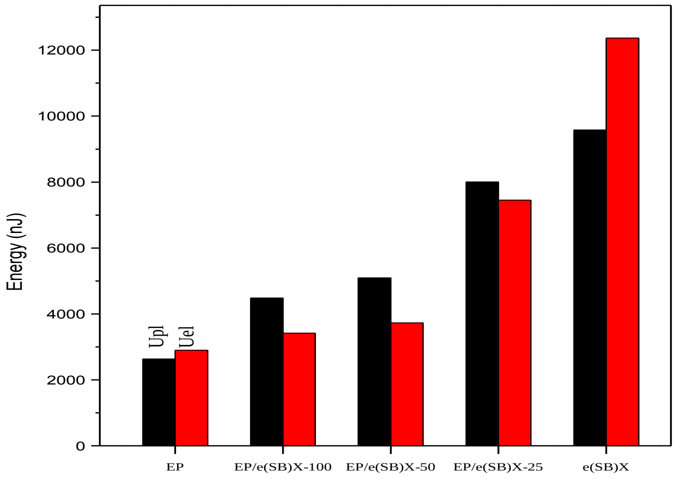

Figure 4.34: Energy bar diagram of EP and EP/e(SB)$_X$ blends with epoxidation degree variation and pure (SB)$_X$; composition of epoxy resin and e(SB)$_X$ in blend is 70/30.

From Figure 4.34, the following observation can be made. For the pure components EP and (SB)$_X$, the energy utilized for elastic deformation during indentation is slightly higher than the plastic deformation energy.

Even though, the amount of total deformation energy may not be significant for the macroscopic mechanical properties. It can be important to correlate with the toughness and deformation behaviour. In Figure 4.35, the difference in epoxidation degree of (SB)x copolymer gives different deformation energy which can be correlated with the morphology. The correlation is rather qualitative.

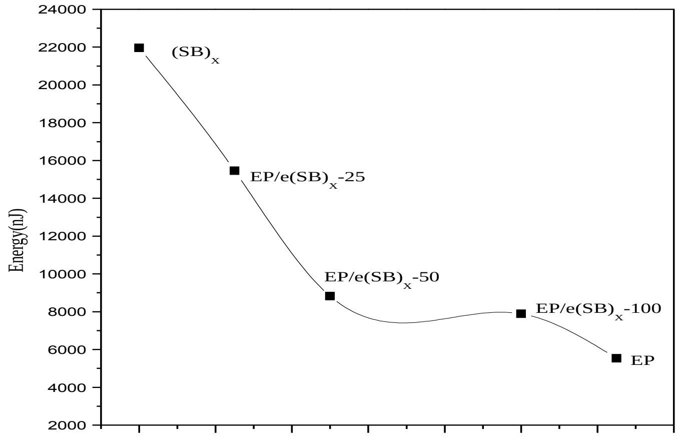

Figure 4.35: Deformation energy diagram plot of (SB)x, epoxy resin (EP) and the epoxidation degree variation of epoxy resin/ BCP blends.

In fact the elastic deformation energy of (SB)x is much higher than the plastic deformation energy which can be correlated with thermoplastic elastomeric properties of the block copolymer [5]. In the blends, the plastic deformation energy predominates implying that a larger part of energy is utilized for plastic deformation which contributes for the toughness of the materials [64, 179].These observations correlate well with observed intense plastic deformation of the blends with the aid of SEM analysis (see Figure 4.37).

The plastic deformation energy for EP is about 2600 nJ. The blends with 30 wt.-% of $e(SB)_X$-50 and $e(SB)_X$-100 have U_{pl} value in the range of 4500-5100 nJ. The value of U_{pl} drastically increase for the blend with 30 wt.-% of $e(SB)_X$-25 with 8000 nJ.

Thus, it can be concluded that the optimum toughness is obtained in EP/$e(SB)_X$-25 blend. However, due to large particle size (4.5 µm, see Figure 4.7) the blend is not transparent. Thus, with respect to toughness/transparent ratio, the optimum epoxidation level of $(SB)_X$ is 50-100 wt.-% when the EP resin is induced with nanostructured morphology of block copolymer.

Indentation plasticity

The concept of indentation plasticity is used for the calculation of microhardness dissipation parameter (MDP). MDP is developed to serve as an indicator of a coating's durability. It is a ratio of the energy of dissipation to the total energy associated with elastic-plastic deformation measured during nanoindentation [155]. The application of this concept is used for the microindentation measurement in this section for nanostructured materials. Microindentation has found a wide application in evaluating coating's "toughness". Based on the equation (5) (section 3.3.4), the MDP was calculated for the determination of plasticity of the EP resin, EP/e(SB)$_X$ blends, and composite and is indexed in the Table 4.18.

Table 4.18 The characteristic microhardness dissipation parameter (MDP) data of specimens

Sample code	MDP
(SB)$_X$	0.43
EP	0.47
EP/e(SB)$_X$-25	0.52
EP/e(SB)$_X$-50	0.58
EP/e(SB)$_X$-100	0.57
EP/eSBS-100	0.56
EP/eSB-100	0.56
EP/OS	0. 56
EP/LS	0. 52
EP/e(SB)$_X$-25/OS	0.73

It can be seen that the pure (SB)$_X$ and epoxy resin have low MDP values which indicate that the plastic deformation is lower in pure (SB)$_X$ and epoxy resin compared to elastic deformation as also observed in Figure 4.39. However, the epoxy resin showed brittle glass likes behaviour as revealed by the SEM micrograph (in Figure 4.41a, section 4.4.5). In contrast, MDP value higher is in the blends and composite which indicate that the latter dissipate the higher amount of energy associated with plastic deformation during microindentation

In terms of plasticity, the plastic deformation is higher in blends and composite which leads to stress relaxation in materials. The easier the stress relaxation proceeds, the larger plasticity is inherent in the material [64,155,156]. Thus, also comparing the plastic strain with the total strain, an indention test directly gives a simple's rough but quick indication of toughness [155]. The blends show the higher indentation plasticity (0.52–0.56) while the nanocomposite with boehmite (EP/e$(SB)_X$-25/OS composite) shows much higher values (0.73) (see Table 4.17).

It can be concluded that the plastic deformation is higher in blends and nanocomposites. However, epoxy resin and pure $(SB)_X$ have low plastic deformation.

4.4.5 Fracture surface analysis

The pure epoxy resins (EP) and blends were investigated using cyro-facture surfaces by scanning electron microscopy (SEM). The fracture surface morphology of the epoxy resin, blends, and nanocomposite has been discussed under the topics: neat epoxy resin, epoxy resin/SBS bends as well as epoxy resin/e$(SB)_X$ blends and epoxy resin/boehmite nanoparticles nanocomposite.

SEM analysis of the fracture surfaces of the blend formed by epoxy resin and $(SB)_X$ block copolymer (a star block copolymer), 70/30 composition by weight, is shown in Figure 4.36.

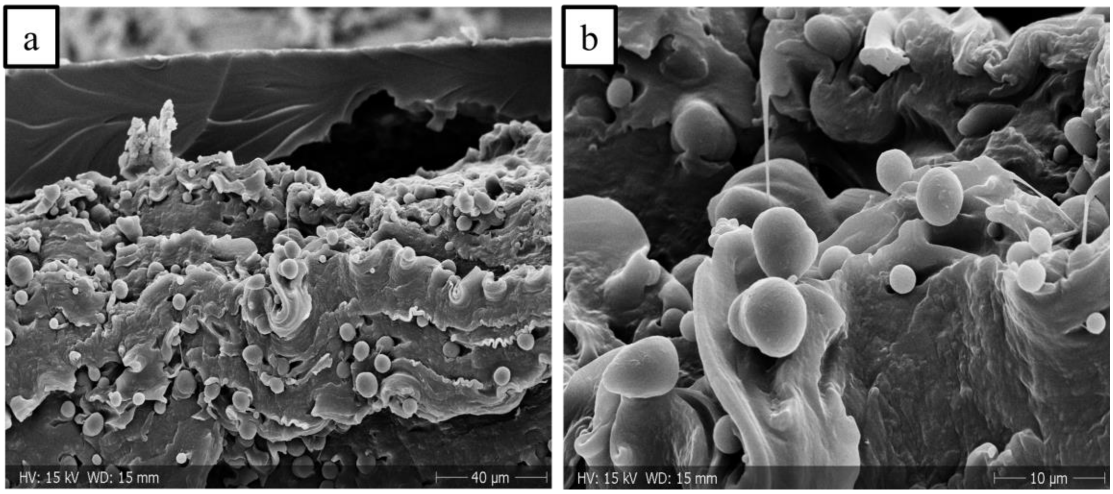

Figure 4.36: Secondary electron mode SEM images of different magnifications of blend between epoxy resin and (SB)x block copolymer in 70/30 composition; a) lower and b) higher magnification.

SEM images of the fracture surface of the blend reveals complete incompatibility with two distinctly separate phases: epoxy resin and $(SB)_X$ block copolymer (see Figure 4.36). These SEM images are typical of incompatible polymer blends in which each phase attempts to minimize the area of contacts with the other polymer [63]. Similar morphologies were observed in incompatible polymer blends, such as polystyrene/ polybutadiene [177], polypropylene/ polystyrene [178], polycarbonate/ polymethyl methacrylate [179] systems, and even in the blends of high and low density polyethylenes [180]. Also in epoxy containing blends, such behavior was frequently observed [82].

Figure 4.36 shows completely segregated polymers: epoxy resin phase (towards the upper part of Figure 4.36a) and an aggregate of block copolymer (towards the centre of micrograph in Figure 4.36a). The block copolymer phase forms a large aggregate of the oval and spherical particles of 25 µm in diameter on the fracture surface of the blend comprising 70% epoxy resin and 30% $(SB)_X$ block copolymer. There is no sign of deformation of any other phases. The resin component breaks in identical manner as the pure epoxy resin. It can be concluded that the fracture of the blend depicted in Figure 4.36 does not dissipate significant amount of energy. There is thus no contribution in toughness enhancement of the blend. The premature fracture is rather promoted by weak interfacial strength of the phases in the blend. These results suggest that either the epoxy resin itself or $(SB)_X$ copolymers need to be chemically modified to produce compatible blends so that the improved thermal and mechanical properties (including toughness) may be expected.

The scanning electron micrographs of the fracture surface of neat epoxy resin are shown in Figure 4.37a in lower and higher magnifications. The neat epoxy resin comprises only one phase. The fracture surface depicts the regions with several cracks-like structures. Many flat terraces may be observed which are typical of brittle materials. This behavior is correlated with the low plasticity in section 4.4.

The earlier works reported in literatures also suggest that the cured epoxy resin becomes hard and brittle due to cross-linking between the epoxy resin and hardener [78,82,106]. The brittleness is connected with inherent chemical structure of the resin comprising chains with bulky groups, cross-linked in a network structures. Additionally, the fracture surface shows that the cracks have propagated rapidly in a definite direction. In summary, the neat epoxy resin is hard and brittle material which breaks in the manner similar to inorganic glasses [92]. It further suggests that the morphology of epoxy resin must be modified to implant the toughness to this material.

Compared to the unmodified $(SB)_X$/epoxy resin blend, epoxidation of $(SB)_X$ has changed the fracture surface morphology as shown in Figure 4.37b. The copolymer was epoxidized to 50 wt.-% and blended with epoxy resin in different weight fraction. Scanning electron micrographs of the blend comprising 70 wt.-% of epoxy resin and

30 wt.-% of e(SB)$_X$ is shown in Figure 4.37b and c. Entirely different morphological pattern is observed in the blend with epoxidized copolymer, e(SB)$_X$-50. The higher magnification SEM image (Figure 4.37b) shows that their fractured surface reveals intense fibrillar structures as a result of large plastic deformation (section 4.4, indentation plasticity). The irrecoverable plastic deformation of the matrix contributes significantly to the better toughness of the material [155].

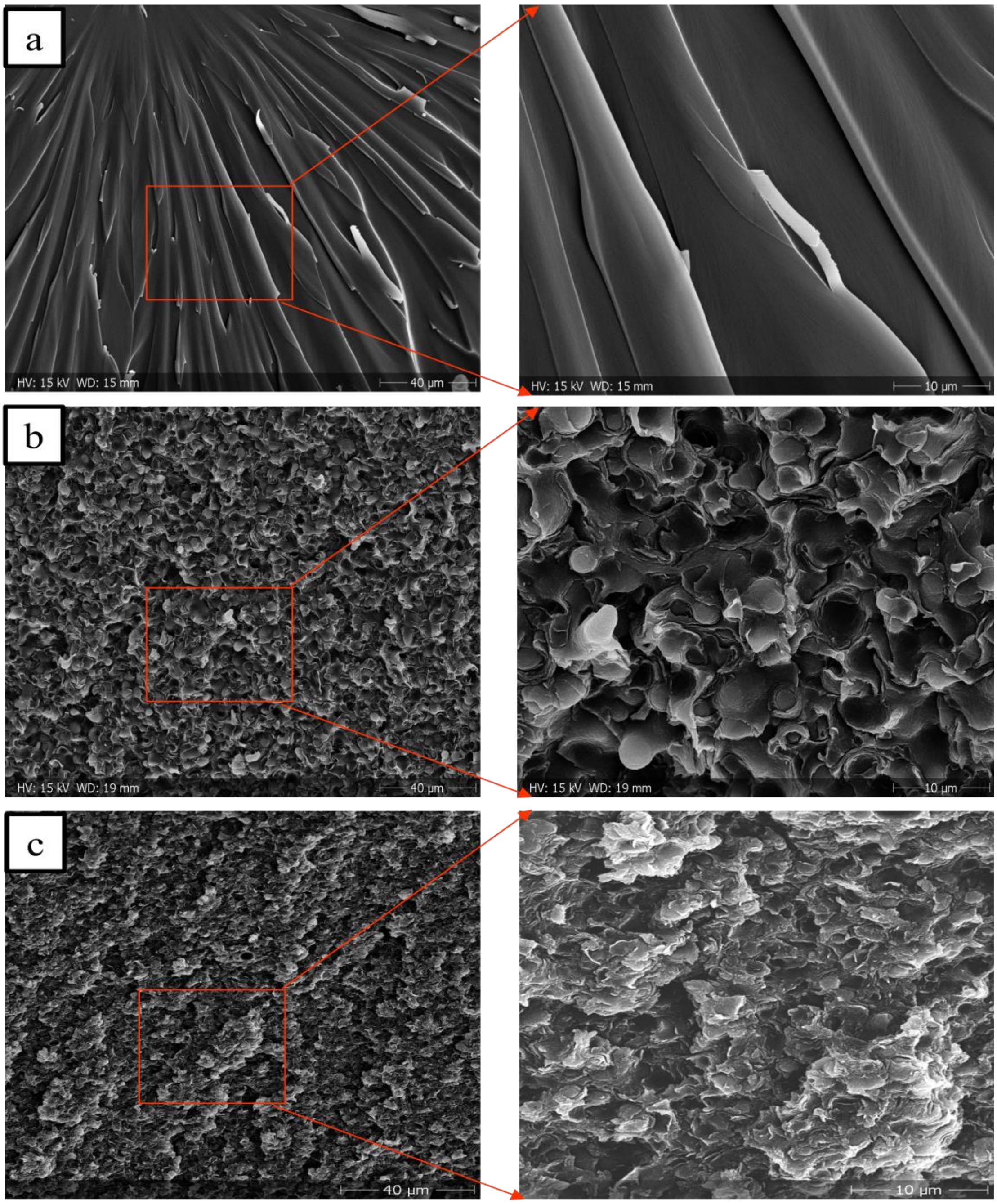

Figure 4.37: Secondary electron mode of left lower and right higher magnification SEM images of; a) an epoxy resin, b) EP/e(SB)$_X$-50 (70/30 composition by weight) blend and c) EP/e(SB)$_X$-50/OS (70/27/3 composition by weight) composite.

Abruptly enhanced surface texturing is generated upon the addition of block copolymer. The e(SB)$_X$-50 modified epoxy resin is with rough and ridgy fracture surface due to the plastic deformation behavior of the epoxy resin as well as well-bound epoxidized block copolymer. Similar result has been observed by Iijima *et. al.* [68] in the preparation of epoxy-terminated poly (aryl ether sulfone) (PSE) and their use as modifiers for epoxy resins. They noticed that PSE modified resin was rough and ridgy based on the plastic deformation of the epoxy matrix itself prior to failure [68]. In the frame of fracture surface morphology, Thompson *et al.* [27] showed the particle voiding and extensive shear deformation with increase in molecular weight of block copolymer in epoxy resin/block copolymer blends. The fracture surface morphology observed in our samples also indicates that the blend undergoes extensive shear deformation and needs more fracture energy during deformation. This is also correlated with the higher plasticity (section 4.4).

Careful inspections of Figure 4.37b reveals that the needles like fibrillar structures surround the disc like structures which are 5 µm in diameter. The discs have their borders slightly deformed and pointed outwards from the fracture surface; a notion of plastic deformation of the microscopic particles.

It should be kept in mind that the observed deformed particles are formed by epoxy resin and also the alter is present in the majority fraction (70 wt.-%). That the majority phase forms the particulate morphology and undergoes plastic deformation during fracture process is a strong evidence of compatibility of the polymer blend. This result also shows that the block copolymer particles toughen using mechanisms similar to those established by Pearson and Yee [32,33,98-100] for the liquid rubber toughened epoxy systems. Fracture surface morphology of the blend comprising 30 parts by weight of epoxidized star block copolymer, e(SB)$_X$-50 (degree of epoxidation 50 wt.-%), demonstrated an internal plastic deformation; a micromechanical requirement for toughness enhancement of the materials (see Figure 4.37b).

The enhancement in toughness often leads to decrease in stiffness or hardness of materials [60], a disadvantage for practical application. In order to compensate this loss in stiffness, a small amount of nanofiller may be fruitful. Thus, a blend nanocomposite with 3 parts by weight of total blend composition was prepared for the same blend as presented in Figure 4.37a and b. The nanofiller were organically modified boehmite. The results are presented in Figure 4.37c.

In higher magnification SEM image (Figure 4.37c), small spherical particle structures of roughly 2.5 to 5 µm in diameter can be observed. These are boehmite nanoparticles which are evenly distributed in the polymer blend matrix. The uniform distribution of nanoparticles should contribute to increase stiffness, toughness, and thermostability of the materials, simultaneously [119-120,145].

From the above discussion, we can conclude that the neat epoxy resin is brittle which breaks like glass. The epoxy resin/e(SB)$_X$ blend as well as its nanocomposites reveals intense plastic deformations as demonstrated by fine fibrillar structures leading simultaneously to enhanced toughness and stiffness of the materials. Besides, it is interesting to note that the fibrillar structures are observed in the blend without nanoparticles (Figure 4.37b); and this persists mere dominantly in the fracture surface of the blends with nanoparticles (Figure 4.37c). In the latter case also a large number of fibrillar tips can be observed which imply much enhanced toughness properties of the blends. The plastic deformation is higher in the blends and nanocomposite.

4.5 Scheme of Structure-Properties Correlations

The synthesis of nanostructured epoxy resin was achieved by the epoxidation of styrene/butadiene block copolymers which served as one of the blends components. The blends were prepared by changing epoxidation degree and architecture of the copolymer as well as composition.

The resins were investigated using different techniques, such as FTIR spectroscopy, electron microscopy, thermogravimetric analysis, differential scanning calorimetry, and mechanical properties by microhardness. It was found that the morphology of the blends was strongly influenced by the degree of chemical modification of the block copolymer. With the increase in the extent of chemical modification, the degree of compatibility among copolymer chains and epoxy segments increases. The nanostructuring was favoured by increased epoxidation level of the copolymer.

At low degree of epoxidation, the macrophase separation occurs with typical particle matrix morphology (Figure 4.38a). The blend remains translucent. At moderate degree of epoxidation, the partial nanostructures formed by microphase separation predominate over a wide range with some large micron sized epoxy particle morphology (Figure 4.38b). The blend remains largely transparent. Likewise, the complete nanostructures is formed by microphase separation at higher degree of epoxidation in which epoxy particles distributed at about 50 nm and PS cylinders in 25 nm sized morphology (Figure 4.38c). The blend thus becomes transparent. The morphology formation of the copolymer is depicted in Figure 4.38.

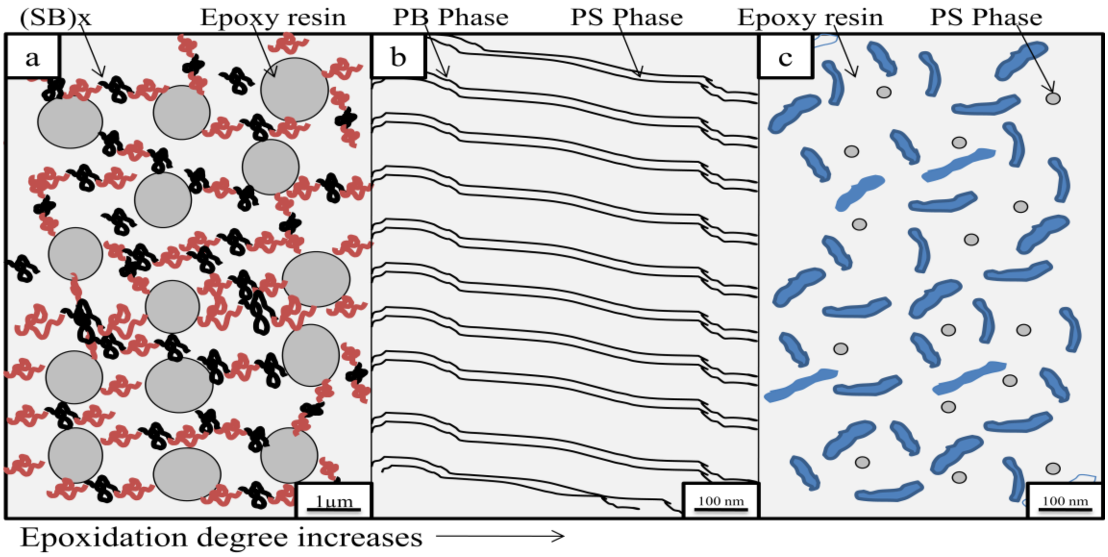

Figure 4.38: Schematic representation of the morphology developed by the investigated epoxy resin/block copolymer system of the epoxidation degree variation.

Hence, the morphologies of the blends were correlated with the deformation behaviour and mechanical properties of the epoxy resin blends. Based on the values of deformation energy calculated from the microindentation measurements, a general picture of toughness evaluation can be traced out as illustrated in Figure 4.39.

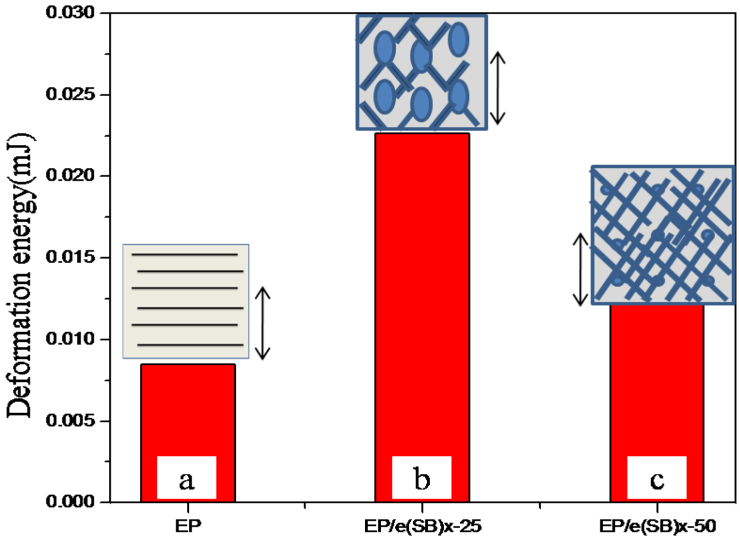

Figure 4.39: Scheme showing morphology-deformation behaviour correlation in the blends of epoxy resin and functionalized block copolymer; the corresponding morphology and deformation structures are sketched above each bar daigram, arrow shows deformation direction.

a) In a pure epoxy resin, the morphology is homogeneous and the material deforms by rapid crack propagation leading to the flat fracture surface. The cracks might have been originated from individual crazes fromed under the action of external load. As a result, the deformation energy is low.

b) In EP/e$(SB)_X$-25 blend, the morphology is comprising of heterogeneous particles and matrix; and the material undergoes the shear deformation leading to the formation of disc and niddle like fibrillar structure. This results in high deformation energy.

c) In EP/e$(SB)_X$-50 blend, the morphology is largely nanostructure and the materials deforms plastically by the formation of shear bands similar to case (b). The deformation energy in this case decreases as matrix is no more a rubbery phase. The same trend is followed when the block copolymer epoxidized to much higher degree is used with the epoxy resin to prepare blends.

CHAPTER – 5

5. CONCLUSION AND RECOMMENDATIONS

Conclusion

As targeted in the objective of the present work, the toughened and transparent epoxy resin blends was fabricated by templating nanostructure using chemically modified styrene/butadiene (SB) based block copolymer. The materials were characterized by different techniques which delivered conclusions on various aspects of the blends.The blends possessed the highly ordered nanostructures with periodicity of approximately 50 nm. The results can be concluded as follows:

1. Styrenic block copolymers based on polystyrene and polybutadiene, including particularly an $(SB)_X$ star block copolymers, were successfully epoxidized to different degrees and various methods of epoxidation using *m*-chloroperoxy benzoic acid (MCPBA), performic acid (PFA), peracetic acid (PAA) and hexafluoro isopropanol (HFIP).
2. The blends were successfully prepared with chemically modified block copolymer with the variation of the epoxidation degree, epoxidation methods, copolymer architecture and blends composition.
3. The nanocomposites of the nanostructured blends with boehmite and layered silicate nanofillers were successfully prepared in which the nanoparticles were homogeneously dispersed.
4. The chemical modification of the copolymers was confirmed by Fourier transform infrared (FTIR) spectroscopy. The intensity of the peaks located at 810 cm^{-1} and 895 cm^{-1} corresponding to oxirane group was found to increase with increasing epoxidation degree. It was found that the epoxidation reaction favoured at *cis*-position of the double bond. All the methods employed for chemical modification were found to be feasible for the epoxidation of the block copolymer. However, the MCPBA method was found to be practically the most suitable one in terms of time, cost and ease of controlling reaction conditions. The FTIR analyses of the blends further indicated the formation of highly cross-linked network between the epoxy rings and amino groups in the investigated blends.

5. Highly ordered nanostructures were induced by the epoxidized block copolymers in the DGEBA based epoxy resin, an amorphous material. Both micro- and nanostructured resins showed tough behaviour. Higher the degree of epoxidation of the block copolymer higher is the ease of formation of epoxide group (which are compatible to epoxy resin) and hence higher will be the degree of nanostructuring. The copolymer architecture has practically no influence on the morphology of the blends with the epoxy resin.
6. The thermostability of the blends was found to be influenced by the epoxidation degree, block copolymer architecture, method and composition, variation. The glass transition temperature (T_g) and specific heat capacity (ΔC_p) of the nanostructured blends remained almost unchanged.
7. The microhardness and hence the elasticity modulus of the blends were found to decrease with the epoxidized block copolymer. In general, the architecture of the block copolymers did not play significant role in the mechanical properties of the blends. The deformation energy was higher in the blends with the copolymer modified to lower degree of epoxidation. The blend with macrophase-separated spherical domains of epoxy resin in blend showed higher toughness and total deformation energy. An optimum mechanical property was achieved when the blends had nanostructured morphology.
8. The deformation micromechanism of the materials was analyzed qualitatively using fracture surface morphology of the materials. In contrast to highly brittle behaviour of the neat thermoset resin, the micro- and nanostructured blends exhibited highly ductile behaviour on the fracture surface.
9. The structure-properties correlation was established based on the analysis of morphology, mechanical properties and deformation structured of the nanostructured blends. The epoxy resin blends as well as their nanocomposites revealed intense plastic deformation demonstrated by the formation of fine fibrillar structures leading simultaneously to enhanced toughness and stiffness of the materials.

Recommendations for Future Works

This study has successfully addressed the issue of templating nanostructures in epoxy resin and characterizing their morphological and mechanical properties. However, there are several questions to be answered in order to fully understand the structure-properties correlations in the blends of epoxy resin with block copolymers. The future works can be concerned with the following aspects.

1. The primary study has indicated that there is no significant influence of block copolymer architectures on the morphology and mechanical properties of blends with epoxy resin over the composition range studied in this work. Thus, considering the significant effect of block copolymer architecture on their phase behavior and properties, the study can be extended to wider composition range in order to fully understand the block copolymer architecture on blends properties.
2. In the present work, the toughness of the blends has been accessed only semi-quantitatively rather qualitatively by micro-indentation experiments and scanning electron microscopy. In future, the samples should be prepared in semi technical scale so that macroscopic deformation tests can be carried so that these properties can be correlated with deformation micromechanisms. Further, the deformation mechanisms should be studied by combining spectroscopic and microscopic methods.

CHAPTER – 6

6. SUMMARY

Styrenic block copolymers are thermoplastic elastomers having nanostructured which have wide applications in the field of material science. One of the applications is used as template to generate the nanostructure in epoxy resin. However, epoxy resin is amorphous and brittle material with lots of potential applications in the field of coating, adhesives to electronic and electric equipments. The aim of study is templating nanostructure in epoxy resin using styrenic block copolymer for improving their properties in the field of application such as electronic, electric equipments, aerospace etc. It can be templated using commercial styrenic block copolymer to toughen epoxy resin with maintaining its transparency. For this purpose, the styrenic block copolymers were subjected to chemical modification in order to make them compatible with epoxy resin. In particular, $(SB)_X$ star block copolymer was successfully epoxidized to different degrees by various methods. The blends and nanocomposite of diglycidyl ether of bisphenol-A (DGEBA) based epoxy resin and epoxidized block copolymers were prepared. The materials were characterized by different techniques such as fourier transform infrared (FTIR) spectroscopy, scanning (SEM) and transmission electron microscopy (TEM), thermogravimetric analysis (TGA), differential scanning calorimetry (DSC), and depth sensing microhardness measurements. The results obtained from these analyses are summarized in the following paragraphs.

The chemical modification of the copolymers was confirmed by Fourier transform infrared (FTIR) spectroscopy. Styrenic block copolymers, particularly an $(SB)_X$ star block copolymers, were successfully epoxidized to different degrees of epoxidation, and various methods using *m*-chloroperoxy benzoic acid (MCPBA), performic acid (PFA), peracetic acid (PAA) and hexafluoro isopropanol (HFIP). The intensity of the peaks assigned at 810 cm^{-1}, 895 cm^{-1} and 1265 cm^{-1}corresponding to half and whole stretching of oxirane group and the peak intensity at 810 cm^{-1} and 895 cm^{-1} was found to increase with increasing epoxidation degree. It was found that the epoxidation reaction preferred at *cis*-position of the double bond. All the methods were found to be suitable for the epoxidation of the block copolymer. However, the MCPBA method was established to be practically the most selective one in terms of time, cost and ease of controlling reaction conditions. The investigated blends further indicated the formation of highly cross-linked network between the epoxy rings and amino groups.

The morphology of blends was investigated using TEM. The blends morphology was formed well ordered nanostructures by the epoxidized block copolymers in the amorphous DGEBA based epoxy resin. This opens up the opportunity of designing transparent nanostructured thermoset resin with tailored stiffness-toughness ratio over a wide range. It has been demonstrated that the epoxidation level of the block copolymer is a key factor to template the nanostructures in the DGEBA based epoxy resin. At low epoxidation degree, the block copolymer shows the inverted macrophase separation with spherical structure of epoxy resin. At higher epoxidation degree, the block copolymer shows higher the ease of formation of epoxide group which also indicate the more compatible to epoxy resin and hence the formation of degree of nanostructuring is also higher. It was found that the copolymer architecture has practically not effect on the morphology of the epoxy resin blends. The homogeneous dispersion of boehmite and layered silicate nanofillers was found in nanocomposites of the nanostructured epoxy blends.

The thermogravimetric analysis shows the blends were thermostable which was found to be influenced by the epoxidation degree, block copolymer architecture, method and composition, variation. The addition of epoxidized block copolymer offers the possibility to increase, besides imparting an enhanced toughness, the thermostability of the materials but lowers the flame retardancy. From the activation energy of decomposition, the cross-linked reaction was found almost unchanged in all blends. The glass transition temperature (T_g) and specific heat capacity (ΔC_p) of the nanostructured blends indicated that they were fully cured and remained almost same.

The mechanical properties such as microhardness and elasticity modulus of the blends were found to decrease with the epoxidized block copolymer. On the other hand, the architecture of the block copolymers was found no significant role in the mechanical properties of the blends. However, the nanofillers show well dispersion and significant improvement in the microhardness properties. 3 wt.-% nano-boehmite was found dramatic increase in microhardness properties in nanostructured blends.

It was found that the deformation energy was higher in the blends with the copolymer modified to lower epoxidation degree. The lower epoxidation degree blend with macrophase-separated spherical domains of epoxy resin showed higher toughness and total deformation energy. The nanostructured morphology of the blends showed an optimum mechanical property. Based on the indentation plasticity, the nanostructured blends and composites showed the highest plastic deformation and microhardness dissipation parameter (MDP).

The deformation micromechanism of the blends was analyzed qualitatively using fracture surface morphology of the materials. In compared to highly brittle behaviour of the neat thermoset resin, the micro- and nanostructured blends showed highly ductile behaviour on the fracture surface with formation of numerous fibrillar structure. The epoxy resin blends as well as their nanocomposites revealed intense plastic deformation demonstrated by fine fibrillar and disc like structures leading simultaneously to enhanced toughness and stiffness of the materials.

REFERENCES

[1] Rohr, T.; Ogletree, D. L.; Svec, F.; Frechet, J. M. J. Surface Functionalization of Thermoplastic Polymers for the Fabrication of Microfluidic Devices by Photoinitiated Grafting. *Adv. Funct. Mater.* **2003**, *13*, 4, pp 264-270.

[2] Amin, S.; Amin, M. Thermoplastic Elastomeric (TPE) Materials and Their Use in Outdoor Electrical Insulation. *Rev. Adv. Mater. Sci.* **2011**, *29*, pp 15-30.

[3] Spontak, R. J.; Patel, N. P. Thermoplastic Elastomers: Fundamentals and Applications. *Curr. Opin. Colloid Interface Sci.* **2000**, *5*, pp 334-341.

[4] Holden, G.; Kricheldorf, H. R.; Quirk, R. P., Eds.; *Thermoplastic Elastomers,* 3rd edition; Hanser Verlag: Munich, **2004**, pp 1-10.

[5] Krause, S. Microphase Separations Zero Approximation. *J. Polym. Sci: Part A*-2, **1969,** *7*, pp 249-252.

[6] Leibler, L. Theory of Microphase Separation in Block Copolymers. *Macromolecules*. **1980,** *13***,** pp 1602-1617.

[7] Lohse D. J.; Hadjichristidis, N. Microphase Separation in Block Copolymers. *Curr. Opin. Colloid Interface Sci.* **1997**, *2*, pp 171-176.

[8] Hamley, I. *The Physics of Block Copolymers*, Oxford University Press: London, UK, **1998**, pp 24-44.

[9] Udipi, K. Epoxidation of Styrene-Butadiene Block Polymers. I. *J. Appl. Polym. Sci.* **1979**, *23*, pp 3301-3309.

[10] Huang, W. K.; Hsiue, G. H ; Hou, W. H. Epoxidation of Polybutadiene and Styrene-Butadiene Triblock Copolymers with Monoperoxyphthalic Acid: Kinetic and Conformation Study. *J. Polym. Sci., Part A: Polym. Chem.* **1988**, *26*, pp 1867-1883.

[11] Hsiue, G. H.; Yang, J. M. Epoxidation of Styrene-Butadiene-Styrene Block Copolymer and Use for Gas Permeation, *J. Polym. Sci., Part A: Polym. Chem.* **1990**, *28*, pp 3761-3773.

[12] Jian, X.; Hay, A. S. Catalytic Epoxidation of Styrene-Butadiene Triblock Copolymer with Hydrogen Peroxide. *J. Polym. Sci., Part A: Polym. Chem.* **1991**, *29*, pp 1183-1189.

[13] Wang, S. M.; Tsiang, R. C. C. Epoxidation of Partially Hydrogenated Styrene-Butadiene Block Copolymers Using Peracetic Acid in A Cyclohexane/Water Heterogeneous System. *J. Polym. Sci., Part A: Polym. Chem.* **1996**, *34*, pp 1483-1491.

[14] Antonietti, M.; Forster, S.; Hartmann, J.; Oestreich, S. Novel Amphiphilic Block Copolymers by Polymer Reactions and Their Use for Solubilization of Metal Salts and Metal Colloids. *Macromolecules.* **1996**, *29*, pp 3800-3806

[15] Hongqiang, L.; Xingrong, Z.; Jianhua, G. Epoxidation of Styrene-Isoprene-Styrene Block Copolymer and Research on its Reaction Mechanism. *J. Wuhan Univ. Technol.-Mater. Sci. Ed.* **2010**, *25*, pp 403-407.

[16] Serrano, E.; Larran˜aga, M.; Remiro, P. M.; Mondragon, I.; Carrasco, P. M.; Pomposo, J. A.; Mecerreyes, D. Synthesis and Characterization of Epoxidized Styrene-Butadiene Block Copolymers as Templates for Nanostructured Thermosets. *Macromol. Chem. Physic.* **2004**, *205*, pp 987–996.

[17] Serrano, E.; Tercjack, A.; Ocando, C.; Larranaga, M.; Parellada, M. D.; Corona-Galvan, S.; Mecerreyes, D.; Zafeiropoulos, N. E.; Stamm, M.; Mondragon, I. Curing Behavior and Final Properties of Nanostructured Thermosetting Systems Modified with Epoxidized Styrene-Butadiene Linear Diblock Copolymers. *Macromol. Chem. Physic.* **2007**, *208*, pp 2281-2292.

[18] Hermel-Davidock, T. J.; Tang, H. S.; Murray, D. J.; Hahn, S. F. Control of The Block Copolymer Morphology in Templated Epoxy Thermosets. *J. Polym. Sci. Pol. Phys.* **2007**, *45*, pp 3338–3348

[19] Blanco, M.; Lopez, M.; Kortaberria G.; Mondragon, I. Nanostructured Thermosets From Self-Assembled Amphiphilic Block Copolymer/Epoxy Resin Mixtures: Effect of Copolymer Content on Nanostructures. *Polym. Int.* **2010**, *59*, pp 523–528.

[20] Bhatnagar, M. S. Epoxy Resins (overview) In: Salomone J.C., ed.; *The Polymeric Materials Encyclopedia*, CRC Press, Inc; Boca Raton, FL, USA, **1996**, pp 1-11.

[21] Augustsson, C. *NM Epoxy Handbook*, 3rd edition; Niels Malmgren AB, Sewden: **2004**, pp 20-40.

[22] Larran˜aga, M.; Mondragon, I.; Riccardi, C. C. Miscibility and Mechanical Properties of an Amine-Cured Epoxy Resin Blended with Poly(ethylene oxide). *Polym. Int.* **2007**, *56*, pp 426-433.

[23] Meng, F.; Yi, F.; Zheng, S. Nanostructured Thermosetting Blends of Phenolic Thermosets and Poly(ethylene oxide)-*block*-poly(propylene oxide)-*block*-poly(ethylene oxide) Triblock Copolymer. *J. Macromol. Sci. Part B.* **2008**, *47*, 3, pp 450-462.

[24] Prolongo, S. G.; Gude, M. R.; Urena, A. Adhesive Strength and Toughness Improvement of Epoxy Resin Modified with Polystyrene-b-Polybutadiene-b-Poly (Methyl Methacrylate) Block Copolymer. *J. Material Sci. Eng.* **2012**, *1*, 2, doi:10.4172/2169-0022.1000109.

[25] Sun, S.; Zhang, M.; Zhang, H.; Zhang, X. Polylactide Toughening with Epoxy-Functionalized Grafted Acrylonitrile–Butadiene–Styrene Particles. *J. Appl. Polym. Sci.* **2011**, *122*, pp 2992-2999.

[26] Kar, S.; Banthia, A. K. Use of Acrylate-Based Liquid Rubbers as Toughening Agents and Adhesive Property Modifiers of Epoxy Resin. *J. Appl. Polym. Sci.* **2004**, *92*, pp 3814-3821

[27] Thompson, Z. J.; Hillmyer, M. A.; Liu, J. (D.); Sue, H. J.; Dettloff, M.; Bates, F. S. Block Copolymer Toughened Epoxy: Role of Cross-Link Density. *Macromolecules*. **2009**, *42*, pp 2333-2335.

[28] Ratna, D. *Handbook of Thermoset Resins*. iSmithers–A Smithers Group Company, United Kingdom: **2009,** pp 248-250.

[29] Lin, L. L.; Ho, T. H.; Wang, C. S. Synthesis of Novel Trifunctional Epoxy Resins and Their Modification with Polydimethylsiloxane for Electronic Application. *Polymer.* **1997**, *38*, 8, pp 1997-2003.

[30] Barcia, F. L.; Amaral, T. P.; Soares, B. G. Synthesis and Properties of Epoxy Resin Modified with Epoxy-Terminated Liquid Polybutadiene. *Polymer*. **2003**, *44*, pp 5811–5819.

[31] Thomas, R.; Durix, S.; Sinturel, C.; Omonov, T.; Goossens, S.; Groeninckx, G.; Moldenaers, P.; Thomas, S. Cure Kinetics, Morphology and Miscibility of Modified DGEBA-Based Epoxy Resin-Effects of a Liquid Rubber Inclusion. *Polymer*. **2007**, *48*, pp 1695-1710.

[32] Pearson R. A.; Yee, A. F. Toughening Mechanisms in Thermoplastic-Modified Epoxies: 1. Modification Using Poly(phenylene oxide). *Polymer*. **1993**, *34*, 17, pp 3658-3670.

[33] Pearson R. A.; Yee, A. F. The Preparation and Morphology of PPO-Epoxy Blends. *J. Appl. Polym. Sci.* **1993**, *48*, pp 1051-1060.

[34] Larrañaga, M.; Arruti, P.; Serrano, E.; de la Caba, K.; Remiro, P. M.; Riccardi, C. C.; Mondragon, I. Towards Microphase Separation in Epoxy Systems Containing PEO/PPO/PEO Block Copolymers by Controlling Cure Conditions and Molar Ratios Between Blocks. Part 2.Structural Characterization. *Colloid Polym. Sci.* **2006,** *284*, pp 1419–1430.

[35] Lipic, P. M.; Bates, F. S.; Hillmyer, M. A. Nanostructured Thermosets From Self-Assembled Amphiphilic Block Copolymer/Epoxy Resin Mixtures. *J. Am. Chem. Soc.* **1998**, *120*, pp 8963-8970.

[36] George, S. M.; Puglia, D.; Kenny, J. M.; Causin, V.; Parameswaranpillai, J.; Thomas, S. Morphological and Mechanical Characterization of Nanostructured Thermosets From Epoxy and Styrene-Block-Butadiene-Block-Styrene Triblock Copolymer. *Ind. Eng. Chem. Res.* **2013**, *52*, pp 9121-9129.

[37] Ocando, C.; Fernandez, R.; Tercjak, A.; Mondragon, I.; Eceiza, A.; Nanostructured Thermoplastic Elastomers Based on SBS Triblock Copolymer Stiffening with Low Contents of Epoxy System. Morphological Behavior and Mechanical Properties. *Macromolecules.* **2013**, *46*, pp 3444-3451.

[38] Serrano, E.; Martin, M. D.; Tercjak, A.; Pomposo, J. A.; Mecerreyes, D.; Mondragon, I.; Nanostructured Thermosetting Systems From Epoxidized Styrene Butadiene Block Copolymers. *Macromol. Rapid Comm.* **2005**, *26*, pp 982-985.

[39] Serrano, E.; Tercjak, A.; Kortaberria, G.; Pomposo, J. A.; Mecerreyes, D.; Zafeiropoulos, N. E.; Stamm, M.; Mondragon, I. Nanostructured Thermosetting Systems by Modification with Epoxidized Styrene-Butadiene Star Block Copolymers. Effect of Epoxidation Degree. *Macromolecules.* **2006**, *39*, pp 2254-2261.

[40] Ocando, C.; Tercjak, A.; Martı´n, M. D.; Ramos, J. A.; Campo, M.; Mondragon, I. Morphology Development in Thermosetting Mixtures Through The Variation on Chemical Functionalization Degree of Poly(styrene-b-butadiene) Diblock Copolymer Modifiers. Thermomechanical Properties. *Macromolecules*. **2009**, *42*, pp 6215-6224.

[41] Kutz, M. *Handbook of Materials Selection*. John Wiley & Sons, Inc., New York, **2002**, pp 336-354.

[42] Michler, G. H.; Baltá-Calleja, F. J., Eds.; *Mechanical Properties of Polymers based on Nanostructure and Morphology*, CRC Press, Boca Raton, USA: **2005**, pp 4-86.

[43] Sperling, L.H. *Introduction to Physical Polymer Science,* 4th edition; A John Wiley & Sons, Inc. Publication, Hoboken, New Jersey, **2006**, pp 168-171, 706-709.

[44] Robeson, L. Historical Perspective of Advances in the Science and Technology of Polymer Blends. *Polymer.* **2014**, *6*, pp 1251-1265.

[45] Matsen, M. W. Phase Behavior of Block Copolymer/Homopolymer Blends. *Macromolecules*, **1995**, *28*, pp 5765-5773.

[46] Ruiz-Pe´rez, L.; Royston, G. J.; Fairclough, J. P. A.; Ryan, A. J. Toughening by Nanostructure. *Polymer.* **2008**, *49*, pp 4475-4488.

[47] Guo, Q.; Figueiredo, P.; Thomann, R.; Gronski, W. Phase Behavior, Morphology and Interfacial Structure in Thermoset/Thermoplastic Elastomer Blends of Poly(propylene glycol)-Type Epoxy Resin and Polystyrene-b-polybutadiene. *Polymer.* **2001**, *42*, pp 10101-10110.

[48] Guo, Q.; Thomann, R.; Gronski, W.; Thurn-Albrecht, T. Phase Behavior, Crystallization, and Hierarchical Nanostructures in Self-organized Thermoset Blends of Epoxy Resin and Amphiphilic Poly(ethylene oxide)-block-poly(propylene oxide)-block-poly(ethylene oxide) Triblock Copolymers. *Macromolecules.***2002**, *35*, pp 3133-3144.

[49] Guo, Q.; Wang, K.; Chen, L.; Zheng, S.; Halley, P. J. Phase Behavior, Crystallization, and Nanostructures in Thermoset Blends of Epoxy Resin and Amphiphilic Star-shaped Block Copolymers. *J. Polym. Sci. Pol. Physic.* **2006**, *44*, pp 975–985.

[50] Lodge, T. P. Block copolymers: Past Successes and Future Challenges. *Macromol. Chem. Physic.* **2003**, *204*, pp 265–273.

[51] Han, C. D.; Kim, J.; Kim, J. K. Determination of the Order-disorder Transition Temperature of Block Copolymers, *Macromolecules.* **1989**, *22*, pp 383-394.

[52] Van Dijk M. A.; Van den Berg, R. Ordering Phenomena in Thin Block Copolymer Films Studied Using Atomic Force Microscopy. *Macromolecules.* **1996**, *28*, pp 6773-6778.

[53] Ruzette, A. V. Leibler, L. Block Copolymers in Tomorrow’s Plastics, *Nature Materials*. **2005**, *4*, pp19-31.

[54] Smart, T.; Lomas, H.; Massignani, M.; Flores-Merino, M. V.; Perez, L. R.; Battaglia, G. Block Copolymer Nanostructures. *Nanotoday*. **2008**, *3*, 3-4, pp 38-46.

[55] Chen, J. T.; Thomas, E. L.; Ober, C. K.; Mao, G. P. Self-assembled Smectic Phases in Rod-coil Block Copolymers. *Science*. **1996**, *273*, pp 343-346.

[56] Otsuka, H.; Nagasaki, Y.; Kataoka, K. Self-assembly of Poly(ethylene glycol)-Based Block Copolymers for Biomedical Applications. *Curr. Opin. Colloid Interface Sci.* **2001**, *6*, pp 3-10.

[57] Zhang, L.; Lin, J.; Lin, S. Self-assembly Behavior of Amphiphilic Block Copolymer/Nanoparticle Mixture in Dilute Solution Studied by Self-consistent-field Theory/Density Functional Theory. *Macromolecules.* **2007**, *40*, pp 5582-5592.

[58] Thompson, R. B.; Ginzburg, V. V.; Matsen, M. W.; Balazs, A. C. Block Copolymer-directed Assembly of Nanoparticles: Forming Mesoscopically Ordered Hybrid Materials. *Macromolecules*. **2002**, *35*, pp 1060-1071.

[59] Mulligan, R. F.; Iliadis, A. A.; Lee, U.; Kofinas, P. Synthesis of Self-assembled Metal-oxide Nanostructures in a Diblock Copolymer Matrix and Integration onto Semiconductor Surface. *Materials Research Society Symposium Proceedings*. **2001**, *642*, J2.11, pp 1-5.

[60] Thomann, Y.; Thomann, R.; Hasenhindl, A.; Mulhaupt, R.; Heck, B.; Knoll, K.; Steininger, H.; Saalwachter, K. Gradient Interfaces in SBS and SBS/PS Blends and Their Influence on Morphology Development and Material Properties. *Macromolecules*. **2009**, *42*, pp 5684-5699.

[61] Wu, S.; Bubeck, C. Macro- and Microphase Separation in Block Copolymer Supramolecular Assemblies Induced by Solvent Annealing. *Macromolecules.* **2013,** *46*, pp 3512-3518.

[62] Vazquez, A.; Lo´pez, M.; Serrano, E.; Valea, A.; Zafeiropoulos, N. E.; Mondragon, I. Structural and Ordering Behavior of Lamellar Polystyrene-block-

polybutadiene-block-polystyrene Triblock Copolymer Containing Layered Silicates. *J. Appl. Polym. Sci.* **2008**, *110*, pp 3624-3637.

[63] Michler, G. H., Ed.; *Electron Microscopy of Polymers*, Springer-Verlag, Heidelberg: **2008**, pp 277-296.

[64] Michler, G. H.; Balta-Calleja, F. J. *Nano- and Micromechanics of Polymers: Structure Modification and Improvement of Properties*, Hanser Verlag, Munich: **2012**, pp 108-109.

[65] Bilyeu, B.; Brostow, W.; Menard, K. P.; Epoxy Thermosets and Their Applications. II. Thermal Analysis. *J. Mater. Educ.* **2000**, *22*, 4-6, pp 107-129.

[66] Unnikrishnan, K. P. Studies on the Toughening of Epoxy Resins, *Ph. D. thesis*, Cochin University, Cochin, India, **2006**.

[67] Gallucci R. R.; Going, R. C. Preparation and Reactions of Epoxy-modified Polyethylene, *J. Appl. Polym. Sci.* **1982**, *27*, pp 425-437.

[68] Iijima, T.; Hiraoka, H.; Tomoi, M. Preparation of Epoxy-terminated Poly (aryl ether sulfone)s and Their Use as Modifiers for Epoxy Resins. *J. Appl. Polym. Sci.* **1992**, *45*, pp 709-721.

[69] Kumar, S. A.; Denchev, Z.; Alaga, M. Synthesis and Thermal Characterization of Phosphorus Containing Siliconized Epoxy Resins. *Eur. Polym. J.* **2006**, *42*, pp 2419-2429.

[70] Ismail, H.; Galpaya, D.; Ahmad, Z. The Compatibilizing Effect of Epoxy Resin (EP) on Polypropylene (PP)/Recycled Acrylonitrile Butadiene Rubber (NBRr) Blends. *Polym. Test.* **2009**, *28,* pp 363-370.

[71] Zhang, J.; Wang, Z.; Ding, G.; Quan, Y.; Chen, Q. The Effect of Epoxy Resin to Reduce the Compression Set of Polysulfide Sealant. *J. Appl. Polym. Sci.* **2012**, *125,* pp 390–395.

[72] Zheng, S.; Gao, R.; Li, J.; Guo, Q. Epoxy resin containing the poly(sily ether): preparation, morphology, and mechanical properties. *J. Appl. Polym. Sci.* **2003**, *89*, pp 505–512.

[73] Wu, C. C.; Lee, W. J. Synthesis and Properties of Copolymer Epoxy Resins Prepared from Copolymerization of Bisphenol A, Epichlorohydrin, and Liquefied Dendrocalamus Latiflorus. *J.Appl. Polym. Sci.* **2010**, *116*, pp 2065-2073.

[74] Zhu, J.; Chandrashekhara, K.; Flanigan, V.; Kapila, S. Curing and Mechanical Characterization of a Soy-based Epoxy Resin System. *J. Appl. Polym. Sci.* **2004**, *91*, pp 3513-3518.

[75] Ahmetli, G.; Deveci, H.; Soydal, U.; Gurler, S. P. Altun, A. Epoxy Resin/Polymer Blends: Improvement of Thermal and Mechanical Properties. *J. Appl. Polym. Sci.* **2012**, *125*, 1, pp 38-45.

[76] Lützen, H.; Bitomsky, P.; Rezwan, K.; Hartwig, A. Partially Crystalline Polyols Lead to Morphology Changes and Improved Mechanical Properties of Cationically Polymerized Epoxy Resins. *Eur. Polym. J.* **2013**, *49*, pp 167–176.

[77] MacKinnon, A. J.; Jenkins, S. D.; McGrail, P. T.; Pethrick, R. A. A Dielectric, Mechanical, Rheological, and Electron Microscopy Study of Cure and Properties of a Thermoplastic-modified Epoxy Resin. *Macromolecules*. **1992**, *25*, pp 3492-3499.

[78] Yadav, R.; Awasthi, P.; Srivastava, D. Studies on Synthesis of Modified Epoxidized Novolac Resin from Renewable Resource Material for Application in Surface Coating. *J. Appl. Polym. Sci.* **2009**, *114,* pp 1471-1484.

[79] Kasemura, T.; Oshibe, Y.; Uozumi, H.; Kawai, S.; Yamada, Y.; Ohmura, H.; Yamamoto, T. Surface Modification of Epoxy Resin with Fluorine-containing Methacrylic Ester Copolymers. *J. Appl. Polym. Sci.* **1993**, *47,* pp 2207-2216.

[80] Wu, J.; Thio, Y. S.; Bates, F. S. Structure and Properties of PBO–PEO Diblock Copolymer Modified Epoxy. *J. Polym. Sci. Pol. Chem.* **2005**, *43*, pp 1950-1965.

[81] Kosonen, H.; Ruokolainen, J.; Nyholm, P.; Ikkala, O. Self-organized Thermosets: Blends of Hexamethyltetramine Cured Novolac with Poly(2-

vinylpyridine)-*block*-poly(isoprene). *Macromolecules.* **2001**, *34*, 9, pp 3046-3049.

[82] Hameed, N.; Sreekumar, P. A.; Francis, B.; Yang, W.; Thomas, S. Morphology, Dynamic Mechanical and Thermal Studies on Poly(styrene-co-acrylonitrile) Modified Epoxy Resin/Glass Fibre Composites. *Composites: Part A.* **2007**, *38*, pp 2422-2432.

[83] Chiu, H. T.; Chiu, S. H.; Wu, J. H. Study on Mechanical Properties and Intermolecular Interaction of Silicone Rubber/Polyurethane/Epoxy Blends. *J. Appl. Polym. Sci.* **2003**, *89*, pp 959-970.

[84] Katsoulis, C.; Kandare, E.; Kandola, B. K. The Effect of Nanoparticles on Structural Morphology, Thermal and Flammability Properties of Two Epoxy Resins with Different Functionalities. *Polym. Degrad. Stab.* **2011**, *96*, pp 529-540.

[85] Siddans, B. B. Epoxy /Clay Nanocomposites: Effect of Clay and Resin Chemistry on Cure and Properties, *M. Sc. Thesis,* Queensland University of Technology: Australia, **2004**.

[86] Liu, P.; Song, J.; He, L.; Liang, X.; Ding, H.; Li, Q. Alkoxysilane functionalized polycaprolactone/polysiloxane modified epoxy resin through sol–gel process. *Eur. Polym. J.* **2008**, *44*, pp 940–951.

[87] Wang, X.; Hu, Y.; Song, L.; Yang, H.; Xing, W.; Lu, H. Synthesis and Characterization of a Dopo-Substitued Organophosphorus Oligomer and its Application in Flame Retardant Epoxy Resins. *Prog. Org. Coat.* **2011,** *71,* pp 72–82.

[88] Lligadas, G.; Ronda, J. C.; Galia`, M.; Ca´diz, V. Development of Novel Phosphorus-Containing Epoxy Resins From Renewable Resources. *J. Polym. Sci., Part A: Polym. Chem.* **2006**, *44*, pp 6717–6727.

[89] Sun, D.; Yao, Y. Synthesis of Three Novel Phosphorus-Containing Flame Retardants and Their Application in Epoxy Resins. *Polym. Degrad. Stab.* **2011**, *96*, pp 1720-1724.

[90] Zhang, W.; Li, X.; Fan, H.; Yang, R. Study on Mechanism of Phosphorusesilicon Synergistic Flame Retardancy on Epoxy Resins, *Polym. Degrad. Stab.* **2012**, *97*, pp 2241-2248.

[91] Chin, H. C.; Chiou, K. C.; Chang, F. C. Reactive Compatibilization of the Poly(Ethylene Terephthalate)/Liquid Crystalline Polymer Blends by Solid Epoxy Resin as a Coupling Agent. *J. Appl. Polym. Sci.* **1996**, *60*, pp 2503-2516.

[92] Chuayjuljit, S.; Soatthiyanon, N.; Potiyaraj, P. Polymer Blends of Epoxy Resin and Epoxidized Natural Rubber, *J. Appl. Polym. Sci.* **2006**, *102*, pp 452–459.

[93] Tjong, S. C.; Meng, Y. Z. Structural-mechanical Relationship of Epoxy Compatibilized Polyamide 6/Polycarbonate Blends. *Mater. Res. Bull.* **2004**, *39*, pp 1791–1801.

[94] Gu, X.; Huang, X.; Wei, H.; Tang, X. Synthesis of Novel Epoxy-Group Modified Phosphazene-containing Nanotube and its Reinforcing Effect in Epoxy Resin. *Eur. Polym. J.* **2011**, *47*, pp 903–910.

[95] Ben Saleh, A. B.; Ishak, Z. A. M.; Hashim A.S.; Kamil, W.A. Compatibility, Mechanical, Thermal, And Morphological Properties of Epoxy Resin Modified With Carbonyl-terminated Butadiene Acrylonitrile Copolymer Liquid Rubber**.** *J. Phys. Sci.* **2009**, *20*, 1, pp 1–12.

[96] Datta, C.; Basu, D.; Roy, A.; Banerjee, A. Mechanical and Dynamic Mechanical Studies of Epoxy/VAC-EHA/HMMM IPN–jute Composite Systems, *J. Appl. Polym. Sci.* **2004**, *91*, pp 958–963.

[97] Zhong, Z.; Zheng, S.; Huang, J; Cheng, X.; Guo Q.; Wei, J. Phase Behaviour and Mechanical Properties of Epoxy Resin Containing Phenolphthalein Poly(ether ether ketone). *Polymer.* **1998**, *39*, 5, pp 1075-1080.

[98] Pearson, R. A.; Yee, A. F. Toughening Mechanisms in Elastomer-modified Epoxies Part 1 Mechanical Studies. *J. Mater. Sci.* **1986**, *21*, pp 2462-2474.

[99] Pearson, R. A.; Yee, A. F. Toughening Mechanisms in Elastomer-Modified Epoxies Part 2 Microscopy Studies. *J. Mater. Sci.* **1986**, *21*, pp 2475-2488.

[100] Pearson, R. A.; Yee, A. F. Influence of Particle Size and Particle Size Distribution on Toughening Mechanisms in Rubber-Modified Epoxies. *J. Mater. Sci.* **1991**, *26*, pp 3828-3844.

[101] Kim, G. M.; Qin, H.; Fang, X.; Sun, F. C.; Mather, P. T. Hybrid Epoxy-Based Thermosets Based on Polyhedral Oligosilsesquioxane: Cure Behavior and Toughening Mechanisms, *J. Polym. Sci., Part B: Polym. Phys.* **2003**, *41*, pp 3299-3313.

[102] Zhao, Z. L.; Zhang, Z.; Feng, X. Q. Experimental and Theoretical Investigations on Toughening Mechanisms of Particles-Reinforced Epoxy Nanocomposites, *9th International Conference on Fracture & Strength of Solids,* Jeju, Korea, June 9-13, **2013**, pp 1-10.

[103] Timmermann, J. F.; Tillman, M. S.; Hayes, B. S.; Seferis, J. C. Matrix and Fiber Influences on the Cryogenic Microcracking of Carbon Fiber/Epoxy Composites. *Composites: Part A*. **2002**, *33*, pp 323-329.

[104] Bussi, P.; Ishida, H. Partially Miscible Blends of Epoxy Resin and Epoxidized Rubber: Structural Characterization of the Epoxidized Rubber and Mechanical Properties of the Blends. *J. Appl. Polym. Sci.* **1994**, *53,* pp 441-454.

[105] Ochi, M.; Mimura, K.; Kiyohara, O.; Tagami, T. Effect of Aramid-CTBN Block Copolymer on Phase Structure and Toughness of Cured Epoxy Resins Modified With Carboxy-terminated Butadiene Acrylonitrile Copolymer (CTBN). *Angew. Makromol. Chem*. **1996**, *240,* pp 17-29.

[106] Francis, B.; Thomas, S.; Jose, J.; Ramaswamy, R.; Lakshmana Rao, V. Hydroxyl Terminated Poly(ether ether ketone) with Pendent Methyl Group Toughened Epoxy Resin: Miscibility, Morphology and Mechanical Properties. *Polymer*. **2005**, *46*, pp 12372–12385.

[107] Kuan, H. C.; Dai, J. B.; Ma, J. A reactive polymer for toughening epoxy resin, *J. Appl. Polym. Sci.* **2010**, *115*, pp 3265–3272.

[108] Declet-Perez, C.; Redline, E. M.; Francis, L. F.; Bates, F. S. Role of Localized Network Damage in Block Copolymer Toughened Epoxies. *ACS Macro Lett.* **2012**, 1, pp 338−342.

[109] Thio, Y. S.; Wu, J.; Bates, F. S. Epoxy Toughening Using Low Molecular Weight Poly(hexylene oxide)-poly(ethylene oxide) Diblock Copolymers. *Macromolecules.* **2006**, *39*, pp 7187-7189.

[110] Liu, J. (D.); Thompson, Z. J.; Sue, H. J.; Bates, F. S.; Hillmyer, M. A.; Dettloff, M.; Jacob, G.; Verghese, N.; Pham, H. Toughening of Epoxies With Block Copolymer Micelles of Wormlike Morphology. *Macromolecules.* **2010**, *43*, pp 7238-7243

[111] Chong, H. M.; Taylor, A. C. The Microstructure and Fracture Performance of Styrene–butadiene–methylmethacrylate Block Copolymer-modified Epoxy Polymers, *J. Mater. Sci.* **2013**, *48*, pp 6762-6777.

[112] Cheng, X.; Chen, Y. X.; Du, Z. L.; Zhu, P. X.; Wu, D. C. Effect of the Structure of Curing Agents Modified by Epoxidized Oleic Esters on the Toughness of Cured Epoxy Resins. *J. Appl. Polym. Sci.* **2011**, *119*, pp 3504-3510.

[113] Ho¨fflin, F.; Ko¨nczo¨, L.; Do¨ll, W.; Morawiec, J.; Mu¨lhaupt, R. Toughening of Epoxy Resins Modified with Polyetherester Block Copolymers: the Influence of Modifier Molecular Architecture on Mechanical Properties. *J. Appl. Polym. Sci.* **2000**, *76*, pp 623-634.

[114] Wu, S.; Guo, Q.; Peng, S.; Hameed, N.; Kraska, M.; Stühn, B.; Mai, Y. W. Toughening Epoxy Thermosets with Block Ionomer Complexes: A Nanostructure-mechanical Property Correlation. *Macromolecules.* **2012**, *45*, pp 3829-3840.

[115] Johnsen, B. B.; Kinloch, A. J.; Mohammed, R. D.; Taylor , A. C.; Sprenger, S. Toughening Mechanisms of Nanoparticle-modified Epoxy Polymers. *Polymer*. **2007**, *48*, pp 530-541.

[116] Gonzalez-Domínguez, J. M.; Anson-Casaos, A.; Díez-Pascual, A. M.; Ashrafi, B.; Naffakh, M.; Backman, D.; Stadler, H.; Johnston, A.; Gomez, M.; Martínez,

M. T. Solvent-free Preparation of High-toughness Epoxy-SWNT Composite Materials. *ACS Appl. Mater. Interfaces.* **2011**, *3*, pp 1441-1450.

[117] Becker, O.; Varley, R.; Simon, G. Morphology, Thermal Relaxations and Mechanical Properties of Layered Silicate Nanocomposites Based Upon High-Functionality Epoxy Resins. *Polymer.* **2002**, *43*, pp 4365-4373.

[118] Ni, C.; Ni, G.; Zhang, L.; Mi, J.; Yao, B.; Zhu, C. Syntheses of Silsesquioxane (POSS)-based Inorganic/Organic Hybrid and the Application in Reinforcement for an Epoxy Resin. *J. Colloid Interface Sci.* **2011**, *362*, pp 94-99.

[119] Zhao, S.; Schadler, L. S.; Duncan, R.; Hillborg, H.; Auletta, T. Mechanisms Leading to Improved Mechanical Performance in Nanoscale Alumina Filled Epoxy. *Compos. Sci. Technol.* **2008**, *68*, pp 2965-2975.

[120] Zhao, S.; Schadler, L. S.; Hillborg, H.; Auletta, T. Improvements and Mechanisms of Fracture and Fatigue Properties of Well-dispersed Alumina/Epoxy Nanocomposites. *Compos. Sci. Technol.* **2008**, *68*, pp 2976-2982.

[121] Wetzel, B.; Rosso, P.; Haupert, F.; Friedrich, K. Epoxy Nanocomposites - fracture and Toughening Mechanisms. *Eng. Fract. Mech.* **2006**, *73*, pp 2375-2398.

[122] Hillmyer, M. A.; Lipic, P. M.; Hajduk, D. A.; Almdal, K.; Bates, F. S. Self-Assembly and Polymerization of Epoxy Resin-amphiphilic Block Copolymer Nanocomposites. *J. Am. Chem. Soc.* **1997,** *119*, pp 2749-2750.

[123] Grubbs, R. B.; Broz, M. E.; Dean J. M.; Bates, F. S. Selectively Epoxidized Polyisoprene-polybutadiene Block Copolymers. *Macromolecules.* **2000,** *33*, pp 2308-2310.

[124] Rebizant, V.; Abetz, V.; Tournilhac, F.; Court, F.; Leibler, L. Reactive Tetrablock Copolymers Containing Glycidyl Methacrylate. Synthesis and Morphology Control in Epoxy-amine Networks. *Macromolecules.* **2003**, *36*, pp 9889-9896.

[125] Ritzenthaler, S.; Court, F.; David, L.; Girard-Reydet, E.; Leibler, L.; Pascault, J. P. ABC Triblock Copolymers/Epoxy-diamine Blends. 1. Keys to Achieve Nanostructured Thermosets. *Macromolecules.* **2002**, *35*, pp 6245-6254.

[126] Noshay, A.; Robeson, L. M. Epoxy/Modifier Block Copolymers. *J. Polym. Sci., Polym. Chem. Ed.* **1974**, *12*, 689-705.

[127] Larrañaga, M.; De la Caba, K.; Eceiza, A.; Corcuera, M. A.; Mondragon, I. Kinetics and Morphology of an Epoxy Resin Modified with PEO-PPO-PEO Block Copolymers. *Proceeding of the 8th Polymers for Advanced Technologies International Symposium* Budapest, Hungary, Sept 13-16, **2005.**

[128] Li, J. G.; Lin Y. D.; Kuo, S. W. From Microphase Separation to Self-organized Mesoporous Phenolic Resin Through Competitive Hydrogen Bonding with Double-crystalline Diblock Copolymers of Poly(ethylene oxide-b-ε-caprolactone). *Macromolecules.* **2011**, *44*, pp 9295-9309.

[129] Yu; R.; Zheng, S. Morphological Transition from Spherical to Lamellar Nanophases in Epoxy Thermosets Containing Poly(ethylene oxide)-block-poly (ε-caprolactone)-block-polystyrene Triblock Copolymer by Hardeners. *Macromolecules.* **2011**, *44*, pp 8546-8557.

[130] Hu, D.; Xu, Z.; Zeng, K.; Zheng, S. From Self-organized Novolac Resins to Ordered Nanoporous Carbons. *Macromolecules.* **2010**, *43*, pp 2960-2969.

[131] Amendt, M. A.; Chen, L.; Hillmyer, M. A. Formation of Nanostructured Poly(dicyclopentadiene) Thermosets Using Reactive Block Polymers. *Macromolecules.* **2010**, *43*, pp 3924-3934.

[132] Grubbs, R. B.; Dean, J. M.; Broz, M. E.; Bates, F. S. Reactive Block Copolymers for Modification of Thermosetting Epoxy. *Macromolecules.* **2000,** *33*, pp 9522-9534.

[133] Guo, Q.; Thomann, R.; Gronski, W.; Staneva, R.; Ivanova, R.; Stuhn, B. Nanostructures, Semicrytalline Morphology, and Nanoscale Confinement Effect on the Crystallization Kinetics in Self-organized Block Copolymer/Thermoset Blends. *Macromolecules.* **2003**, *36*, pp 3635-3645.

[134] Ritzenthaler, S.; Court, F.; Girard-Reydet, E.; Leibler, L.; Pascault, J. P. ABC Triblock Copolymers/Epoxy-diamine Blends. 2. Parameters Controlling the Morphologies and Properties. *Macromolecules.* **2003**, *36*, pp 118-126.

[135] Ramos, J. A.; Espósito, L. H.; Fernández, R.; Zalakain, I.; Goyanes, S.; Avgeropoulos, A.; Zafeiropoulos, N. E.; Kortaberria, G.; Mondragon, I. Block Copolymer Concentration Gradient and Solvent Effects on Nanostructuring of Thin Epoxy Coatings Modified with Epoxidized Styrene-butadiene-styrene Block Copolymers. *Macromolecules.* **2012**, *45*, pp 1483-1491.

[136] Fernandez, R.; Ramos, J. A.; Esposito, L.; Tercjak, A.; Mondragon, I. Reversible Optical Storage Properties of Nanostructured Epoxy-based Thermosets Modified with Azobenzene Units. *Macromolecules.* **2011**, *44*, pp 9738-9746.

[137] Fan, W.; Wang, L.; Zheng, S. Double Reaction-induced Microphase Separation in Epoxy Resin Containing Polystyrene-block-poly(ε-caprolactone)-block-poly-(n-butyl acrylate) ABC Triblock Copolymer. *Macromolecules.* **2010**, *43*, pp 10600-10611.

[138] Yi, F.; Zheng, S.; Liu, T. Nanostructures and Surface Hydrophobicity of Self-assembled Thermosets Involving Epoxy Resin and Poly(2,2,2-trifluoroethyl acrylate)-*block*-poly(ethylene oxide) Amphiphilic Diblock Copolymer. *J. Phys. Chem. B.* **2009,** *113,* pp 1857-1868.

[139] Hu, D.; Zheng, S. Morphology and Thermomechanical Properties of Epoxy Thermosets Modified with Polysulfone-block-polydimethylsiloxane Multiblock Copolymer. *J. Appl. Polym. Sci.* **2011**, *119,* pp 2933-2944.

[140] Zhang, Y.; Shi, W.; Chen, F.; Han, C. C. Dynamically Asymmetric Phase Separation and Morphological Structure Formation in the Epoxy/Polysulfone Blends. *Macromolecules.* **2011**, *44,* pp 7465-7472.

[141] Akiyama, S.; Kobori, Y.; Sugisaki, A.; Koyama, T.; Akiba, I. Phase Behavior and Pressure Sensitive Adhesive Properties in Blends of Poly(styrene-*b*-isoprene-*b*-styrene) with Tackifier Resin. *Polymer.* **2000**, *41*, pp 4021-4027.

[142] Soares, B. G.; Dahmouche, K.; Lima, V. D.; Silva, A. A.; Caplan, S. P.C.; Barcia, F. L. Characterization of Nanostructured Epoxy Networks Modified with Isocyanate-terminated Liquid Polybutadiene, *J. Colloid Interface Sci.* **2011**, *358*, pp 338-346.

[143] Mijovic, J.; Shen, M. Sy, J. W.; Mondragon, I. Dynamics and Morphology in Nanostructured Thermoset Network/Block Copolymer Blends During Network Formation. *Macromolecules.* **2000,** *33,* pp 5235-5244.

[144] Serrano, E.; Kortaberria, G.; Arruti, P.; Tercjak, A.; Mondragon, I. Molecular Dynamics of an Epoxy Resin Modified with an Epoxidized Poly(styrene–butadiene) Linear Block Copolymer During Cure and Microphase Separation Processes, *Eur. Polym. J.* **2009**, *45*, pp 1046-1057.

[145] Ocando, C.; Tercjak, A.; Mondragon, I. Nanostructured Systems Based on SBS Epoxidized Triblock Copolymers and Well-dispersed Alumina/Epoxy Matrix Composites. *Comp. Sci. Technol.* **2010**, *70*, pp 1106-1112.

[146] Tercjak, A.; Gutierrez, J.; Martin, M. D.; Mondragon, I. Transparent Titanium Dioxide/Block Copolymer Modified Epoxy-based Systems in the Long Scale Microphase Separation Threshold. *Eur. Polym. J.* **2012**, *48*, pp16-25.

[147] Kosmidou, T. V.; Vatalis, A. S.; Delides, C. G.; Logakis, E.; Pissis, P.; Papanicolaou , G. C. Structural, Mechanical and Electrical Characterization of Epoxy-amine/Carbon Black Nanocomposites. *eXPRESS Polym. Lett.* **2008**, *2*, 5, pp 364-372.

[148] Song , S. H.; Park , K. H.; Kim , B. H.; Choi , Y. W.; Jun , G. H.; Lee , D. J.; Kong , B. S.; Paik , K. W.; Jeon, S. Enhanced Thermal Conductivity of Epoxy–graphene Composites by Using Non-oxidized Graphene Flakes with Non-covalent Functionalization. *Adv. Mater.* **2013**, *25*, pp 732-737.

[149] Teng, C. C.; Ma, C. C. M.; Lu, C. H.; Yang, S. Y.; Lee, S. H.; Hsiao, M. C.; Yen, M. Y.; Chiou, K. C.; Lee, T. M. Thermal Conductivity and Structure of Non-covalent Functionalized Graphene/Epoxy Composites. *Carbon.* **2011**, *49*, pp 5107-5116.

[150] Tang, L. C.; Wan, Y. J.; Yan, D.; Pei, Y. B.; Zhao, L.; Li, Y. B.; Wu, L. B.; Jiang, J. X.; Lai, G. Q. The Effect of Graphene Dispersion on the Mechanical Properties of Graphene/Epoxy Composites. *Carbon*. **2013**, *60*, pp 16-27.

[151] Pavlidou, S.; Papaspyrides, C. D. A Review on Polymer-layered Silicate Nanocomposites. *Prog. Polym. Sci.* **2008**, *33*, pp 1119-1198.

[152] Xie, H. Q.; Chen, Y.; Yang, W.; Xie, D. Synthesis and Characterization of Maleated Ionomers via Ring-opening Reaction of Epoxidized Styrene-butadiene Rubber with Potassium Hydrogen Maleate and Study of Their Behavior as Compatibilizer, *J. Appl. Polym. Sci.* **2006**, *101*, pp 792-798.

[153] Lach, R.; Kim, G. M.; Adhikari, R.; Michler, G. H.; Grellmann, W. Indentation Methods for Characterizing the Mechanical and Fracture Behaviour of Polymer Nanocomposites. *Nep. J. Sci. Technol.* **2012**, *13*, 2, pp 115-122.

[154] Lach, R.; Michler, G. H.; Grellmann, W. Microstructure and Indentation Behaviour of Polyhedral Oligomeric Silsesquioxanes-modified Thermoplastic Polyurethane Nanocomposites. *Macromol. Mater. Eng.* **2010**, *295*, 5, pp 484-491.

[155] Zhang, S.; Zhang, X. Toughness Evaluation of Hard Coatings and Thin Films, *Thin Solid Films*. **2012**, *520*, pp 2375-2389.

[156] Fox-Rabinovich, G.S.; Beake, B. D.; Endrino, J. L.; Veldhuis, S. C.; Parkinson, R.; Shuster, L. S.; Migranov, M. S. Effect of Mechanical Properties Measured at Room and Elevated Temperatures on the Wear Resistance of Cutting Tools with TiAlN and AlCrN Coatings, *Surf. Coat. Technol.* **2006**, *200*, pp 5738-5742.

[157] Hsiue, G. H.; Yang J. M. Epoxidation of Styrene–butadiene–styrene Block Copolymer and Use for Gas Permeation. *J. Polym. Sci., Part A: Polym. Chem.* **1990**, *28*, pp 3761-3773.

[158] Chaisuriyathepkul, A.; Klinpituksa, P.; Phinyocheep, P.; Nakason, C.; Kittipoom, S. Synthesis of Acrylated Styrene–isoprene–styrene Copolymer. *e-Polymers.* **2008**, *141*.

[159] Phinyocheep, P.; Phetphaisit, C. W.; Derouet, D.; Campistron, I.; Brosse, J. C.; Chemical Degradation of Epoxidized Natural Rubber Using Periodic Acid: Preparation of Epoxidized Liquid Natural Rubber. *J. Appl. Polym. Sci.* **2005**, *95*, pp 6-15.

[160] Mustata, F.; Tudorachi, N.; Rosu, D. Curing and Thermal Behavior of Resin Matrix for Composites Based on Epoxidized Soybean Oil/Diglycidyl Ether of Bisphenol A. *Composites: Part B.* **2011**, *42*, pp 1803-1812.

[161] Theophanides, T.; Ed. *Infrared Spectroscopy – Materials Science, Engineering and Technology*, Chapter 13, **2012,** pp 261-284.

[162] Shokralla; S. A.; Al-Muaikel, N. S. Thermal Properties of Epoxy (DGEBA)/Phenolic Resin (Novolac) Blends. *The Arabian J. Sci. Eng.* **2010**, *35*, 1B, pp 7-14.

[163] Denq, B. L.; Chiu, W. Y.; Lin, K. F.; Fuh, M. R. S. Thermal Degradation Behavior of Epoxy Resin Blended with Propyl Ester Phosphazene. *J. Appl. Polym. Sci.* **2001**, *81*, pp 1161-1174.

[164] Gracik, T. D.; Long, G. L. Prediction of Thermoplastic Flammability by Thermogravimetry, *Thermochim. Acta*. **1992**, *212*, pp 163–170.

[165] Hsiue, G. H.; Wei, H. F.; Shiao, S. J.; Kuo, W. J.; Sha, Y. A. Chemical Modification of Dicyclopentadiene-based Epoxy Resins to Improve Compatibility and Thermal Properties. *Polym. Degrad. Stab.* **2001**, *73*, pp 309-318.

[166] Ho, T. H.; Leu, T. S.; Sun, Y. M.; Shieh, J. Y. Thermal Degradation Kinetics and Flame Retardancy of Phosphorus-containing Dicyclopentadiene Epoxy Resins. *Polym. Degrad. Stab.* **2006**, *91*, pp 2347-2356.

[167] Yao, F.; Wu, Q.; Lei, Y.; Guo, W.; Xu, Y. Thermal Decomposition Kinetics of Natural Fibers: Activation Energy with Dynamic Thermogravimetric Analysis. *Polym. Degrad. Stab.* **2008**, *93*, pp 90-98.

[168] Lee, J. Y.; Shim, M. J.; Kim, S. W. Thermal Decomposition Kinetics of an Epoxy Resin with Rubber-modified Curing Agent. *J. Appl. Polym. Sci.* **2001**, *81*, pp 479-485.

[169] Tripathi, G.; Srivastava, D. Study on the Effect Of Carboxyl Terminated Butadiene Acrylonitrile (CTBN) Copolymer Concentration on the Decomposition Kinetics Parameters of Blends of Glycidyl Epoxy and Non-Glycidyl Epoxy Resin. *Int. J. Org. Chem.* **2011**, *1*, pp 105-112.

[170] Lee, J. Y.; Lee, H. K.; Shim, M. J.; Kim, S. W. Thermal Decomposition Characterization of Epoxy Network Chemically Toughened with Liquid Rubber Using Dynamic TG Analysis. *J. Industrial Eng. Chem.* **2000**, *6*, 4, pp 250-255.

[171] Sharma, A.; Agarwal, D.; Singh, J. Study of Curing Kinetics and Thermal Degradation of UV Curable Epoxy Acrylate Resin. *e-J. Chem.* **2008**, *5*, 4, pp 904-913.

[172] .Shukla, S. K.; Srivastava, D. Epoxy/Resole Blends – A Study of its Degradation Kinetics. *Indian J. Chem. Technol.* **2001**, *8*, pp 357-361.

[173] Gupta, N. Varma, I. K. Curing of Diglycidyl Ether of Bisphenol A by Aromatic Diamines and Thermal Behaviour of Cured Resins. *Die Angewandte Makromolekulare Chemie*, **1998**, *263*, pp 41-45.

[174] Raditoiu, V.; Gabor, R.; Nicolae, C. A.; Dumitrache, L.; Raditoiu, A.; Mihailescu, M. Damping Properties of Some Epoxy Resin – Liquid Crystalline Dyestuff Composites. *University Politehnica of Bucharest Sci. Bull.* **2014,** *76*, 1, pp 223-230.

[175] Saiter, A.; Devallencourt, C.; Saiter, J. M.; Grenet, J. Fragility Behavior of Melamine Formaldehyde Three Dimensional Network. *Mater. Lett.* **2000**, *45*, pp 180-185.

[176] Flores, A.; Ania, F.; Balta–Calleja, F. J. From the Glassy State to Ordered Polymer Structures: A Microhardness Study. *Polymer*. **2009**, *50*, pp 729-746.

[177] Joseph, S.; Thomas, S. Morphology, Morphology Development and Mechanical Properties of Polystyrene/Polybutadiene Blends. *Eur. Polym. J.* **2003**, *39*, 1, pp 115-125

[178] Macaúbas, P. H. P.; Demarquette, N. R. Morphologies and Interfacial Tensions of Immiscible Polypropylene/Polystyrene Blends Modified with Triblock Copolymers. *Polymer*. **2001**, *42*, 6, pp 2543-2554.

[179] Lim, D. S.; Kyu, T. Phase Separation Dynamics of Polycarbonate/Polymethyl Methacrylate Blends. I. Temperature Jumps into an Immiscibility Loop. *J. Chem. Phys.* **1990**, *93*, 6, pp 3944-3950.

[180] Potschke, P.; Bhattacharyya, A. R.; Janke, A. Morphology and Electrical Resistivity of Melt Mixed Blends of Polyethylene and Carbon Nanotube Filled Polycarbonate. *Polymer*. **2003**, *44*, pp 8061-8069.

[181] Berkessel, A. In: *Modern Oxidation Methods;* Backvall, J. E.; Ed., Wiley-VCH, Weinheim, **2010,** pp 117-136.

Appendix – 1

1) The reaction involving the epoxidation of SBS block copolymer with meta-chloroperoxy benzoic acid (MCPBA) is illustraed in Figure Ap-1 taking functionalization of an SBS triblock copolymer as an example.

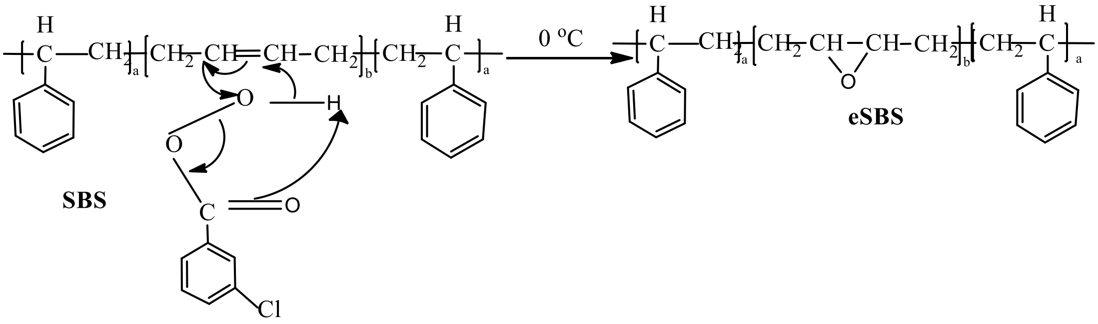

Figure Ap-1 Epoxidation reaction of SBS triblock copolymer by MCPBA as epoxidizing agent; the C=C double bonds were changed into the epoxide groups.

Appendix – 2

2) In order to find the optimum method of chemical modification of the butadiene blocks, various reagent (particularly the peracids) were used. One of the method using MCPBA was described eariler. The different peracids were metachloroperxy benzoic acid (MCPBA), performic acid (PFA) and peracetic acid (PAA). Among them PFA will be formed using the followed reaction shown in Figure Ap.-2.1.

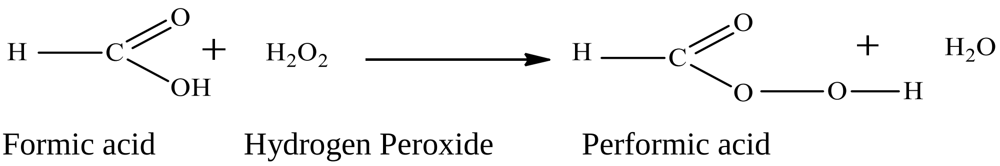

Figure Ap-2.1 Reaction of formation of performic acid from fromic acid and hydrogen peroxide

The general reaction can be represented as follows in Figure Ap-2.2.

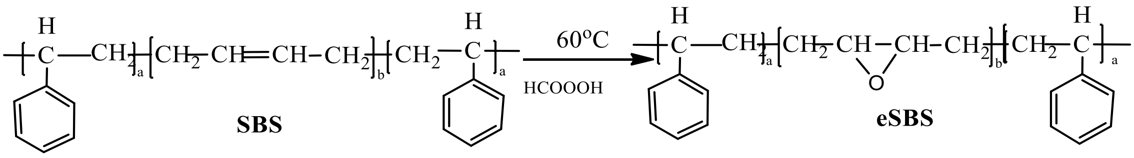

Figure Ap-2.2 Scheme of epoxidation reaction of SBS block copolymer using PFA method; the butadiene block undergoes chemical modification resulting in epoxide groups

Appendix – 3

Additionally, hexafluoro isopropanol (HFIP) method was used in other systems [181] which was used as new method for SBS copolymers. In a standard experiment, two grams of SBS was dissolved in the 25 mL chloroform. The solution was maintained at 0 °C and well stirred with magnetic stirrer. 2 mL of hexafluoro isopropanol was added drop wise to the solution and 0.04 g phenylarsonic acid was added in the solution. After 10 minutes of addition of phenyl arsenic acid, white precipitate was observed. The reaction mixture was heated up to 60 °C for 2 hour. The rest of the procedure was same as MCPBA method. The general epoxidation reaction is described in Figure Ap-3.1.

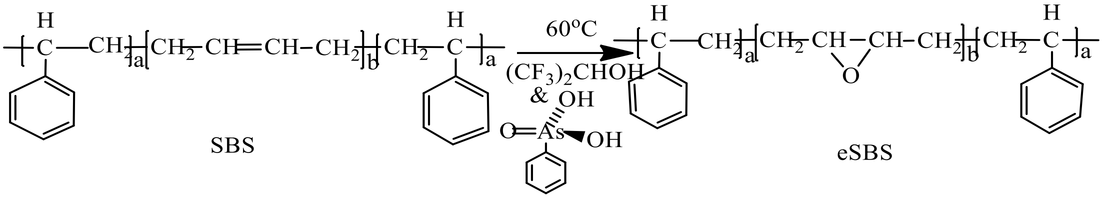

Figure Ap-3.1 Epoxidation reaction of SBS triblock copolymer using HFIP method; the C=C double bonds were changed into the epoxide group [181]

The mechanism of this reaction is illustrated in Figure Ap-3.2.

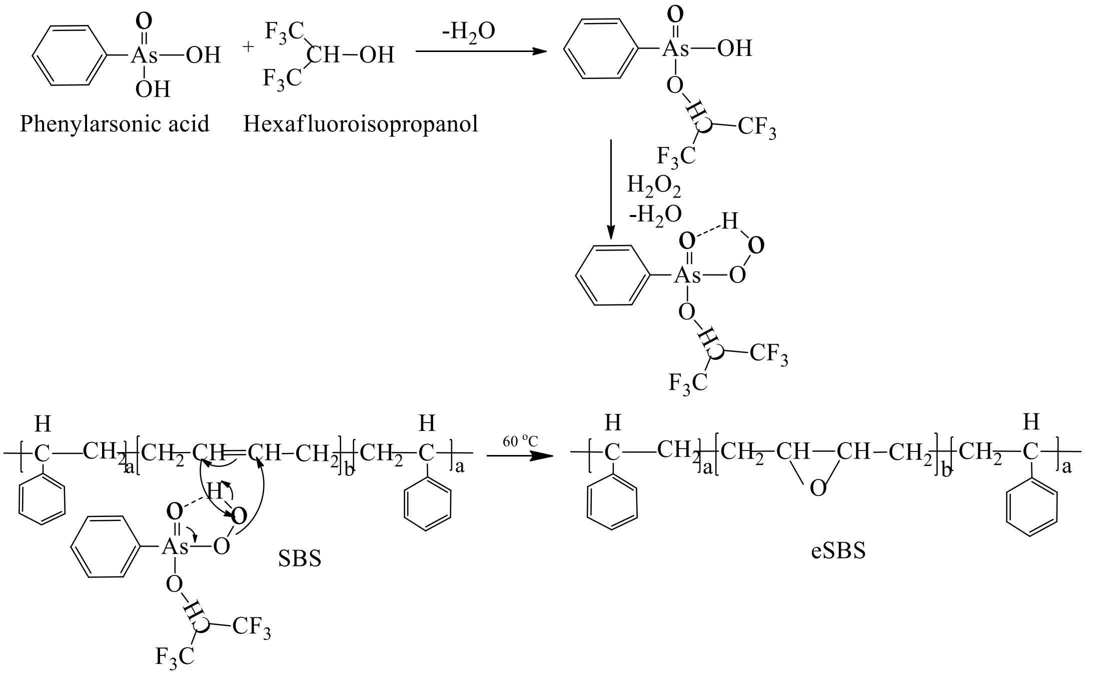

Figure Ap-3.2 The mechanism of epoxidation reaction of SBS block copolymer using HFIP method; the C=C double bonds were changed into the epoxide group by using hexafluoroisopropanol and phenylarsonic acid [181]

Appendix – 4

3) Picture of Teflon mold

Fig-App.-4 A photograph of teflon mold.

LIST OF PUBLISHED PAPERS

1. International Publications

- **R. Pandit**, G. H. Michler, R. Lach, W. Grellmann, J. M. Saiter, A. Berkessel, R. Adhikari, Epoxidation of styrene/butadiene star block copolymer by different methods and characterization of the blends with epoxy resin, *Macromolecular Symposia,* Vol. 341, Page No. 67 – 74, **2014**.
- **R. Pandit**, J. Giri, G. H. Michler, R. Lach, W. Grellmann, B. Youssef, J. M. Saiter, R. Adhikari, Effect of epoxidation of diene component of SBS block copolymer on morphology and mechanical properties, *Macromolecular Symposia,* Vol. 315, Page No. 152-157, **2012.**

2. National Publications

- **R. Pandit,** A. Berkessel, R. Lach, W. Grellmann, R. Adhikari, Synthesis and characterization of nanostructured blends of epoxy resin and block copolymers, *Nepal Journal of Science and Technology* Vol. 13, No. 1 Page No. 81-88, **2012**.

- **R. Pandit,** B. Youssef, J. M. Saiter, R. Adhikari, Investigations into morphology and mechanical properties of epoxidized polystyrene/polybutadiene/polystyrene (SBS) triblock copolymer, *Journal of Nepal Chemical Society*, Vol. 28, Page No. 42-47, **2011.**

LIST OF SCIENTIFIC PRESENTATIONS

- **R. Pandit,** S. P. Khatiwada, R. Lach, W. Grellmann, H. H. Le, S. Henning, R. Adhikari, Effect of copolymer architecture and composition on nanostructured thermosetting resin blends. **16th ISEPD** (Nepal), 2015, *oral presentation*

- **R. Pandit**, G. H. Michler, W. Lebek, R. Lach, W. Grillmann, J. M. Saiter, A. Berkessel, R.Adhikari, Blends of epoxy resin and SBS block copolymers: morphology and mechanical behaviour. Kathmandu Symposia in Advanced Materials, (Nepal), 2014, *poster presentation*

- **R. Pandit**, G. H. Michler, W. Lebek, R. Lach, W. Grillmann, J. M. Saiter, A. Berkessel, R.Adhikari, Epoxidation of styrene/butadiene star block copolymer by different methods and characterization of the blends with epoxy resin. 2014 IUPAC World Polymer Congress (MACRO-2014) Chiangmai, (Thailand), 2014, *poster presentation*

- **R. Pandit,** G. H. Michler, R. Lach, W. Grillmann, J. M. Saiter, A. Berkessel, R. Adhikari, Synthesis and Characterization of blends of epoxy resin and SBS block copolymers. International conference on Emerging Trends in Science and Technology, Biratnagar (Nepal), 2014, *oral presentation*

- **R. Pandit,** G. H. Michler, R. Lach, W. Grillmann, J. M. Saiter, A. Berkessel, R. Adhikari, Tolaring morphology and mechanical behavior of blends of epoxy resin and SBS block copolymers. 5th Asian colloidal and surface chemistry (India), 2013, *oral presentation*

- **R. Pandit,** G. H. Michler, R. Lach, W. Grillmann, J. M. Saiter, A. Berkessel, R. Adhikari, Thermal and mechanical behaviour of nanostructured epoxy resin/SBS block copolymers blends. 2nd Microsymposium on applied sciences-2013(Nepal), 2013, *oral presentation*

- **R. Pandit,** R. Lach, W. Grillmann, A. Berkessel, R. Adhikari, Synthesis and Characterization of epoxy resin and SBS block copolymers blends. ROSAM, (France), 2013, *poster presentation*

- **R. Pandit**, R. Lach, W. Grillmann, A. Berkessel, R. Adhikari, Synthesis and characterization of nanostructured epoxy resin and SBS blends. POLYCHAR 21, world forum of advanced materials (Korea), 2013, *oral presentation*
- **R. Pandit,** R. Lach, W. Grillmann, A. Berkessel, R. Adhikari, « "Synthesis and characterization of epoxy resin and SBS block copolymers blends" » KASAM-2012, Kathmandu symposia on advanced materials-2012, *poster presentation*
- **R. Pandit**, J. Giri, G. H. Michler, R. Lach, W. Grellmann, B. Youssef, J. M. Saiter, R. Adhikari, Effect of epoxidation of Diene Component of SBS Block Copolymer on Morphology and Mechanical Properties.International Conference, POLYCHAR 20, Croatia 26-31 March 2012, *poster presentation*
- **R. Pandit,** R. Lach, W. Grillmann, A. Berkessel, R. Adhikari, Influence of epoxidation on mid diene component of the block copolymer on mechanical properties. ICAMN-2011, International Conference on Advanced Materials and Nanotechonolgy, Kathmandu-2011, *Oral presentation*
- **R. Pandit**, J. Giri, G. H. Michler, R. Lach, W. Grellmann, B. Youssef, J. M. Saiter, R. Adhikari, Morphology and properties of epoxidized styrenic block copolymers. Second International Conference on Recycling and Reuse of Materials (ICRM-2011) conducted by Centre for Nanoscience and Nanotechnology and Institute of Macromolecular Science and Engineering (IMSE), Mahatma Gandhi University, Kerala, India, Aug 5-7, 2011, *poster presentation*
- **R. Pandit**, J. Giri, G. H. Michler, R. Lach, W. Grellmann, B. Youssef, J. M. Saiter, R. Adhikari, Effect of Epoxidation of middle diene blocks on Morphology and properties of SBS Block copolymer. International Conference on World Forum of Advance materials, **POLYCHAR 19** conducted by Nepal Polymer Institute and Tribhuvan University, Kathmandu, Nepal, March 20-25, 2011, *poster presentation*